

https://dspace.org/

A dual oral intestinal film for pulsatile release of a mood stabilizing agent in the treatment of schizoaffective disorder

Hoosain, Famida Ghulam

2016

http://hdl.handle.net/10539/21403

Hoosain, Famida Ghulam (2016) A dual oral intestinal film for pulsatile release of a mood stabilizing agent in the treatment of schizoaffective disorder, University of the Witwatersrand, Johannesburg, <http://hdl.handle.net/10539/21403>

Downloaded from a DSpace repository. https://dspace.org/

A DUAL ORAL INTESTINAL FILM FOR PULSATILE RELEASE OF A MOOD STABILIZING AGENT IN THE TREATMENT OF SCHIZOAFFECTIVE DISORDER

FAMIDA GHULAM HOOSAIN

A thesis submitted to the Faculty of Health Sciences, University of the Witwatersrand, Johannesburg, in fulfilment of the requirements for the degree of Doctor of Philosophy

Supervisor:

Professor Viness Pillay
Department of Pharmacy and Pharmacology, University of the Witwatersrand, South Africa

Co-Supervisors:
Professor Yahya E. Choonara and Dr Lisa C. du Toit
Department of Pharmacy and Pharmacology, University of the Witwatersrand, South Africa

Johannesburg, 2016

DECLARATION

I, Famida Ghulam Hoosain, declare that this thesis is my own work. It is being submitted for the degree of Doctor of Philosophy of Pharmacy in the Faculty of Health Sciences at the University of the Witwatersrand, Parktown, Johannesburg, South Africa. It has not been submitted before for any other degree or examination at this or any other university.

……..

Signed this …….. day of January 2016

PUBLICATIONS

Famida G. Hoosain, Yahya Choonara, Lomas Tomar, Pradeep Kumar, Charu Tyagi, Lisa du Toit, Viness Pillay. Bypassing P-Glycoprotein Drug Efflux Mechanisms: Possible Applications in Pharmacoresistant Schizophrenia Therapy. Journal of BioMed Research International, 2014, 1-21. Article ID 484963 [Review Article]. ISI, IF: 1.579.

Famida G. Hoosain, Yahya Choonara, Pradeep Kumar, Lomas Tomar, Charu Tyagi, Lisa du Toit, Viness Pillay. An Epichlorohydrin-Crosslinked Semi-Interpenetrating GG-PEO Network as a xerogel Matrix for Sustained Release of Sulpiride. American Association of Pharmaceutical Sciences, *AAPS PharmSciTech*, 2014, 15(5). [Research Article], ISI, IF: 1.641.

Famida G.Hoosain, Lomas K.Tomar, Pradeep Kumar, Charu Tyagi, Lisa C. du Toit, Yahya E. Choonara, Viness Pillay. Fabrication and characterization of Poly (ethylene) oxide- Gellan Gum semi –Interpenetrating Polymer Network Matrix (XePoMas) oral dosage form for the delivery of a low bioavailable active. (To be submitted to American Association of Pharmaceutical Sciences, *AAPS PharmSciTech)*.

Famida G. Hoosain, Yahya Choonara, Pradeep Kumar, Lisa du Toit, Viness Pillay. A Novel Dual-layered Oral Device for Delivery of Two Bioactives in the Treatment of Schizoaffective Disorder. (To be submitted to *The Journal of Pharmaceutical Sciences, JPharmSci*).

Appendix 11.1

RESEARCH PRESENTATIONS

Famida Ghulam Hoosain, Vines Pillay, Yahya Choonara, Lisa du Toit, Pradeep Kumar. A novel semi-Interpenetrating polymer network (IPN) matrix system for the delivery of sulpiride in schizophrenia. **(*Abstract Publication*)**. Boehringer Ingelheim Young Scientist Competition, 35th Conference of the Academy of Pharmaceutical Sciences 2014.

Famida Ghulam Hoosain, Viness Pillay, Yahya Choonara, Lisa du Toit and Pradeep Kumar. A Novel Dual Layered Oral Semi-Interpenetrating Polymer Network Xerogel Matrix-Bioadhesive Intestinal Patch System for the Individualistic Delivery of Antipsychotics and Mood Stabilizing Agents in Schizoaffective Disorder. **(*Poster Presentation*)**. The 2015 International AAPS Annual Meeting and Exposition, Orange County Convention Centre, Orlando Florida, USA.

Famida Ghulam Hoosain, Viness Pillay, Yahya Choonara, Lisa du Toit and Pradeep Kumar. A Novel Dual-layered Oral Device for Delivery of Two Bioactives in the Treatment of Schizoaffective Disorder. **(*Podium Presentation*)**. The 2015 Academy of Pharmaceutical Sciences of the Pharmaceutical Society of South Africa (APSSA) Conference, Cedar Woods of Sandton, Conference Centre.

Famida Ghulam Hoosain, Viness Pillay, Yahya Choonara, Lisa du Toit and Pradeep Kumar. A Novel Dual Layered Oral Matrix-Bioadhesive Intestinal Patch System for the Delivery of Antipsychotics and Mood Stabilizing Agents in Schizoaffective Disorder. **(*Poster Presentation*)**. School of Therapeutic Sciences Research Day, University of the Witwatersrand, Johannesburg, South Africa, 2015.

Appendix 11.2

PATENT FILED

Xerogel-Intestinal Patch Dual Layered Matrix Tablet. Famida Ghulam Hoosain, Viness Pillay, Yahya Choonara, Lisa du Toit, Pradeep Kumar ~PCT.

ACKNOWLEDGMENTS

Foremost and most importantly I would like to thank Almighty God, the most Beneficent and Merciful for providing me with the opportunity and guidance to complete my PhD degree. Without the guidance and blessings You have bestowed upon me I would have not made it this far. All praises are due to You.

I would like to thank my parents, Razia and Abdul Razack Ghulam Hoosain, mere words cannot possibly translate my immense gratitude for all the love, unwavering support and motivation throughout my life. It is due to your sacrifices and prayers that I have come this far and I hope to continue making you proud.

To my brother Mohammed Faraaz, sister Dr Shenaaz Banu, and sister in law Shakira I would like to thank you for all the moral support and encouragement. A special thanks to my sister for always being there for me and going beyond your call of duty for me, you are a sister, friend and mother figure.

To Professor Viness Pillay, thank you for the opportunity given to me in allowing me to complete my PhD under your supervision. Your dedication to excellence and the field of drug delivery has allowed me the chance to attain not only scientific skills but valuable life lessons. Thank you for providing students like myself the opportunity to follow our dreams and be a part of a prestigious research group such as the Wits Advanced Drug Delivery Platform (WADDP).

To my co-supervisors Dr Lisa du Toit and Professor Yahya Choonara for their help and commitment in guiding my research to completion, the time and effort you devoted has only made the completion of this thesis so much easier. A special thanks to Pradeep Kumar for imparting boundless knowledge to me and always making himself available to assist, for always sharing words of encouragement and being a source of motivation. I wish you all success in your future endeavours.

I would especially like to acknowledge my friends who are more like family, to my sisters and colleagues Tasneem Suleman and Naeema Mayet you have been a constant source of humorous motivation for me thank you for all the help and good memories in all aspects of my life. To my colleagues who turned out to be my closest friends Fatima Choonara, Poornima

Ramburrun and Karmani Murugan for all the laughs, happy times, encouragement and assistance.

To my colleagues Steven Mufamadi, Nonhlanhla Masina, Felix Mashingaidze, Ahmed Seedat, Angus Hibbins, Tasneem Rajan, Khadija Rhoda, Thiresen Govender, Teboho Kgesa, Martina Manyikana, Kealeboga Mokolobate, Khadija Rhoda, Fatema Mia, Mpho Ngoepe, Gillian Mahumane, Dimitris Georgiou, Sunaina Inderman, Mershen Govender, Latavia Singh, Jonathan Pantshwa, Pierre Kondiah, Olufemi Akilo, Khuphukile Madida, Zikhona Hayiyana, Margaret Siyawamwaya and Mduduzi Sithole for their assistance and friendship.

To Mr Sello Ramarumo, Mr Kleinbooi Mohlabi, Mr Bafana Temba, Ms Pride Mothobi, and MsPhumzile Madondo for their invaluable assistance with the effective management of the laboratories.

To the staff of the Central Animal Services (CAS) at the University of the Witwatersrand, Mr Nico Douths, Sr. Mary-Ann Costello, Mr Patrick Selahle, Sr. Amelia Rammekwa, Ms Kershnee Chetty, and Ms Lorraine Setimo for being very obliging and always making their skills available to my disposal for the duration of my *in vivo* studies.

To the Wits Department of Pharmacy and Pharmacology staff, Mr David Bayever, Ms Nompumelelo Damane, Mrs Neelaveni Padayache, Ms Shira Moch, Professor van Zyl and Professor Paul Danckwerts thank you for all the guidance, support and inspiration.

The financial assistance of the National Research Foundation (NRF) towards this research is hereby acknowledged. Opinions expressed and conclusions arrived at, are those of the author and are not necessarily to be attributed to the NRF. The completion of this research would not have been achievable without the assistance from NRF of South Africa, their support is deeply appreciated.

One who treads a path in search of knowledge has his path to Paradise made easy by God

-Prophet Mohammed (S.A.W)-

ABSTRACT

Oral drug delivery is acknowledged by many as the idyllic method of drug delivery due to its versatility and convenience of administration. Nevertheless, the bioavailability of drugs delivered via the oral route remains disputed. Classically, conventional marketed drug delivery systems release drugs in inconstant and unpredictable manners, leading to sub-therapeutic and in some cases toxic drug doses. Consequently, patient compliance is compromised, in turn having an effect on the success of the therapeutic intervention in question. One such limitation occurs in the treatment of Schizophrenia, with patients unable to comply with treatment due to multiple administration requirements. Sulpiride, an antipsychotic agent, displays notable efficiency in reducing both positive and negative symptoms of Schizophrenia. However, sulpiride has a low bioavailability and thus therapy requires the use of large doses, and hence multiple administrations. In addition, a large percentage of Schizophrenic patients present with concomitant mood disorders, namely 'Schizoaffective' disorder, which further necessitates the use of mood stabilizing agents. As a result, patients end up with a huge pill burden and are unable to comply with therapy and this leads to reduced clinical outcomes.

A dual layered, xerogel-bioadhesive intestinal patch drug delivery system (ODLS) was thus designed, formulated, and evaluated for the site-specific delivery of two bioactives in the treatment of Schizophrenia with concomitant mood disorders in a time controlled-idiosyncratic manner. Ultimately easing compliance to complicated treatment regimens, enhancing bioavailability and improving patient compliance. The ODLS essentially comprises of a bi-layered tablet, layer one comprised of a sustained release semi-interpenetrating polymer network (s-IPN) xerogel and a layer two of embedded pulsatile release bioadhesive intestinal patches, with the system as a whole enteric coated for protection. Intestinal patches encompassed in layer two are fabricated of a backing layer, a drug loaded layer, a mucoadhesive layer, and a mucus cleaving layer. The ODLS employs a combination of sustained and pulsatile drug release mechanisms, in addition to intestinal retentive mechanisms. Furthermore, the system physically protects the drug delivery system from acidic or proteolytic degradation within the human gastro-intestinal tract. The present study utilized the use of bioadhesion for site-specific and gastro retentive drug delivery, with crosslinking being employed for rate-modulated drug delivery. Sulpiride and sodium valproate were selected as model drugs for the sustained release xerogel layer and the pulsatile bioadhesive patch layer respectively in this study as sulpiride is an antipsychotic with low bioavailability yet good antipsychotic activity and sodium valproate is the mainstay drug treatment for mood disorders in schizophrenia. Therefore, sulpiride would profit from the sustained release as it would improve bioavailability and hence patient compliance, whereas sodium valproate would benefit from the pulsatile release so as to avoid the well-known resistance to therapy due to prolonged exposure to drug. Thus these drugs would gain benefit from the site-specific controlled drug delivery offered by the ODLS.

The primary aim of the sustained release s-IPN xerogel was to ensure delayed release of drug over 24 hours thus decreasing the need for multiple administrations and to maintain a steady state drug concentration. Film casting, a versatile technique was utilized in the fabrication of polymeric films to develop the bioadhesive intestinal patches. Preliminary in vitro investigations led to identification of a combination of polymers and crosslinking agent best suited to develop the system. A central composite design was employed for system optimization. The xerogel layer demonstrated that zero-order drug release was achieved after the crosslinking procedure. Delayed drug release fundamentally decreases the number of doses required daily and thus patient compliance and clinical efficacy is improved. The pulsatile release layer displayed distinct triphasic drug release after assembly of the intestinal patches, pulsatile release of drugs fundamentally reduced resistance to drug therapy as well as reducing pill burden. Furthermore, in vitro analysis of the ODLS showed that the xerogel layer behaved superiorly in terms of controlling drug delivery in a site-specific and prolonged fashion in comparison to a marketed gold standard. There exists no gold standard for pulsatile delivery of sodium valproate hence the pulsatile layer was tested against the marketed standard administered as a single dose. In vitro findings were substantiated by in vivo analysis in a white pig model. Results indicated that the systemic bioavailability of sulpiride was higher than the gold standard and drug release was prolonged in a zero-order fashion over 24 hours. Sodium valproate released in a triphasic manner over 24 hours thus reducing the risk of treatment resistance and decreased pill burden.

To summarize, the ODLS was able to overcome the many challenges associated with oral drug delivery in schizoaffective disorder, by simplification of complicated treatment regimens, and hence improving bioavailability of drug delivery orally. The benefits associated with oral drug delivery have evidently been exploited by the present study, producing a versatile drug delivery system which can successfully deliver two bioactives simultaneously via individualistic release patterns, thus treating both conditions with a single oral dosage form with a single daily administration.

DEDICATION

This thesis is dedicated to the source of my unwavering strength, my perpetual inspiration, my enduring motivation, my beloved parents

Razia and Abdul Razack Ghulam Hoosain

For teaching me the importance of education and the value of perseverance; and for all that I am today.

TABLE OF CONTENTS

DECLARATION……i

PUBLICATIONS……...ii

RESEARCH PRESENTATIONS……...iii

PATENT FILED……iv

ACKNOWLEDGEMENTS……...v

ABSTRACT……..vii

DEDICATION……..viii

LIST OF ABBREVIATIONS……..xxvii

LISTOF EQUATIONS……....xxix

LIST OF FIGURES……xxxi

LIST OF TABLES……...xxxix

CHAPTER 1
INTRODUCTION AND MOTIVATION FOR STUDY

1.1. Background to the Study……1

1.2. Rational and Motivation for the Study……6

1.3. Mechanism by which Dual Drug Delivery will be achieved with the ODLS…….....7

1.4. Novelty of the Study…….....10

1.5. Aim and Objectives of the Study……..10

1.6. Synopsis of the Thesis…….....13

1.7. Concluding Remarks……15

CHAPTER 2
BYPASSING P-GLYCOPROTEIN DRUG EFFLUX MECHANISMS: POSSIBLE APPLICATIONS IN PHARMACORESISTANT SCHIZOPHRENIA THERAPY

2.1. Introduction……16

2.2. Structure and Function of the Intestine and P-gp Intestinal Expression in Drug Delivery……..20

2.3. Structure and Function of the BBB and P-gp Expression in Drug Delivery……..23

2.4. P-gp Efflux Transporter Structure and Mechanism of Action……..27

2.5. P-gp in Schizophrenia Therapy…….....29

2.6. P-gp Substrates and Inhibitors……31

2.7. Novel Drug Delivery Systems and Pharmaceutical Excipients Capable of CNS and Intestinal Delivery via P-gp Bypass or Inhibition with a Potential Applicability in Schizophrenia Therapy……33

2.7.1. Formulation excipients utilized as P-gp inhibitors…….....33

2.7.2. Chemosensitizers……..33

2.7.3. Natural polymers……34

2.7.4. Synthetic polymers……34

2.7.5. Solvents and surfactants ……38

2.8. Drug Delivery Systems with P-gp Modulatory and Enhanced Intestinal Absorption Applications……39

2.8.1. Bestatin-improved intestinal absorption by co-administration of a P-gp inhibitor.....39

2.8.2. Enhanced intestinal absorption of ganciclovir by P-gp inhibition using Pharmaceuticalexcipients…….....39

2.8.3. Self-emulsifying drug delivery systems…….....40

2.8.4. Double coated nanocapsules for enhanced intestinal absorption and bioavailability of a P-gp substrate……40

2.8.5. Novel polymeric P-gp inhibitor for enhanced intestinal drug delivery……41

2.8.6. Influence of intestinal P-gp on absorption of furosemide a P-gp substrate……..41

2.9. Drug Delivery Systems with P-gp Modulation and Enhanced BBB Absorption……...42

2.9.1. Nanocarriers……..43

2.9.2. Surfactant-polymer nanoparticles overcome P-gp-mediated drug efflux……..43

2.9.3. Lipid-based nanoparticles……44

2.9.4. Transferrin-conjugated nanoparticles for delivery across the BBB……45

2.9.5. Paclitaxel-polymer micelles to overcome multidrug drug resistance (MDR)……45

2.9.6. Polyethylene glycol-660 hydroxystearate nanocapsules……46

2.9.7. Immunoliposomes in bypassing P-gp……47

2.9.8. PAMAM-drug complex for delivery across the BBB……48

2.9.9. Poly (D, L-lactide) nanosuspensions of risperidone……49

2.9.10. Natural Vesicular Exosomes as Drug Delivery Systems to Possibly Bypass P-gp Efflux.....49

2.10. Concluding Remarks…….....52

CHAPTER THREE

PRELIMINARY FORMULATION AND CHARACTERIZATION OF THE EPICHLOROHYDRIN-CROSSLINKED semi- INTERPENETRATING POLYMER NETWORK XEROGEL MATRIX

3.1. Introduction……53

3.1.1. Preliminary formulation design……57

3.2. Materials and Methods……..58

3.2.1. Materials…….....58

3.2.2. Polymer blending and crosslinking…….....59

3.2.3. Fabrication of xerogel polymer matrix system……59

3.2.4. Determining the upper and lower limit variables of the formulation required for input into the Central Composite Design……...60

3.2.5. Validation and determination of chemical transitions upon crosslinking……60

3.2.6. Identification of optimization variables for degree of swelling and erosion……60

3.2.7. Surface morphological analysis……...61

3.2.8. Determination of the physiomechanical properties of the s-IPN xerogel matrix system via textural analysis……...61

3.2.9. Construction of calibration curve for the determination of sulpiride release from the s-IPN xerogel matrix……61

3.2.10. Identification of optimization variables via *in vitro* drug release studies……..62

3.3. Results and Discussion……62

3.3.1. Analysis of chemical transitions upon crosslinking……...62

3.3.2. Pre-formulation evaluation of the swelling and erosion characteristics of the s-IPN xerogel……64

3.3.3. Assessment of surface morphological characteristics……...64

3.3.4. Evaluation of textural analysis studies…….....66

3.3.5. Construction of a calibration curve for the ultraviolet spectrophotometric determination of sulpiride……...67

3.3.6. Assessment of *in vitro* drug release……68

3.3.7. Determining the upper and lower limits of the formulation variables required for input into the Central Composite Design……69

3.4. Concluding Remarks……71

CHAPTER 4

FABRICATION AND STATISTICAL OPTIMIZATION OF THE NOVEL EPICHLOROHYDRIN-CROSSLINKED semi-INTERPENETRATING GG-PEO XEROGEL NETWORK MATRIX TABLET

4.1. Introduction……72

4.2. Materials and Methods……..74

4.2.1. Materials……74

4.2.2. Construction of a Randomized Central Composite Design for the optimization of the s-IPN xerogel matrix component of the ODLS……74

4.2.3. Synthesis of crosslinked s-IPN xerogel……....75

4.2.4. Preparation of the s-IPN xerogel matrix tablets……76

4.2.5. Physiomechanical evaluation of fabricated s-IPN xerogel matrix tablets……77

4.2.5.1. Brinell hardness number, deformation, rigidity, and resilience determination…….....77

4.2.6. Surface morphological analysis…….....78

4.2.7. Chemical composition analysis…….....79

4.2.8. Thermal transition examination……..79

4.2.9. Response surface analysis of the employed responses……79

4.2.10. Water content determination employing Karl- Fischer Analysis (KF)……79

4.2.11. Powder flow characterization studies…….....80

4.2.11.1. Angle of repose…….....80

4.2.11.2. Carr's Compressibility Index and Hausner ratio……80

4.2.12. Swelling and erosion studies……81

4.2.13. *In vitro* drug release studies……..82

4.3. Results and Discussion……82

4.3.1. Assessment of the physiomechanical properties of the s-IPN xerogel matrix component of the ODLS……...82

4.3.2. Assessment of the surface morphology of the s-IPN xerogels as per design……86

4.3.3. Chemical compositional assessment of the s-IPN xerogels……..88

4.3.4. Thermal analysis of the crosslinked s-IPN xerogel……90

4.3.5. Response surface analysis of the Box-Behnken design……92

4.3.6. Influence of water content as determined via titrimetric analysis……...98

4.3.7. Flow properties of powdered-drug loaded xerogel……...99

4.3.8. Analysis of the swelling behavior……100

4.3.9. *In vitro* drug release analysis……103

4.3.10. Response optimization of s-IPN xerogel matrix……...108

4.4. Concluding Remarks……...109

CHAPTER 5

CHARACTERIZATION AND FURTHER EVALUATION OF THE OPTIMIZED ORAL S-IPN XEROGEL MATRIX FORMULATION

5.1. Introduction……...110

5.2. Materials and Methods……111

5.2.1. Materials…….....111

5.2.2. Fabrication of optimized s-IPN Gellan Gum- Poly (ethylene) oxide xerogel matrix……...112

5.2.3. Characterization of vibrational transitions of optimized s-IPN xerogel……112

5.2.4. Characterization of thermal transitions of the optimized s-IPN xerogel by Differential Scanning Calorimetry and Thermogavimetric Analysis……112

5.2.5. *In vitro* drug release studies……..113

5.2.6. Morphological and surface structure analysis……113

5.2.7. Porositometric analysis……113

5.2.8. Assessment of degree of mucoadhesion of the optimized xerogel matrix……..114

5.2.9. Elucidation of the pertinent rheological properties of the optimized s-IPN xerogel……115

5.2.10. Textural characterization of the optimized s-IPN xerogel matrix tablet……..115

5.2.11. Gravimetric swelling and erosion studies……115

5.2.12. Determination of the diffusion, swelling and erosion fronts……117

5.2.13. Magnetic Resonance Image (MRI) analysis of the swelling behavior of the optimized xerogel matrix tablets……117

5.3. Results and Discussion……...117

5.3.1. Inter and intra- polymeric interaction validation of the optimized crosslinked xerogel……117

5.3.2. Thermal analysis of the optimized crosslinked PEO-GG based xerogel by Differential Scanning Calorimetry and Thermogavimetric Analysis……119

5.3.3. Construction of calibration curve for ultraviolet spectrophotometric determination of bioactive release from optimized s-IPN xerogel matrix……122

5.3.4. *In vitro* drug release determination of optimized s-IPN xerogel matrix tablets……122

5.3.5. Assessment of the surface morphology of the optimized crosslinked xerogel……124

5.3.6. Determination of xerogel porosity……126

5.3.7. Determination of degree of mucoadhesion……127

5.3.8. Rheological characterization of non-drug loaded xerogel polymeric solution employed in matrix formation……...127

5.3.9. Mechanical evaluation and validation of structural integrity of the optimized xerogel matrix……128

5.3.10. Gravimetric swelling and erosion analysis……129

5.3.11. Evaluation of the diffusion, swelling and erosion fronts of the matrix system……132

5.3.12. Magnetic Resonance Imaging of the optimized s-IPN xerogel matrix tablet……135

5.4. Concluding Remarks……...137

CHAPTER 6

PRELIMINARY DESIGN OF THE MULTI-LAYERED BIOADHESIVE POLYMERIC INTESTINAL PATCH FOR PULSATILE DRUG DELIVERY (IPRPS)

6.1. Introduction……...138

6.1.1. Selection of independent variables for input into a Central Composite Design……..140

6.2. Materials and Methods……144

6.2.1. Materials…….....144

6.2.2. Construction of a Randomized Central Composite Design for optimization of the bioadhesive multilayered intestinal patch component of the ODLS……144

6.2.3. Fabrication of mucoadhesive lectin fused hypromellose-chitosan blend and drug loaded layer……...146

PART I: Preliminary Mucoadhesive Layer Characterization……...147

6.3. Physiomechanical and Physiochemical Characterization of the Mucoadhesive Layer……...147

6.3.1. Chemical transitional characterization of the lectin amalgamated mucoadhesive layer of the intestinal patches……...147

6.3.2. Thermal analysis of polymeric material employed in the formulation of the mucoadhesive layer of the intestinal patch……147

6.3.3. Mucoadhesive analysis of the mucoadhesive layer……..148

6.3.4. Evaluation of the swelling behavior of the mucoadhesive layer……...148

6.3.5. Textural analysis of formulated mucoadhesive film layer……148

6.3.5.1. Determination of the tensile properties and Young's modulus of the intestinal mucoadhesive films via NanoTensile analysis……..149

6.3.6. Elucidation of the pertinent rheological properties……150

6.3.7. Response surface analysis of the employed responses……...150

6.4. Results and Discussion……...150

6.4.1. Chemical composition elucidation of the mucoadhesive layer of the intestinal patches……150

6.4.2. Thermal appraisal of polymeric components of the mucoadhesive film layer……152

6.4.3. Clarification of the mucoadhesive properties of the mucoadhesive layer……...153

6.4.4. Assessment of the gravimetric swelling characteristics of the mucoadhesive layer……155

6.4.5. Mechanical strength appraisal of the mucoadhesive film layer……156

6.4.6. Assessment of Rheological characteristics of the mucoadhesive polymeric solutions of the multi-layered intestinal patch……157

6.4.7. Response surface analysis of the Central Composite design……..158

PART II: Preliminary Drug Loaded Layer Characterization……164

6.5. Physiomechanical and Physiochemical Characterization of the Drug Loaded Layer…….164

6.5.1. Determination of the chemical vibrational transition of the crosslinked drug loaded layer of the bioadhesive multilayered intestinal patch……164

6.5.2. Thermal event analysis of the drug loaded layer of the bioadhesive multi-layered intestinal patch……..164

6.5.3. Textural analysis of the drug loaded layer……...164

6.5.4. Appraisal of swelling behavior of the drug loaded layer……164

6.5.5. Determination of the Rheological Properties……..164

6.5.6. Construction of a calibration curve for the ultraviolet spectrophotometric determination of valproic acid……..165

6.5.7. *In vitro* drug release from the drug loaded layer of the bioadhesive multi-layered intestinal patch……...165

6.5.8. Response surface analysis of the employed responses……...166

6.6. Results and Discussion……...166

6.6.1. Elucidation of chemical vibrational transitions of the drug loaded layer……..166

6.6.2. Thermal characteristics of the drug loaded layer……168

6.6.3. Tensile assessment of the drug loaded layer……169

6.6.4. Appraisal of swelling behavior of the drug loaded layer……170

6.6.5 Assessment of rheological characteristics…….....171

6.6.6. *In vitro* drug release from the drug loaded layer……172

6.6.7. Response surface analysis of the Central Composite design……..174

6.6.8. Response optimization of the mucoadhesive and drug loaded layer of the bioadhesive multilayered intestinal patch……...177

6.7. Concluding Remarks……...179

CHAPTER 7

FABRICATION AND CHARACTERIZATION OF THE STATISTICALLY OPTIMIZED MULTI-LAYERED BIOADHESIVE INTESTINAL PATCH FOR PULSATILE BIOACTIVE RELEASE

7.1. Introduction……...180

7.2. Materials and Methods……183

7.2.1. Materials…….....183

7.2.2. Preparation of the respective layers of the optimized bioadhesive intestinal patches……184

7.2.3. Physiomechanical and Physiochemical Characterization of the layers of the Optimized Multilayered Bioadhesive Intestinal Patches……..185

7.2.3.1. Evaluation of membrane uniformity…….....185

7.2.3.2. Determination of the tensile properties and Young's Modulus of the respective layers of the optimized bioadhesive multilayered intestinal patch……186

7.2.3.3. Analysis of surface morphology of the optimized mucoadhesive and drug loaded layers……187

7.2.3.4. Evaluation of the polymeric structural and vibrational frequency vibrations of the optimized mucoadhesive and drug loaded layers……188

7.2.3.5. Evaluation of the degree of swelling and its effect on mucoadhesive characteristics of the optimized patch layers upon intestinal environment exposure…188

7.2.3.6. Characterization of thermal transitions employing Differential Scanning Calorimetry.....189

7.2.3.7. Ex vivo determination of mucoadhesive properties via textural analysis……...189

7.2.3.8. In vitro perfusion studies.....190

7.2.3.9. Ex vivo drug permeation studies……...191

7.2.3.9.1. Integrity evaluation of the intestinal mucosal tissue.....192

7.2.3.10. In vitro drug release analysis……...193

7.3. Results and Discussion…….....193

7.3.1. Physical characterization of optimized patch layers: Analysis of membrane uniformity……193

7.3.2. Assessment of the tensile properties and Young's Modulus of the optimized intestinal patch layers……194

7.3.3. Evaluation of surface morphology of the optimized mucoadhesive and drug loaded layers……..195

7.3.4. Appraisal of the polymeric structural and vibrational frequency variations of the optimized mucoadhesive and drug loaded layers……197

7.3.5. Elucidation of the degree of swelling and its effect on mucoadhesive characteristics of the optimized patch layers upon intestinal environment exposure……201

7.3.6. Analysis of thermal transitions……..202

7.3.7. *Ex vivo* determination of mucoadhesive properties via textural analysis and a comparative evaluation via *ex vivo* perfusion……205

7.3.8. *Ex vivo* drug permeation studies……..207

7.3.8.1. Porcine intestinal mucosa integrity evaluation……209

7.3.9. *In vitro* drug release analysis……209

7.4. Concluding Remarks……...211

CHAPTER 8

IN VIVO ANALYSIS OF THE DUAL LAYERED ORAL DRUG DELIVERY SYSTEM COMPONENTS IN RELATION TO MARKETED GOLD STANDARD FORUMULATIONS

8.1. Introduction……...212

8.2. Materials and Methods……....213

8.2.1. Materials…….....213

8.2.2. Preparation of system components……214

8.2.3. Habituation of pigs prior to drug study commencement……214

8.4.4 Surgical implantation of a chronic catheter into the left jugular vein……215

8.4.5 Administration of the marketed gold standards and the optimized system formulations to the Large White Pig model……217

8.2.6. Blood sampling protocol from the surgically implanted jugular vein catheter…….....219

8.3. Quantification of *In Vivo* Release of the Model Drugs Employed Utilizing Ultra-Performance Liquid Chromatography Analysis……221

8.3.1. Preparation of calibration standards……222

8.3.2. Calibration sample preparation of plasma employing liquid-liquid extraction……222

8.3.3. Validation of liquid-liquid extraction methodologies……..223

8.3.4. Construction of calibration curves for the quantification of sulpiride and sodium Valproate release from the dual-layered oral device……..223

8.4. Pharmacokinetic Modeling Employing Non-compartmental and Compartmental Algorithms……224

8.4.1. Pharmacokinetic analysis: *in vitro-in vivo* correlation establishment……..224

8.5. Results and Discussion……...225

8.5.1. Behavioral evaluation of pig's post-surgical implantation of the jugular vein catheter and administration of the optimized formulations……...225

8.5.2. Validation of the extraction procedure……225

8.5.3. *In vivo* release of sulpiride and sodium valproate in the Large White Pig model from the dual-layered oral device components……..225

8.5.4. Interpretation of the extravascular compartmental and non-compartmental pharmacokinetic model analysis……..230

8.5.5. Establishment of an *in vitro-in vivo* correlation……235

8.6. Concluding Remarks……...238

CHAPTER 9

CONCLUSIONS, RECOMMENDATIONS AND FUTURE OUTLOOK

9.1. Conclusions……..239

9.2. Recommendations……...240

9.3. Future Outlook…….....241

10. References……242

11. Appendices…….....269

11.1. Publications……..269

11.1.1. Review Paper……...269

11.1.2. Research Paper 1……270

11.1.3. Research Paper 2……271

11.1.4. Research Paper 3……272

11.2. Research Presentations…….....273

11.3. Animal Ethics Clearance Certificate……277

LIST OF ABBREVIATIONS

AESC - Animal Ethics Screening Committee

AIC - Akaike's Information Criterion

ANOVA - Analysis of Variance

AUC - Area under the Curve

BET - Brunauer-Emmett-Teller

BHN - Brinell hardness number

BJH - Barrett, Joyner and Halenda

CA - citric acid

$CaCl_2$ - calcium chloride

CCI - Carr's compressibility index

CHT - chitosan

CMC - carboxymethylcellulose

DDS - drug delivery system

DL - drug loaded layer

DoE - Design of Experiments

EC - Ethylcellulose

EPI - epichlorohydrin

FDC - Franz diffusion cell

FTIR - Fourier Transform Infrared

GG - gellan gum

GIT - gastro-intestinal tract

HCL - hydrochloric acid

HPM- hypromellose

IPN - interpenetrating polymer network

IS - internal standard

IVIVC - *in vitro-in vivo* correlation

MDF - maximum displacement force

MDT - mean dissolution time

MRI - Magnetic Resonance Imaging

Mw - molecular weight

n - Sample size

NAC - N-acetyl- cysteine

NAW - narrow absorption window

NT - NanoTensile

ODLS - oral dual-layered system

PBS - phosphate buffered saline

PDA - photodiode array

PEO - poly (ethylene oxide)

PEO - polyethylene oxide (Polyox® WSR 303)

P-gp- P-glycoprotein

R^2 - correlation coefficient

RF - resistance reduction factor

RSM - response surface methodology

SBC - Schwarz's Bayesian Criterion

SD - standard deviation

SE - Standard error of weighted residuals

SEM - Scanning Electron Microscopy

s-IPN - semi interpenetrating polymer network

SS - Sum of squares of residuals

TA - textural analysis

T*g* - glass transition temperature

TGA - Thermogavimetric analysis

UPLC - ultra performance liquid chromatography

UV - Ultraviolet-visible

WA - work of adhesion

LIST OF EQUATIONS

Equation 2.1: Brain Efflux Index……26

Equation 3.1: Brinell hardness number……...61

Equation 3.2: Resilience……61

Equation 4.1: Brinell hardness number……78

Equation 4.2: Resilience……78

Equation 4.3: Angle of Repose…….....80

Equation 4.4: Carr's compressibility index…….....80

Equation 4.5: Hausner's ratio……80

Equation 4.6: Swelling ratio……81

Equation 4.7: Dynamic swelling ratio……81

Equation 4.8: % water uptake……81

Equation 4.9: % erosion…….....82

Equation 4.10: Equilibrium water uptake…….....82

Equation 4.11: MDT (Mean Dissolution Time)

Equation 4.12: Young's modulus…….....85

Equation 4.13: Deformation……86

Equation 4.14: derived formula from textural deformation……86

Equation 4.15: derived formula from textural deformation……86

Equation 4.16: ANOVA analysis mean % erosion……..93

Equation 4.17: ANOVA analysis total MDT…….....93

Equation 4.18: ANOVA analysis mean % swelling……93

Equation 4.19: % water content……98

Equation 4.20: degree of crosslinking effect on swelling……102

Equation 4.21: Fick's law of diffusion……102

Equation 4.22: fraction of drug released per unit time……102

Equation 4.23: Effect of dynamic swelling on drug release……102

Equation 4.24: Levenberg Marquardt equation……105

Equation 4.25: Sherwood number…….....106
Equation 4.26: diffusion coefficient…….106
Equation 4.27: diffusion matrix……106
Equation 5.1: % mucoadhesion……..115
Equation 5.2: Dynamic swelling ratio……116
Equation 5.3: Equilibrium water content……116
Equation 5.4: % water uptake……116
Equation 5.5: % erosion……...116
Equation 6.1: % mucoadhesion…….....148
Equation 6.2: equilibrium swelling ratio…….....148
Equation 6.3: Young's modulus……..149
Equation 6.4: ANOVA analysis Young's modulus……...159
Equation 6.5: ANOVA analysis % mucoadhesion……...159
Equation 6.6: ANOVA analysis MDT drug loaded layer…….....175
Equation 7.1: % swelling……188
Equation 7.2: Work of adhesion…….....190
Equation 7.3: permeation flux…….....192
Equation 7.4: Fick's law derived flux……192
Equation 7.5: resistance reduction factor……192
Equation 8.1: extraction yield %.....223

LIST OF FIGURES

Figure 1.1: Illustration of various restrictions to oral drug delivery and studies conducted to overcome them…….....3

Figure 1.2: Potential applications of the ODLS……7

Figure 1.3: Componential configuration of the ODLS prototype, where a) represents the dual layered oral drug delivery system and b) represents the multilayered bioadhesive intestinal patch with its respective polymeric film layers…….8

Figure 1.4: Technology utilized to enhance bioavailability in the development of the ODLS.....9

Figure 1.5: Schematic illustration depicting mechanism of drug release from the ODLS; a) xerogel matrix; b) adhesive intestinal patch layer; c) illustration of individual patch archetype; and d) dual layered oral dosage form (ODLS)……12

Figure 2.1: (a) Description of the aetiological complexity of schizophrenia (van Os et al., 2010) (b) Stages of schizophrenia progression (Tandon et al., 2009)……...20

Figure 2.2: Drug Efflux by P-glycoprotein in the intestine (Estudante et al., 2013)……22

Figure 2.3: Schematic representation of the cross section of the BBB cerebral capillary (Blasi et al., 2007)…….24

Figure 2.4: Respective locations of the drug efflux proteins on brain capillary endothelial cells that collectively form the BBB (Löscher and Potschka, 2005 (3)……25

Figure 2.5: (a) Structural configuration of P-gp, MRP, and BCRP (Aouali et al., 2005) (b) Diagrammatic representations of the “Vacuum Cleaner” and Flippase model of P-gp function (Sharom, 2014)……..28

Figure 2.6: Mechanism of inhibition of the P-gp efflux pump (Kumar and Sinha, 2013)……38

Figure 2.7: TEM images of lipid based nanoparticles; arrows show the lipid bilayer thickness (Mandal et al., 2013)…….....44

Figure 2.8: TEM micrographs showing the surface morphology of drug loaded micelles (Wang et al., 2011)…….46

Figure 2.9: (a) (A) P-gp interacts with substrates in the plasma membrane and digoxin (substrate) is effluxed from the lipid bi-layer. (B) Cellular uptake of digoxin facilitated by Immunoliposomes-targeted to transferrin receptor and taken up via receptor-mediated endocytosis (Huwyler et al., 2002) (b) (A) 2D Schematic representation of a dendrimer. (B) 3D representation of a dendrimer (Svenson, 2009)……48

Figure 3.1: Types of IPNs (Chikh et al., 2011; Banerjee et al., 2010)…….56

Figure 3.2: FTIR spectra of a) gellan gum, b) PF 5, c) PF 1 and d) PEO……...63

Figure 3.3: Illustration of the % swelling and erosion for all preliminary formulations……..64

Figure 3.4: SEM micrographs of a) PEO, b) GG, c) PF 5 and d) PF 1…….65

Figure 3.5: Graphical illustration of Brinell hardness numbers and respective standard deviations for preliminary formulations…….....66

Figure 3.6: Percentage resilience and respective standard deviations of the respective pilot study formulations…….....67

Figure 3.7: Calibration curve of sulpiride in PBS at λ_{300}……68

Figure 3.8: Fractional release profiles of preliminary formulations……69

Figure 4.1: (a) Digital images of s-IPN xerogel after precipitation in acetone at 3 hours and (b) s-IPN xerogel polymer matrix tablets compressed employing the *Carver Press 3851-0*……..76

Figure 4.2: Diagrammatic representation of Brinells Hardness Number for Box Behnken Statistical formulations depicting the effect of polymer concentration and crosslinking density on the hardness and mechanical strength of formulations……...84

Figure 4.3: Illustration of the difference of Resilience between all statistical Box-Behnken design formulations with variances in chemical composition……85

Figure 4.4: SEM Micrographs of PEO (A), GG (B), F1(C), F7 (D), and xerogel F9 (E)……87

Figure 4.5: FTIR Spectra of crosslinked s-IPN xerogel F1 (f), F7(c), F9 (d), as well as pure PEO (b) and GG (a) depicting the change within chemical structure via the identification of specific functional groups within the spectra obtained. Pink and green spectra correspond to PEO and GG respectively with black, red and blue representing formulations 1, 7 and 9 respectively……88

Figure 4.6: DSC Thermograms of s- IPN xerogel Formulations F1(c), F7 (d), F9 (e), as well as PEO (b) and GG (a) at a heating rate of 10˚C/ min from 10- 300˚C under nitrogen atmosphere……92

Figure 4.7: Residual plots for the responses a) mean % erosion b) drug release (MDT) c) mean % swelling……...94

Figure 4.8: Response surface and contour plots depicting the effects of gellan gum (GG), poly (ethyleneoxide) (PEO) and epichlorohydrin (EPI) on mean % matrix erosion……96

Figure 4.9: Response surface and contour plots depicting the effects of gellan gum (GG), poly (ethyleneoxide) (PEO) and epichlorohydrin (EPI) on drug release (total MDT)……..97

Figure 4.10: % water content obtained for 15 design formulations employing Karl- Fischer analysis……99

Figure 4.11: a) Graphical illustration of calculated angle of repose and Carr's compressibility index b) Graphical illustration of Hausner ratio…….....100

Figure 4.12: Graphical representation of Swelling characteristics (a and b) of crosslinked xerogel formulations vs. a non crosslinked blend to assist in identification of the influence of polymer ratio as well as crosslinker density on the swelling and erosion capabilities of formulations based on chemical variations on exposure to an aqueous environment (pH 6.8)……....103

Figure 4.13: Graphical illustration of the *in vitro* fractional drug release vs. time of sustained release s-IPN xerogel matrix tablets in comparison to release profiles of PEO-GG blend formulations……..104

Figure 4.14: Desirability plots representing the levels of GG, PEO and EPI required to synthesize the optimized formulation……109

Figure 5.1: FTIR spectra of (a) crude GG; (b) optimized s-IPN xerogel and (c) PEO……118

Figure 5.2: DSC Thermograms of a) Gellan Gum b) Optimized s-IPN xerogel c) Polyethylene Oxide…….....120

Figure 5.3: TGA thermogram of optimized s-IPN xerogel……121

Figure 5.4: Plots of drug release based on the respective mathematical models ……123

Figure 5.5: SEM images of A) optimized xerogel before swelling B) optimized xerogel after swelling C) pure polyethylene oxide D) pure gellan gum……125

Figure 5.6: (a) Textural analysis Force vs. Time profile for the optimized xerogel matrix tablet and (b) Textural analysis Force vs. Time profile for the PEO-GG blend tablet….....129

Figure 5.7: (a) % water uptake vs. time and (b) % erosion vs. time of the optimized xerogel matrix tablet…….....131

Figure 5.8: The theoretical fronts observed for s-IPN xerogel matrix systems and the respective digital images obtained during the front movement study conducted for the optimized matrix tablet……..133

Figure 5.9: Graphical representation of the fronts present and their positions over a 24 hour test period……133

Figure 5.10: MRI imagery of xerogel matrix tablets over 24 hours……...135

Figure 6.1: Assembly of the bioadhesive multilayered intestinal patches……...139

Figure 6.2: Mechanism of polymeric film formation by the film casting method……..140

Figure 6.3 : FTIR spectra of native polymers a) chitosan, b) hypromellose, c) citric acid and d) lectin employed in the fabrication of the mucoadhesive films and e) a representative design formulation……151

Figure 6.4: DSC thermograms of the native polymers a) chitosan, b) citric acid, c) hypromellose and d) lectin employed in the fabrication of the mucoadhesive layer and e) a representative design formulation……153

Figure 6.5: Percentage adhesion of mucoadhesive films to mucus for all 20 design formulations…….....154

Figure 6.6: Percentage swelling of mucoadhesive layer design formulations over 24 hours…….....155

Figure 6.7: Residual plots for the responses a) Young's Modulus b) % Mucoadhesion…….....160

Figure 6.8: Response surface and contour plots depicting the effects of citric acid (CA), chitosan (CHT) and hypromellose (HPM) on Young's Modulus……...162

Figure 6.9: Response surface and contour plots depicting the effects of citric acid (CA), chitosan (CHT) and hypromellose (HPM) on % mucoadhesion……163

Figure 6.10: Calibration curve of sodium valproate in PBS at λ_{215}……165

Figure 6.11: FTIR spectra of native polymers a) alginate, b) Eudragit RS 100 and d) calcium chloride employed in fabrication of drug loaded layer and c) a representative design formulation……167

Figure 6.12: DSC thermograms of the native polymers a) alginate, b) calcium chloride and c) Eudragit RS100 employed in the fabrication of drug loaded layers and d) a representative design formulations……..168

Figure 6.13: Percentage swelling of the drug loaded design formulations over 24 hours…….....170

Figure 6.14: *In vitro* fractional drug release profiles for all design formulations……173

Figure 6.15: Residual plot for the response MDT……..175

Figure 6.16: Response surface and contour plots depicting the effects of Eudragit® RS100 and $CaCl_2$ on the MDT…….....176

Figure 6.17: Desirability plots representing the levels of chitosan, hypromellose, citric acid, Eudragit® RS100 and calcium chloride required to synthesize the respective optimized bioadhesive multilayered patch layers, a) bioadhesive layer and drug loaded layers b) 2h, c) 10h and d) 18h……178

Figure 7.1: Illustration of a) the wetting theory and b) the diffusion theory of mucoadhesion…….....182

Figure 7.2: Illustration of NanoTensile® sample preparation and set-up……187

Figure 7.3: Pictorial illustration of the Franz diffusion cell set up……..191

Figure 7.4: Typical stress-strain NanoTensile® profile of a) mucus cleaving layer b) optimized mucoadhesive layer c) optimized drug loaded layer and d) backing layer……...195

Figure 7.5: Scanning electron micrographs depicting the surface morphology of a) optimized drug loaded layer and b) the optimized mucoadhesive layer c) optimized drug loaded layer after swelling and d) optimized mucoadhesive layer after swelling……197

Figure 7.6: FT-IR spectra of native polymers a) chitosan; b) hypromellose; c) citric acid; and d) lectin employed in fabrication of e) the optimized mucoadhesive layer……199

Figure 7.7: FT-IR spectra of native polymers a) Eudragit®RS100; b) alginate and c) calcium chloride employed in the fabrication of d) optimized 2hour; e) optimized 10hour and f) optimized 18hour drug loaded layer formulations……200

Figure 7.8: Schematic illustration of the proposed process resulting in the fluctuations observed in swelling and hence in mucoadhesion characteristics of the optimized formulations……201

Figure 7.9: Graphical illustration of the variations in degree of swelling and erosion of a) optimized mucoadhesive layer b) optimized drug loaded layers and c) the mucus cleaving layer……..202

Figure 7.10: DSC thermograms of A) the optimized mucoadhesive layer (e); and native polymers a) CHT; b) hypromellose; c)citric acid; d) lectin WGA and B) the optimized drug loaded layers 2,10 and 18 hours (d-f); and the native polymers a) Eudragit®RS100; b) alginate and c) calcium chloride……..204

Figure 7.11: Typical textural profile demonstrating the MDF (N) and WA (AUC_{FD}) (mJ)……205

Figure 7.12: A comparison of a) Maximum Detachment Force (MDF)(N) and b) Work of Adhesion (AUC_{FD}) (mJ) of intestinal patch layers in phosphate buffered saline (pH 6.8) (n=3; SD < 0.025)……206

Figure 7.13: Schematic illustration of perfusion study observations……207

Figure 7.14: *Ex vivo* permeation profile of sodium valproate across excised porcine intestinal mucosa (n=3; SD ≤0.02 in all cases)……208

Figure 7.15: Schematic illustrating ideal drug release profile requisite for the bioadhesive multilayered intestinal patch system……210

Figure 7.16: Drug release profile of the optimized bioadhesive multilayered intestinal patch device……211

Figure 8.1: Summary of system assembly……..213

Figure 8.2: Farm unit, housing, daily habituation (feeding and behavioral learning) of the Large White Pig……...215

Figure 8.3: Digital images demonstrating a) oxygen supply to animal after anesthesia; b) administration of injections and c) shaving of the surgical area (indicated by red circle)…….216

Figure 8.4: Digital images of surgical implantation of the jugular catheter……..217

Figure 8.5: Sequential digital images depicting the process of dosage administration…....218

Figure 8.6: Schematic illustrating the quantity of pigs required and the procedural steps involved during *in vivo* studies……...220

Figure 8.7: Calibration curves of a) sulpiride at 300nm and b) sodium valproate at 215nm……226

Figure 8.8: Typical chromatograms of a) sulpiride in plasma and b) sodium valproate in plasma; with their respective internal standards…….227

Figure 8.9: Plasma drug concentration profile depicting the release behavior over 24 hours of Control (Sulpiride alone), optimized s-IPN xerogel matrix oral device and, Conventional……228

Figure 8.10: Plasma drug concentration profile depicting the release behavior over 24 hours of the optimized bioadhesive multilayered intestinal patch oral device pulsatile component and conventional 200mg……....229

Figure 8.11: Drug release profiles of the *in vitro* and *in vivo* a) sulpiride and b) sodium valproate release from the Dual-layered oral system obtained via deconvolution analysis…….236

Figure 8.12: Regression plot showing the relationship between the fraction of (a) sulpiride and (b) sodium valproate absorbed *in vivo* and the fraction released *in vitro*…..……237

LIST OF TABLES

Table 2.1: The net uptake of bioactive by the brain depends on the difference between the influx and efflux processes (Schermann, 2002)……...26

Table 2.2: Brief overview of P-gp inhibitors/substrates and the corresponding IC50 values of inhibitors…….....31

Table 2.3: Summarized list of polymer & surfactant P-gp inhibitors and their mechanism of action……...35

Table 2.4: Summary of reviewed systems……51

Table 3.1: Summary of the common advantages and features of IPNs (Banerjee et al., 2010)……55

Table 3.2: Compositions of pilot study formulations…….59

Table 3.3: The identified variables and their corresponding upper and lower limits for input into the Central Composite Design…….70

Table 4.1: Box-Behnken design template for the statistically derived 15 s-IPN xerogel formulations and their respective chemical compositions……...75

Table 4.2: Test parameters used during Texture Analysis as per standard protocol for solid dosage forms…….....77

Table 4.3: Comprehensive table of data obtained from textural analysis describing the mechanical properties of the s-IPN xerogel matrix tablets……83

Table 4.4: ANOVA analysis for the measured responses……93

Table 4.5: Design formulations and their corresponding R^2 values fitted into the zero-order and higuchi model equations…….107

Table 4.6: Formulation constraints employed for response optimization……108

Table 5.1: Parameters utilized for the evacuation and heating phases in degassing of the optimized s-IPN……114

Table 5.2: Zero order kinetic data ……122

Table 5.3: Summary of porosity data obtained for the optimized xerogel……126

Table 6.1: The identified variables and their corresponding upper and lower limits for input into the Central Composite Design……...143

Table 6.2: Mucoadhesive layer Central Composite statistical design……..145

Table 6.3: Drug loaded layer Central Composite statistical design……..146

Table 6.4: Experimental average values obtained from NanoTensile (NT) and Textural analysis (TA) of mucoadhesive layer design formulations……156

Table 6.5: Effect of polymer concentration on viscosity for the mucoadhesive layers……157

Table 6.6: ANOVA analysis for the measured responses……..159

Table 6.7: Experimental average values obtained from NanoTensile (NT) and Textural analysis (TA) for the drug loaded design formulations……....169

Table 6.8: Effect of polymer concentration on viscosity……171

Table 6.9: ANOVA analysis for the measured responses……..175

Table 6.10: Formulation constraints employed for response optimization……..177

Table 7.1: Outline of optimized patch layer compositions……..185

Table 7.2: Optimized patch layers and their respective average weight and thickness……193

Table 7.3: Experimental values obtained from NanoTensile® and Textural Analysis of optimized patch layers……..194

Table 7.3: Sodium valproate flux and permeability coefficient as determined via *ex vivo* permeability analysis……...209

Table 8.1: Mobile phases and priming solvents used for determination of sulpiride and sodium valproate in plasma samples……....222

Table 8.2: Compartmental analysis of plasma sulpiride data after extravascular input without and with lag……..231

Table 8.3: Compartmental analysis of plasma sodium valproate data after extravascular input without and with lag……232

Table 8.4: Results of the non-compartmental analysis of plasma sulpiride and sodium valproate data after extravascular input…….....234

CHAPTER 1
INTRODUCTION AND MOTIVATION FOR STUDY

1.1. Background to the Study

Consideration of the absorption of oral dosage forms is a crucial forethought in drug delivery system development. Oral routes are favored for being less invasive, being a more physiologically natural route leading to ease of administration and improved patient compliance. Nonetheless, in comparison to entry of drug into direct systemic circulation via intravenous dosing, there exist additional factors affecting the availability of drugs after oral administration (Musther et al., 2014).

These factors include, degradation within the gastrointestinal tract (GIT), metabolism within the gut wall and liver, permeability through the gastrointestinal epithelium, as well as inadequate drug release from the delivery system (Musther et al., 2014). In addition, if the drug is not released in sufficient concentrations at the site of absorption, the drug will be unable to reach effective plasma concentrations to accomplish the anticipated therapeutic outcome (Davis, 2005). The oral bioavailability of many drugs is further compromised in drugs classified as Narrow Absorption Window (NAW) drugs, where the therapeutic window of several drugs is restricted by their short circulating half-life and absorption via a well-defined segment of the GIT (Streubel et al., 2006).

Once the dosage form passes the absorption window, the drug becomes neither bioavailable nor clinically effective (Bakde et al., 2012). Many drugs are poorly absorbed or sensitive to the gastric environment; thus conventional oral delivery systems need to undergo modifications or novel drug delivery systems need to be designed and developed so as to efficiently administer NAW drugs (Shen and Mitragotri, 2002; Bakde et al., 2012). Additionally, it has been shown that drug efflux pumps such as the P-glycoprotein (P-gp) (an ATPase, energy-dependent transmembrane drug efflux pump) plays a vital role in modifying the pharmacokinetics of many drugs and is thereby related to the observed poor bioavailability (Varma et al., 2003). It has gradually been attaining significance in research aimed at enhancing drug absorption due to its distribution at the site of drug absorption (Varma et al., 2003).

Pharmacokinetic limitations posed by narrow absorption windows and efflux pumps lead to frequent dosing of various drugs to attain the required therapeutic effect. This results in pill burdens and thus reduced patient compliance (Bakde et al., 2012). Patients with chronic illness

often present with concomitant conditions, hence requiring a greater number of drugs and thus problems with adherence to treatment becomes a greater challenge. One crucial contributing factor of adherence to treatment is a simplified dosing schedule and frequency of drug administration. Numerous comprehensive review studies have advocated that adherence is superior to drugs that have a once daily dosing schedule compared with those requiring multiple doses (Kruk and Schwalbe, 2006). Many studies have been conducted on the possibility of simple dosing regimens, where a delivery system has the ability to deliver multiple drugs for an extended period of time, thereby reducing the administration dose and frequency (Kruk and Schwalbe, 2006). The above detailed limitations to oral drug delivery are further outlined in Figure 1.1 with the corresponding strategies employed to overcome them.

An idyllic drug delivery system ought to achieve two requisites, 1) to deliver drug at a specified rate over the duration of treatment, and 2) allow for site-specific targeting. These requirements lead to the necessity for controlled release technologies that are able to improve therapeutic efficiency of a drug via precise spatial targeting, thereby decreasing the dose and number of oral administrations (Varma et al., 2004).

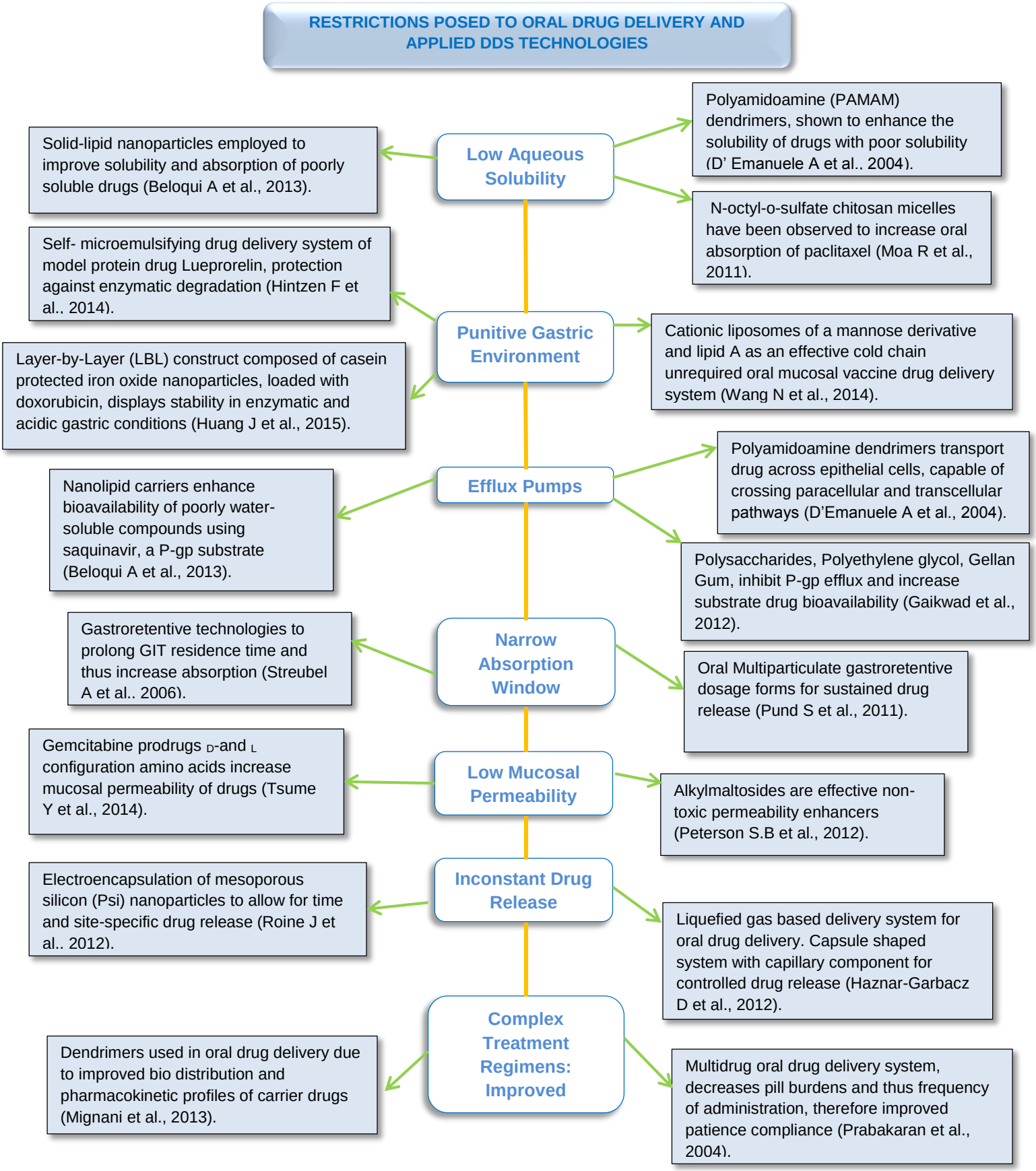


Figure 1.1: Illustration of various restrictions to oral drug delivery and studies conducted to overcome them.

Amongst others the most common technologies developed to achieve controlled drug release include bilayered tablets, gastroretentive systems, and polymer matrices. The introduction of matrix tablets in the context of controlled drug release systems has provided a revolution for novel drug delivery technology of pharmaceutical salience. The rate of drug release from a matrix system is governed by the type and amount of polymer utilized in the formulation process (Modi et al., 2011; Korbely et al., 2012).

Schizophrenia is a neurodegenerative disorder associated with reduced mental abilities and the decreased level of social functioning due to the occurrence of symptoms such as hallucinations, delusions and emotional affect. Of significant importance in the treatment of schizophrenia is non-adherence to therapy, which leads to relapse and hospitalization thereby causing greater costs being incurred in treatment programs and poor prognosis. Researchers have thus suggested that the use of long-acting controlled drug delivery systems may significantly improve compliance (Olivares et al., 2009), hence the need for zero-order sustained release delivery systems in the treatment of schizophrenia becomes apparent.

However, schizophrenia is known to commonly present as schizoaffective disorder, which is defined as an acute concomitant mood syndrome presenting with a fundamental schizophrenic symptom (Levinson et al., 1999). Treatment of schizoaffective disorder thus requires combination therapy so as to combat symptoms of schizophrenia and the mood disorder, thus the concurrent use of antipsychotics and mood stabilizing agents. Mood stabilizing agents employed easily undergo degradation by metabolic enzymes and thereby develop resistance thus requiring three times a day dosing to prevent treatment resistance and non-adherence due to the higher risk of adverse effects.

This results in complex treatment regimens which patients find difficult to adhere to, thus the use of time-programmed (pulsatile) drug delivery systems is useful as it reduces the number of administrations required.

Pulsatile drug delivery systems allow for the release of drug immediately after a defined lag time according to circadian rhythms or dosing requirements. This pattern of drug delivery becomes useful in the case of chronic therapy as drug resistance and side effects are often seen, the likelihood of such effects are less with pulsatile delivery systems as the desired concentration of drug is released only at predetermined time intervals (Mandal et al., 2010; Rasve et al., 2011).

Overall, pulsatile release systems have been designed due to the subsequent reasons (Nagar et al., 2010):

i. Chronopharmacotherapy of disease states, in which circadian rhythms play a vital role in disease pathophysiology.

ii. To circumvent degradation of drugs within the upper GIT.

iii. Programmed drug delivery, due to the fact that continuous drug release leads to instabilities in normal feedback mechanisms within the body and the development of drug resistance.

iv. For drugs that develop biological tolerance, and are targeted to specified sites in the GIT.

Various formulation techniques exist for the development of pulsatile drug delivery system; they are generally classified as single-unit and multiple-unit systems. However, they function on the same rudimentary principles of erosion and dissolution; swelling and alterations in membrane permeability (Roy and Shahiwala, 2009).

One possible relatively unexplored approach to pulsatile drug delivery is the use of bioadhesive intestinal multilayered patch systems. Patches comprise of layers of thin, flexible polymeric films; when the patch attaches to the intestinal wall, drug flows through the epithelial lining into circulation at a rate controlled by the film that is preprogrammed to maintain drug at an effective level (drug loaded layer) (Tao and Desai, 2005).

Membranous drug delivery systems such as intestinal patches have the advantage of being layered with the incorporation of various excipients into the different layers, where the layers of the system can perform differing functions, including drug encapsulation, protection of the system, and mucoadhesion, therefore allowing for gastric retention (Shen and Mitragotri, 2002; Tao and Desai, 2005).

So as to overcome the challenges of oral drug delivery, the drug delivery system proposed in the present thesis is designed to deliver two bioactives targeted to the intestine, for a prolonged period of time via idiosyncratic or individual drug release patterns i.e. sustained (zero-order) and pulsatile, within a single dosage form; in interest of overcoming the drawbacks observed in the treatment and clinical outcomes of patients with schizoaffective disorder. The proposed oral dual layered s-Interpenetrating Polymer Network (s-IPN) xerogel-bioadhesive intestinal patch oral drug delivery system (ODLS), consists of a dual layered tablet of which layer one comprises the s-IPN xerogel matrix allowing for site-specific sustained release of sulpiride an antipsychotic and layer two comprises the embedded bioadhesive multilayered intestinal patches for pulsatile release of valproic acid, with each patch consisting of a mucus cleaving layer, bioadhesive layer, drug loaded layer and a backing layer.

1.2. Rational and Motivation for the Study

Schizophrenia is one of the major psychiatric disorders that have been shown to greatly impair the quality of life of patients and their caregivers, creating an enormous financial burden on society (Peuskens et al., 1999). As noted previously non adherence to therapy is a common cause for relapse leading to greater costs incurred in treatment programs and poor prognosis. Research has indicated the use of sustained drug delivery systems may considerably advance compliance (Olivares et al., 2009).

Sulpiride is effective in the treatment of acute and chronic schizophrenia, poor lactation, depression, anxiety, tardive dyskinesia and tension (Soares et al., 2011), with a low bioavailability of 30 % (Chitneni et al., 2011). Psychiatric therapy with sulpiride involves high dosages of up to 2400mg/day thus requiring multiple administrations in a day (Barnes et al, 2006; Rossiter and Blockman, 2010). Therefore the issue of diminished patient compliance is evident. In addition, it is has been ascertained that a majority of schizophrenic patients present with concomitant mood disorders which is collectively known as schizoaffective disorder; defined in *Chapter 1, Section 1.1.* Treatment of schizoaffective disorder entails combination therapy so as to combat symptoms of schizophrenia and the co-occurring mood disorder, thus concurrent use of antipsychotics and mood stabilizing agents such as valproic acid is a necessity. This places a huge pill burden upon the patient or caregiver and thus leads to reduced patient compliance and hence poor clinical outcomes.

Thus a dual site-specific delivery system would allow for the delivery of two therapeutic agents in a single dosage form, as a once daily dose, hence improving the bioavailability and patient compliance; with no risk of drug interactions occurring despite dual delivery within a single dosage form. The proposed ODLS can successfully achieve such individualistic drug delivery, whereby the system releases sulpiride (antipsychotic) in a sustained manner from the s-IPN xerogel and valproic acid (mood stabilizing agent) in a pulsatile release pattern via intestinal patches at different absorption sites in the intestine via bioadhesion of the respective carrier systems. Furthermore, the ODLS has further therapeutic applications, as illustrated in Figure 1.2.

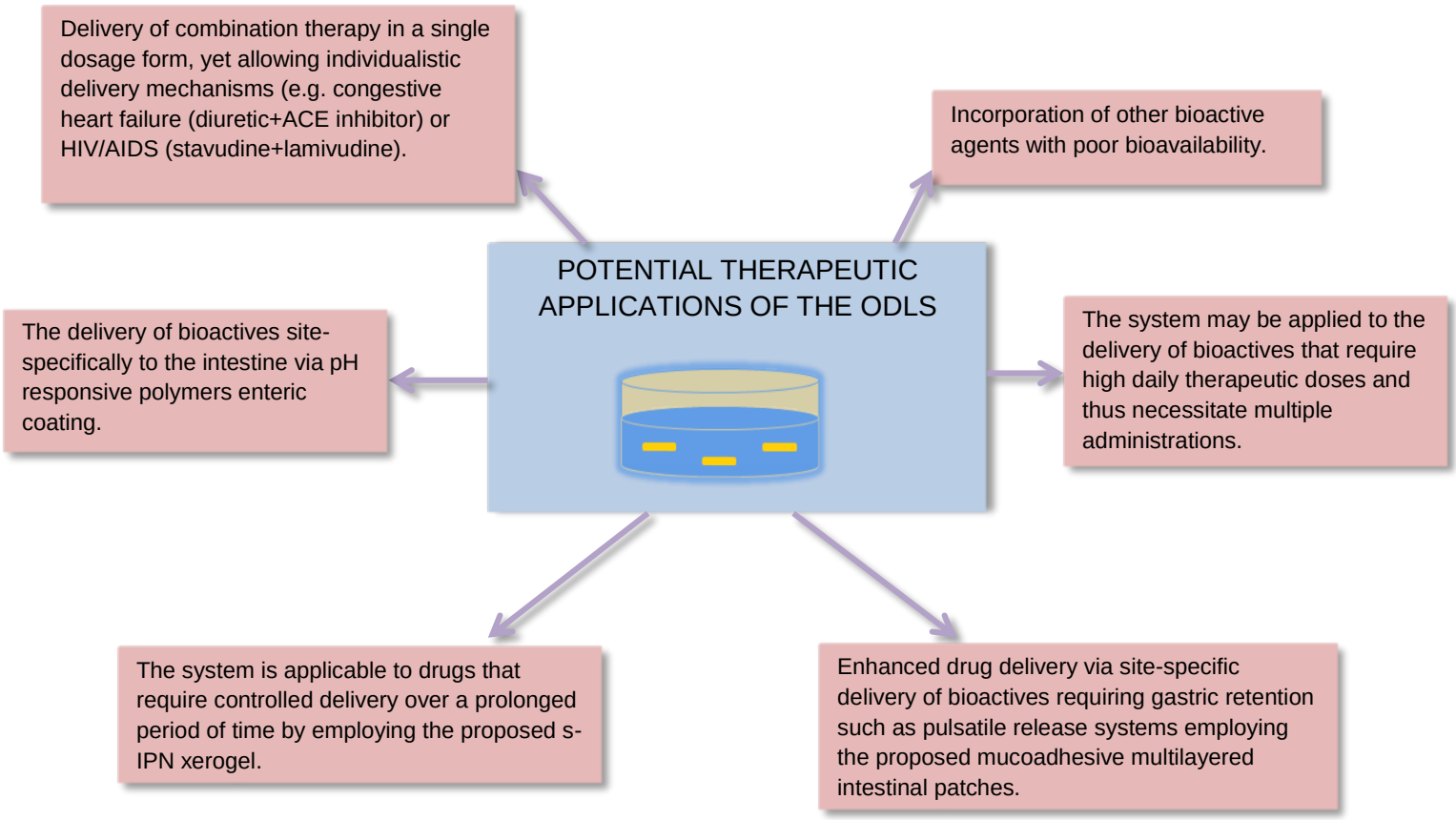


Figure 1.2: Potential applications of the ODLS.

1.3. Mechanism by which Dual Drug Delivery will be achieved with the ODLS

The diagrammatic representation of the ODLS in Figure 1.3a represents the dual layered oral drug delivery system, with layer 1 comprising the s-IPN xerogel for zero-order sustained release, and layer 2 consisting of embedded bioadhesive multilayered intestinal patch for pulsatile release. Figure 1.3b illustrates the layers of the intestinal patch with i) being the N-acetyl cysteine mucus cleaving layer ii) the Lectin conjugated bioadhesive layer iii) Crosslinked Eudragit RS 100: Alginate drug loaded layer and iv) Ethyl cellulose impermeable backing layer. Once the dosage form is ingested, the enteric coated tablet will pass into the intestine protected, in the vicinity of the small intestine the enteric coating will dissolve away and the dual layered tablet will divide into the s-IPN xerogel and intestinal patch components respectively; both components attach to the intestinal wall via a process of mucoadhesion. Layer one, which is the s-IPN xerogel will release drug in a controlled manner over 24 hours, while layer 2 comprising of the three multilayered bioadhesive patches will be released from the tablet via erosion. The released patches will adhere to the intestinal wall via mucus cleaving initiated by the N-acetyl cysteine layer and later by the lectin

conjugated bioadhesive layer; drug release will be modulated by the degree of crosslinking within the respective drug loaded layers, to allow for pulsatile release. Leakage and loss of drug into the intestinal contents will be prevented by the impermeable backing layer.

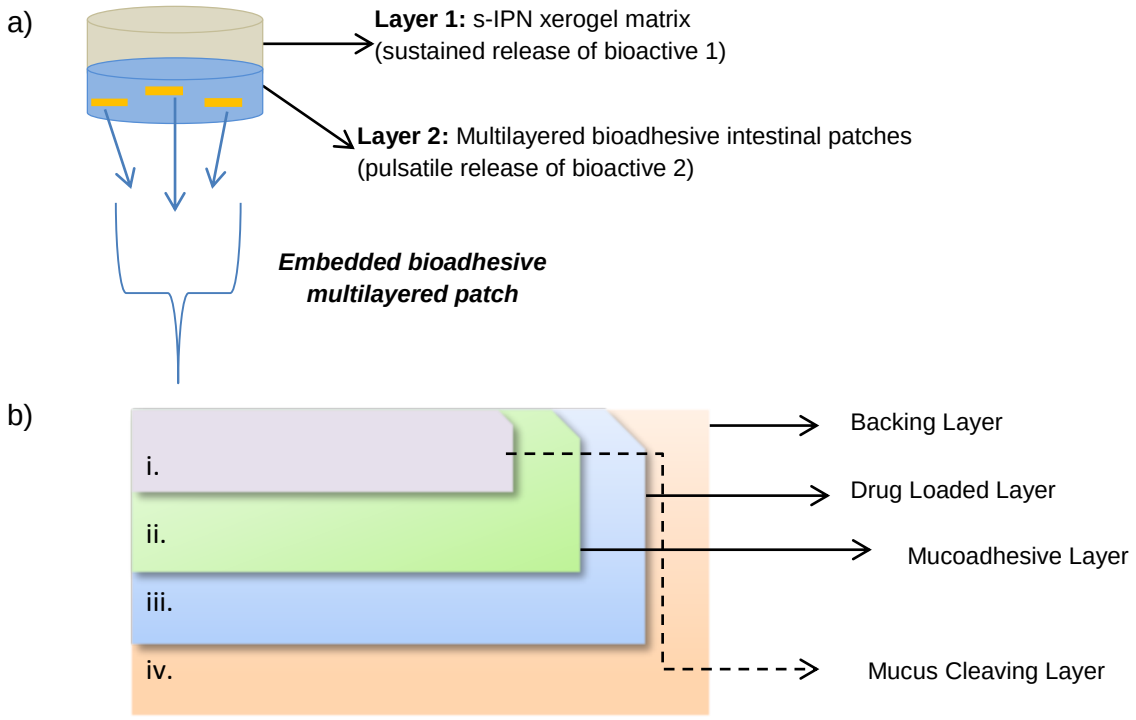
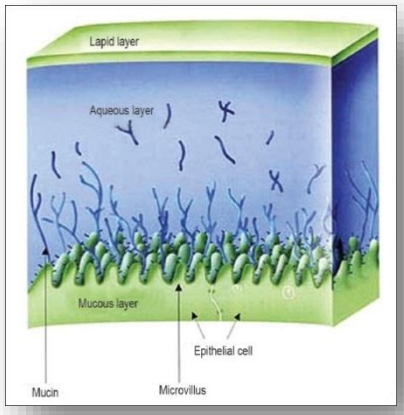


Figure 1.3: Componential configuration of the ODLS prototype, where a) represents the dual layered oral drug delivery system and b) represents the multilayered bioadhesive intestinal patch with its respective polymeric film layers.

In an effort to improve bioavailability, patient compliance, and evade drug resistance, the proposed ODLS employed technology outlined in Figure 1.4 to develop a single dosage form for segregated idiosyncratic drug delivery.







Mucoadhesion-Mucus Cleavage

- Site-specific drug delivery.
- Isolated and idiosyncratic drug delivery-no drug interactions.
- Gastroretentive thus retains DDS at site of absorption for prolonged time period.

Crosslinking- s-IPN

- Drug entrapped in polymer networks-prolonged drug delivery time, one tablet, once daily-improved compliance.
- Averts variable and excessive drug release.

Protective Coating

- Physical protection of DDS from the harsh environment of the stomach.
- Unidirectional release via impermeable backing layer-thus improved absorption and bioavailability.

Figure 1.4: Technology utilized to enhance bioavailability in the development of the ODLS.

1.4. Novelty of the Study

The novelty of this study lies in the mode of idiosyncratic/individualistic drug delivery, which was achieved via the use of two novel drug delivery strategies. The dual component system will be able to avoid high pill burdens, reduced patient compliance, poor bioavailability and treatment resistance by administering two bioactive agents in a single dosage form; yet, allowing individual release kinetics suited to the treatment regimens of each. Furthermore, the formulation process involved the novel crosslinking of poly (ethylene) oxide with gellan Gum employing epichlorohydrin as the crosslinking agent to form a semi-interpenetrating polymer network xerogel, which in turn allowed for zero-order sustained drug release kinetics. The incorporation of lecithin as an excipient within the xerogel further added to the novelty as the model drug, sulpiride is a known substrate of the P-glycoprotein (P-gp) efflux transporter and lecithin is a known inhibitor of the P-gp transporter along with the other polymers utilized in the formulation thus improving bioavailability even further. Novelty of the system was extended with the design and fabrication of the multilayered bioadhesive intestinal patches, with the innovation laying in the use of N-acetyl cysteine within the mucus cleaving layer and lectins being conjugated to the mucoadhesive layer to enhance bioadhesion and thus retention time of the intestinal patches allowing for pulsatile release over 12 hours; which is highly beneficial in schizoaffective disorder, with drug resistance arising with the use of valproic acid. The development of the dual layered tablet encompassing both systems greatly reduces the number of administrations required to a single dose daily and thus increases compliance, reduces the risk of resistance and improves clinical outcomes.

1.5. Aim and Objectives of the Study

Aim: Pharmaceutical fabrication and prototyping of an adaptable multifunctional double layered semi-IPN xerogel-bioadhesive intestinal patch matrix tablet (ODLS) for the treatment of schizophrenia and associated mood disorder to improve versatility and multifunctionality of currently available treatment regimens. The proposed ODLS ensures idiosyncratic release of the incorporated drugs via the mechanism illustrated in Figure 1.5.

The aforementioned ODLS will be formulated to meet the following design criteria:

1. For purposes of sustained release the matrix tablet component should allow for sufficient drug entrapment within the xerogel pores so as to allow for prolonged delivery rates.

2. The crosslinked xerogel in combination with lecithin should improve the bioavailability of the bioactive.

3. The candidate drug must remain protected from enzymatic degradation within the gastro-intestinal tract until it is in contact with the site of delivery which is the small intestine.

4. For purposes of pulsatile release the intestinal patch component should be sufficiently bioadhesive to allow for prolonged residence time in the small intestine.

5. To allow for adequate drug absorption, drug leakage from the intestinal patch component should be prevented.

6. To attain pulsatile release of the drug from the intestinal patch component, drug should be efficiently trapped in a drug loaded layer, thereby controlling drug release profiles.

Objectives:

For pragmatic fulfillment of the aim and design strategy, the following objectives are apparent:

i) To design and formulate a novel physically stable s-IPN xerogel matrix through the process of crosslinking which results in the sustained zero-order release of entrapped drug.

ii) To characterize the s-IPN xerogel matrix component of the ODLS, the following tests will be conducted: Fourier Transform Infrared (FTIR) Spectroscopy; Scanning Electron Microscopy (SEM) imaging; Differential Scanning Calorimetry (DSC).

iii) To design and fabricate the novel bioadhesive multilayered intestinal patch component of the ODLS via a process of crosslinking and solvent casting, for pulsatile release of entrapped drug.

iv) To characterize the bioadhesive multilayered intestinal patch component, the following tests were conducted: Fourier Transform Infrared (FTIR) Spectroscopy; Scanning Electron Microscopy (SEM) imaging; Differential Scanning Calorimetry (DSC), and Rheology.

v) Swelling and erosion studies were conducted on the s-IPN xerogel and the bioadhesive patches to evaluate the rate of polymer swelling and erosion and its possible effect on drug release.

vi) Clinical potential of the prototype ODLS components, based on their ability to meet the design criteria *in vitro*, will be ascertained in the Large White Pig model in terms of *in vivo* release kinetics and biocompatibility.

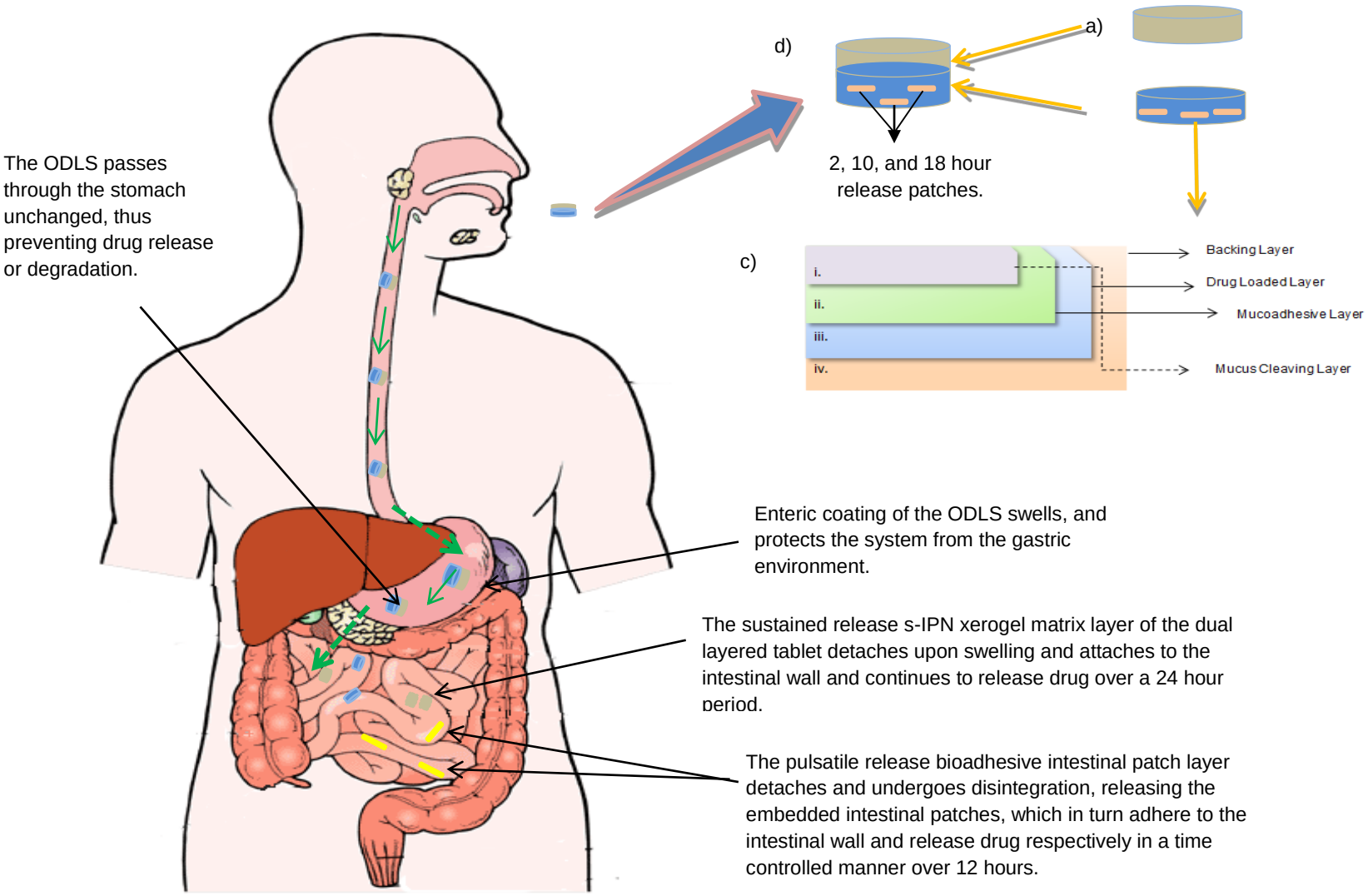


Figure 1.5: Schematic illustration depicting mechanism of drug release from the ODLS; a) xerogel matrix; b) adhesive intestinal patch layer; c) illustration of individual patch archetype; and d) dual layered oral dosage form (ODLS).

1.6. Synopsis of the Thesis

Chapter One of this thesis provides an introduction and background to this study and highlights the rationale, aim, objectives, novelty and potential beneficial applications of this study.

Chapter Two of this thesis provides a comprehensive literature review, focusing on the presence and function of P-glycoprotein efflux transporters in the intestine and Blood Brain Barrier. It further describes the role of P-gp in limiting the oral bioavailability of drugs that are substrates, and approaches investigated in the management of other disease states in terms of polymers and drug delivery systems which are capable of P-gp inhibition or by-pass; and their possible application in the treatment of schizophrenia.

Chapter Three of this thesis describes the pre-formulation and development of the s-IPN xerogel component of the ODLS; and the preliminary formulation methods investigated. In addition, formulation parameters were established to allow for Construction of a Central Composite Design.

Chapter Four of this thesis describes the preparation of variants of the s-IPN xerogel as constructed according to a randomized, Face-centered Central Composite Design. In addition, physiomechanical and physiochemical characteristics were analyzed in order to determine the *in vitro* performance in simulated intestinal conditions.

Chapter Five of this thesis describes the preparation of the optimized s-IPN xerogel component of the ODLS via Response Surface Methodology. The applicability of the design was analyzed. Furthermore, comprehensive *in vitro* physiomechanical and physiochemical evaluation was analyzed.

Chapter Six of this thesis describes the pre-formulation and development of the bioadhesive multilayered intestinal patch components; namely the mucoadhesive and drug loaded layers of the ODLS. It describes the film formation techniques, and provides an overview of the parameters affecting film formation as well as an introduction to mucoadhesion, including the various mechanism of mucoadhesion. It further details the fabrication of variants of the respective bioadhesive multilayered intestinal patch layers as constructed according to a randomized, Face-centered Central Composite Design,

Chapter Seven of this thesis describes optimization using Response Surface Methodology. Furthermore, *in vitro* physiomechanical and physiochemical characterization of the system was analyzed to determine the *in vitro* performance.

Chapter Eight of this thesis describes the preparation of the remaining layers of the bioadhesive multilayered intestinal patch component of the ODLS. It includes a comparative analysis of the ODLS components with a marketed 'gold standard' formulation in terms of both *in vitro* and *in vivo* drug release behavior. Furthermore, it contains an explanation of the *in vivo* animal studies undertaken in the large pig model. Assessment of the ODLS's biocompatibility and drug release behavior were highlights in this chapter. In addition, dosage administration and blood sample collection procedures are described.

Chapter Nine of this thesis presents the conclusions and recommendations for future work.

1.7. Concluding Remarks

This chapter aimed to highlight the limitations and challenges associated with oral drug delivery, particularly the effects of poor oral drug bioavailability and the most common approaches to overcome these limitations. In addition, the rationale, aim, objectives, and novelty of the current study was discussed. The focus of the chapter was a description of the ODLS, with specific emphasis on the architectural assembly and functioning of the various components. The need and advantages of such systems in the treatment of schizoaffective disorder due its respective clinical limitations were also addressed.

CHAPTER 2
Bypassing P-Glycoprotein Drug Efflux Mechanisms: Possible Applications in Pharmacoresistant Schizophrenia Therapy

2.1. Introduction

The effectiveness of drug treatments for numerous disease states such as cancer, infectious diseases, and central nervous system (CNS) disorders (epilepsy, depression, and schizophrenia) is limited by poor therapeutic outcomes or drug resistance. The outcomes of drug treatment can be viewed as an interchange of several gene products that have an effect on pharmacokinetics and pharmacodynamics. These gene products mainly include metabolizing enzymes and drug transporters and alterations within any of these gene products may lead to a reduction in clinical outcomes (Löscher and Potschka, 2005). In particular, the clinical treatment and management of CNS disorders necessitate that a sufficient amount of drug must enter the brain. The use of oral drug delivery systems is beneficial in the treatment of neurodegenerative disorders as compliance to therapy becomes challenging (Nassar et al., 2009). However, an imperative factor determining the entry of drug molecules into the brain via oral administration is its absorption through the intestinal epithelium and the permeability of the blood-brain barrier (BBB). Passive diffusion across the intestinal epithelium is dependent on many physiochemical characteristics of drugs such as lipophilicity, molecular weight, and hydrophobic bonding (Takano et al., 2006). The same principle applies to passive diffusion across the BBB, although passive diffusion across the BBB is limited to small lipophilic molecules. Active efflux of the drug into the intestine and from BBB endothelium back into the blood are the most important mechanisms underlying reduced brain uptake of active drug molecules post oral dosing (Elsinga et al., 2004).

The development of drug delivery systems involved in the treatment of neurodegenerative disorders requires a vital consideration of achievable brain concentrations. Factors that impact the brain uptake and concentrations of drugs include (i) the extent of intestinal absorption after oral administration, (ii) the rate and extent of transport across the BBB into the brain, (iii) metabolic stability of the drug, and (iv) the active transport out of the intestine and brain endothelium via efflux pump transporters. There are three classes of transporters that have been associated with the efflux of drugs-monocarboxylic acid transporters, organic ion transporters, and multidrug resistance transporters. This remarkable system of transporters provides a viable mechanism through which the permeation of CNS targeted drugs into the brain is effectually decreased. The

action of these efflux transporters at the level of the intestine and BBB may be demonstrated clinically as the reduced effectiveness of drug therapy targeted at CNS disorders (Taylor, 2002).

In addition, various multispecific transport proteins have also been identified within the intestine and BBB. Some of these belong to the ATP-binding cassette (ABC) superfamily of transporters with P-glycoprotein (P-gp), multidrug resistance associated protein (MRP), and breast cancer resistance protein (BCRP) as representative examples (Elsinga et al., 2004; van Wetering et al., 2009). P-gp is a membrane transporter of the ABC superfamily located within both the intestinal epithelium and the BBB thus playing a dynamic role in the bioavailability of orally administered drugs employed in the treatment of neurodegenerative disorders (Demeule et al., 2002]. We propose that drug molecules intended for the treatment of CNS disorders must be capable of bypassing the P-gp efflux pump at the intestinal and BBB levels so as to attain effective brain concentrations.

Regardless of the vast advances in brain research outputs, neurodegenerative and psychiatric disorders remain the world's leading causes of disability, morbidity, and mortality (Lalatsa et al., 2011). Dysfunctions in the P-gp efflux transporter have already been suggested to play a role in the development of neurodegenerative disorders, such as Parkinson's and Alzheimer's diseases. Genetic variations in theMDR1 gene associated with reduced P-gp function at the BBB have been related to a higher risk of Parkinson's disease. The reduced function of the P-gp efflux pump has been noted in most neurodegenerative disorders. It has been hypothesized that the decreased P-gp function in the BBB may increase the risk and hence the incidence of neurological diseases (Bartels et al., 2009). In schizophrenia genetic variations of the ABCB1 (ATP-binding cassette subfamily B) gene also known as the MDR1 (multidrug resistance) gene have been described as the predisposing factors for schizophrenia and other neurodegenerative diseases. They have also been employed as determinants of treatment response to antipsychotics (Lin et al., 2006). As in other neurodegenerative diseases the BBB may be compromised by way of the inflammatory and neurodegenerative processes (Stolp and Dziegielewska, 2009); hence the functionality of P-gp is influenced by the inflammatory responses (Roberts and Gorlski, 2008). As discussed previously, there exists a reduction of P-gp function in progression of neurodegenerative diseases. Conversely, there is evidence of increased P-gp function in patients presenting with schizophrenia (Bartels et al., 2008).

Schizophrenia is a neurodegenerative disorder that is known to affect approximately 1% of the world's population (van Os et al., 2010), with a further 25% of patients approximated to be afflicted

by the disease experiencing non-remitting sickness (Pharoah et al., 2006). The disorder is characterized by disturbances of perception, thought, and volition, with significant impairment in social and occupational functioning. Studies have shown that roughly 10% of schizophrenic patients commit suicide. A recent study showed that more than 70% of patients diagnosed with chronic schizophrenia discontinued their antipsychotic drug therapy, due to poor effectiveness or tolerability (Nnadi and Malhotra, 2007; American psychiatric association, 1994; Kulhara et al., 2001; Khin et al., 2012; Kingdon et al., 2010; Falkai and Möller, 2012; Insel, 2010).

Schizophrenia is clinically characterized by the incidence of symptoms such as hallucinations and delusions which are collectively termed “positive” symptoms whereas symptoms pertaining to expression of emotional dullness and social withdrawal are recognized as “negative” symptoms (Pharoah et al., 2006). Figure 2.1(a) diagrammatically depicts the symptom cascade. Schizophrenia is widely characterized via a successive course that involves three distinct phases, namely, phase 1 (premorbid) defined by cognitive, motor, and societal dysfunction, phase 2 (prodromal) which is characterized by weakened positive symptoms and accompanying deteriorating functionality, and phase 3 (plateau) in which the positive psychosis defining symptoms are less conspicuous and the negative symptoms including cognitive deficits are generally predominant (Tandon et al., 2009). Figure 2.1(b) illustrates the clinical stages of schizophrenia progression.

It has been discovered that “pharmacoresistant schizophrenia” is a noteworthy obstacle to the successful management of the disease within the clinical setting. The prevalence of pharmacoresistant schizophrenia is understood to be approximately 12.9 to 48% of all schizophrenic patients and persists regardless of the use of drug combination treatment regimens with possible therapeutic efficacy. Majority of patients presenting with treatment resistant schizophrenia are on atypical antipsychotic medication. Recent *in vitro* studies have shown that drugs such as amisulpride, risperidone, quetiapine, and clozapine have a varying degree of affinity for the P-gp efflux transporter (Bebawy and Chetty, 2008; Boulton et al., 2002; El Ela et al., 2004). An additional study was conducted to determine the effect that cyclosporine A, a P-gp inhibitor, has on the brain uptake of amisulpride (a recognized P-gp substrate). *In vitro* and *in vivo* results displayed that amisulpride when co-administered with 50mg/kg of cyclosporine A showed an increase and prolonged antipsychotic effect. The area under the curve (AUC) in serum and the brain was increased in cyclosporine co-treated rats. These data points indicated a pharmacokinetic interaction between cyclosporine A and amisulpride which is most likely due to P-gp inhibition (Schmitt et al., 2006). Thus, the expression and function of the P-gp efflux

transporter have been recently implicated in the occurrence of pharmacoresistant schizophrenia. Antipsychotic drugs have also been shown to stimulate the catalytic activity of P-gp providing additional evidence of the participation of P-gp-mediated drug extrusion processes in restraining CNS penetration of these drugs. It has been suggested that some of the principles observed with the combination treatment of P-gp-mediated drug resistance in cancer may be applied to elucidate the involvement of P-gp in drug-resistant schizophrenia. There exists a greatly emergent body of evidence supporting the role of P-gp on the efflux of antipsychotic agents from the BBB; however limited consideration has been focused on the modulation of P-gp function by polymeric materials, excipients, and drug delivery systems used in other P-gp modulated treatment-resistant disease states (Bebawy and Chetty, 2008).

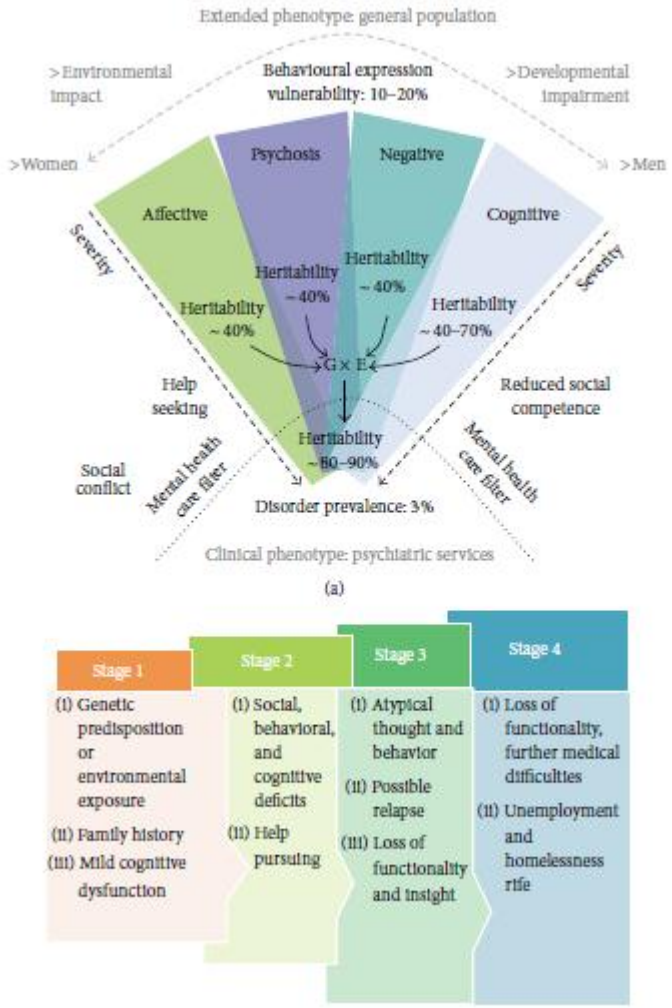


Figure 2.1: (a) Description of the aetiological complexity of schizophrenia (van Os et al., 2010) (b) Stages of schizophrenia progression (Tandon et al., 2009).

2.2. Structure and Function of the Intestine and P-gp Intestinal Expression in Drug Delivery

The absorption of drugs via the oral route is always under examination due to the fact that good bioavailability indicates that the drug is able to reach systemic circulation. Oral drug absorption is affected by both drug properties and the physiology of the gastrointestinal tract (GIT) (Pang, 2003). Oral bioavailability is a collective outcome of fraction absorbed, fraction escaping gut-wall elimination, and the fraction avoiding hepatic elimination. The factors that affect the bioavailability are divided into physiological, physiochemical, and biopharmaceutical factors (El-kattan and Varma, 2012). The sequence of actions determining the systemic availability of drug molecules subsequent to their oral administration is well acknowledged. However, for particular drugs, the process leading to drug absorption and bioavailability is complex. Certain mechanisms may

involve poor drug solubility, poor permeability, degradation (enzymatic/ non-enzymatic), and first pass hepatic metabolism (Takano et al., 2006). Following oral dosing, drug molecules cross the luminal membrane via a diversity of mechanisms that comprise of passive diffusion or active transport. Passive diffusion is divided into two pathways, the paracellular and transcellular pathway, in which the paracellular pathway drug molecules are absorbed via diffusion and convection volume flow through the water filled intercellular space (El-kattan and Varma, 2012).

The active transport pathway is mediated by transporters and is divided into influx and efflux. The applicability of the various routes is determined by the compounds physiochemical properties and their relative affinity for various transport proteins. Enterocytes express several transporters belonging to the Adenosine triphosphate (ATP) binding cassette (ABC) superfamily and solute carrier (SC) super families, on the apical and basolateral surface of membranes with the function of influx and efflux of endogenous substances. A wide diversity of transporters are expressed in enterocytes; however, only a select few have been implicated in the intestinal absorption of drugs. ABC transporters utilize ATP to power the transport and are thus called primary active transporters. Solute carrier (SLC) transporters employ ion gradients (H+, Na+, and Ca++) across the membrane by active carriers. ABC transporters that are expressed in the intestine include P-glycoprotein (P-gp), breast cancer resistant protein (BCRP), and multidrug resistance protein (MRP), which are localized on the brush border membrane of enterocytes. Efflux transporters mechanistically limit the enterocytic levels of their respective substrates by reducing uptake and facilitating efflux, whereas SLC transporters which include peptide transporter (PepTI) and organic anion polypeptide transporter (OATP1A2) amongst others are secondary active transporters that employ energy coupling mechanisms (El-kattan and Varma, 2012; Schlessinger et al., 2013).

During oral absorption, in addition to the physical processes mentioned above (solubility, permeability, etc.), P-gp mediated efflux across the apical membrane has an effect on the rate and concentration of drug diffusing across the basolateral membrane and thus entering general circulation from the intestine. It has been estimated that 50–60% of new and 40–50% of existing drugs molecules are lipophilic in nature and more than 25% of these agents are known P-gp substrates (Nassar et al., 2009). Pumps in the intestinal epithelium transport substrates from the intestinal lumen to the general blood circulation (Wagner et al. P-gp identifies with a diversity of structurally and pharmacologically dis, 2001) similar hydrophobic substances. The P-gp efflux pump transporter restricts the influx into and facilitates efflux from enterocytes of its substrates. Therefore, the P-gp efflux transporter is recognized as a determining factor of oral bioavailability and intestinal efflux of drugs (Takano et al., 2006). In the human intestine, P-gp is highly expressed

on the apical surface of superficial columnar epithelial cells of the colon and ileum (Figure 2.2) while expression decreases proximally into the jejunum, duodenum, and stomach (Takano et al., 2006).

Since the oral route of drug administration is the most preferred as previously mentioned, it is vital to overcome the absorption barrier posed by the P-gp efflux transporter (Nassar et al., 2009). Additionally, as discussed earlier P-gp plays a role in restricting cellular uptake of drugs from the general blood circulation into the brain due to its presence within the BBB as well. Research outputs have shown that intestinal P-gp can be inhibited by various compounds resulting to an increase in oral absorption of P-gp substrate drugs (Takano et al., 2006).

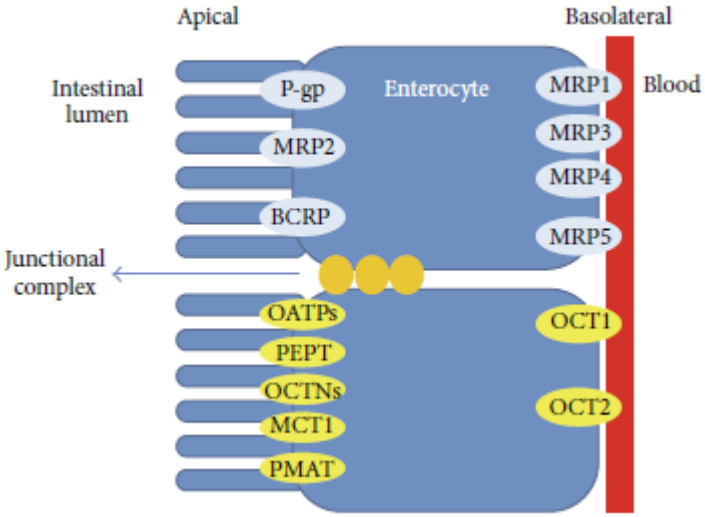


Figure 2.2: Drug Efflux by P-glycoprotein in the intestine (Estudante et al., 2013).

Physiological factors that influence oral drug absorption are absorption rate of a drug, which is a function of drug absorption via the GIT and gastro intestinal transit time, which influences the systemic exposure of rapidly, dissolved, and highly absorbed drugs. Intestinal transit time impacts the absorption of drugs with limited mucosal permeability and carrier-mediated uptake and drugs that are subjected to intestinal degradation. In addition, the degree of ionization plays a key role in determining drug dissolution rate and the passive permeability across the GIT. The pH at the absorption site is also a vital factor in allowing or inhibiting the dissolution and absorption of many ionizable drugs (El-kattan and Varma, 2012).

In addition, there are biopharmaceutical factors that influence oral drug absorption; amongst these is the salt form of a drug molecule which changes the coulombic attraction between the drug molecule and its respective counter ion thus altering the potential energy when in a solid state. This is usually associated with an alteration of the pH of the diffusion layer at the surface of the dissolving solid, thereby greatly increasing the solubility of the drug molecule. The amorphous form alternatively tends to improve the dissolution rate and solubility significantly compared to its crystalline form which increases the rate and degree of oral absorption (El-kattan and Varma, 2012). Apart from these mechanisms, the small intestine has the ability to metabolize drugs via a diversity of pathways involving phase I and phase II reactions, which in turn may cause a restriction in oral bioavailability. CYP3A4 is the most abundant cytochrome P450 enzyme within the intestinal enterocytes that is implicated in the metabolic elimination of many drugs (El-kattan and Varma, 2012).

2.3. Structure and Function of the BBB and P-gp Expression in Drug Delivery

The BBB is a specialized system of capillary endothelial cells as shown in Figure 2.3, which assists in protecting the brain from harmful substances within the blood stream, while supplying the brain with nutrients that are necessary for proper function. The BBB has many functions, including maintenance of the internal environment of the brain, protection of the brain from fluctuations in ionic composition, and drainage of cerebrospinal fluid and interstitial fluid. Due to its protective function the BBB restricts transport of substances into the brain via both the physical (tight junctions) and the metabolic (enzyme) barriers (Kaur et al., 2008; Hawkins and Davis, 2005).

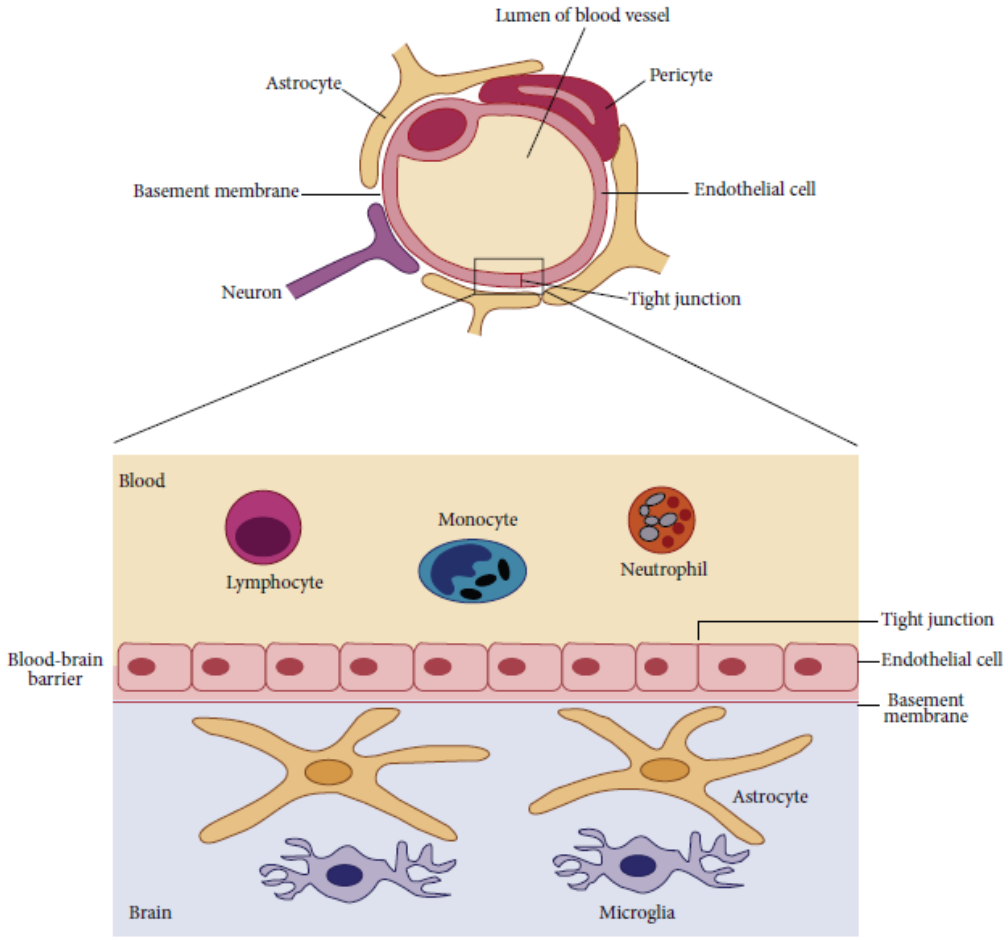


Figure 2.3: Schematic representation of the cross section of the BBB cerebral capillary (Blasi et al., 2007).

The BBB is composed of a monolayer of brain capillary endothelial cells. The limitation of drug uptake by the BBB arises via the presence of tight junctions between adjacent capillary endothelial cells and the relative lack of fenestrae as well as pinocytotic vesicles within the endothelial cell monolayer. In turn, brain capillary endothelial cells are surrounded by an extracellular matrix, pericytes, and astrocyte foot processes. Once a drug molecule enters the brain, either via transport across the BBB after systemic administration or by direct administration into the CNS, the drug may return to the blood via three ways: (1) It may pass through the capillary endothelial cells of the brain, (2) cross the epithelial cells of the choroid plexus, (3) or return to systemic circulation by bulk flow of cerebrospinal fluid that effectively results in reabsorption at the arachnoid villi (Taylor, 2002). The BBB is known to express a high degree of active efflux transporter proteins, including, as mentioned previously, P-gp, MRP-1, and BCRP. Lipophilic

molecules of approximately 500–600 Daltons may diffuse passively into the CNS. However, the vast majority of molecules of a molecular weight greater than 600

Daltons do not cross the BBB (Figure 2.4). Therefore in order to reach the brain, most drug molecules must cross the BBB via an interaction with specific transporters occurring at the luminal surface of the endothelial cells (Löscher and Potschka, 2005; Löscher and Potschka, 2005 (2); Löscher and Potschka, 2005 (3); Lee et al., 2001).

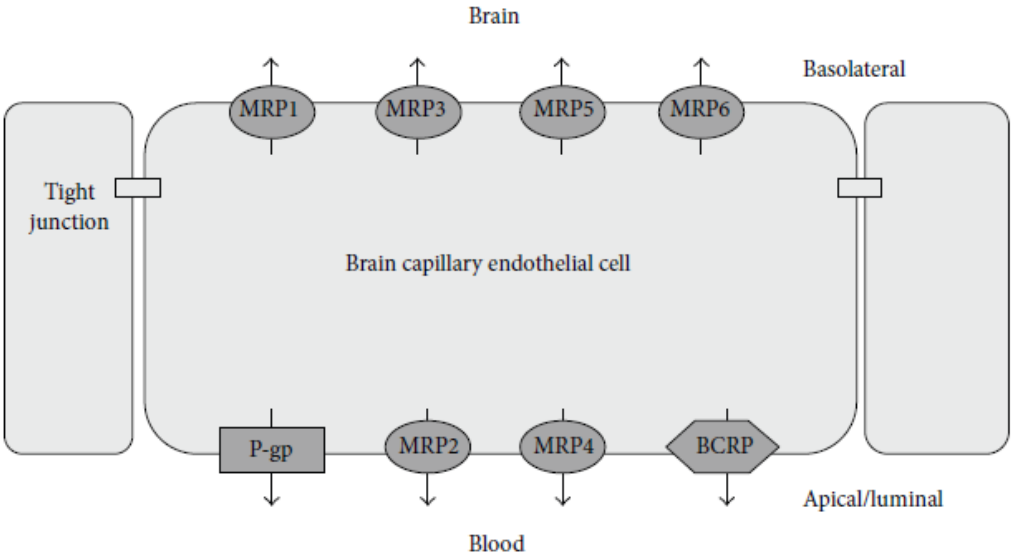


Figure 2.4: Respective locations of the drug efflux proteins on brain capillary endothelial cells that collectively form the BBB (Löscher and Potschka, 2005 (3).

The pharmacodynamics and pharmacokinetics of CNS targeted drugs are determined by their unbound concentrations in the extracellular fluid of the brain. Several *in vivo* and *in vitro* procedures are accessible to study these properties. The efflux transport across the BBB is an imperative process utilized in the explanation of the mechanism of the apparent restricted cerebral distribution of drugs after their systemic administration. To examine the BBB efflux transport mechanism under *in vivo* conditions, an intracerebral microinjection technique has been developed and newly estimated as the BEI (Brain Efflux Index). BEI is defined as the relative percentage of drug that is effluxed from the ipsilateral (does not cross the opposite hemisphere of the amount of drug injected into the cerebrum as shown:

$$BEI\% = \frac{Amount\ of\ drug\ effluxed\ at\ the\ BBB}{Amount\ of\ drug\ injected\ into\ the\ BBB} \times 100$$

Equation 2.1

However, limitations of the BEI method are that only one data point may be obtained for a single intracerebral injection, and the concentration the drug in the cerebrum cannot be accurately determined (Misra et al., 2003). The net uptake of a drug molecule by the brain via the BBB depends on the overall difference between the uptake and efflux processes (Table 2.1) Brain uptake of drug molecules is controlled by various factors, including the systemic disposition of the drug as well as the properties of the endothelial cells. Thus, permeability of endothelial cells and their ability to metabolize drugs actively regulate the amount of drug crossing the BBB in both directions (Schermann, 2002).

Table 2.1: The net uptake of bioactive by the brain depends on the difference between the influx and efflux processes (Schermann, 2002)

Blood Lumen	Endothelial Cell	Extracellular Fluid
(i) Blood systemic exposure	Influx Clearance →	
(ii) Drug blood cell and protein binding	(i) Drug permeability	Drug disposition
	(ii) Drug metabolism	
	Efflux Clearance ←	

In recent years it has become well perceived that the activity of the P-gp in the BBB plays a restrictive role with regard to the net cerebral uptake of many therapeutic drugs. Owing to its unspecific substrate affinities, P-gp restricts the achievable cerebral concentration of various medications and may be a crucial factor in the phenomenon of pharmacoresistance

(La Foug'ere et al., 2010; Schinkel, 1999; Aller et al., 2009). P-gp is a prototypical multidrug resistance (MDR) transporter; its discovery was based on its ability to confer drug resistance to cancer cells. P-gp, a phosphoglycoprotein, acts as an unrestrained energy-dependent efflux pump (Taylor, 2002). Given that P-gp efflux accountability can be a key obstacle for CNS therapeutic drugs to cross the BBB and reach the target, the interactions of the CNS targeted drugs with the P-gp transporter may lead to the lack of CNS activity as a result of the minimized brain penetration.

Therefore the estimation and understanding of the significance of P-gp mediated efflux transporter have become an important stage in the discovery and development of CNS delivery strategies (Miller et al., 2008).

2.4. P-gp Efflux Transporter Structure and Mechanism of Action

In response to the inefficiency in conventional delivery mechanisms, a great amount of research efforts have lately focused primarily on the development of new strategies to allow for a greater efficacy in the delivery of drug molecules to the CNS. In particular, these research efforts have focused on the modulation of P-gp efflux transporters within the BBB (Gabathuler, 2010). P-gp is presently the most widely studied member of the ABC transporter family and has been shown to transport an extensive list of substrates with a great degree of structural diversity (Matsson et al., 2009). P-gp is a type of energy-dependent ATPase transmembrane drug efflux transporter. It is a 1280-long amino acid glycoprotein, expressed as a single chain structure containing two homologous portions of equal length, each portion consisting of 6 transmembrane domains and two ATP binding regions separated by a flexible polypeptide linker portion (Varma et al., 2003; Rosenberg et al., 2003), (Figure 2.5 (a), (Aouali et al., 2005; Sharom, 2014).

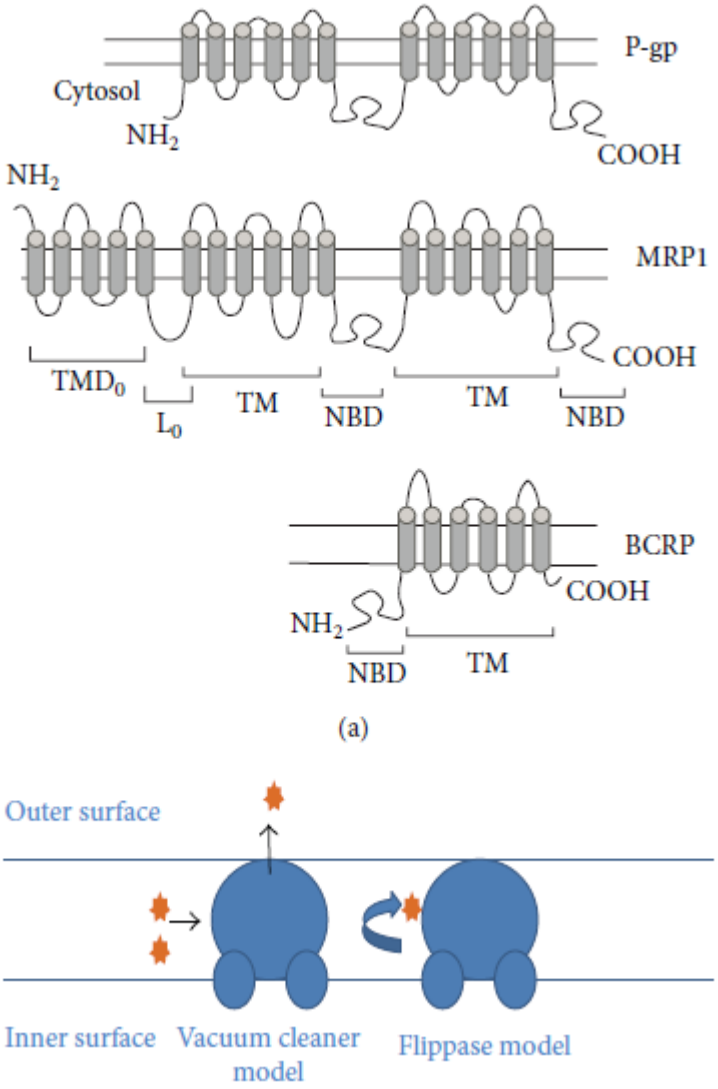


Figure 2.5: (a) Structural configuration of P-gp, MRP, and BCRP (Aouali et al., 2005) (b) Diagrammatic representations of the "Vacuum Cleaner" and Flippase model of P-gp function (Sharom, 2014).

There are numerous models to explain the mechanism of efflux by the P-gp transporter. The three most predominant models, pore, flippase l, and the hydrophobic vacuum cleaner model, are commonly used to explain the mechanism of efflux (Figure 2.5 (b). The vacuum cleaner model hypothesizes that P-gp recognizes substrates embedded in the inner leaflet of the plasma membrane; the substrate is then transported through the protein channel out of the cell (Sharom, 2014). Within the perspective of this model, P-gp binds directly to the substrate molecules that are located on the plasma membrane and pumps them out of the cell by recognizing the substrates as foreign bodies (Fardel et al., 1996). The pore model is described as an interaction of P-gp with

drugs within the boundaries of the cytosol, followed by efflux out of the cell via protein channels. The hypothesized flippase model explains drug efflux as a “flipping” of drug molecules from the inner leaflet to the outer leaflet of the cell against a concentration gradient. These drug molecules then undergo diffusion to reach the extracellular space (Fardel et al., 1996). However, the flippase model is the most generally received model and increasing amounts of evidence have made it the most favoured amongst all (Constantinides and Wasan, 2007; Higgins and Gottesman, 1992; Sauna et al., 2001).

2.5. P-gp in Schizophrenia Therapy

Antipsychotic drugs and other pharmacological agents used to treat psychiatric illness must cross the BBB to reach the target sites within the CNS to be able to exert their therapeutic effects. Antipsychotic drugs are crucial treatment options for symptoms of schizophrenia. The first generation or conventional antipsychotics include drugs that have high affinity antagonism of dopamine D2 receptors. The second generation antipsychotics or atypical agents include drugs with a lower D2 receptor affinity and a far greater affinity for other neuroreceptors (Wang et al., 2009). Recently, it has become progressively evident that drug transporters situated within the BBB play a fundamental role in the pharmacokinetics of several drugs with therapeutic implications. There are strong indications for an impaired integrity of the BBB in schizophrenia, such as increased intracerebral concentrations of the soluble intercellular adhesion molecule-1 (sICAM). Furthermore, the concentration of immunoglobulin and albumin is raised in cerebrospinal fluid in 30% of schizophrenic patients. P-gp function has been reported to be reduced in the progression of neurodegenerative diseases (de Klerk et al., 2010).

Wang and co-workers (Wang et al., 2004) conducted a study employing the abcb1a/b knockout mouse model with a functional deficiency in P-gp. By utilizing ATPase activity as a marker for P-gp activity, an *in vitro* study provided evidence that various atypical antipsychotic drugs such as risperidone and olanzapine may be effectively effluxed by P-gp. In a subsequent *in vivo* study utilizing the abcb1a gene knockout mouse model, results depicted that P-gp restricted the brain penetration of olanzapine, as the resulting brain concentration was 3-fold higher in the abcb1a knockout mice than as the comparative control mice (Wang et al., 2004). Risperidone is an atypical antipsychotic drug that has potent antagonistic affinities toward serotonin 5-HT2 and dopamine D2 receptors. Risperidone is recognized for its effectiveness against both positive and negative symptoms of schizophrenia. An *in vitro* study by Nakagami and co-workers (Nakagami et al., 2005) of the activity of P-gp against a range of antipsychotic agents showed that P-gp is likely to influence the absorption of all atypical antipsychotics to various degrees (Nakagami et al., 2005).

In addition to other studies relating to P-gp function the activity of the P-gp transporter at the level of the BBB can be studied *in vivo* via Positron emission tomography (PET) with [11C] verapamil as a PET tracer. PET seems to be a suitable means of *in vivo* valuation of P-gp functionality in humans and allows for the quantification of BBB/P-gp function in neurodegenerative disorders. The PET brain imaging study with the use of [11C] verapamil as a radiotracer was conducted on schizophrenic patients and a comparative healthy control group. Data obtained from the study showed a regionally reduced [11C] verapamil uptake within the temporal cortex and basal ganglia of schizophrenic patients versus healthy controls. These results have been interpreted as an increase in P-gp function in the brain of schizophrenic patients. These findings are of immense worth since an increase in P-gp function may be pertinent for the clinical progression of schizophrenia. An increase in P-gp function leads to reduced uptake of antipsychotic agents and may thus be associated with poor clinical outcomes (de Klerk et al., 2010).

A further study by Kirschbaum and co-workers (Kirchbaum et al., 2008) found that the ATPase activity assay displayed high affinity of the antipsychotic risperidone for P-gp. *In vivo* studies conducted in mice and humans revealed variations in brain and serum concentrations for both risperidone and its active metabolite, 9-hydroxyrisperidone, which was recently approved as a new antipsychotic paliperidone. In comparison, the conventional antipsychotic haloperidol which displays a high antagonistic activity at dopamine D2 receptors is poor substrate of Pgp. Behavioural changes in the mdr 1a/1b knockout mice in comparison to the wild-type mice allow for the investigation of P-gp-dependent variations in the expression degrees of the CNS which leads to functional dispositions. Motor impairment on a rotarod physical task is characteristic of antipsychotic related D2 receptor antagonism [de Klerk et al., 2010; Kirschbaum et al., 2008)

This very hypothesis was applied to mdr 1a/1b and wild-type mice after administration of either the known substrate risperidone or a poor substrate haloperidol. Results revealed distinctively different profiles in motor effects by the antipsychotic drug risperidone which was dependent on P-gp expression. Brain concentrations of risperidone and its 9-hydroxyrisperidone metabolite were 10-fold higher for the first three hours in knockout mice versus wild-type mice. The increased concentration reflects the change in dose response seen in the behavioural task. The results establish for the first time the strong association between physical functionality and P-gp-dependent brain concentrations. Pharmacokinetic data of this study displayed a 10-fold higher brain level of risperidone and a 20-fold higher brain level of 9-hydroxyrisperidone in mdr1a/1b mice as compared to wild type mice. Conclusively, antipsychotic drugs are effectively transported by the P-gp efflux transporter (Kirschbaum et al., 2008).

In conclusion, an additional study was conducted on the atypical antipsychotic aripiprazole. To assess the role of Pgp in the distribution and penetration of aripiprazole within the BBB, mice deficient in the P-gp gene were dosed intraperitoneally with 2 μg/g of aripiprazole. Wild type mice were administered the same dose as the gene deficient mice. The results showed that deficiency of P-gp had a drastic effect on drug concentrations within the brain. Thus aripiprazole has been characterized as a transportable substrate of P-gp (Wang et al., 2009).

2.6. P-gp Substrates and Inhibitors

In an attempt to estimate the effects of P-gp *in vivo*, a range of *in vitro* P-gp assays have been developed so as to categorize compounds as P-gp substrates or inhibitors (Table 2.2). One such assay is the Transwell-based assays using polarized cell lines such as Madin-Darby Canine kidney (MDCK) cell line. The MDCK cell line may be stably transfected with human MDR1 orMdr1a. Comparing the efflux ratios betweenMDR1- MDCK and MDCK, Transwell assays are able to provide a measure of the specific human P-gp-mediated efflux activity (Kirschbaum et al., 2008).

Table 2.2: Brief overview of P-gp inhibitors/substrates and the corresponding IC50 values of inhibitors.

Inhibitor	IC_{50}	References
Haloperidol	Potent	(Doan et al., 2002)
Fluoxetine Chlorpromazine Paroxetine Sertraline	Moderate	(Doran et al., 2005; Doan et al., 2002)
Risperidone 9-hydroxyrisperidone Sulpiride Zolpidem	Low	(Doran et al., 2005; Doan et al., 2002)
Loperamide*		(Doran et al., 2005)
Verapamil* Quinidine*	Moderate	(Feng et al., 2008; Doran et al., 2005)
Prednisone*	Low	Doran et al., 2005)

Potent (P) inhibition (IC50 < 10 μM), moderate (M) inhibition (10 μM ≤ IC50 < 50

Another generally used P-gp *in vitro* assay is the P-gp ATPase assay for assessing drugs that demonstrate P-gp interactions as substrates. The standard reagent of the ATPase assay is a membrane preparation from insect cells that are vastly expressive of human P-gp. Functional human P-gp will transport P-gp substrates across the membrane thus resulting in the release of inorganic phosphates (Feng et al., 2008). In addition, the *in vitro* calcein AMP-gp inhibition assay can be utilized to detect compounds that inhibit the P-gp-mediated efflux, via employing a fluorescent P-gp substrate, calcein. The calcein assay is capable of differentiating between various Pgp inhibitors from non-inhibitors by measuring the resultant fluorescence of calcein (Feng et al., 2008)

A further *in vitro* approach in studying the P-gp activity is the use of P-gp knockout mice in comparison to wild-type mice. P-gp knockout mice are genetically modified animals in which both genes that are homologous to the human MDR1 gene have been disrupted, resulting in a viable line of animal models. An assessment of the brain plasma area under the curve (AUC) ratio in knockout mice as compared to wild type mice has become a standard experimental methodology to determine whether P-gp-mediated efflux poses a possible obstacle to the activity of CNS targeted drugs *in vivo* (Löscher and Potschka, 2005; Doran et al., 2005; Hitchcock, 2012).

P-gp exhibits significant capability to bind and transport a wide range of structurally and functionally dissimilar compounds. Typical drug substrates include typical and atypical antipsychotics as well as anticancer agents. P-gp also interacts with yet another group of hydrophobic agents, known as chemomodulators, that is, calcium channel blockers and phenothiazine's. Chemomodulators belong to two categories, those that are transport substrates themselves and thereby compete for efflux and those that exert their effects by binding to and blocking drug efflux without themselves being transported out of the cell (Bebawy and Chetty, 2008).

In general, P-gp can be inhibited via (i) blocking the drug binding site competitively/noncompetitively/allosterically, (ii) by interfering with ATP hydrolysis, and (iii) by altering the integrity of the cell membrane lipids (Varma et al., 2003) Based on their specificity and affinity, P-gp inhibitors are categorized into three generations: First generation inhibitors are pharmacological actives, which are in clinical use for other indications but have been shown to inhibit P-gp. Second and third generation inhibitors specifically modulate P-gp, with the second generation inhibitors lacking the pharmacological activity of its first generation counterparts and with a higher affinity for P-gp. The third generation inhibitors have a 10-fold higher affinity and potency to inhibit P-gp (Bebawy and Chetty, 2008).

2.7. Novel Drug Delivery Systems and Pharmaceutical Excipients Capable of CNS and Intestinal Delivery via P-gp Bypass or Inhibition with a Potential Applicability in Schizophrenia Therapy

2.7.1. Formulation excipients utilized as P-gp inhibitors.

Approaches to bypass the P-gp efflux pump may be to combine the target drug with either another P-gp pump substrate or an inhibitor; on the other hand there is the novel approach of combining the active drug molecule with a lipid or polymer excipient which is capable of P-gp inhibition. The initial approach is effective in its inhibitory potential; however it involves the use of a second pharmaceutically active agent that increases the risk of drug-drug interactions; thus in retrospect the use of inhibitory excipients has nonspecific pharmacological action and therefore the possibility of systemic effects and drug interactions is eliminated (Constantinides and Wasan, 2007).

2.7.2. Chemosensitizers

Chemosensitizers, also termed reversal agents, are one such approach; they inhibit the efflux pump and increase the absorption of drugs intracellularly; and thus the co-administration with clinically relevant compounds has become a common practice (Gohel et al., 2011). Chemosensitizers function by acting as competition at the P-gp substrate binding site or by blockade of ATP hydrolysis; drugs such as verapamil, cyclosporine A, and antisteroidal agents such as tamoxifen are classified as 1st generation P-gp modulators. However high concentrations of these agents are required for this purpose and thus lead to pronounced side effects; thus the development of 2nd generation chemosensitizers was prompted. This nevertheless proved to exhibit the same limitations.

To circumvent limitations observed with the 1st and 2nd generation P-gp chemosensitizers, 3rd generation chemosensitizers have been developed utilizing the supremacy of combinational chemistry and Structure Activity Relationships (SARs). These agents are non-competitive inhibitors that result in alterations in protein conformation, thus modulating P-gp substrates; they include elacridar and tariquidar amongst others (Montesinos et al., 2012). Further research conducted depicted evidence that drug delivery systems in combination with P-gp modulators could considerably enhance pharmacokinetics of the P-gp modulator and in addition reduce the pharmacokinetic interactions with P-gp substrates. Cremophor EL was one of the excipients employed in the above mentioned study which showed promising activity as a P-gp modulator (Montesinos et al., 2012). Furthermore, in an experimental study conducted by Choo and co-workers tariquidar, a P-gp modulator in combination with propylene glycol, 5% dextrose, and ethanol, was able to inhibit P-gp function at the BBB in high doses (Choo et al., 2006), thus

displaying a possible application in improving CNS permeability of drugs employed in neurodegenerative diseases. In another research study it has been shown that GF120918 (elacridar) a known 3rd generation P-gp modulator is capable of increasing the brain uptake of paclitaxel (P-gp substrate) 5- fold (Kaur et al., 2009).

2.7.3. Natural polymers

The natural gums are classified as polysaccharides that consist of multiple sugar groups that bonded together to create much larger molecules; they offer the advantages of being sustainable, biodegradable, and biologically safe; these natural gums are known to form gels that depict a high degree of network formation. Gums are capable of undergoing grafting and crosslinking reactions and through such reactions they may form hydrogels, xerogels, and nanoparticles which have a very important function in the inhibition of the P-gp efflux transporter (Choo et al., 2006). Chitosan, a cationic polysaccharide in combination with nucleotides to form nanosystems, may enhance the permeability of drug molecules into the CNS via opening of tight junctions, and the formulation of nanosystems incorporating chitosan and nucleotides will enable this purpose (Werle and Bernkop-Schnürch, 2008). Natural polymers such anionic gums, for example, xanthan and gellan gum, as well as alginates, have been shown to inhibit the action of the P-gp efflux pump at concentrations of 0.05% and 0.5mg/mL, respectively (Hunter et al., 1994). In the presence of xanthan gum studies have shown increased concentration of P-gp substrates such as vinblastine and doxorubicin. Alginate flavicam demonstrated an increase in the intracellular concentration of doxorubicin in everted gut sac cells (Werle, 2008).

2.7.4. Synthetic polymers

Synthetic polymers are synthesized via polymerization reactions and the modification of natural polymers or via the complexation of natural polymers with naturally occurring agents such as fatty acids (Werle, 2008). Synthetic polymers such as PEG 400, at concentrations between 1 and 20%, increased accumulation of digoxin due to the inhibition of the P-gp drug efflux pump (Shen et al., 2006; Hugger et al., 2002). Similar studies conducted employing Pluronic P85 and Vitamin E D-α-Tocopheryl polyethylene glycol 1000 succinate on the digoxin uptake in rats have further proven that pluronic blocked copolymers are capable of inhibiting the P-gp efflux pump and enhancing substrate uptake (Johnson et al., 2002). Furthermore, studies have shown that pluronic P85 has an inhibitory action on the ATPase enzyme that is involved in the functioning of the P-gp efflux pump proteins, thus resulting in inhibitory reactions between these proteins and the P-gp substrates (Batrakova et al., 2001). In a study conducted by Batrakova and co-workers who have shown the increased brain concentration of digoxin in mdr1 knockout mice and wild type mice

treated with Pluronic P85, it was clearly demonstrated that Pluronic P85 delayed the residence time and concentration of digoxin in the brain (Batrakova et al., 2001). Commonly occurring polymers that act as P-gp inhibitors are listed in Table 2.3.

Table 2.3: Summarized list of polymer & surfactant P-gp inhibitors and their mechanism of action.

Polymer and Surfactant based P-gp efflux Inhibitors	Applications	References
Natural Polymers:		
Xanthan Gum Gellan Gum Alginates	Inhibition of the P-gp efflux transporter by the presence of polysaccharide d-mannose monomers, increasing concentration of substrates e.g. vinblastin and doxorubicin.	(Hunter et al., 1994)
Synthetic Polymers:		
PEG 400 PEG-PEI PEG 300	Changes the microenvironment of Caco-2 cell membranes, leading to modifications in membrane fluidity.	(Hunter et al., 1994; Werle, 2008)
Pluronic® P85	Results in ATPase inhibition and ATPase reduction. As well as membrane fluidization.	(Werle, 2008; Hugger et al., 2002; Johnson et al., 2002)
Thiomers	Thiol groups interact with cysteine in the P-gp transmembrane channel, forming disulfide bonds. Thus the allosteric change blocks efflux.	(Batrakove et al., 2001)

Research studies have been conducted to evaluate the inhibitory properties of PEG on the P-gp efflux pump. The study involved the grafting PEG to polyethyleneimine (PEI) and then undergoing a thiolation reaction employing γ- thiobutyrolatone to formulate a novel grafted thiomer. The grafted PEG was then evaluated based on its effect on the transport of Rhodamine–123, a well-known P-gp substrate. Results depicted that the cellular uptake of Rhodamine-123 was improved with the grafted-thiolated PEG as compared to free drug solutions.

Oral administration of many drug substances is limited due to the poor bioavailability and systemic uptake which is directly linked to the presence and action of the P-gp efflux pump. In an attempt to overcome this limitation there has been the development of P-gp pump inhibitors; however due to the abovementioned set back of requiring high doses, none of them have been approved for oral administration due to the risk of systemic side effects. Thus polymeric Pgp inhibitor incorporation into drug delivery systems as excipients provides a valuable approach; they show a high inhibitory potential and due to their great molecular weights they are not absorbed from the gastrointestinal system and thus eliminate any possible systemic effects. Previous studies determined the inhibition of P-gp by PEG's by their effect on the elevated permeability of substrate drug molecules such as taxol and doxorubicin within caco-2 monolayers (Iqbal et al., 2010). PEGylated sorbitans that are esterified with fatty acids are commonly known as polysorbates. The most extensively studied group of the Polysorbates is polyoxyethylene sorbitans monolaurates, known by the trade name Tween; these agents have been found to enhance the accumulation of daunorubicin within tumor cells (Werle, 2008).

Poloxamers also fall within the category of synthetic polymers and are also known as Pluronics. Specifically, Pluronic P85 has been studied for its inhibitory effect on the function of the P-gp efflux pump. Two main areas that P85 is used for its inhibitory properties are in the BBB and cancer chemotherapy (Werle, 2008). The mechanism of inhibition has been dedicated to a reduction in ATP and inhibition of ATPase enzymes as well as lipid membrane fluidization (Batrakova et al., 2001; Batrakova et al., 2001(2). Pluronic brings about a reduction in ATP levels within bovine endothelial cells; the ATP depletion was reasoned to be as the result of the inhibition of cellular metabolism (Batrakova et al., 2004).

Additionally, mixed micelles synthesized from a combination of poloxamer 407 and D-α-Tocopheryl polyethylene glycol 1000 succinate (TPGS 1000) have the potential of elevating the clinical efficiency of drugs by increasing the amount of drug in the interior of the cell by inhibiting P-gp efflux transporters (Saxena and Hussain, 2012). TPGS 1000 is classified as a water soluble vitamin that consists of a lipophilic head and hydrophilic PEG tail. The mechanism by which TPGS 1000 inhibits the P-gp pump has been proposed as a combination of membrane fluidization, ATP depletion, and prevention of substrate binding. Research on the effect of pluronic block polymers on the accumulation of digoxin has proven the hypothesized inhibition of Pgp efflux transporters by Pluronic polymers. The treatment of various substrates with Pluronic polymers displayed an increase in apical to basolateral transport, thus displaying Pgp inhibition (Werle, 2008; Batrakova et al., 2001; Batrakova et al., 2001(2).

Thiomers, yet another group of synthetic polymers, are characterized as polymers containing a thiol moiety within their chemical structure; the presence of the thiol moiety allows for the formation of disulfide bonds between the cysteine groups, of the P-gp pump, for example, α chitosanthiobutylamidine (Werle and Hoffer, 2006). The mechanism of thiomer mediated inhibition of the P-gp efflux pump is depicted in Figure 2.6. Improved transmucosal transport of Rhodamine-123 a P-gp substrate in the company of thiolated chitosan, produced by linking of amino groups of chitosan and thiol groups (Bernkop-Schnurch et al., 2003), was displayed by Bernkop-Schnurch et al. due to P-gp transporter inhibition. Thiomers are not absorbed from the GIT due to their high molecular weight; therefore systemic side effects are eliminated and their use as pharmaceutical excipients for their P-gp inhibitory properties is greatly beneficial (Iqbal et al., 2010). As described above the P-gp efflux pump is made up of 12 transmembrane units; these units in turn form channels through which P-gp substrates pass through to exit the cell; two of the 12 units display cysteine subunits. Thiomers are theorized to enter the channels of the P-gp pump and thereafter form disulfide bonds with the cysteine subunits; in this manner the transport of drug molecules out of the cell is hindered and thus there is an inhibition of P-gp efflux pump action (Werle and Bernkop-Schnurch, 2008). Thiolated chitosan is a directly compressible excipient which may therefore be formulated into matrix tablets (Bernkop-Schnurch et al., 2003).

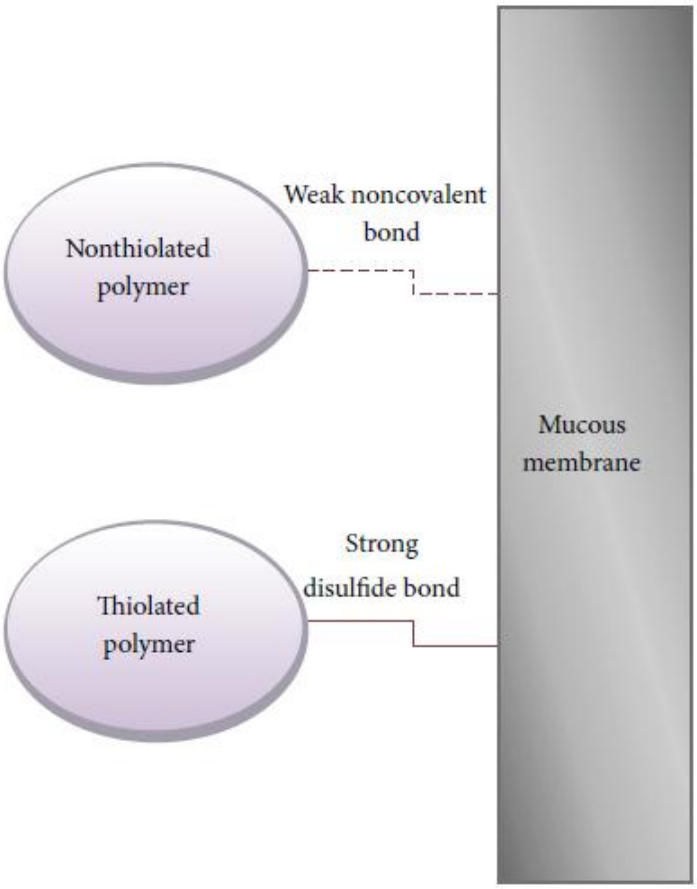


Figure 2.6: Mechanism of inhibition of the P-gp efflux pump (Kumar and Sinha, 2013)

2.7.5. Solvents and surfactants

Both surfactants and solvents act by interaction with the polar heads of the lipid bilayers thereby adjusting hydrogen bonding and ionic forces and have the potential to insert themselves between the nonpolar tails of the lipid bilayer. These interactions cause the fluidization of the lipid membrane and thus P-gp inhibition. Non-ionic surfactants such as Tween and Span possess Pgp transporter inhibitory potential; these agents are also hydrophobic and thus rendered less toxic (Bansal et al., 2009). Surfactants are furthermore important in the formulation process of nanoparticles. Various research outputs have shown that the efficiency of surfactants as P-gp inhibitors is based on their respective chemical structures. Surfactants such as Solutol HS15, Tween 80, and Cremophor EL contain Polyethylene glycol on the hydrophilic portions of their structures, which have displayed the ability to increase intracellular concentrations of epirubicin in human colorectal carcinoma cells, thereby confirming that surfactants act as P-gp modulators

(Montesinos et al., 2012). In a study conducted by Rege and co-workers (Rege et al., 2002) the effect of Tween 80, Cremophor EL, and vitamin E TPGS on the P-gp efflux transporter in caco-2 cell monolayers was investigated. Results showed that all three surfactants inhibited P-gp and Tween 80 and Cremophor EL increased the apical to basolateral permeability of Rhodamine 123 (P-gp substrate) within a concentration range of 0-1mM. Whereas vitamin E TPGS contributed an inhibitory effect at a concentration of 0.025mM (Rege et al., 2002).

2.8. Drug Delivery Systems with P-gp Modulatory and Enhanced Intestinal Absorption Applications

The following section will focus on the strategic design of drug of delivery systems studied for their aptitude to enhance bioactive delivery through the intestinal epithelia by P-gp modulation and/or inhibition with a future applicability in schizophrenia therapy.

2.8.1. Bestatin-improved intestinal absorption by co-administration of a P-gp inhibitor.

A study by Huo and co-workers (Huo et al., 2013) has shown the enhancement effect of P-gp inhibitors on the intestinal absorption of bestatin. The study showed that when bestatin and cyclosporine A were co-administered orally, the resultant plasma concentration of bestatin was considerably increased. Cyclosporine A and Verapamil, commonly utilized P-gp inhibitors, can eliminate the efflux pump mediated by P-gp, resulting in improved intestinal absorption of the co-administered P-gp substrate. The study by Huo and co-workers (Huo et al., 2013) displayed a 90% increase in bestatin intestinal absorption seen in the C_{max} and AUC with the addition of cyclosporine A (Huo et al., 2013).

2.8.2. Enhanced intestinal absorption of ganciclovir by P-gp inhibition using pharmaceutical excipients

Several studies have shown that P-gp inhibitors such as verapamil and cyclosporine A are capable of enhancing the bioavailability of a variety of drugs. However, such inhibitors are pharmacologically active agents and thus may cause toxic effects. In addition, these agents are absorbed into the bloodstream and can interact with P-gp in other organs that it is expressed in. On the other hand, pharmaceutical excipients, which are utilized as inert excipients in drug delivery formulations, are being investigated as superior class of P-gp inhibitors. Several studies have shown that these excipients can greatly improve the intestinal absorption of a wide range of drugs by P-gp inhibition.

These excipients are non-absorbable; thus there will be no unnecessary P-gp inhibition in other organs. A study conducted by Li and co-workers (Li et al., 2011) studied the effects of common

excipients on the intestinal absorption of ganciclovir, a substrate of P-gp in rats. The *in vitro* transferal from mucosa to serosa as well as the *in situ* transepithelial permeation was evaluated. Selected excipients within a concentration range of 0.1–1% w/v were shown to increase the concentration of ganciclovir transported in an everted gut sac model. Results depicted a significant increase in permeability of ganciclovir by all excipients employed in the study. The effects of EL-35 and F-68 were dose-dependent but that of PEG 400 and Tween 80 were not. The results observed confirm that the improvement of intestinal absorption of ganciclovir via the use of excipients is due to inhibition of P-gp inhibition mediated drug efflux. The mechanism of F-68 inhibition of P-gp is due to its blocking effect on the binding site of the Pgp efflux transporter, whereas PEG 400, tween-80, and EL-35 are due to alteration in the membrane fluidity of P-gp (Li et al., 2011).

2.8.3. Self-emulsifying drug delivery systems

This is another drug delivery approach that may prove useful in bypassing the P-gp pump due mainly to the presence of surfactants such as Tween 80 that have been identified as P-gp inhibitors (Rege et al., 2002). SMEDD's consisting of vitamin E (oil phase) and surfactants have been shown to enhance the solubility and bioavailability of paclitaxel (a P-gp substrate) owing to their P-gp inhibitors activity. An advantage of using SMEDD's is their capability to incorporate and solubilize high concentrations of P-gp inhibitors. Many studies have been conducted to improve the oral bioavailability of this chemotherapeutic agent so as to increase clinical outcomes; it has been proven that P-gp plays a vital role in the bioavailability of paclitaxel; the study conducted by Woo and co-workers shows that the use of KR-30031 a verapamil analogue with P-gp inhibitory effects in combination with paclitaxel improved the bioavailability of the later (Woo et al., 2003). Nanocapsules have been used as a drug delivery system to improve the oral bioavailability of the P-gp substrate Tacrolimus, which was incorporated into nanocapsules with the use of polymethacrylate polymers. Results depicted that the bioavailability was between a ranges of 2.45- and 4.9-fold compared to the commercially available formulation (Nassar et al., 2009).

8.2.4. Double coated nanocapsules for enhanced intestinal absorption and bioavailability of a P-gp substrate

An experimental study performed by Nassar and co-workers (Nassar et al., 2009) proposes the use of double coated nanocapsules to improve the bioavailability of a P-gp substrate, Tacrolimus. Using caco- 2 cells and intestinal rat segment the effect of encapsulation of Tacrolimus on P-gp was evaluated. The double coated nanocapsules prevented its molecular recognition by the Pgp efflux transporter in caco-2 cells. The conclusive results show that the nanocapsule delivery

system is a great platform for intestinal absorption of lipophilic drugs which are P-gp substrates. The oral bioavailability of Tacrolimus was 4.9- and 2.45-fold greater when compared to a marketed product (Nassar et al., 2009).

2.8.5. Novel polymeric P-gp inhibitor for enhanced intestinal drug delivery

Many drugs are unable to be administered via the oral route owing to poor absorption into the systemic circulation due to intestinal P-gp efflux pumps. In order to circumvent this obstacle many types of efflux pump inhibitors have been developed. Yet, many of these inhibitors have not been approved for oral use due to their systemic side effects. A noteworthy alternative would be polymeric based efflux pump inhibitors, displaying greatly efficient inhibitory action and no systemic side effects because it is unabsorbed into the intestine due to its high molecular mass. In a study conducted by Iqbal and co-workers (Iqbal et al., 2010) a novel thiolated copolymer, thiolated PEG-g-PEI copolymer, was synthesized. The novel thiolated copolymer showed a significantly greater effect on the intestinal absorption of Rho- 123, a P-gp substrate as compared to other P-gp inhibitors. In addition, the thiolated copolymer was able to increase the intestinal uptake of Rho-123 up to 3.26-fold in comparison to a system lacking a P-gp inhibitor. In addition to enhancing the absorption of Rho-123 the novel thiomer was also capable of decreasing the basolateral to apical transport across the rat intestinal mucosa segment. The study has thus provided evidence that the novel thiomer has a great applicability in improving bioavailability of P-gp substrate drugs (Iqbal et al., 2010).

2.8.6. Influence of intestinal P-gp on absorption of furosemide a P-gp substrate

Furosemide is a loop diuretic employed in the clinical treatment of congestive heart failure and hypertension. Pharmacokinetics of furosemide show that it has incomplete absorption from the gastrointestinal tract after oral dosing. P-gp efflux pumps have been implicated as the possible cause for reduced absorption; however no complete evidence exists. The intestinal absorption of furosemide was evaluated in the presence and absence of verapamil utilizing the rat intestinal sac model in an experimental study conducted by Al-Mohizea (Al-Mohizea, 2010).

Results obtained from the study depict low drug permeability in the non-everted rat intestinal sac. This replicates the drug transference from the mucosal to serosal region which imitates the *in vivo* environment. In contrast, when observed in the everted rat intestinal sac, drug displayed a noticeably greater transport as compared to transport across the non-everted intestinal sac. These results clearly indicate the involvement of the P-gp pump and because the defined function of the P-gp efflux transporter is to pump drug back into the intestine subsequent to absorption, the observed outcomes indicate a greater transintestinal permeation from the serosal to mucosal

region. The ratio of serosal to mucosal and mucosal to serosal permeability was discovered to be 5.6 and this was advocated for the possible role of P-gp efflux transporter in the intestinal uptake of furosemide. The effect of verapamil hydrochloride, a P-gp efflux pump inhibitor, on furosemide absorption was employed to confirm the results obtained from the intestinal sac model experiment.

It was shown that the presence of verapamil increased the mucosal to serosal transport of furosemide noticeably compared to the control lacking verapamil. This observation is due to the inhibitory effect of verapamil on the P-gp efflux pump, which prevents transport of drug back into the mucosal region. The ratio of serosal to mucosal and mucosal to serosal permeability was reduced from 5.6 in the absence of verapamil to 1.28 in its presence. These results confirm the mechanistic effect of the P-gp efflux pump on intestinal absorption. Furthermore, the current study evaluated the effect of Tween 80 and HPβCD, two commonly employed pharmaceutical excipients, on the intestinal uptake of furosemide. The results displayed a permeation improvement effect for Tween 80 but not for HPβCD. This in turn inferred a substantial increase in the mucosal to serosal permeability of furosemide. Tween 80 was shown to decrease the ratio of serosal: mucosal to mucosal: serosal permeability (5.6 to 1.08). This provides evidence that Tween 80 is a noteworthy P-gp efflux pump inhibitor (Al-Mohizea, 2010).

2.9. Drug Delivery Systems with P-gp Modulation and Enhanced BBB Absorption

The following section will focus on drug delivery systems that have been studied for their unique ability to enhance BBB permeability of drug agents via P-gp inhibition and/or bypass with a prospective application in schizophrenia therapy. The effective non-invasive treatment of neurological diseases is frequently restricted by poor access of bioactives into the central nervous system (CNS). Many therapeutic agents do not freely permeate into brain tissue due to the presence of the BBB and its associated P-gp efflux pump transporter. Recent advances in drug delivery technology have provided promising solutions to overcome these challenges.

The use of drug delivery systems with the ability to bypass or inhibit the P-gp efflux transporter has shown a great improvement in CNS bioavailability and hence enhanced therapeutic outcomes. Furthermore, nanocarriers ranging from polymeric nanoparticles, solid lipid nanoparticles, liposomes, dendrimers, and micelles have been studied for their ability to deliver CNS therapeutics and have displayed success in the treatment of CNS diseases such as brain tumors and alzheimer's (Wong et al., 2012) Hence, we propose the use of these delivery systems in the treatment of schizophrenia so as to bypass the BBB and its efflux transporters.

2.9.1. Nanocarriers

Nanoparticles can gain access to the brain via numerous mechanisms. These mechanisms acting either alone or in combination can explain the transport of therapeutically bioactive agents across the BBB: (i) adsorption and pooling of nanoparticles in the capillaries of the brain, followed by adsorption to the capillary wall, which provides a concentration gradient across the blood capillaries located in the brain cells; therefore this may enhance the transport of bioactives across the endothelial cell monolayer and thus increase the uptake of the bioactive into the brain, (ii) receptor-mediated endocytosis of nanoparticles across the BBB, followed by internalization of the complex and release of the bioactives within brain cells, (iii) transcytosis, nanoparticles with bound bioactives, which can undergo transcytosis through the endothelial cell monolayer and gain access to the brain capillaries, (iv) inhibition of the P-gp efflux transporter and coating nanoparticles with specific Pgp inhibitory substances, such as polysorbate 80 that may possibly inhibit the P-gp, (v) membrane permeabilization effect that involves solubilization of the endothelial cell lipids via the use of surfactants, which leads to membrane fluidization and enhanced permeability of the BBB, and (vi) disruption of the BBB, thus opening tight junctions located between endothelial cells of the BBB; nanoparticles may assist in permeation of bioactives through tight junctions (Agarwal et al., 2009).

Nanocarriers are colloidal systems that include polymeric micelles, nanoparticles, lipid nanocapsules, and liposomes among others. Many of these systems have been designed and developed for indications in various CNS disorders to enhance brain uptake of the CNS targeted bioactives via Pgp transporter activity modulation.

2.9.2. Surfactant-polymer nanoparticles overcome P-gp-mediated drug efflux

Nanoparticles improve the therapeutic efficacy of an encapsulated drug by increasing and prolonging the delivery of the drug within the cell. Aerosol OT-alginate nanoparticles were employed in evaluating their delivery capabilities in brain tumor cells overexpressing P-gp. Rhodamine 123 and doxorubicin were employed as model P-gp substrates. Uptake studies using Rhodamine loaded nanoparticles showed a substantial increase in drug accumulation in resistant cells. The energy-dependent nanoparticle accumulation within cells proposes the contribution endocytosis in nanoparticle uptake. Nanoparticle doses of greater than 200 μg/mL were shown to be the minimum concentration to improve drug accumulation (Chavanpatil et al., 2007; Fortuna et al., 2011).

2.9.3. Lipid-based nanoparticles

Paclitaxel loaded lipid nanoparticles (Figure 2.7) utilizing Brij 78 displayed IC50 values 9-fold greater than when formulated with taxol. The study established that lipid nanoparticles were able to inhibit the synthesis of the microemulsion precursor. Temporary and reversible reductions in ATP were observed with blank nanoparticles and free Brig 78.Therefore, the greater degree of P-gp substrate accumulation was elucidated by a synergistic combination of nanoparticle with Brig 78, where nanoparticles improve the brain uptake of the bioactive by partially bypassing the P-gp transporter and drug efflux is restricted via the release of Brig 78 from the nanoparticles (Constantinides and Wasan, 2007; Montesinos et al., 2012; Mandal et al., 2013).

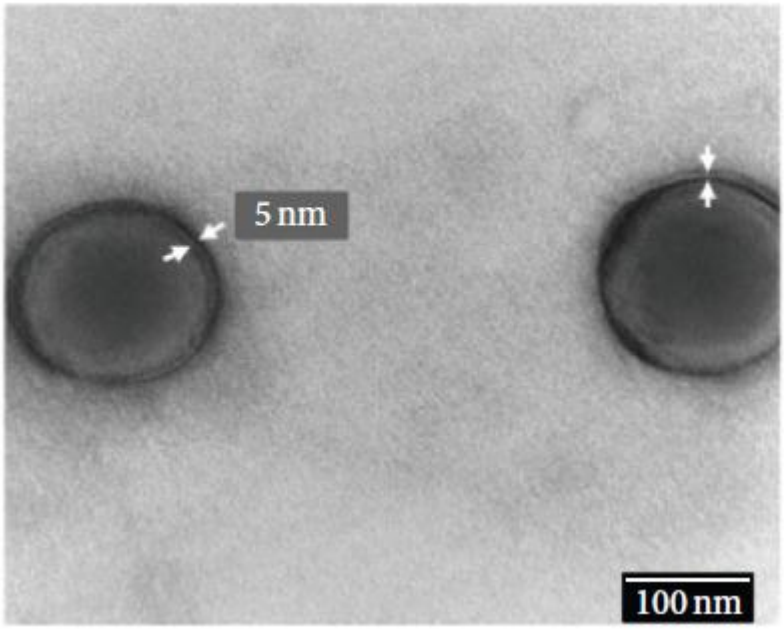


Figure 2.7: TEM images of lipid based nanoparticles; arrows show the lipid bilayer thickness (Mandal et al., 2013).

In other studies, lipid nanocapsules loaded etoposide were synthesized due to their hypothesized reversal of multidrug resistance by the use of P-gp inhibitory surfactants during formulation.

P-gp inhibitory activity of the etoposide loaded lipid nanocapsules was independent of size. The proposed mechanism was cell uptake followed by intracellular P-gp inhibition thus allowing for a higher intracellular drug concentration (Lamprecht and Benoit, 2006). In a further research study the formulation of lipid nanocapsules was achieved by the use of tricaprylic acid, polyethylene glycol 660, and soybean lecithin, for the delivery of the therapeutic agent, paclitaxel, to caco- 2 cells; results showed that the oral bioavailability of paclitaxel was greatly improved possibly due to the ability of lipid nanocapsules to inhibit the P-gp efflux activity; this mechanism is primarily due to the fact that the surface layer of nanocapsules being phospholipids thus resulting in P-gp inhibition via P-gp substrate site competition (Roger et al., 2010).

2.9.4. Transferrin-conjugated nanoparticles for delivery across the BBB.

Transferrin-conjugated nanoparticles of poly (lactide) - D-α-Tocopheryl polyethylene glycol succinate diblock copolymer were formulated via the nano precipitation method with encapsulated docotaxel. Results from the study showed via IC50 data that transferrin-conjugated nanoparticles were 23.4–229% more efficient than the control, PLGA nanoparticles. Thus based on results obtained transferrin conjugated nanoparticles showed to be effective in delivery of drugs across the BBB (Gan and Feng, 2010).

2.9.5. Paclitaxel-polymer micelles to overcome multidrug drug resistance (MDR).

Micelles form from the spontaneous association of amphiphilic copolymers in aqueous phase and are characterized by a diameter no greater than 100 nm (Figure 2.8). The attractive force that leads to micellization is based on the interaction between the electrostatically neutral and hydrophobic portions of the copolymer. Self-assembly of the micelle only begins when the copolymer concentration reaches a threshold value generally referred to as the critical micelle concentration (CMC) (Wang et al., 2011).

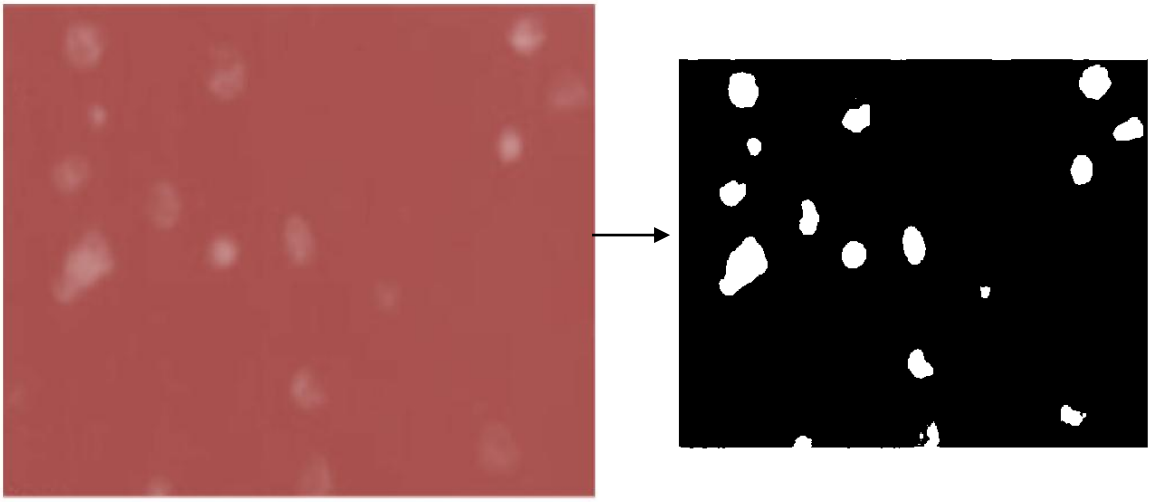


Figure 2.8: TEM micrographs showing the surface morphology of drug loaded micelles (Wang et al., 2011)

Verapamil is a known P-gp inhibitor as well a reversal agent used in reversal of resistance associated with P-gp. Within the context of this study, paclitaxel, a P-gp substrate, in combination with verapamil, was encapsulated into micelles utilizing DOMC-FA (deoxycholic acid methylated chitosan-Folic acid). Resulting data showed that the conjugation of folate on to micelles displayed a higher brain tumor cell uptake of the loaded micelles, possibly via folate receptor-mediated endocytosis. Micelles consisting of the combination of verapamil and paclitaxel showed a higher cellular accumulation of paclitaxel as compared to micelles lacking verapamil (Danson et al., 2004).

In another study, mixed micelles of hydrophobic and hydrophilic pluronic L61 and F127 with encapsulated doxorubicin were formulated. Results observed depicted elevated cellular concentrations of drug to P-gp inhibition displayed via modification of intracellular drug transport (Fortuna et al., 2011).

2.9.6. Polyethylene glycol-660 hydroxystearate nanocapsules

Nanocapsules encapsulated with etoposide (substrate) in combination with P-gp inhibiting surfactants, namely, PEGHS (polyethylene glycol-660 hydroxystearate), were formulated with results depicting an increased bioavailability of etoposide (Roger et al., 2010; B'eduneau et al., 2006). Further studies showed that lipid nanocapsules of paclitaxel formulated by triglycerides of

capric and caprylic acids increased the uptake of drug molecules by MDR1 cells; the half-life of paclitaxel was also prolonged from 21 minutes initially to 5 hours (Wong et al., 2012).

2.9.7. Immunoliposomes in bypassing P-gp

The overexpression of P-gp has been associated with the development of multidrug resistance in cancer cells. Methods employed in overcoming the multidrug resistance frequently involve the co-administration of inhibitors of the P-gp transporter (Figure 2.9(a). Within the context of this study, the hypothesis that immunoliposome-based drug delivery systems may be employed as alternatives to overcome multidrug resistance has been explored. Since immunoliposomes penetrate target cells via receptor-mediated endocytosis, which in turn allows for the bypass of membrane related P-gp transporters, targeting of immunoliposomes was accomplished by via the use of an antitransferrin receptor monoclonal antibody (OX26

MAb).The incorporation of radiolabelled digoxin andOX26- immunoliposomes improved the cellular uptake of digoxin by a factor of 25 in immortalized rat brain endothelial cells. The cellular uptake as well as intracellular accumulation of the digoxin loaded liposomes was determined by acid washing of the cells and further confirmed via confocal microscopy studies. This *in vitro* study proposes that immunoliposome based drug delivery systems can be utilized to bypass P-gp and therefore deliver bioactives to the cytosol of target cells (Huwyler et al., 2002). Furthermore there is the novel approach of combining substrates and P-gp inhibitors within liposomal delivery systems; clinical trials were performed via the formulation of liposomes encapsulating PSC 8339, a recognized P-gp efflux inhibitor in combination with the drug molecule, doxorubicin; results observed depicted an increase in drug delivery potential with no alteration to the pharmacokinetic or pharmacodynamic character of the drug molecule (Krishna et al., 1999; Lee et al., 1992).

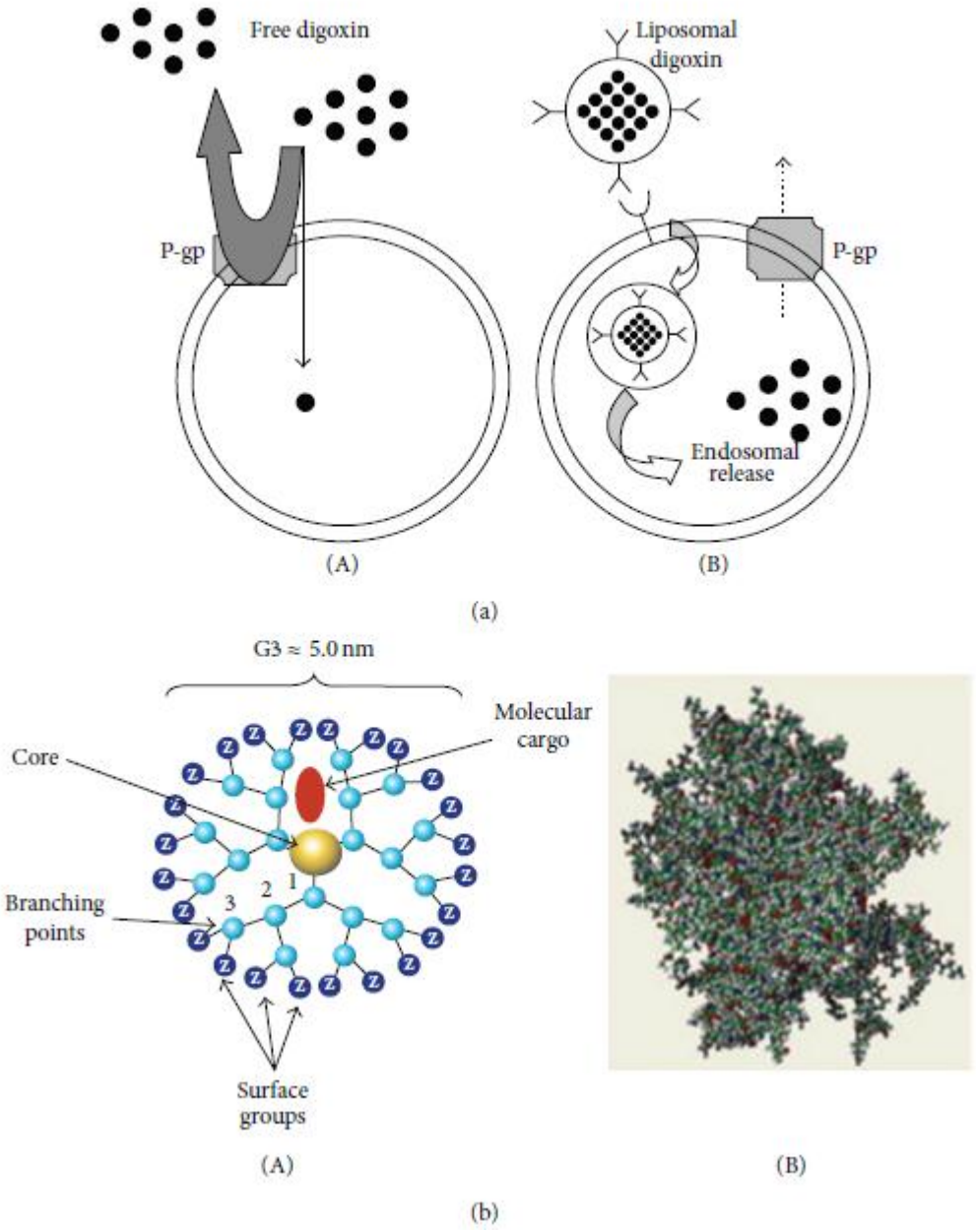


Figure 2.9: (a) (A) P-gp interacts with substrates in the plasma membrane and digoxin (substrate) is effluxed from the lipid bi-layer. (B) Cellular uptake of digoxin facilitated by Immunoliposomes-targeted to transferrin receptor and taken up via receptor-mediated endocytosis (Huwyler et al., 2002) (b) (A) 2D Schematic representation of a dendrimer. (B) 3D representation of a dendrimer (Svenson, 2009).

2.9.8. PAMAM-drug complex for delivery across the BBB

Dendrimers are defined as synthetic macromolecules that have a well-defined structural configuration. It is made up of a centrally located core and branched units that stem from the core

(Figure 2.9 (b) (Werle, 2008; Gillies and Fr'echet, 2005).The mechanism by which dendrimers inhibit P-gp is via endocytosis; the dendrimer passes into the cell interior; this inhibition process could be due to cell membrane alterations and ATPase inhibition; research has shown that P-gp substrates that are encapsulated within dendrimers show an increased intracellular concentration (Gohel et al., 2011). Polyamidoamine (PAMAM) dendrimers belong to a new avenue of P-gp inhibition research; these dendrimers are known to improve the solubility of low solubility drugs. In the current study doxorubicin was chosen as the bioactive agent. Polyamidoamine (PAMAM) dendrimers were exploited as an effective carrier of doxorubicin. Data obtained from the fluorescence intensity assay and fluorescent microscopy displayed that cellular uptake of the PAMAM-doxorubicin complex was 6-fold greater than that of free doxorubicin. These results provide evidence that the novel PAMAM-bioactive complex is a simple yet highly efficacious system, with a great capability to cross the BBB and thus delivery CNS targeted drug successfully (Cui et al., 2009).

Propanolol, a P-gp substrate, was encapsulated within PAMAM dendrimers, due to its poor solubility. Conjugation of propanolol with PAMAM dendrimers was found to allow for bypass of the P-gp efflux pump and therefore enhance the drug concentration within target cells (D'Emanuele et al., 2004; Svenson, 2009).

2.9.9. Poly (D, L-lactide) nanosuspensions of risperidone.

Nanosuspensions are dispersed systems comprising fine particles of drug molecules in the form of crystals. Nanosuspensions are known commonly to incorporate highly lipophilic compounds; these therapeutic agents are stabilized in solution via the use of surfactants. The large surface area afforded by the fine particles assists in enhancing bioavailability to the brain tissue, atovaquone coated by polysorbates in the form of a nanosuspension increased activity in mice presenting with encephalitis (Wong et al., 2012). Employing Pluronic F-68 (P-gp inhibitor) nanosuspensions were formulated containing risperidone and poly-lactide; they have been found to display better clinical outcomes in psychotic disorders via P-gp inhibition (Muthu and Singh, 2009).

2.9.10. Natural Vesicular Exosomes as Drug Delivery Systems to Possibly Bypass P-gp Efflux.

Extracellular vesicles are defined as cell derived membrane vesicles with a characteristic (phospho) lipid bilayer that allows for cell to cell communication. Microvesicles are sized between 50 and 2000 nm, whereas exosomes are between 40 and 150 nm. Exosomes are produced by the formation of intraluminal vesicles in multivesicular bodies. Fusion of multivesicular bodies with

the plasma membrane results in secretion of intraluminal vesicles which are in turn referred to as exosomes once released into the extracellular space. Due to their respective sizes and natural functionality, microvesicles and exosomes seem to be model candidates for drug delivery (van der Meel et al., 2014). A study conducted by van Dommelen and co-workers provided the initial evidence of biotechnological modification of vesicular exosomes; immature dendritic cells was derived from mouse bone marrow as a source of exosomes. These were then loaded with exogenous siRNA for delivery. The BBB was chosen as the target site due to it being a vital obstacle to the delivery of drugs to the CNS. The study displayed specified delivery of siRNA to neurons in the brain with no corresponding toxicity. In another study performed, exosomes were used to deliver anti-inflammatory drugs to the brain via the intranasal route. It was proven that exosomes administered in this manner are potential delivery vehicles for small molecules, by enhancing biological stability and passage across the BBB; these systems may be extended to include a wider range of therapeutic agents (Dommelen et al., 2012). Findings from research studies conducted thus far indicate that a vesicular exosomal-based formulation could be a valuable implement in future for the treatment of neurodegenerative disorders (Haney et al., 2015). A comprehensive summary of the various drug delivery systems, polymers, and drugs employed in their formulation process and their respective applications is provided in Table 2.4.

Table 2.4: Summary of reviewed systems.

DRUG DELIVERY SYSTEM	POLYMER	DRUG	APPLICATION	References
Nanocarrier (Nanospheres)	Polyethylene glycol Polybutylcyanoarylate, Alginate, Polyethylene glycol, poly lactic –co-glycolic acid, poly lactic acid.	Doxorubicin, Clozapine, Methotrexate, Saquinavir, zidovudine	Drug molecule is delivered to the cell nucleus and thus avoids recognition by the BBB and intestinal p-gp efflux pump.	(Wong et al., 2012; Wong et al., 2006; Kuo and Chen, 2006).
Liposomes	Phospholipids and Cholesterol	Epirubicin, Cisplatin, Methotrexate, Doxorubicin	Inhibits p-gp efflux transporter by interaction with phospholipids, the system may also incorporate p-gp inhibitors.	(Krishna et al., 1999; Lee et al., 1992).
Polymer Nanoparticles	Acrylic polymers such as poly-butyl-cyanoacrylate(PBCA)	Loperamide and Doxorubicin	Bypasses the p-gp due it its nanosize.	(Wong et al., 2006)
Dendrimers	Mannosylated poly(propyl eneimine), Polyethylene glycol-poly (amidoamine)	Vinblastine, Doxorubicin and Propranolol (intestinal)	Inhibits p-gp efflux by bypassing the pump	(Gillies and Fr'echet, 2005; Cui et al., 2009; D'Emanuele et al., 2004).
Nanogels	Cationic and non- ionic polymers , NVP/NIPAM	Anti-sense phosphorothioate oligonucleotides (SODN), 5-Fluorouracil	Allows for the incorporation of p-gp inhibitors. Polysorbate coating of nanogel increases brain accumulation from 0.18 to 0.52%.	(Wong et al 2012; Yallapu et al., 2011).
Micelles	Pluronics® L61 and F127, P85	Doxorubicin, Digoxin, Paclitaxel, Ritonavir, Vinblastine	1. Inhibits p-gp efflux and also involves intracellular drug transport modification thereby avoiding the p-gp efflux pump. 2. Drug permeability in monolayered BBB model by P-gp substrates increased from 1.6 to 29 fold. No change in digoxin concentration in mdr1 knockout mice.	(Wong et al., 2012; Nasongkla et al., 2006; Mo et al., 2011).
Hydrogels	(hydroxypropyl) methacrylamide	Cyclosporine A and Doxorubicin	Inhibits the p-gp efflux transporter by incorporation of drugs such as cyclosporine A that are p-gp inhibitors.	(Kim and Chu, 2000).
Lipid Nanocapsule	PEG- HS (poly ethylene glycol- 660 hydroxy Stearate), poly-methacrylate polymers and HPMC Triglycerides of capric and caprylic acids, Solutol	Etoposide and Tacrolimus Paclitaxel	1. Inhibits p-gp efflux by incorporation of surfactant based p-gp inhibitors. 2. Paclitaxel uptake increased in MDR1 expressing cells, the half-life in brain prolonged from 21min to > 5h.	(Wong et al., 2012; Roger et al., 2010)
Self- emulsifying drug delivery systems	Poly-methacrylate polymers Medium chain triglyceride, PEG 400, Polysorbate 80, Cremophor EL Capmul MCM-C8, CremophorEL and Pluronic L-121	Paclitaxel and Tacrolimus Penfluridol (Schizophrenia therapeutic agent) Irinotecan	Inhibits p-gp efflux by incorporation of surfactant based p-gp inhibitors e.g. Tween Enhances solubilization of drug and thus effective brain concentrations. Increased oral bioavailability by P-gp modulation	(Zhuang et al., 2011; Negi et al., 2013)
Nano suspension	Pluronic® F68	Resperidone	p-gp efflux inhibition by employing polymers that inhibit the p-gp transporter, such as Pluronic®	(Muthu and Singh, 2009).

2.10. Concluding Remarks

Central nervous system (CNS) disorders such as schizophrenia are becoming increasingly prevalent, with limitations in social and physical functionality of patients being reduced. Treatment outcomes associated with schizophrenia therapy are reduced due to pharmacoresistance, which leads to a reduction in patient compliance. The P-glycoprotein (P-gp) efflux transporter located within the blood-brain barrier restricts the uptake of drugs and other molecules within the CNS; furthermore it has been implicated in the occurrence of pharmacoresistant schizophrenia. Therefore, research studies conducted in regards to the role of the P-gp transporter in CNS drug delivery prove to be a noteworthy avenue so as to improve schizophrenia treatment outcomes.

CHAPTER THREE

PRELIMINARY FORMULATION AND CHARACTERIZATION OF THE EPICHLOROHYDRIN-CROSSLINKED semi- INTERPENETRATING POLYMER NETWORK XEROGEL MATRIX

3.1. Introduction

Drug release from a suitable dosage form at predetermined times and rates, presents as a primary challenge for pharmaceutical scientists. Despite significant progress being made in the field of controlled drug release, numerous objectives still remain to be investigated for treating chronic clinical pathologies. Among the variety of natural and synthetic polymers that may be employed in formulations aimed to optimize drug release rates, polysaccharides are of particular interest. This is due to the fact that polysaccharides are abundant and have a great diversity of composition and characteristic properties that allow for tailored modifications. Furthermore, hydrogels composed of crosslinked polysaccharides have been commonly researched and evaluated for their use in novel controlled drug release dosage forms (Coviello et al., 2007). In addition, modified hydrogels, such as xerogels, which is broadly defined as an open network formed by the removal of all solvents and swelling agents from a gel, resulting in a porous structure (Rey-Raap et al., 2015) which may be exploited in the controlled and site-specific delivery of drugs.

Over the last decade, carbohydrate and biodegradable polymers have been expansively employed in the development of controlled release formulations for drugs with short plasma half-life. Among the array of polymers utilized, hydrophilic biopolymers are the most appropriate for oral applications in regard to their merits in contrast with synthetic polymers. The significance of biocompatible and biodegradable polymers is constantly increasing within the pharmaceutical industry due to their ability to form crosslinked 3-dimensional network gels. Systems derived from such reactions have been given a great amount of attention as a potential strategy to deliver drug molecules in a controlled release manner (Banerjee et al., 2010). In this respect Interpenetrating Polymer Networks (IPNs) and semi-Interpenetrating Polymer Networks (s-IPNs) have arose as novel and innovative biomaterials for drug delivery (Liu and Park, 2009).These network systems display physio-chemical properties that may be significantly different from those of the macromolecular constituents. Polymer network properties can be modified and tailored by the type of polymer and its respective concentration, by the crosslinking method employed as well as the preparation procedure utilized (Matricardi et al., 2013).

IPNs are defined as combinations of two or more polymer networks synthesized in juxtaposition (Sperling et al., 1994). The IUPAC definition for an IPN is "*A polymer comprising two or more networks which are at least partially interlaced on a molecular scale but not covalently bonded to each other and cannot be separated unless chemical bonds are broken. A mixture of two or more preformed polymer networks is not an IPN"* the last statement of this definition focuses on the point that the difference between an IPN and a blend. The polymer entanglement of crosslinked polymer in an IPN results in miscibility as compared to the incompatible polymer blends (Matricardi et al., 2013). Types of IPNs are outlined in Figure 3.1.

Semi-IPNs differ from IPNs in the sense that they comprise of one linear polymer entrapped within the network of another polymer. The IUPAC definition for an s-IPN is "*A polymer comprising one or more linear or branched polymer(s) characterized by the penetration on a molecular scale of at least one of the networks by at least some of the linear or branched macromolecules"* s-IPNs are distinguished from IPNs due to the fact that its constituent linear or branched polymers can be separated from the constituent polymer network without breaking chemical bonds (Chikh et al., 2011).

Table 3.1: Summary of the common advantages and features of IPNs (Banerjee et al., 2010).

Advantages of IPNs	***Characteristic Features of IPNs***
1) When an IPN gel is synthesized from two polymers at a specified temperature, the physical phase separation amid the individual polymers would be virtually improbable due to the zero-viscosity of the gel.	1) Undergoes swelling in solvents without dissolving.
2) IPN formulations are good candidates in taking advantage of synergistic characteristics from individual polymers involved in its formulation process.	2) Systems formed from IPNs benefit from the properties that are representative of each polymer employed.
3) IPNs have been shown to improve the phase stability of the resultant biomaterial.	3) Polymer comprising two or more polymer networks which are partially interpenetrating on a molecular level but are not necessarily covalently bonded to each other and may or may not be separated unless chemical bonds are broken depending on the type of IPN formed.
4) IPNs enhance the mechanical properties of the resultant system.	4) IPNs have been indicated in the design and development of controlled release drug delivery systems.
5) Any present thermodynamic incompatibility may be overcome via interlocking of network segments, which is produced by mixing.	

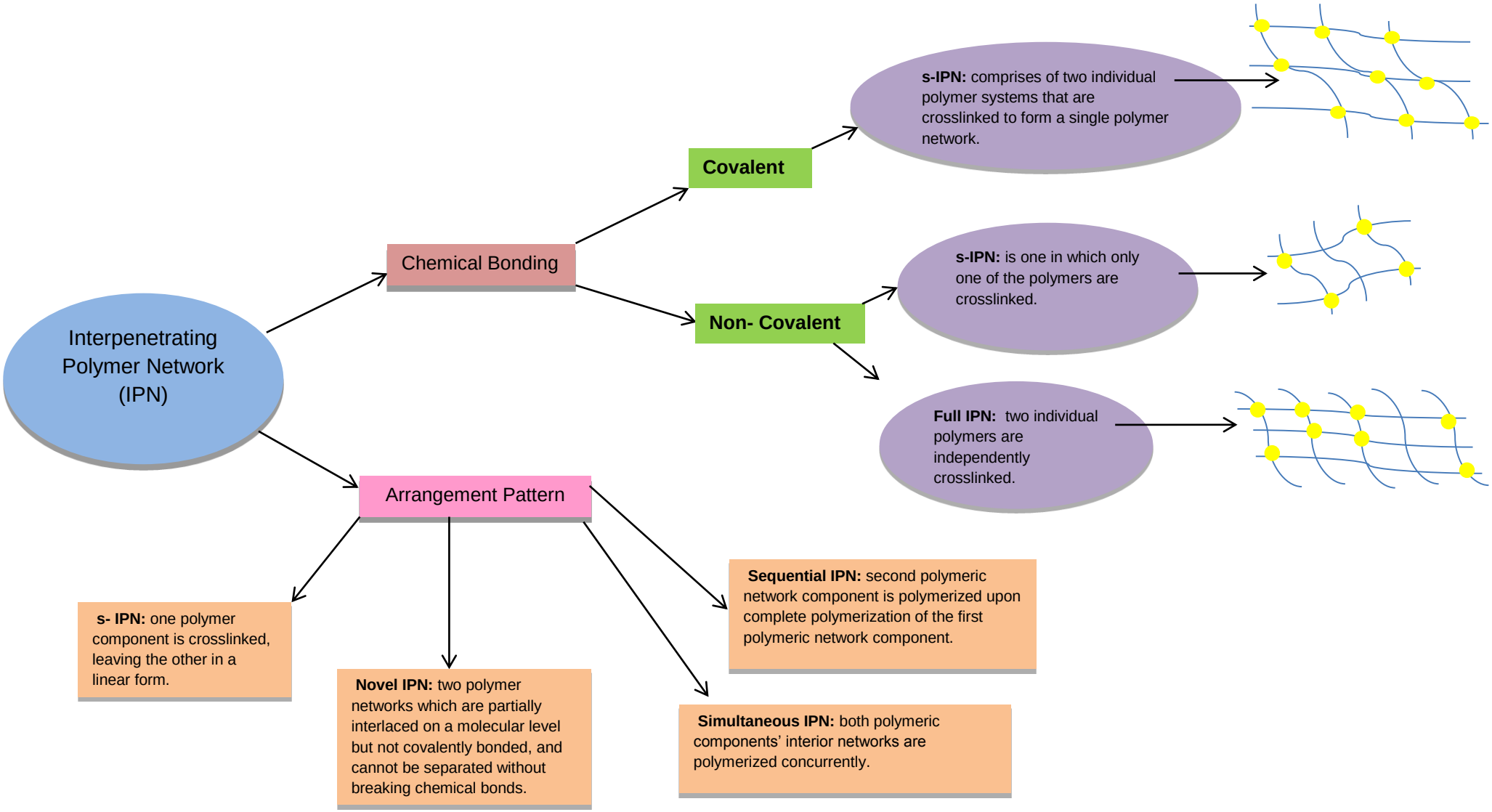


Figure 3.1: Types of IPNs (Chikh et al., 2011; Banerjee et al., 2010).

IPN based drug delivery systems are specifically designed to deliver drugs at a predetermined rate with minimal fluctuations for a desired duration.

-*Tablets*

IPNs formulated as oral dosage forms such as tablets has displayed great potential for controlled drug release. IPNs prepared from chitosan and Carbopol polymer complexes may be used as a sustained release matrix tablet. The solid structure of the IPN based tablets has shown great *in vivo* drug release potential via blending of hydrophilic polymer complexes with a hydrophobic polymer (Ghada and Mina, 2008).

-*Sheets/Films*

Polymeric sheets or films are commonly prepared via solvent casting methods. Their applications vary from transdermal to buccal drug delivery. A polymeric biomaterial comprising an interpenetrating network of a polyol (allyl carbonate) and an epoxy resin prepared via polymerizing the poly (allyl carbonate) by radical initiation and partially polymerizing an epoxy resin forming solution via acid catalysis has been applied as a wound dressing (Banerjee et al., 2010).

-*Sponges*

IPN based sponges have the ability to easily absorb large amounts of tissue exudates, allow for smooth adherence to a wet wound site, while keeping the wound site dry and providing protection against physical harm and secondary bacterial infection. IPN sponges have been employed successfully in the treatment of severe burns as well as a dressing for a wide array of other wound types (Kim et al., 2007).

-*Hydrogel*

Hydrogels are commonly used as drug carriers due to the ease of manufacturing and administration. The advantage of hydrogels for their clinical applications is their ability to produce a large surface area. The combination of natural and synthetic polymers provides mechanical stability and biological acceptance, in addition, acquiring synergistic characteristics of both polymers (Suri and Christine, 2009).

3.1.1. Preliminary formulation design

The rational identification of a candidate system for further optimization was the elemental focus of the current chapter. The subsequent experimental studies were conducted to provide a logical comparison of the effect of crosslinking on the chemical structure of the formulated xerogel, textural analysis of the xerogel matrix, surface morphological analysis to determine the resultant

surface structure, and dissolution studies of the various preliminary formulations developed; in addition, to determine their respective potential in designing a targeted sustained release drug delivery system.

Preliminary formulation studies involved, evaluating the selected polymers for their chemical structure, morphological surface structure, tensile strength and dissolution characteristics. Further modifications and inclusion of excipients was then undertaken to develop a candidate system. The identification of variables with upper and lower limits was paramount for further optimization of the s-IPN xerogel component of the ODLS.

3.2. Materials and Methods

3.2.1. Materials

Biocompatible and biodegradable polymers investigated included poly (ethyleneoxide) (PEO) (Polyox™, WSR303) and Gellan gum (GG) (Gelzan™CM) obtained from Sigma Aldrich (Pty) Ltd. (St Louis, MO, USA). Sulpiride employed as the model drug and epichlorohydrin (EPI) 99% used as a crosslinking agent were purchased from Sigma Aldrich (Pty) Ltd. (St Louis, MO, USA). Lecithin sourced from Merck (Pty) Ltd. (Modderfontein, South Africa) was used as a formulation excipient to enhance bioavailability. Carboxymethylcellulose sodium (CMC) and magnesium stearate utilized within the tablet forming process were purchased from Sigma Aldrich (Steinham, Germany). All other reagents employed were of analytical grade and used without further purification. De-ionized water was obtained from a Milli-Q water purification system (Milli-Q, Millipore, Billerica, MA, USA).Phosphate buffered saline (PBS) was prepared using sodium hydroxide (NaOH, Mw=40.00g/mol) and sodium chloride (NaCl, Mw=58.44g/mol) obtained from Saarchem (Wadeville, Gauteng, South Africa), hydrochloric acid (HCl, 32%w/v) purchased from Rochelle Chemicals (Johannesburg, South Africa) and potassium dihydrogen phosphate (KH2PO4, Mw=136.09g/mol) obtained from Riedel-de Haen (Sigma-Aldrich Laborchemikalein GmbH, Germany) in double-deionized water (Milli-Q System, Millipore, Bedford MA, USA).

3.2.2. Polymer blending and crosslinking

Polymeric solutions of poly (ethyleneoxide) (Polyox®), 1-2.5 %$^{w}/_{v}$ and gellan gum 0.5-1%$^{w}/_{v}$ were prepared using deionized water (Rowe et al., 2006). The Polyox® and Gellan gum solutions were combined in 1:4 ratios and allowed to stir on a magnetic stirrer for 30 minutes until homogenous. Thereafter 5M NaOH (1.2mL) was added to the gel and stirred till homogenous, after which epichlorohydrin (EPI) (0.4-0.8 %$^{v}/_{v}$), a crosslinking agent, was added drop wise to the blend using a syringe. Formulation compositions are listed in Table 3.1. The solution was then allowed to stir for a further 3 hours. Lecithin, the selected formulation excipient was prepared by dissolving lyophilized soybean lecithin in deionized water. The desired quantity of the lecithin solution (1%$^{v}/_{v}$) was added to the crosslinked s-IPN xerogel while undergoing continuous stirring (da Fonseca et al., 2008).

Table 3.2: Compositions of pilot study formulations.

PRELIMANRY FORMULATION COMPOSITIONS
PF 1: 1%$^{w}/_{v}$ GG, 2%$^{w}/_{v}$ PEO, 0.4%$^{v}/_{v}$ EPI
PF 2: 1% $^{w}/_{v}$ GG, 2.5% $^{w}/_{v}$ PEO, 0.8% $^{v}/_{v}$ EPI
PF 3: 0.5% $^{w}/_{v}$ GG, 2% $^{w}/_{v}$ PEO, 0.4% $^{v}/_{v}$ EPI
PF 4: 0.5% $^{w}/_{v}$ GG, 2.5% $^{w}/_{v}$ PEO, 0.8% $^{v}/_{v}$ EPI
PF 5: 1% $^{w}/_{v}$ GG, 1% $^{w}/_{v}$ PEO, 0.8% $^{v}/_{v}$ EPI
PF 6: 1% $^{w}/_{v}$ GG, 1% $^{w}/_{v}$ PEO, 0.4% $^{v}/_{v}$ EPI

3.2.3. Fabrication of xerogel polymer matrix system

The homogenous s-IPN xerogel was then allowed to stir at a high speed on a magnetic stirrer, to allow for the crosslinked s-IPN xerogel to sufficiently blend with the lecithin. After which it was removed and precipitated in a small volume of acetone for approximately 10 minutes. The precipitated xerogel was then placed on a glass petri dish and dried in laboratory fumehood at room temperature overnight. The dried xerogel was then crushed into a powder using a mortar and pestle. The xerogel powder was then mixed with surfactant (1.5mg magnesium stearate),

which allows for the stabilization of the polymer particles (Bassett and Hamilec, 2009), carboxymethylcellulose sodium a tablet filler, and sulpiride the model drug to form the porous xerogel-polymer drug loaded matrix. The porous xerogel matrix system was then compressed into an oral dosage form (tablet) using *a* Carver Tablet Compressor (model 3851-0), the tablets were 0.9×0.9cm in size.

3.2.4. Determining the upper and lower limit variables of the formulation required for input into the Central Composite Design

Following the identification of the most appropriate polymer combination to be utilized in the fabrication of the s-IPN xerogel matrix drug delivery system, upper and lower limits of the formulation variables were determined for input into a Central Composite Factorial Design. Determination of the variables involved combining the polymers in various ratios with corresponding variances in crosslinker concentration followed by tablet compression as detailed in *Chapter 3, Section 3.2.1 and 3.2.2.,* and thereafter assessing whether the formulations satisfied the following criteria:

- Demonstrated physical properties that could withstand and undergo tableting.
- Demonstrated good physiomechanical characteristics appropriate for oral dosing.
- Displayed morphological structure conducive to sustained drug delivery.
- Polymers were successfully crosslinked to form the s-IPN xerogel.
- Controlled drug release over the desired period of time (24 hours).

3.2.5. Validation and determination of chemical transitions upon crosslinking

The FTIR spectra of PEO, GG and the crosslinked s-IPN xerogel were recorded using an FTIR Spectrophotometer (Perkin Elmer Spectrum 100, FT-IR Spectrometer) fitted with a universal ATR Polarization Accessory (Perkin Elmer Ltd., Beconfield UK). Wavelengths were recorded between 4000 and 650cm^{-1} and FTIR spectrums of absorbance and % transmittance against distance was obtained.

3.2.6. Identification of optimization variables for degree of swelling and erosion

Evaluation of the degree of swelling and erosion of the s-IPN xerogel was conducted. Respective pre-formulation samples were weighed and placed in 250mL beakers containing 200mL potassium phosphate buffer (pH 6.8; 37˚C) and allowed to swell over a 24 hour period. At predetermined time intervals tablets were removed from the buffer and weighed after removing

surface water with absorbent tissue paper on a calibrated electronic scale. The mean % swelling and erosion were calculated.

3.2.7. Surface morphological analysis

SEM was employed in determining the surface morphology of crude PEO and GG, as well as evidence of the synthesis of an s- IPN xerogel within the crosslinked formulations with the aid of the generated microscopic images. It further assisted in identifying the differences in physical morphology and characteristics of the crude polymers as compared to the crosslinked xerogel. Dried xerogel samples before tableting and native polymers were placed on steel studs and sputter coated with carbon and gold palladium shadowing using the Phenom™ G2 Pro SEM (FEI Company, and Hillsboro, Oregon, USA) by employing various magnifications.

3.2.8. Determination of the physiomechanical properties of the s-IPN xerogel matrix system via textural analysis

The Brinell hardness test was employed to determine the strength of tablets where a load of 5kg was applied to the surface of the tablets via a steel indenter of 3.175mm in diameter. Thus the diameters of the resultant indentation on the surface of the tablets were measured and the Brinells Hardness Number (BHN) was calculated using the following equation:

$$Brinell\ Hardness\ Number = 2F/(\pi D(D - (D^2 - d^2)$$

Equation 3.1

Where, F=load on the indenting tool (force generated in kg), D=diameter of the spherical probe indenter (3.175mm), and d=diameter at the rim of the impression made (depth 0.5mm) (Choonara et al., 2006).

By plotting a force vs. time graph resilience was calculated when a strain of 10% is applied with the use of the following equation:

$$Resilience = \left(\frac{Area\ 2:3}{Area\ 1:2}\right) \times 100$$

Equation 3.2

3.2.9. Construction of calibration curve for the determination of sulpiride release from the s-IPN xerogel matrix

Employing Ultraviolet (UV) spectroscopy and a sequence of known concentrations (0.2-1mg/mL) of sulpiride in Phosphate Buffered Saline (PBS) (pH 6.8; 37˚C), a calibration curve was constructed. The linear curve was plotted with use of the detected absorbance of sulpiride as the dependent variable and the concentration of sulpiride as the independent variable. A statistical illustration of the degree at which the function relates the set of values (R^2 value) was calculated for the curve.

3.2.10. Identification of optimization variables via *in vitro* drug release studies

Dissolution studies were carried out utilizing a USP type II apparatus (Caleva, model 7ST) at 50rpm and 37˚C in 900mL of potassium phosphate buffer (pH 6.8) with the addition of a stainless steel mesh ring, which fits under the paddle into the lower part of the standard dissolution vessel. 5mL of dissolution medium was withdrawn manually at predetermined time intervals during the 24 hour study and replaced with an equal volume of fresh dissolution medium to ensure sink conditions were maintained. The samples were then analyzed for drug release via ultraviolet spectrometry (WinAspect Spectro-analytical software, Analytik Jena AG), at a wavelength of 291nm employing a calibration curve obtained for the drug (Strübing et al., 2008).

3.3. Results and Discussion

3.3.1. Analysis of chemical transitions upon crosslinking

Pilot Fourier Transform Infrared Spectroscopy (FTIR) studies were conducted to determine the success of crosslinking poly (ethyleneoxide) (PEO) with gellan gum (GG), a novel concept. Thus a preliminary experiment was conducted by formulating a 1% PEO solution and a 1% GG solution, these were then combined and crosslinked using epichlorohydrin as described in *Chapter 3, Section 3.2.2*. FTIR is defined as being the absorption of electromagnetic radiation through a sample and the vibrations observed due to specific chemical bonds present. As new bonds are formed there is the appearance of new bands or shifts in bands that suggest chemical bonds are being formed or broken. FTIR is useful in that it can provide information about the chemical bonding and change in chemical nature of a formulation due to crosslinking reactions.

Based on visual observation it can be seen that the system is stable and homogenous allowing for a well-structured gel system. FTIR has shown that GG and PEO have similar bands; however gellan lacks the aromatic C-H bond which is still present in the crosslinked gel, the shift in bands

of saturation also shows that bonds have been broken and new bonds created between GG and PEO.

FTIR was then conducted on both crude polymer solutions and on the crosslinked formulation to determine the success of the crosslinking procedure. The FT-IR spectra depicted in Figure 3.2d of PEO displayed functional groups present, such as that of O-H functional groups characteristic of alcohols in a range of 3200-3600cm^{-1}, and C≡C stretching depicted at wavenumber range of 2100- 2260cm^{-1}. A broad band at 2850-2960cm^{-1} relating to C-H stretching in alkane groups is observed as a characteristic functional group of GG, seen in Figure 3.2a, in addition, all preliminary formulations display this band (Coates, 2000).

Results in Figure 3.2 below depicted that there were shifts in the peaks relating to double C=C bonds (alkenes) at 1640- 1680cm^{-1} and the addition of an aromatic ring corresponding to C-H group at 675- 870 cm^{-1} (aromatic ring/ alkenes 675-1000cm^{-1}), thus the shifts in peaks and the additional aromatic structure prove that crosslinking was successful and the PEO and GG did form new bonds.

The introduction of amine groups was found in formulations that consisted of a higher percentage crosslinker, at a wavelength of 3360.17cm^{-1} (Coates, 2000). Preliminary formulations also showed C=C stretch at a wavelength of 1500cm^{-1} (Coates, 2000), which corresponds to a conjugational asymmetrical stretch, occurring when the ratio of polymers is 1:2 and crosslinker is at an intermediate density.

The results that were received has shown that the crosslinking process has been successful with the appearance of new bonds that were clearly depicted by the bands displayed in FTIR, this provides a novel approach and will allow for the enhanced bioavailability of sulpiride by combining the effects of polymers.

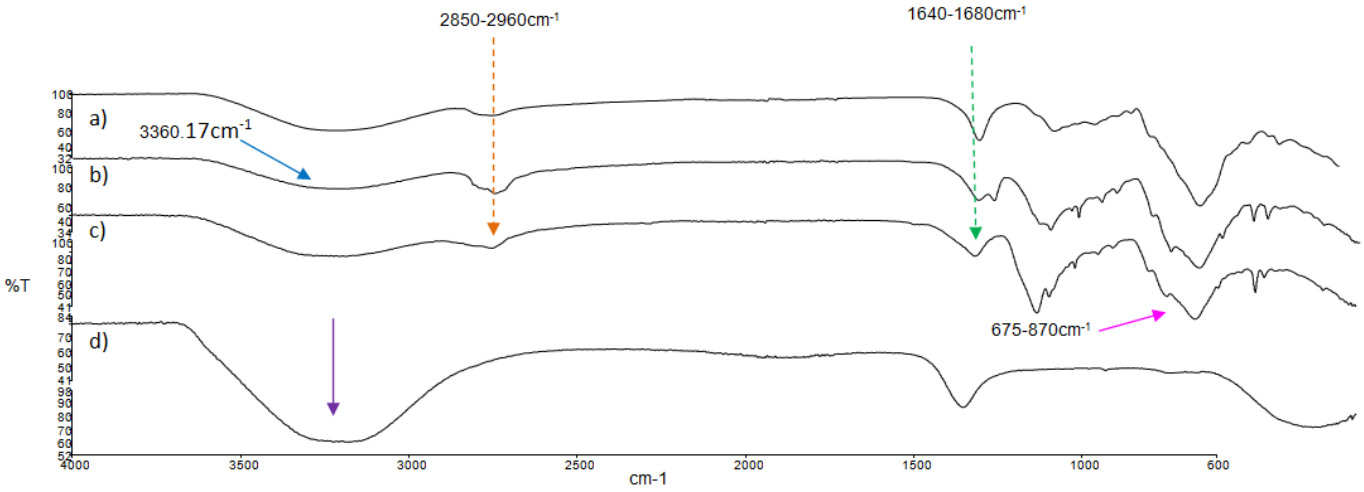


Figure 3.2: FTIR spectra of a) gellan gum, b) PF 5, c) PF 1 and d) PEO.

3.3.2. Pre-formulation evaluation of the swelling and erosion characteristics of the s-IPN xerogel

The mean percentage swelling and erosion of the preliminary s-IPN xerogel samples were investigated by observing the variation in sample weight over a predetermined time interval; Figure 3.3 shows the mean percentage swelling and erosion respectively. All formulations displayed appreciable swelling and erosion, it was noted that preliminary formulations with increased polymer concentrations had a corresponding rise in swelling and erosion. On the other hand, a lower concentration of crosslinking agent led to an increase in percentage swelling. It has been indicated that swelling is controlled by the rate of hydration when in contact with aqueous medium. Therefore, the degree of swelling and erosion affect drug release kinetics, due to drug release being delayed with an increase in swelling of the delivery system (Sriamornsak et al., 2007).

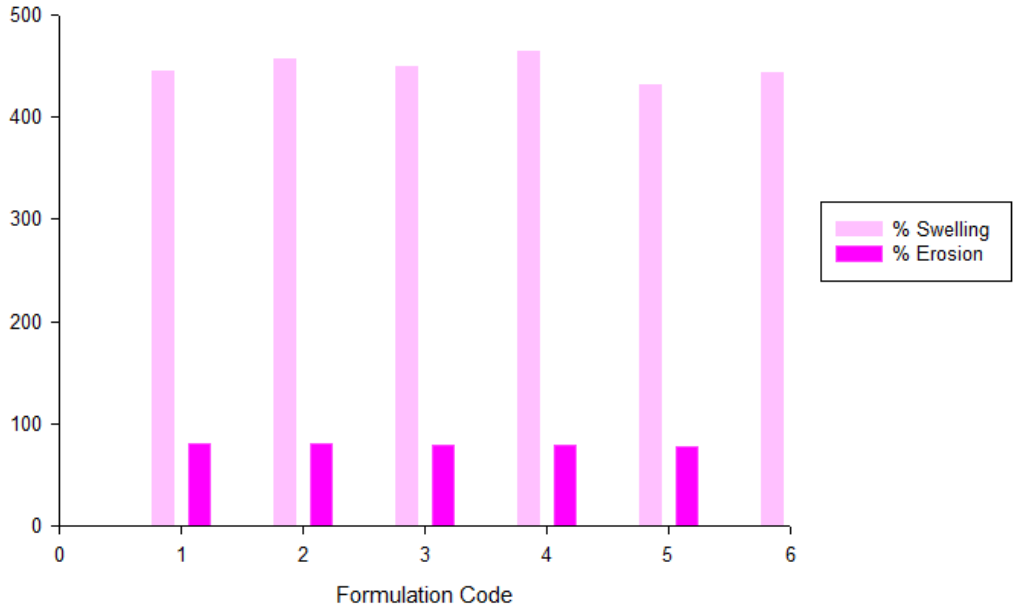


Figure 3.3: Illustration of the % swelling and erosion for all preliminary formulations.

3.3.3. Assessment of surface morphological characteristics

The surface morphology of PEO, GG, and preliminary formulations are shown with the use of scanning electron microscopy (SEM) imagery in Figure 3.4. The SEM micrograph of pure PEO (Figure 3.4a) shows distinct tightly clumped polymer particles with an uneven surface structure and absence of pores, conversely SEM images of GG (Figure 3.4b) indicate clear polymer "ribbons" with smooth surfaces apart from the occasional occurrence of slight ridges. Comparatively, SEM micrographs of preliminary crosslinked s-IPN xerogel formulations (Figure 3.4c/d) display a definite modification in surface structure. They exhibit a vastly porous surface morphology, which proves the crosslinking reaction to be effective and the subsequent formation of an s-IPN xerogel. s-IPN crosslinking of the respective polymer in effect forms the porous structure, in addition to this the drying procedure allows for the fabrication of the xerogel aspect which also involves the formation of air filled pores. The overall porosity of the resultant s-IPN xerogel formulations permits sustained release of bioactive from within the pores of the polymer network.

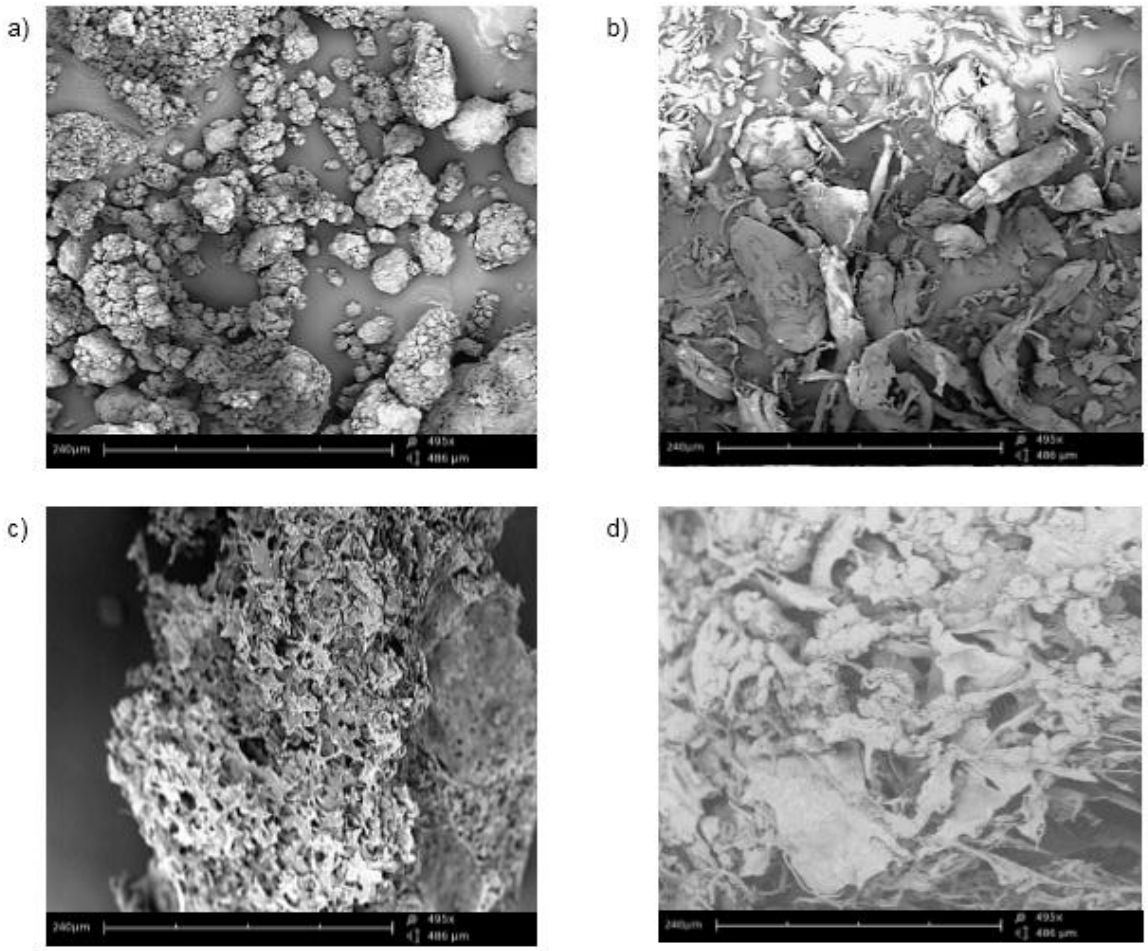


Figure 3.4: SEM micrographs of a) PEO, b) GG, c) PF 5 and d) PF 1.

3.3.4. Evaluation of textural analysis studies

Textural analysis data graphs were utilized to evaluate the physiomechanical characteristics of the preliminary crosslinked s-IPN xerogel matrix tablets when a uniaxial force of compression is applied. From the graphs of force vs. distance obtained it was observed that the resultant curves displayed sharp peaks which indicate that the s-IPN xerogel matrix offers a greater degree of resistance to the force applied.

The mechanical strength of the s-IPN xerogel matrix was further illustrated via assessment of the brinells hardness number as seen in Figure 3.5. It was observed that the brinells hardness number is proportional to the density of crosslinking and polymer ratios, thus the strength of the matrix was increased with a corresponding increase in crosslinker concentration and a higher overall polymer concentration.

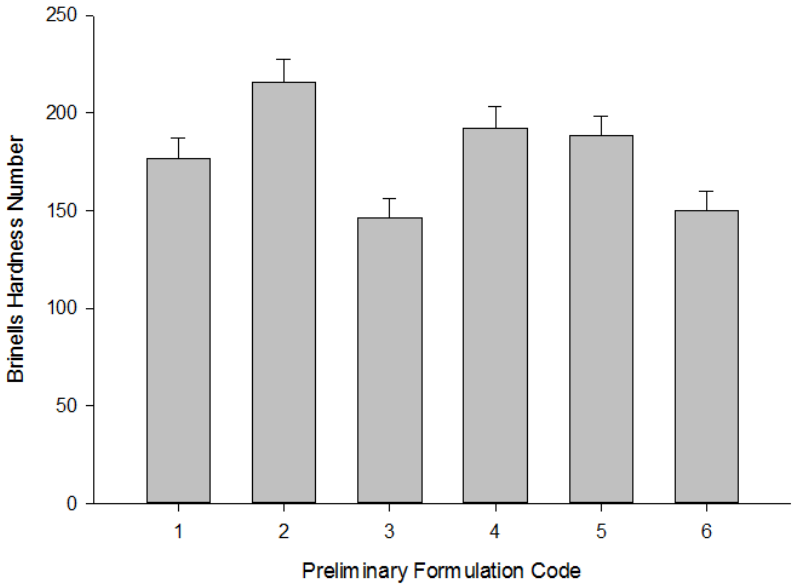


Figure 3.5: Graphical illustration of Brinell hardness numbers and respective standard deviations for preliminary formulations.

Furthermore, the physiomechanical properties of the preliminary formulations were evaluated with the use of the percentage resilience derived from the force vs. time textural analysis graphs as shown in Figure 3.6. Percentage resilience is yet another parameter employed to determine the mechanical strength of polymer systems, it has been indicated that the percentage resilience of the s-IPN xerogel matrix is directly proportional to the polymer concentration ratio and the degree of crosslinking. It can thus be seen that preliminary formulations with a greater polymer ratio and crosslinking density displayed a corresponding increase in matrix resilience; this may be accredited to the greater network formation, leading to a highly structured interpenetrating polymer system. Therefore, in conclusion all preliminary formulations displayed satisfactory physiomechanical strength; however those with higher polymer and crosslinker concentrations were marginally enhanced.

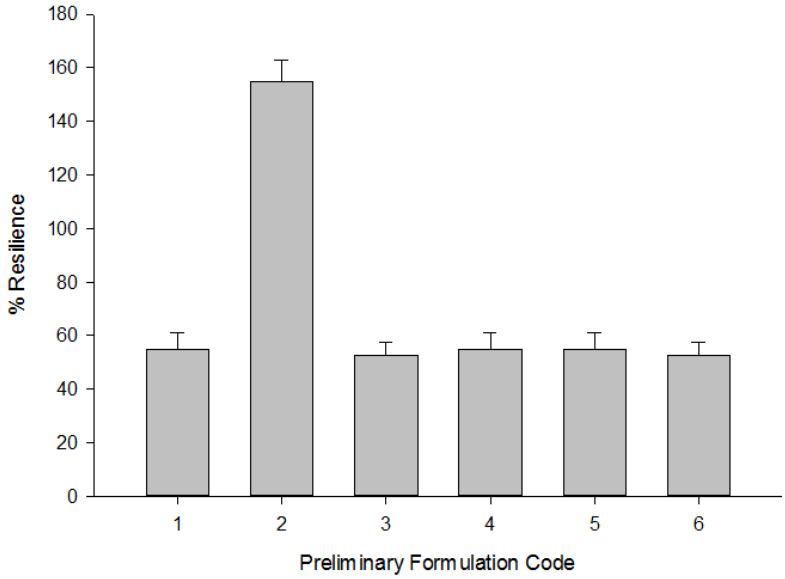
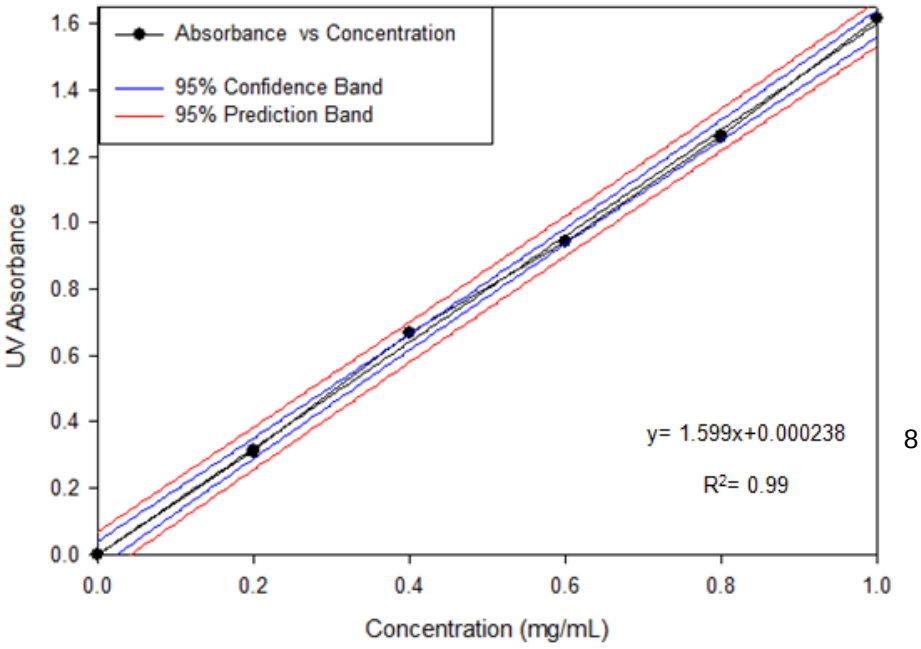


Figure 3.6: Percentage resilience and respective standard deviations of the respective pilot study formulations.

3.3.5. Construction of a calibration curve for the ultraviolet spectrophotometric determination of sulpiride

Utilizing UV spectroscopy, it was established that sulpiride exhibits a maximum wavelength at λ_{300}, consistent with published literature on the absorption peak of sulpiride being at 300nm (Parikh et al., 2010; Phapale et al., 2010). Using a series of known concentrations (0.2-1mg/mL) of sulpiride in PBS, a calibration curve at $\lambda_{300}$was conducted (Figure 3.7). The linear curve was plotted with the observed absorbance of sulpiride as the dependent variable and the concentration of sulpiride as the independent variable (Figure 3.7). The obtained R^2 value of the calibration curve was 0.99 (Figure 3.7), indicating a perfect correlation.



8

Figure 3.7: Calibration curve of sulpiride in PBS at λ_{300}.

3.3.6. Assessment of *in vitro* drug release

So as to determine the release of drug from the crosslinked s-IPN xerogel matrix, dissolution studies were conducted in simulated intestinal conditions as described in *Chapter 3, Section 3.2.10*. The fractional release vs. time graphs for the preliminary s-IPN xerogel matrix formulations are shown in Figure 3.8.

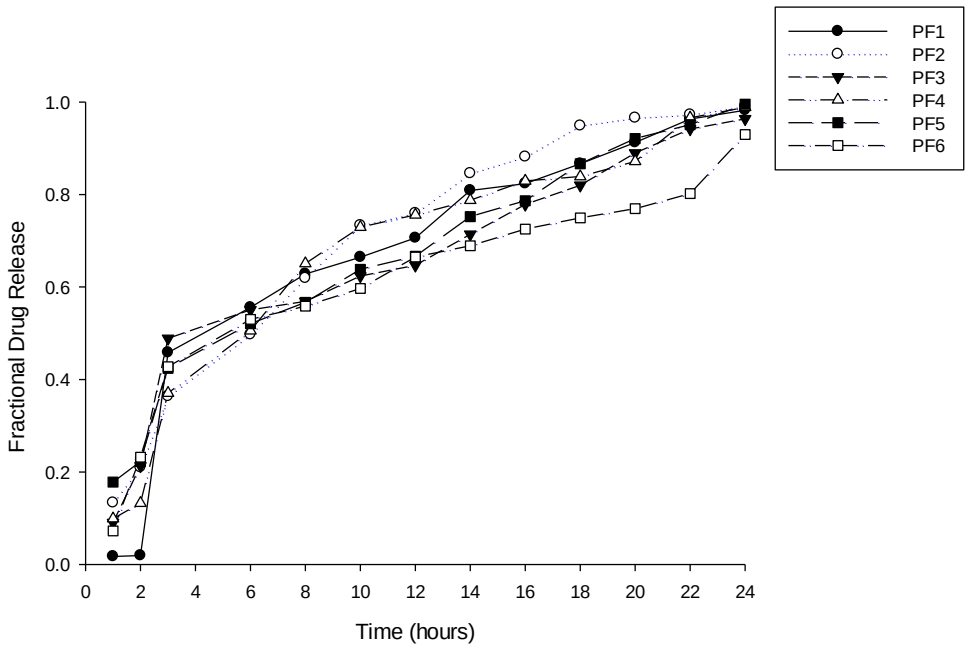


Figure 3.8: Fractional release profiles of preliminary formulations.

From the drug release profiles it can be seen that all preliminary formulations provided sustained drug release over the predetermined 24 hour test duration, it can clearly be seen that variations on polymer ratios and crosslinker density have an effect on the resultant drug release profiles. In particular, PF 6 displays an initial lag phase which may be attributed to the possible free uncrosslinked polymer chains, which swell extensively and uncontrollably leading to a delay in drug release as drug becomes entrapped within the matrix due to a thick outer gel layer. All remaining formulations display slight variances in drug release pattern; however they all perform effectively in prolonging drug release over the desired period due to their porous structure, allowing for entrapment of drug within these polymer network pores and thus controlling drug release.

3.3.7. Determining the upper and lower limits of the formulation variables required for input into the Central Composite Design

Subsequent to identification of the polymer combinations for the s-IPN xerogel matrix, the upper and lower limit variables of the formulations was determined. The resultant variables are illustrated in Table 3.2. The limits were determined via ensuring that the formulated tablets met the criteria identified in *Chapter 3, Section 3.2.4.*

Table 3.3: The identified variables and their corresponding upper and lower limits for input into the Central Composite Design.

Polymer	**Lower Limit (%w/v)**	**Upper Limit (%w/v)**
GG	0.5% - Anything <0.5% did not form a sufficiently viscous gel and thus could not be used in the formation of a xerogel.	1% - Formulations comprised of >1% formed viscous solutions that resulted in a solid mass.
PEO	1% - solutions of <1% were viscous but not of an appropriate consistency to be crosslinked to form a xerogel and could not be precipitated.	2.5% - Formulations containing > 2.5% was difficult to dissolve and resulted in solutions that presented with hydrated clumps and were too sticky to work with.
Crosslinker		
EPI	0.4% - crosslinking with < 0.4% was not successful. When precipitated, PEO would dissolve out of xerogel into acetone.	0.8% - formulations comprising >0.8% formed highly brittle xerogels that did not withstand the tableting process.

3.4. Concluding Remarks

Preliminary studies led to the rational identification of the formulation variables that were most appropriate for the development and further optimization of the s-IPN xerogel matrix component of the ODLS. Due to their ability to control drug release and novelty in regard to the crosslinking reaction, GG and PEO were chosen as the crude polymers to undergo crosslinking for the formation an s-IPN xerogel.

An essential outcome of this chapter was to ensure that the fabricated s-IPN xerogel was successfully crosslinked by the use of epichlorohydrin, that controlled drug release was achieved in a sustained manner, and that good mechanical properties were provided for oral administration. This chapter functioned to identify the candidate formulation range which resulted in the identification of 3 variables, with their corresponding upper and lower limits, for input into a Central Composite Design. The Central Composite Design, which is detailed in Chapter 4, was conducted with the purpose of further optimization of the s-IPN xerogel matrix component of the ODLS.

CHAPTER 4

FABRICATION AND STATISTICAL OPTIMIZATION OF THE NOVEL EPICHLOROHYDRIN-CROSSLINKED semi-INTERPENETRATING GG-PEO XEROGEL NETWORK MATRIX TABLET

4.1. Introduction

Formulation optimization based on statistical approaches, utilizing a systematic Design of Experiments (DoE), is broadly practiced to enhance the outcomes of formulation design in the development of Drug Delivery Systems, due to it being an effective and cost efficient tool that is able to afford the most optimal formulation in response to the most desired formulation characteristics (Singh et al., 2004; Singh et al., 2005). So as to ensure the efficacious implementation of an experimental design, the experimental objectives and the parameters to be investigated need to be clearly defined. By means of preliminary studies, detailed in *Chapter 3*, a prototype formulation led to the identification of independent variables (i.e. polymer and crosslinker concentration) which influenced the measured responses (i.e. drug release, mean % swelling and mean % erosion).

To achieve the desired characteristics and advantages of a Drug Delivery System, it is necessary to determine whether factors involved in the formulation process will impact characteristics of the resulting formulation. In the course of the preliminary studies, one or more procedural formulation process variables or factors were intentionally varied to determine the effect the variance may have on the measured responses (Singh et al., 2004; Singh et al., 2005). Outcomes indicated that varying the components, specifically, the polymer and crosslinker concentration of the system resulted in alterations that would influence drug release properties of the system. However, employing this methodology in formulation design is a costly and time-consuming process and obtaining an optimized formulation is not a certainty. In order to overcome this limitation of formulation design, the use of a statistically sound experimental Central Composite Design may be employed; which is an optimization strategy that exploits lesser experimental runs, has a reduced level of time–consumption and produces an accurate optimized formulation via systematic and methodical approach.

The Response Surface Methodology (RSM) was elected in implementation of the design strategy as factors affecting formulation characteristics were identified in *Chapter 3*, thereby facilitating the optimization procedure. The ultimate objective of utilizing the RSM was to enable the identification

of the most appropriate combination of formulation components that would accomplish an optimal formulation for the s-IPN xerogel matrix component of the ODLS.

RSM is frequently used in Central Composite Designs to aid researchers in the identification of optimal framework of experimental factors which provide the maximum or minimum value of the measured response. Fundamentally RSM is an assemblage of both mathematical and statistical strategies for empirical prototype assembly grounded on literal experiments or experimental derived observations (He et al., 2005; Raissi and Farsani, 2009).

Based on the preliminary results obtained from *Chapter 3*, the formulation component (input variables) that influenced the drug release characteristics, degree of crosslinking, and physiomechanical properties of the formulation (measured responses) were identified in conjunction with their upper and lower limits. Factors with their corresponding factor levels were selected for the s-IPN xerogel matrix component of the ODLS so that a mathematical model was generated. Polymers, crosslinking agent, and the model drug employed in the system design are outlined below:

Gellan gum (GG), a natural polysaccharide with low toxicity, was employed as one of the polymer components of the crosslinked s-IPN xerogel matrix. It is a high molecular weight hydrophilic anionic deacetylated polysaccharide which is produced by the fermentation of Shingomonas Elodea; the organism is aerobic, gram negative, and non-pathogenic. Its chemical structure consists of four linked monosaccharides, one molecule of rhamnose, one molecule of glucuronic acid, and two glucose molecules (Singh et al., 2011). GG functions as a gelling agent in many foods and pharmaceutical products. The hydrophilic nature of GG has been exploited in the present study to ensure sustained drug release via means of water penetration, dissolution, polymer swelling and erosion. Hydrophilic polymers have been extensively employed in controlled drug delivery (Du¨rig and Fassihi, 2002). The concentration range selected for optimization of the s-IPN xerogel component of the ODLS was based on preliminary studies detailed in *Chapter 3* and was determined to be 0.5-1g.

Poly (ethyleneoxide) (PEO), a non-ionic water soluble polymer, was employed as the other polymer components of the crosslinked s-IPN xerogel matrix. Research has shown it is capable of retarding the release of drugs and thus its use in controlled release formulations is widespread. The mechanism of drug release from poly (ethyleneoxide) based delivery systems are centered on swelling and erosion of the polymer. The chemical structure consists of an epoxide ring, two corners of the molecule have –CH2- links, with the third corner having oxygen. These poly (ethyleneoxide) water soluble polymers may be crosslinked to form gels with great water retention

properties. Poly (ethyleneoxide) is non- toxic and biodegradable and thus well suited for use within the pharmaceutical scope of drug delivery systems (Cappello et al., 2006). Its use in controlling drug delivery has been exploited in the present study to ensure sustained release of the selected bioactive over a 24 hour period.

Epichlorohydrin (EPI), an epoxide agent, was used as a crosslinking agent for the formation of an s-IPN between GG and PEO. It is colorless sweet chloroform smelling liquid at room temperature. It is used in the production of many synthetic materials as well as in the crosslinking of starch and in the production of pharmaceutical products (National Toxicology Program, 2011; Kittipongpatana and Kittipongpatana, 2013).

Sulpiride (5- (aminosulfonyl)-N- f1-ethyl-2-pyrrolidinylgmethyl-2-methoxybenzamide) is a known selective dopamine D2 antagonist, with both antipsychotic and antidepressant action, it displays poor aqueous solubility (Chiba et al., 2011; Sigma Aldrich, MDS (±) Sulpiride, Germany).

4.2. Materials and Methods

4.2.1. Materials

Gellan gum (GG) (Gelzan™CM), poly(ethyleneoxide) (PEO) (Polyox™, WSR303), (±) sulpiride, epichlorohydrin (EPI) 99%, carboxymethylcellulose sodium (CMC) and magnesium stearate were purchased from Sigma Aldrich (Steinham, Germany), while acetone (Analytical grade) and sodium hydroxide (assay min. 97%) were purchased from Merck (Darmstadt, Germany). All other reagents employed were of analytical grade and used without further purification.

4.2.2. Construction of a Randomized Central Composite Design for the optimization of the s-IPN xerogel matrix component of the ODLS

A model independent approach (Minitab® V15, Minitab Inc. PA, USA) was employed for optimization of the s-IPN xerogel. The input factors or independent variables were the concentration of GG: PEO and concentration of the crosslinking agent EPI. These were studied at three levels each, and the DoE generated 15 experimental runs (formulations). Statistical optimization was employed to ascertain the ideal combination of polymers and crosslinker required to achieve the desired drug release profile, swelling, erosion and matrix resilience efficacies. Table 4.1 summarizes the derived factor combinations of the 15 experimental runs studied and their conversion of the coded levels to the experimental units utilized during the study. The coded variables chosen for the statistical design were; total Mean Dissolution Time (MDT), mean % swelling and mean % erosion. Whereas, parameters for the design were set as the concentrations of PEO $\%^{w}/_{v}$, epichlorohydrin (mL), GG (g).

Table 4.1: Box-Behnken design template for the statistically derived 15 s-IPN xerogel formulations and their respective chemical compositions.

F#	PEO Concentration ($\%^{w}/_{v}$)	GG (g)	EPI-Crosslinker Volume (mL)
F1	2.5	1	0.6
F2	2.5	0.75	0.8
F3	1.75	0.75	0.6
F4	1.75	0.75	0.6
F5	1	0.75	0.8
F6	1	1	0.6
F7	1.75	1	0.4
F8	1	0.5	0.6
F9	1.75	1	0.8
F10	1.75	0.5	0.8
F11	1	0.75	0.4
F12	1.75	0.75	0.6
F13	2.5	0.5	0.6
F14	1.75	0.5	0.4
F15	2.5	0.75	0.4

4.2.3. Synthesis of crosslinked s-IPN xerogel

s-IPN xerogels were synthesized in accordance with the Box-Behnken statistical experimental design shown in Table 4.1. Polymeric solutions of PEO of varying concentrations in distilled water were prepared ranging from 1-2.5%$^{w}/_{v}$; once a homogenous solution was achieved, GG ranging between 0.5-1g was added to the above mentioned solutions and allowed to further homogenize and form a viscous polymer blend.

Once GG was appropriately dissolved, epichlorohydrin (EPI) was added drop-wise allowing for a period of stirring between each drop, within a range of 0.4-0.8mL followed by further stirring with a magnetic stirrer for 30 minutes to allow for effective crosslinking to occur. The resulting viscous, slightly opaque gel was poured into a beaker of acetone (50mL), and allowed to precipitate for approximately 3 hours. Thereafter the precipitated gel was drained of all the excess acetone using a laboratory strain and placed in a petri dish, and air dried under the influence of a fumehood for a further 24 hours. The resultant s-IPN xerogel is then crushed into a uniform powder using a mortar and pestle and electrical grinder for formulation of sustained release s-IPN xerogel matrix tablets as depicted in Figure 4.1.



(a) (b)

Figure 4.1: (a) Digital images of s-IPN xerogel after precipitation in acetone at 3 hours and (b) s-IPN xerogel polymer matrix tablets compressed employing the *Carver Press 3851-0.*

4.2.4. Preparation of the s-IPN xerogel matrix tablets

s-IPN xerogel matrix tablets were prepared consisting of a 50mg sulpiride to 100mg s-IPN xerogel using the direct compression method. All tablet excipients including the xerogel with the exception of magnesium stearate were mixed with equal concentrations initially after which the concentration of each excipient gradually increased until all weighed out excipients were added. Magnesium stearate was added and mixed for a further 2 minutes. The dry blend of powdered excipients was directly compressed using a hand operated Carver Press (Model 3851-0, S/N 43000-904, Wabash, IN, USA) at a pressure of 5 tons.

4.2.5. Physiomechanical evaluation of fabricated s-IPN xerogel matrix tablets

The matrix tablets of PEO-GG xerogel, crude GG, and crude PEO were evaluated by textural analysis studies to determine the physiomechanical properties of the tablets. Parameters such as hardness, deformation, rigidity, and matrix resilience were obtained. PEO-GG xerogel, GG, and PEO tablets, 5mm in thickness respectively were evaluated from (force vs. distance) and (force vs. time) profiles generated on a TA.XT*plus* Texture Analyzer (Stable Microsystems, Surrey, UK) equipped with a 2mm flat cylindrical probe,5kg load cell and Texture Exponent (V3.2) software for processing of data. Matrix tablets were secured on a raised platform fitted with a 5mm diameter central hole. A central probe with a weight of 5kg was lowered on to the surface of the tablet (Covielloa et al., 2005), in accordance with the test parameters listed in Table 4.2.

Table 4.2: Test parameters used during Texture Analysis as per standard protocol for solid dosage forms

Parameters	**Test Settings**
Test mode	Compression
Pre-Test	1mm
Test	0.5mm
Post-Test	1mm
Target Mode:	
Distance - Strain	0.5mm- 10%
Trigger Force	0.05N

4.2.5.1. *Brinell hardness number, deformation, rigidity, and resilience determination*

The Brinell hardness test was employed to determine the hardness of tablets where a load of 5kg was applied to the surface of the tablets via a steel indenter of 3.175mm in diameter. Thus the

diameters of the resultant indentation on the surface of the tablets were measured and the Brinell Hardness Number (BHN) was calculated using Equation 4.1.

$$Brinell\ Hardness\ Number = 2F/(\pi D(D - (D^2 - d^2)$$

Equation 4.1

Where, F=load on the indenting tool (force generated in kg), D=diameter of the spherical probe indenter (3.175mm), and d=diameter at the rim of the impression made (depth 0.5mm) (Choonara et al., 2006).

Deformation and rigidity was determined from evaluating the area under the curve (AUC) as well as the gradient from the force vs. distance graph. By plotting a force vs. time graph the values for 1:2 and 2:3 (values for the peak anchors) were obtained, thereby resilience was then calculated when a strain of 10% is applied with the use of Equation 4.2.

$$Resilience = \left(\frac{2:3}{1:2}\right) \times 100$$

Equation 4.2

4.2.6. Surface morphological analysis

Scanning Electron Microscopy (SEM) was employed to determine the surface morphology of crude PEO and GG, as well as provide evidence of the synthesis of an s-IPN within the crosslinked xerogel formulations with the aid of the generated microscopic images. It further assisted in identifying the differences in physical morphology and characteristics of the crude polymers as compared to the crosslinked xerogel. Dried xerogel samples before tableting and native polymers were placed on steel studs and sputter coated with carbon and gold palladium shadowing using the Phenom™ G2 Pro SEM (FEI Company, and Hillsboro, Oregon, USA) by employing various magnifications.

4.2.7. Chemical composition analysis

The FTIR spectra of PEO, GG and the crosslinked s-IPN xerogels were recorded using an FTIR Spectrophotometer (Perkin Elmer Spectrum 100, FT-IR Spectrometer) fitted with a universal ATR Polarization Accessory (Perkin Elmer Ltd., Beconfield UK). Wavelengths were recorded between 4000 and 650cm^{-1} and FTIR spectrums of absorbance and % transmittance against distance was obtained.

4.2.8. Thermal transition examination

DSC analysis was conducted for PEO, GG and the s- IPN- xerogels using a Mettler Toledo, DSC 1 , STAR^{E} System (Schwerzenback, Switzerland) at a heating rate of 10˚C/min from 25-300˚C under the constant flow of nitrogen gas. Accurately weighed samples of each formulation (±10mg) were placed into aluminum sample holders covered and a central pin hole made. Indium metal (99.99%) was used to calibrate the DSC with regards to temperature and enthalpy (Kreye et al., 2012).

4.2.9. Response surface analysis of the employed responses

Minitab® statistical software (V15, Minitab Inc., PA, USA) was utilized to perform the response surface analysis of the various response variables. The results were demonstrated employing response surface and contour plots which were derived for the measured responses (drug release and degree of swelling and erosion), based on the experimental model.

4.2.10. Water content determination employing Karl- Fischer Analysis (KF)

KF analysis was conducted for all formulations within the study using the Mettler Toledo V30 Volumetric KF Titrator, with methanol as the moisture standard. Accurately weighed out xerogel samples of 0.01g were placed within the solvent bath after a baseline drift of zero was achieved, under continuous vigorous stirring with a magnetic stirrer until the titration end point is reached. All samples were tested to determine water content with results obtained in % water content per sample (Scaccia, 2005).

4.2.11. Powder flow characterization studies

4.2.11.1. *Angle of repose*

The angle of repose is the angle formed between the horizontal bench surface and the cone-shaped mass of powdered xerogel. A glass funnel, 5cm in height from the base to the orifice was employed. The funnel was secured 4cm above the bench surface. Thereafter, the powdered xerogel was poured through the funnel orifice, a cone shaped mass of xerogel formed. The height (h) and radius(r) of the cone-shaped mass were recorded. The angle of repose was thus calculated as per Equation 4.3 below (Shah et al., 2008):

$$\Theta = \tan^{-1}(h/r)$$

Equation 4.3

4.2.11.2. *Carr's Compressibility Index and Hausner ratio*

Bulk (ρbulk) and tapped (ρtap) densities were recorded employing methods as described in the USP. Samples were poured into a 10mL graduated measuring cylinder. The bulk density was measured after tapping the cylinder twice on a flat bench top surface. Thereafter the tapped volume was recorded after tapping in increments of 10, 15, 20, 30, 50, and 100 taps (Shah et al., 2008)

The recorded bulk and tapped densities were utilized to calculate the Carr's compressibility index (Equation 4.4) and Hausner ratio (Equation 4.5) respectively.

$$CI = \frac{\rho_{tap} - \rho_{bulk}}{\rho tap} \times 100$$

Equation 4.4

$$HR = \frac{\rho_{tap}}{\rho_{bulk}}$$

Equation 4.5

4.2.12. Swelling and erosion studies

A study to evaluate the swelling, erosion and water uptake characteristics of the tablets was conducted. Whereby the respective tablets were weighed and placed in 250mL beakers containing 200mL potassium phosphate buffer pH 6.8 at room temperature and allowed to swell over a 24 hour period. Tablets were at predetermined time intervals removed from the buffer and weighed after removing surface water with absorbent paper on a calibrated electronic scale. The swelling ratios, erosion and water uptake % was calculated using Equations 4.6-4.10 (Özerogluand Birdal, 2009).

$$Swelling\ Ratio = \frac{Wt}{Wo}$$

Equation 4.6

Where, Wt. =weight of the tablet at time t, and WO=initial weight of the tablet.

$$Dynamic\ Swelling\ Ratio\ (S) = \frac{Wt - Wo}{Wo}$$

Equation 4.7

Where, Wt. =weight at time t, and WO=initial weight of the tablet.

$$Water\ Uptake\ \% = \frac{Ws - Wo}{Wo} \times 100$$

Equation 4.8

Where, Ws=weight of the swollen tablet, and WO=weight of the initial tablet.

$$\%\ Erosion = \frac{Wo - We}{We} \times 100$$

Equation 4.9

Where, WO=initial weight of the tablet, and we=weight of the test after the erosion test (Reddy et al., 2012).

$$Equilibrium\ Water\ Content(EWC\%) = \frac{Weq - Wo}{Weq} \times 100$$

Equation 4.10

Where, Weq=weight at equilibrium, and WO=weight of the initial tablet (Murthy et al., 2006; Reddy et al, 2012).

4.2.13. *In vitro* drug release studies

Dissolution studies were carried out utilizing a USP type II apparatus (Caleva, model 7ST) at 50rpm and 37˚C in 900mL of potassium phosphate buffer (pH 6.8) with the addition of a stainless steel mesh ring, which fits under the paddle into the lower part of the standard dissolution vessel. 5mL of dissolution medium was withdrawn manually at predetermined time intervals during the 24 hour study and replaced with an equal volume of fresh dissolution medium to ensure sink conditions were maintained. The samples were then analyzed for drug release via Ultraviolet spectrometry (WinAspect Spectro-analytical software, Analytik Jena AG), at a wavelength of 291nm employing a calibration curve obtained for the drug (Strübing et al., 2008). The Mean Dissolution Time (MDT) was calculated for all samples, the concept of MDT relates to the average time required for dissolution of a drug delivery system. MDT can be arithmetically calculated from experimental dissolution data using Equation 4.11:

$$MDT = \frac{ABC}{W_{\infty}}$$

Equation 4.11

Where W_{∞} is the asymptote of dissolved amount of drug and ABC is the area between the cumulative dissolution curve and W_{∞} (Rinaki et al., 2003).

4.3. Results and Discussion

4.3.1. Assessment of the physiomechanical properties of the s-IPN xerogel matrix component of the ODLS

Textural analysis data profiles were employed to study the mechanical properties of the crosslinked s-IPN xerogel matrix tablets in comparison to the PEO-GG blend tablets alone when a uniaxial compression force was applied to the tablets. The work of deformation energy which is

calculated as the area under the curve (AUC) of the force-distance curve points to the deformation and rigidity of the tablets. The force-distance curves obtained is a measure of the force of resistance encountered by the probe infiltration as a function of the travelled distance into the tablet. A low resistance is depicted by a low slope which further illustrates that the strength of the tablet is low, while a sharp increase in force, a higher slope as the test probe penetrates deeper into the tablet corresponds to a greater strength (Pillay and Fassihi, 2000). From the profiles of force-distance obtained there was a display of both a high and sharp curve as well as short curve, s-IPN xerogel matrix tablets had a greater resistance to the force applied than to the comparative; namely; PEO-GG blend tablets. This may be further highlighted by calculating the gradients of the various force-displacement curves as indicated in Table 4.3, whereby the gradient shows the rigidity of the tablets tested, data indicates that the crosslinked PEO-GG xerogel tablets have an greater rigidity than the PEO-GG blend as a consequence of the new formed polymer chain strength, with Formulation 10 (F10) displaying the highest rigidity.

Table 4.3: Comprehensive table of data obtained from textural analysis describing the mechanical properties of the s-IPN xerogel matrix tablets.

Formulation Code	***Force (N)***	***BHN No.***	***Deformation (AUC)***	***Rigidity (N.mm)***	***Resilience %***
F1	46.67	236.00	0.011	96.412	145.00
F2	41.43	209.69	0.008	88.945	54.62
F3	40.38	204.40	0.008	84.674	143.80
F4	39.38	199.00	0.008	83.754	141.78
F5	42.67	215.96	0.009	89.565	155.81
F6	44.64	225.90	0.010	93.264	44.60
F7	48.00	242.94	0.011	101.104	45.66
F8	39.41	199.50	0.008	83.607	54.92
F9	44.64	225.90	0.010	93.625	54.80
F10	48.21	244.00	0.011	101.332	45.63
F11	42.86	216.90	0.009	91.720	56.17
F12	39.38	199.00	0.008	83.754	141.65
F13	42.07	212.93	0.009	87.998	55.00
F14	39.68	200.80	0.008	81.759	42.39
F15	47.14	238.59	0.011	98.587	54.99

The same applied for deformation, the crosslinked xerogel tablet showed a lower level of deformity whereas the PEO -GG blend tablet showed the highest value of deformation due to the high

binding properties and loose bonds between polymer molecules. The Brinell hardness and resilience of design formulations are represented graphically in Figures 4.2 and 4.3, respectively.

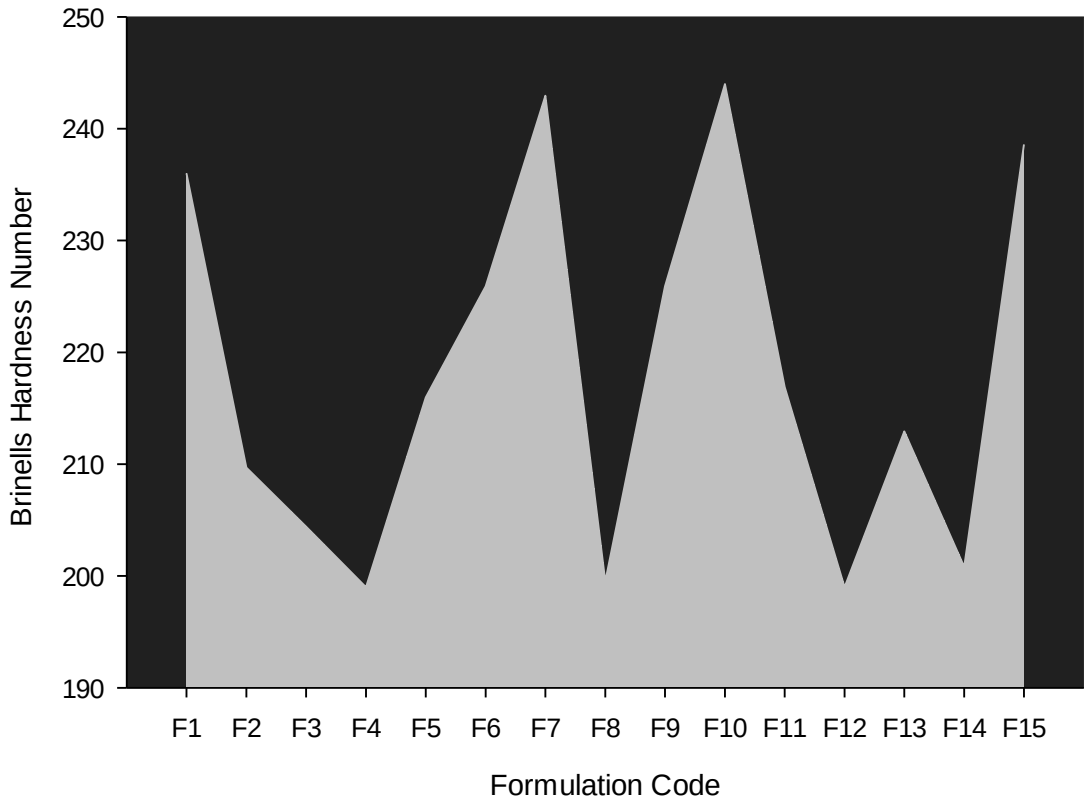


Figure 4.2: Diagrammatic representation of Brinells Hardness Number for Box Behnken Statistical formulations depicting the effect of polymer concentration and crosslinking density on the hardness and mechanical strength of formulations

To determine the resilience of the tablets a strain of 10% was applied to the tablets whereby a textural analysis profile was generated of Force (N) - Time (sec) to the 1:2 and 2:3 ratios, after which the resilience was calculated as depicted in Table 4.3 above.

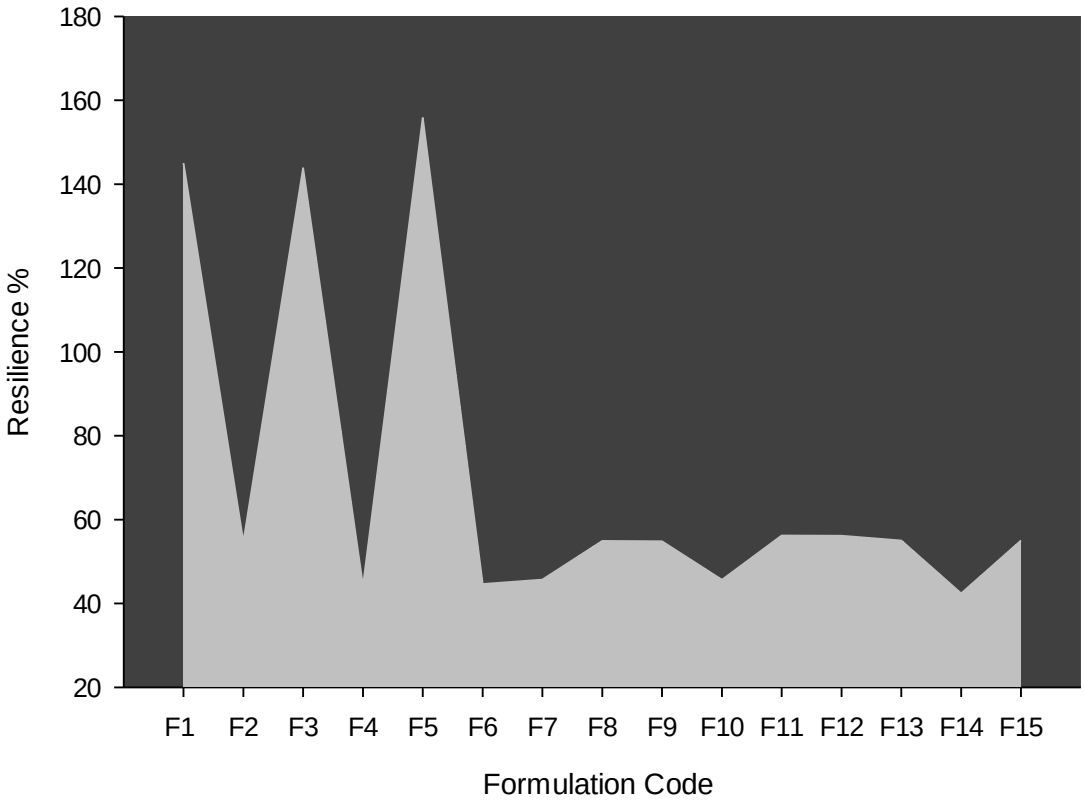


Figure 4.3: Illustration of the difference of Resilience between all statistical Box-Behnken design formulations with variances in chemical composition.

From the results obtained it can be seen that the s-IPN xerogel matrix formulation F5 has the greatest % resilience than its comparatives, which may be attributed to the greater mechanical strength of the crosslinked xerogel due to a greater concentration of crosslinker being used. The strain applied as well as the deformation of the xerogel was directly proportional to the compression force applied. In addition, the applied stress and deformation was inversely proportional to the radius and diameter of the indenter probe. This can be confirmed theoretically, from the principles of Young's modulus (*E*) and Equations 4.12-4.15 (Ruvalcaba et al., 2009).

$$\hat{o} = -E(\ddot{e} - 1)$$

Equation 4.12

Where, $\hat{o}$ is the applied stress, and $\ddot{e}$ is the deformation (Khalid et al., 2002)

$$E^{2/3} = \frac{KF^{2/3}}{R^{1/3}d}$$

Equation 4.13

Where, *R* is the indenter radius, *d* is the displacement of the indenter, and *F* is the compression force. Equating 4.12 and 4.13, the relations shown in Equations 4.14 and 4.15 can be deduced.

$$\hat{o}\ and\ \ddot{e} \propto F$$

Equation 4.14

$$\hat{o}\ and\ \ddot{e} \propto 1/R$$

Equation 4.15

4.3.2. Assessment of the surface morphology of the s-IPN xerogels as per design

Scanning electron micrograms displayed in Figure 4.4 displays the surface morphology of pure PEO, GG, and crosslinked s-IPN xerogel formulations F1, F7 and F9 that showed distinct alterations after precipitation in acetone and drying under the influence of a fumehood. The SEM micrographs show that the s-IPN xerogel formulations are highly porous as compared to the pure PEO and GG. The average particle size ranged from approximately 240-486µm. The drastic change in surface morphology between the native polymers and crosslinked s-IPN xerogels shows that the modification of these polymers was successful. The resultant porous nature of the s-IPN xerogel furthermore allows for the sustained release of the active from within the interpenetrating network formed. Formulations with a greater degree of crosslinking display a reduced free volume of polymer matrix, which thus delays the passage of drug through the matrix (Kulkarni et al., 2011 (1); Kulkarni et al., 2011 (2).

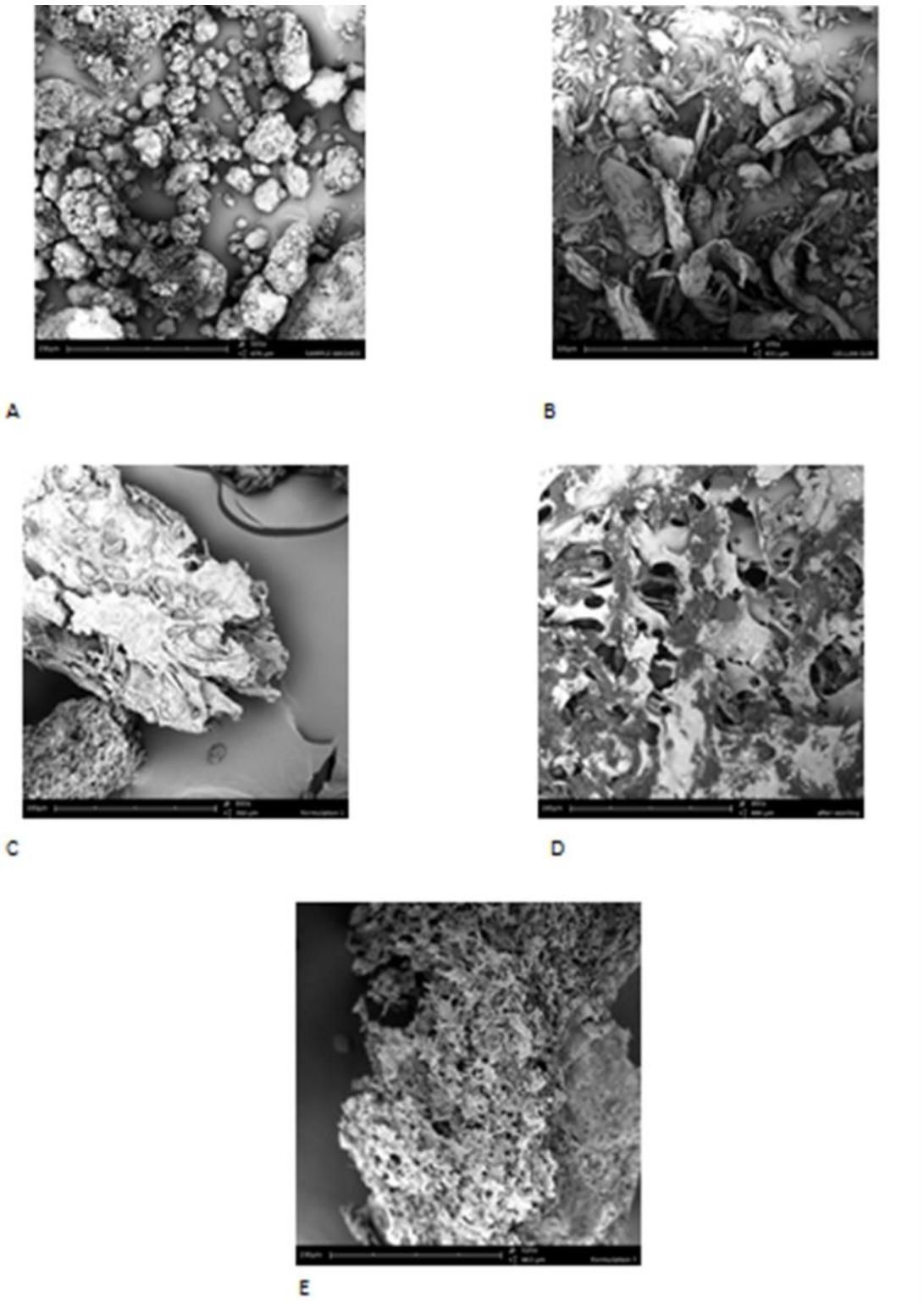


Figure 4.4: SEM Micrographs of PEO (A), GG (B), F1(C), F7 (D), and xerogel F9 (E).

4.3.3. Chemical compositional assessment of the s-IPN xerogels

FT-IR may be used as a 'fingerprint' tool to determine which molecules can differentiate between the xerogel formulations and its precursors such as GG and PEO by using comparisons of known compound consistency. Figure 4.5 below represents the FTIR spectrum obtained for PEO, GG, xerogel F1, F7 and F9 as a function of % transmittance against wavelength.

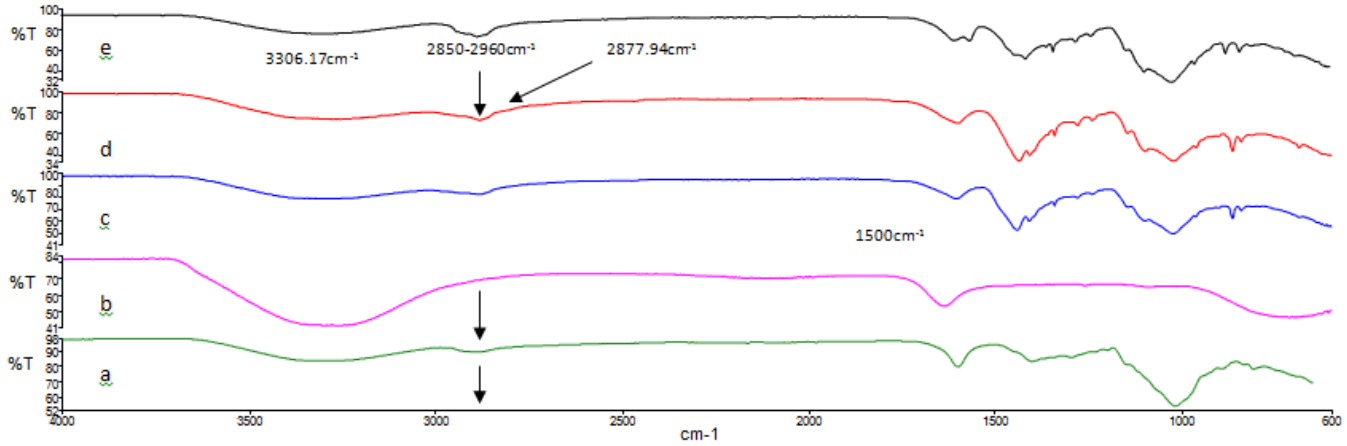


Figure 4.5: FTIR Spectra of crosslinked s-IPN xerogel F1 (f), F7(c), F9 (d), as well as pure PEO (b) and GG (a) depicting the change within chemical structure via the identification of specific functional groups within the spectra obtained. Pink and green spectra correspond to PEO and GG respectively with black, red and blue representing formulations 1, 7 and 9 respectively.

Modifications in chemical structure of the s-IPN xerogel formulations were analyzed employing FT-IR spectroscopy, which assists in identifying interactions of parent polymers upon chemical reactions such as crosslinking. The current observation of crosslinking was optically detected by noted change in solution viscosity as well as opacity on completion of the crosslinking reaction. The FT-IR spectra of PEO depicted the functional groups present within the chemical compound by determining characteristic bands such as that of O-H functional groups characteristic of alcohols in a range of 3200-3600cm^{-1}, and C≡C stretching depicted at wavenumber range of 2100-2260cm^{-1}. Furthermore the spectrum for crude GG depicts an important peak at a range of 2850-2960cm $^{-1}$ which corresponds to C-H stretching band (Coates, 2000), and is found in all design formulations as a characteristic GG absorption. On experimental evaluation of the FT-IR data set it has been inferred that changes in the polymer ratios and crosslinking density have an effect on the vibrational frequencies observed. A broad band in the range of 2850-2960cm^{-1} relating to C-H

stretching (Coates, 2000) in alkane functional groups is observed in all s-IPN xerogel formulations, characteristic of GG.

Due to the presence of NaOH within the crosslinking reaction, it leads to the breakdown of O-H bonds (Adel et al., 2010) thus causing these hydrogen and oxygen molecules to interact with other molecules, forming new functional groups. This chemical phenomenon leads to the addition of alkene groups with C-H stretching at higher wavelengths of 3276cm^{-1}(Coates, 2000), as depicted by the highlighted peak in Figure 4.5 of F7. This confers a greater degree of conjugation thereby improving stability and as an extension the physiomechanical properties of the polymer network synthesized. In addition a strong band relating to the O-H bonding groups within the range of 3200-3600cm^{-1} (Coates, 2000), is observed in s-IPN xerogels that had an intermediate ratio of polymers relating to the presence of alcohols or phenols. There also exist shifts in the spectrum with the varying crosslinking density. The introduction of N-H amine groups is found in F1, 2, 3, 5, and 10, at a wavelength of 3360.17cm^{-1} (Coates, 2000) this is due to the increase in crosslinker density, therefore promoting bond formation, the absence of the amino groups within the remaining formulations indicates the absence of amino groups for bonding reactions, this occurrence could be due to the reduced concentration of GG and increased density of EPI within these formulations which thereby creates steric hindrance.

F9 showed C=C stretch at a wavelength of 1500cm^{-1} (Coates, 2000), highlighted in the FT-IR spectra in Figure 4.5, which corresponds to a conjugational asymmetrical stretch, occurring when the ratio of polymers is 1:2.5 and crosslinker is at an intermediate density. C-H stretching within the aromatic ring structure which is derived from the structure of pure GG, was observed with all formulations with the resulting incorporation of a C-O functional group within the aromatic structure at a wavelength of 1080cm^{-1} (Coates, 2000). Furthermore methyl and methylene functional groups were introduced within formulations with a higher concentration of crosslinker due to the introduction of $RCH=CH_2$ bridges extending from the aromatic ring backbone. Aliphatic ethers represented by wavelengths occurring at 1060-1150cm^{-1} were observed in s-IPN xerogels that consisted of PEO at a concentration of 1.75%$^{w}/_{v}$. C-N stretching occurred between 1560-1650cm^{-1} in formulations that had crosslinking density of 0.6mL, these peaks tend to occur at higher vibrational frequencies and are known to be associated with the degree of crosslinking (Adel et al.,2010) and polymer network formation resulting in a change within the structural configuration of the molecules, thus formulations with higher degrees of crosslinking was found to have wavelengths shifting to the greater end of the spectrum. From the data obtained from the FT-IR spectra of all compounds tested it can be seen that there are distinct changes within the chemical structure with the addition and removal of certain functional groups. Shifting of the aromatic ether

occurs in F1, 3, 4, 8 and 11 which all have a crosslinking concentration of 4.4%$^{v}/_{v}$. There is a disappearance of the C-H in plane bending from xerogel formulations consisting of a polymer ratio of 0.75: 1.75%$^{w}/_{v}$ thus describing an effect of polymer concentrations of the C-H bonding. Furthermore individual formulations show characteristically new bands, such as the addition of an alkyne and amine group in F1 as well as methyl groups in F7 and F9.

Chemical crosslinking entails the use of a crosslinking agent to allow a linkage between two polymer chains. The actual crosslinking reaction of both synthetic and natural polymers is accomplished via the reaction between their functional groups with crosslinkers such as epichlorohydrin. Chemical crosslinking largely implicates the introduction of new functional groups and molecules between the polymeric chains to thereby produce crosslinked chains (Syed et al., 2011). This theoretical explanation thus accounts for the additional functional groups and chemical orientation seen in the FT-IR spectra of the crosslinked s-IPN xerogel formulations as compared to the spectra of PEO and GG. All of the observations help to conclude that polymer concentration as well as crosslinking density has an effect on the formation of semi Interpenetrating networks as observed by peaks within the FT-IR spectra.

4.3.4. Thermal analysis of the crosslinked s-IPN xerogel

Differential Scanning Calorimetry (DSC) is employed to determine the well as the crystallization temperature of the crude polymers, pure Gelzan™ CM, GG and pure PEO WSR303 as compared to crosslinked s-IPN xerogel. The procedure follows a thermal analytical method that maintains all test samples at a constant temperature throughout the experimental procedure, whereas the sample temperature holder increases in a linear manner. The DSC thermogram of pure PEO shown in Figure 4.6, displays a pronounced endothermic peak at 73.86˚C which corresponds to the crystalline melting (Tm) temperature of crude PEO (Ibrahim and Johan, 2012).Glass transition of pure PEO occurs at approximately 65.72˚C. An exothermic peak at 190.51˚C depicts melting of stable modification. Figure 4.6 also depicts the thermogram of GG (Gelzan™ CM), shows an endothermic peak at 62.98˚C which is due to endothermic peaks only appearing at GG concentrations of ^{w} and lower with these peaks disappearing at concentrations greater than 8% (Izumi et al., 1999).

The glass transition temperature (Tg) is directly proportional to the crosslinking density, thus as seen in the DSC curves for design formulations it is clearly visible that there is an increase in the Tg with a corresponding increase in the crosslinker concentration ranging between 64.95-65.92˚C.Melting peaks for all design formulations remained within a stable, constant range

between 106-107˚C; however there was a slight reduction noted in the melting temperature when the ratio of polymers was reduced , this phenomenon has been described earlier by the Sanchez-Eby theory which states that a reduction in melting temperature is due to a reduction in the heat of fusion present within the reaction, this results because with lower concentrations of polymers there is a greater degree of non-crystallizable units (Zo-li, 2005).

The melting peaks observed were broad due to the partial crystalline nature of the polymers, this occurs due to the size distribution of crystallites. Melting is then followed by a broad exothermic crystallization peak, the surface of the xerogel which after melting forms a rigid envelope leads to crystallization which involves the transition of the polymeric material from a liquid to a crystalline solid, with repeated units forming rigid structure crystallization (Mettler Toledo, 2000). It was found that the temperature of crystallization was shifted to higher temperatures with a corresponding increase in crosslinker and polymer concentrations with broad peaks depicting that with an increase in crosslinking the crosslinks appear within the amorphous regions, thus allowing a greater crystalline peak (Reis and Pruitt, 2005). A prominent crosslinking peak is also noted within the crosslinked s-IPN xerogel formulations, thus proving the crosslinking reaction of GG-PEO employing epichlorohydrin. This peak is representative of the crosslinking reaction that occurs upon heating of the sample called curing. These crosslinking peaks are observed with formulations with a higher concentration of crosslinking agent, but absent from those with a reduced crosslinker concentration, most prominent around the temperature of 215˚C.

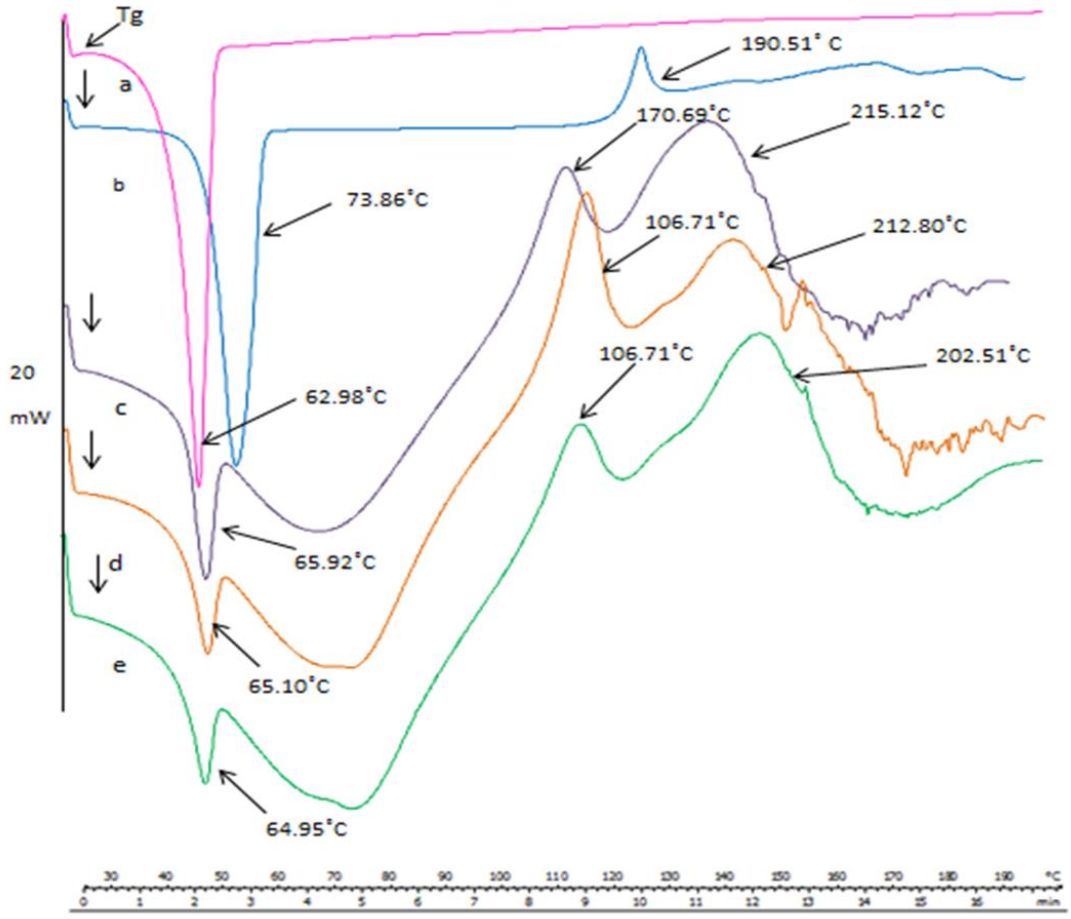


Figure 4.6: DSC Thermograms of s- IPN xerogel Formulations F1(c), F7 (d), F9 (e), as well as PEO (b) and GG (a) at a heating rate of 10˚C/ min from 10- 300˚C under nitrogen atmosphere.

4.3.5. Response surface analysis of the Box-Behnken design

With the purpose of determining the relationship between the response variables and predictor variables, a complete ANOVA analysis was performed of the measured formulation responses (Figure 4.7, Table 4.4), drug release, swelling and erosion. The aptness of the multiple regression models are accessed via residual analysis. Residual plots for drug release (total MDT), mean % swelling and mean % erosion are depicted in Figure 4.7. The hypotheses of a multiple linear regression model is that the response variables are independent and ordinarily distributed, arbitrary variables with constant variance and means depending linearly on the explanatory variables (Larsen and McCleary, 1972; Huynh, 2000). Resilient linear relationships were observed for all response variables as indicated by the confined clustering of the partial residuals. The scatter plot of the residual, in which the residuals were plotted against the model predictions, is objectively uniform and radiate in the vicinity of zero. They generally displayed irregular scatter i.e. no specific trends, indicating none of the underlying hypotheses of the multiple regression

analysis were obviously breached; some deviations (outlying points) and some widely spread points were observed indicative of a degree of non-constant variance (du Toit et al., 2013). The normal probability plots of the residuals fell on a straight line demonstrating the data to be normally distributed with no affirmation of unidentified variables. Definite patterning was not observed in any of the variable plots, indicating non-contravention of the assumptions of zero means and constant variance of the regression model notwithstanding the presence of a few outlying points in these plots. Deviations could have resulted from experimental error. The histograms for drug release and erosion were largely symmetrical thus supporting the probability plots of constant and uniform distribution. The attained histogram for swelling depicted an absence of symmetry suggestive of a random error of the data set. The scatter plot, which is the residual vs. observation order, depicts the performance of the model. Scatter plots stayed within constant scale indicating non-arbitrary error. A full ANOVA was conducted and shown in Table 4.4.

Table 4.4: ANOVA analysis for the measured responses.

Response Variables	**p-values**		
	Drug Release	*% Swelling*	*% Erosion*
[GG]	0.152	0.025	0.055
[PEO]	0.734	0.148	0.112
[EPI]	0.618	0.814	0.872

The complete regression equations generated for drug release, mean % swelling and mean % erosion are indicated below;

$$Mean\ \%\ Erosion = 102.194 - 41.5[GG] - 9.424[PEO] + 3.521[EPI]$$

Equation 4.16

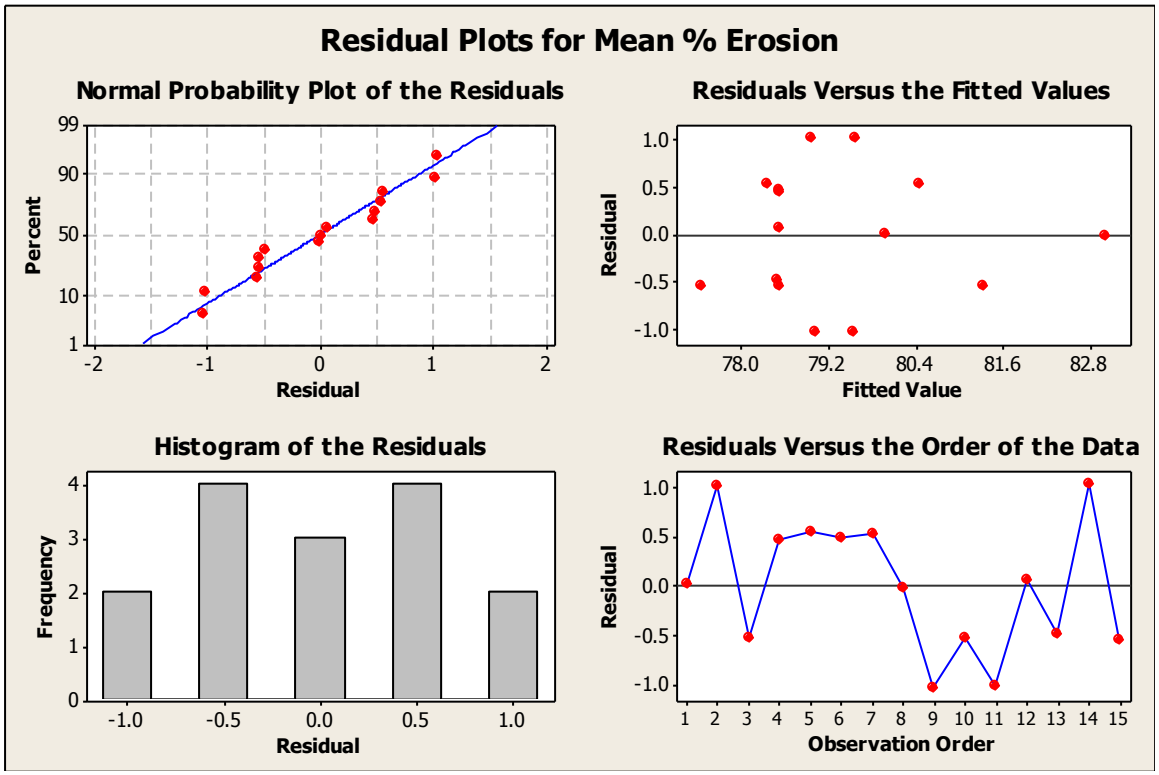
$$Drug\ Release\ (Total\ MDT) = -18.968 + 99.504[GG] + 6.250[PEO] - 39.221[EPI]$$

Equation 4.17

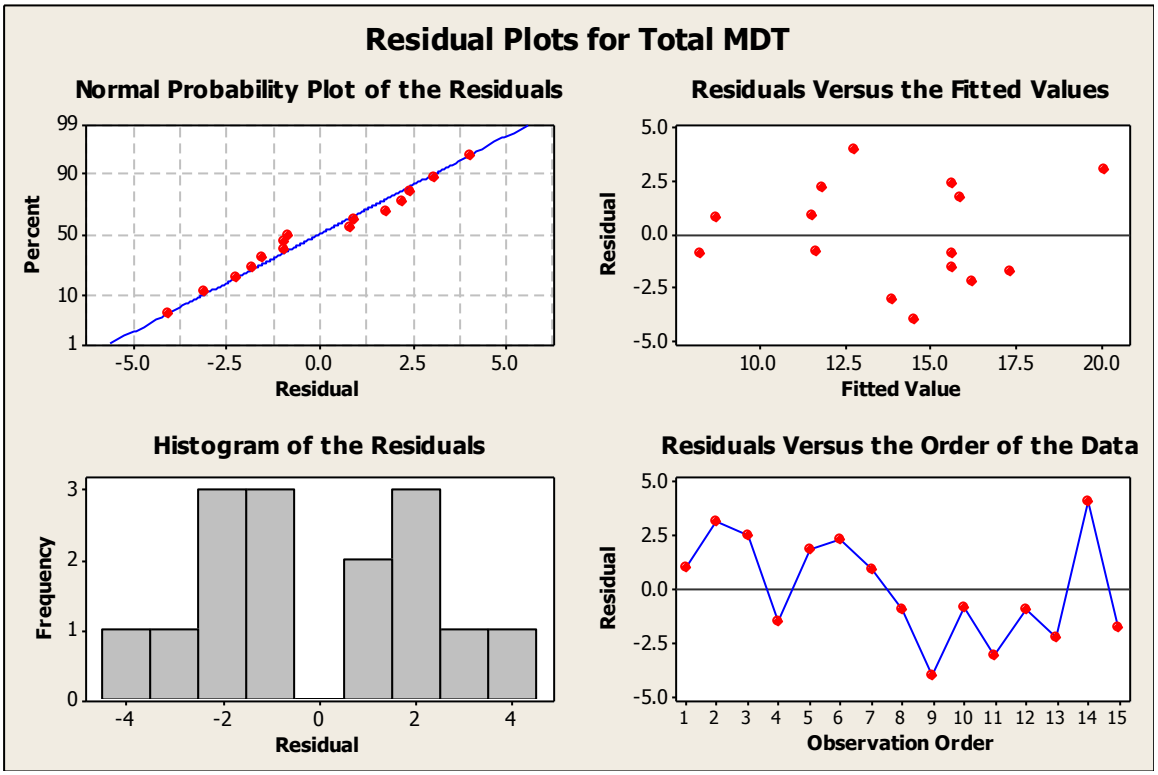
$$Mean\ \%\ Swelling = 1017.20 - 1020.11[GG] - 161.85[PEO] + 99.63[EPI]$$

Equation 4.18

(a)


Residual Plots for Mean % Erosion
Normal Probability Plot of the Residuals
Percent
Residual
Residuals Versus the Fitted Values
Residual
Fitted Value
Histogram of the Residuals
Frequency
Residual
Residuals Versus the Order of the Data
Residual
Observation Order

(b)


Residual Plots for Total MDT
Normal Probability Plot of the Residuals
Percent
Residual
Residuals Versus the Fitted Values
Residual
Fitted Value
Histogram of the Residuals
Frequency
Residual
Residuals Versus the Order of the Data
Residual
Observation Order

(c)

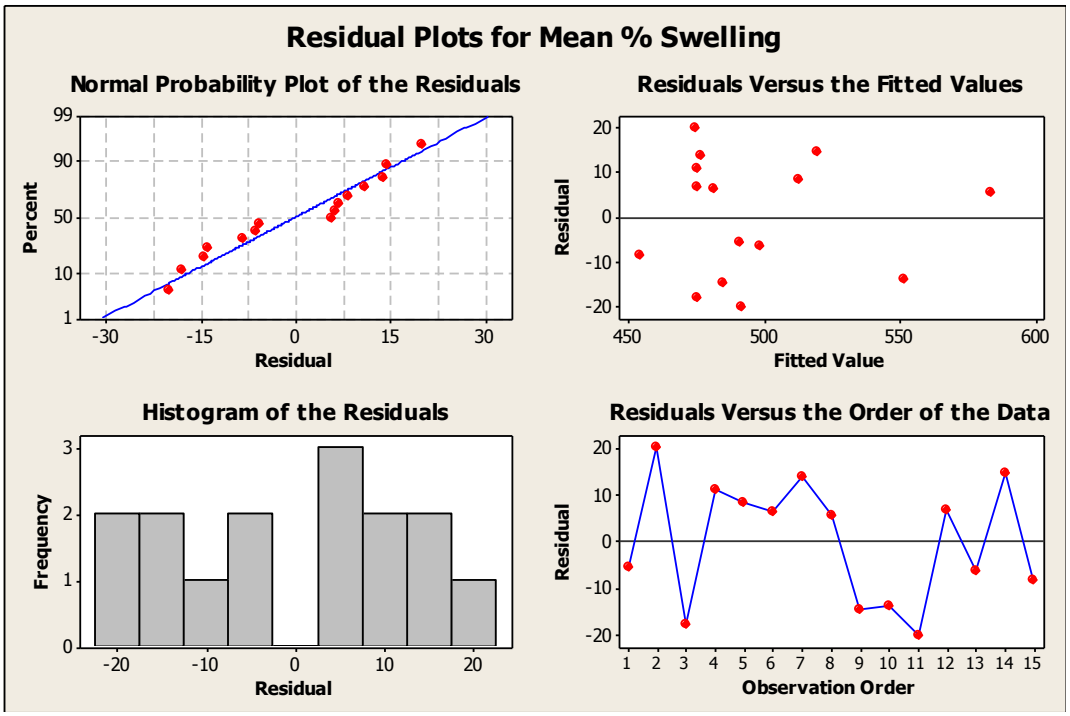


Figure 4.7: Residual plots for the responses a) mean % erosion b) drug release (MDT) c) mean % swelling.

Matrix erosion, drug release and polymer swelling are vital parameters influencing the resultant drug release profile from the s-IPN xerogel matrices. The integration of swelling, erosion and diffusion assists in achieving the desired zero-order drug release profile. Data plots were utilized to illustrate the purposeful relationship between the experimental variables and achieved responses. The effects of the GG, PEO and EPI on erosion are depicted in Figure 4.8 GG: PEO ratio of 1g: 0.8%$^{w}/_{v}$ displayed lower percentage erosion, whereas a GG: PEO ratio of approximately 0.5g:2.5%$^{w}/_{v}$ displayed an increase in matrix erosion. Higher concentrations of EPI of > 0.6mL enhanced the erosion capability with both polymers employed in the system design.

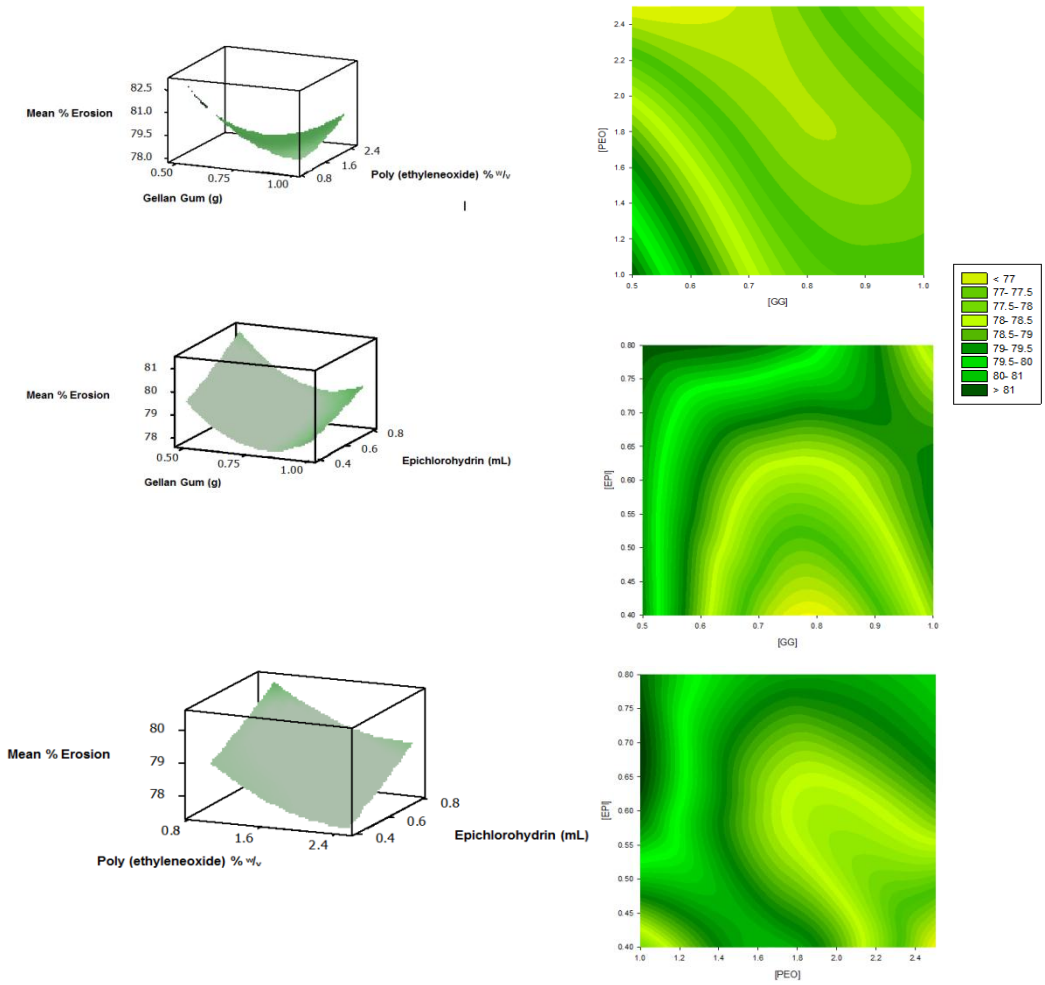


Figure 4.8: Response surface and contour plots depicting the effects of gellan gum (GG), poly (ethyleneoxide) (PEO) and epichlorohydrin (EPI) on mean % matrix erosion.

GG at a concentration of 0.5g and PEO at 1.5 % $^{w}/_{v}$ show desirable MDT as seen in Figure 4.9. The ratio of 0.8mL EPI to 1g GG derived an anticipated MDT of 12.5. It was observed that an increase in concentration of GG and PEO resulted in a corresponding increase in MDT. An increase in the concentration and volume of the respective polymers and crosslinker leads to an increase in the bulk volume of the xerogel matrix thus causing a reduction in drug release as drug has to pass through a greater bulk of s-IPN xerogel polymer network. Thus the concentration of GG had a significant interaction on the desired system responses.

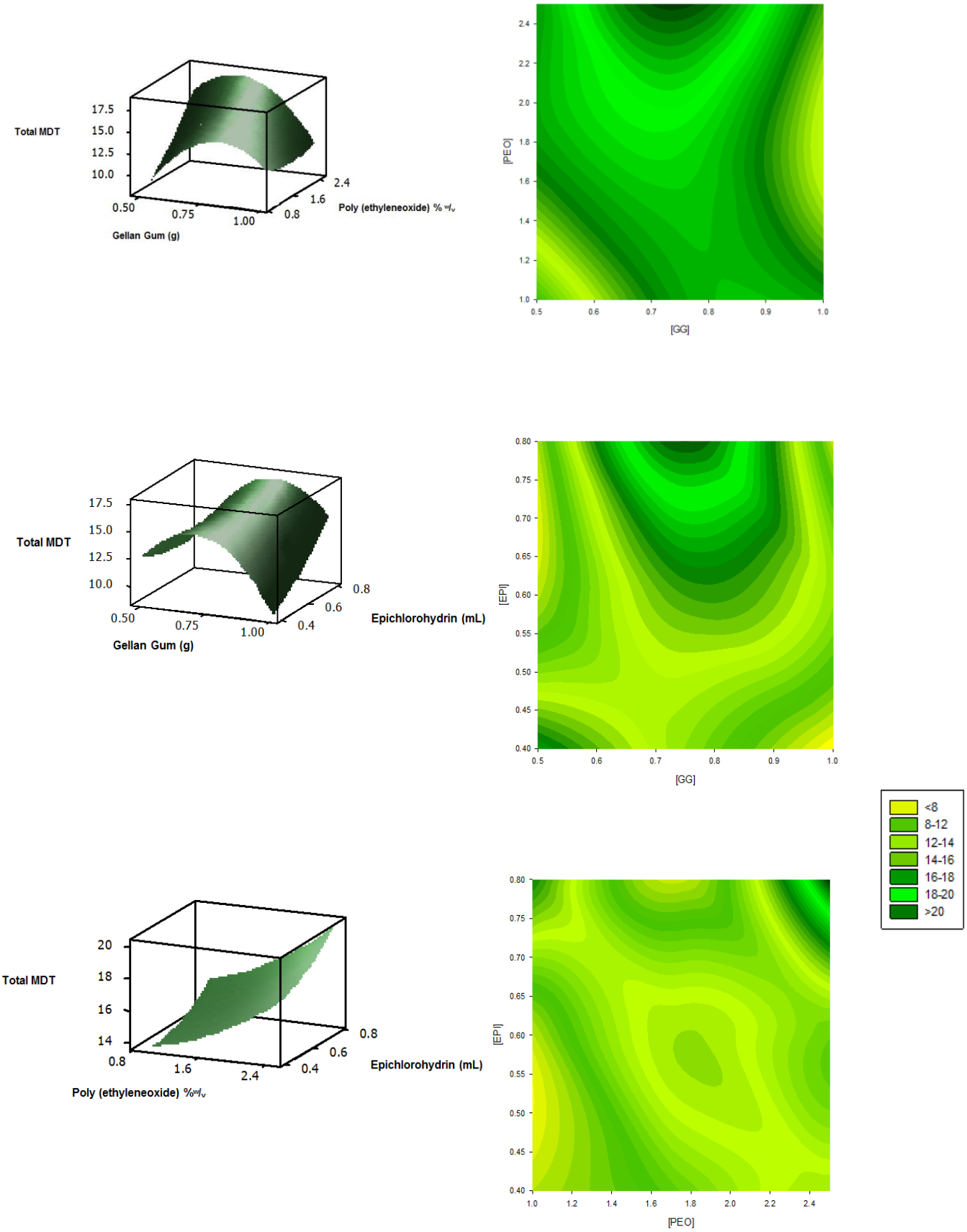


Figure 4.9: Response surface and contour plots depicting the effects of gellan gum (GG), poly (ethyleneoxide) (PEO) and epichlorohydrin (EPI) on drug release (total MDT).

An observed ratio of 2.4 $\%^{w}/_{v}$ PEO and 1g GG greatly raises the mean % swelling. Furthermore, a reduction in concentration of the respective polymers results in a corresponding decrease in swelling. The reduction in swelling could be attributed to the reduced polymer chain entanglement leading to rigidity of the s-IPN xerogel matrix. Conversely, an increase in volume of crosslinker employed >0.6 mL results in an intermediate to low percentage of mean swelling. An approximate mean % swelling of ≥ 200% is considered appropriate to attain the desired prolonged release profile. A greater degree of swelling provides a matrix barrier to drug release thus sustaining drug release over 24 hours.

4.3.6. Influence of water content as determined via titrimetric analysis

The percentage water content was obtained for all Box-Behnken design formulations employing a sample size of 0.01g. Results obtained ranged between 3.149-11.454% water content using Equation 4.19.

$$\%\, Water\ Content = \frac{Volume\ at\ Equlibrium\ (ml) \times Amount\ of\ water\ in\ standard\ (methanol) mg/ml}{Weight\ of\ sample\ (mg)} \times 100\%$$

Equation 4.19

Formulations depicted varying degrees of water capacity based on the ratio of polymer and crosslinker content. Formulations with an a higher concentration of polymer and crosslinker in overall showed a higher percentage of water content whereas; formulations with lower polymer and crosslinker concentrations depicted a reduction in water content. This is possibly due to the greatly hydrophilic nature of PEO and GG, as well as the high degree of water content found in EPI. Ideally water contact of a solid dosage form should be kept to a minimum due to adverse effects it may have on the physical and chemical characteristics of the pharmaceutical product (Szakonyi and Zelkó, 2012).) However, in the current study it can be seen that although the water content is on the greater spectrum it's mostly due to the hydrophilic nature of the parent polymers and the crosslinking agent used. The water content for design formulations are shown in Figure 4.10.

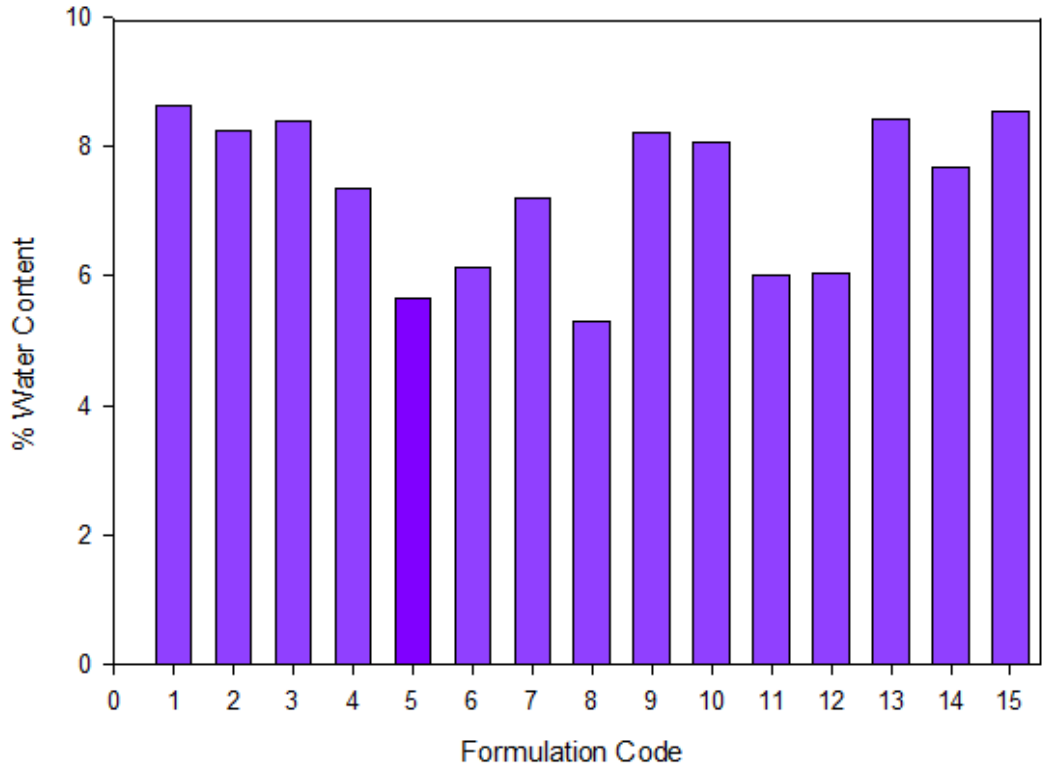


Figure 4.10: % water content obtained for 15 design formulations employing Karl-Fischer analysis.

4.3.7. Flow properties of powdered-drug loaded xerogel

The angle of repose, Carr's compressibility index and Hausner ratio were measured for all design formulations and the results are illustrated in Figure 4.11. The angle of repose calculated for all design formulations ranged from 20.48 to 34.4˚, with majority of the formulations falling within the 20˚ range. The angle of repose, which is a customary characterization tool used to determine pharmaceutical powder flow. Flowability is based on the angle of repose obtained via the calculation. A value of <30˚ specifies excellent flow, while values >56˚ indicates poor flow properties (Shah et al., 2008). Based on the results obtained, formulations were rated as having excellent to good flow characteristics.

In contrast, the Carr's compressibility (CCI) index and Hausner ratio (HR) were also calculated based on equations 4.4 and 4.5 outlined in *Chapter 4, Section 4.2.11.* The CCI and HR were found to range from 9-31 and 1.1-1.45 respectively. CCI is a measure of powder bridge strength and HR is a degree of interparticulate friction. In theory, lower values for CCI and HR respectively dictate better flow properties. A CCI value of <10 or HR <1.1 is indicated as excellent flow, whereas CCI >38 and HR >1.6 is considered poor flow (Schnaare et al., 2005). Therefore, based on the data

obtained, flow of the powdered drug loaded xerogel was rated as excellent to good established by CCI and HR.

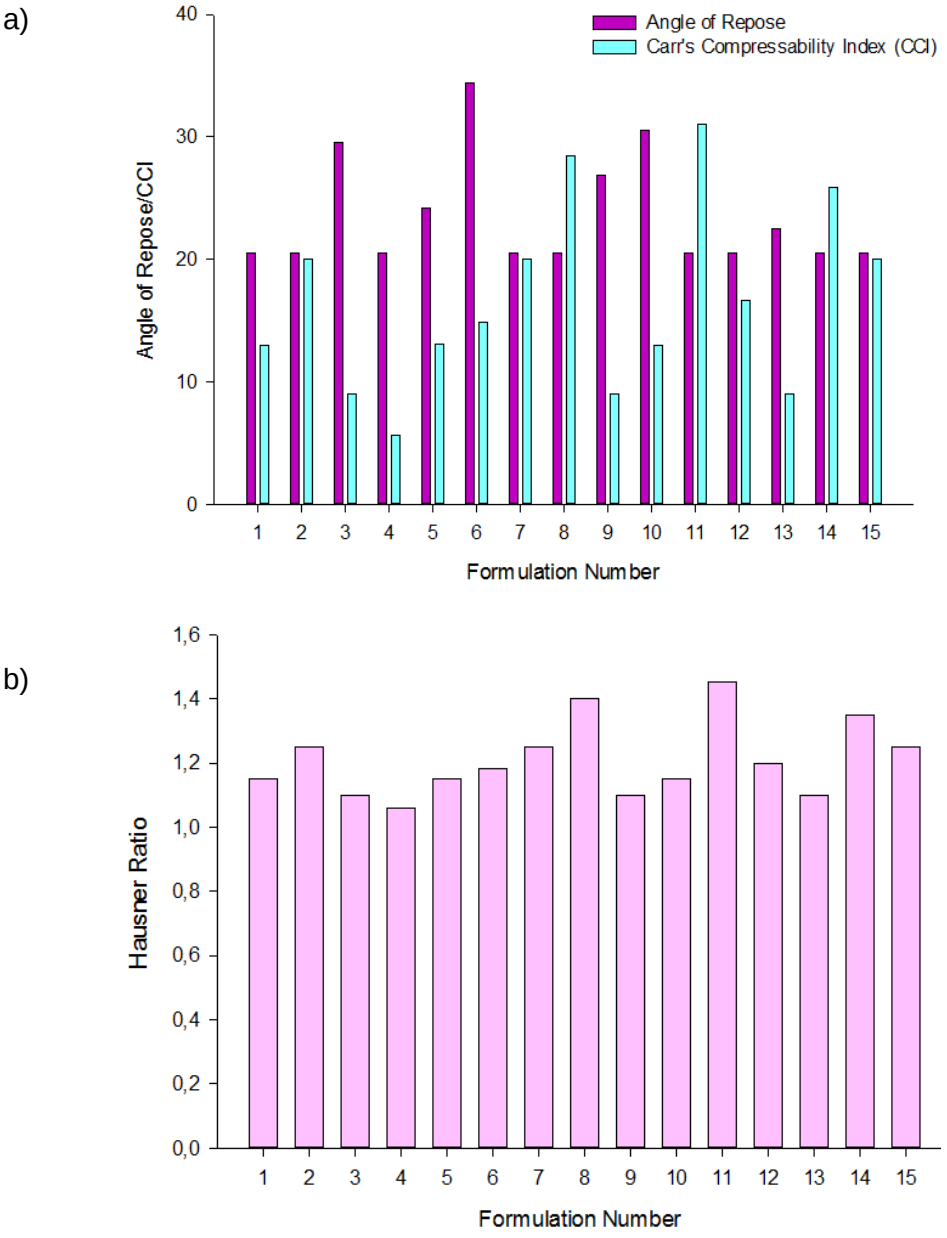


Figure 4.11: a) Graphical illustration of calculated angle of repose and Carr's compressibility index b) Graphical illustration of Hausner ratio.

4.3.8. Analysis of the swelling behavior

In this study the dynamic swelling, in terms of water uptake and erosion of the s-IPN xerogel and PEO-GG blend tablets, were analyzed by monitoring the change in weight over a pre-determined

period of time. Figure 4.12 indicates the percentage of water uptake and thus swelling over a period of time for the varying crosslinked s-IPN xerogel formulations as well as the PEO-GG blend tablets. The porosity of the polymeric material in question such as GG is a predominant feature that determines its swelling ability. In theory an increase in porosity leads to greater initial rates of water uptake and a greater level of equilibrium swelling (Ferrero et al., 2010). Porosity affects the rate of dissolution, when a porous polymeric delivery system is placed in direct contact with dissolution medium, release of the drug must be headed by the penetration of dissolution medium into the pores. Pores close to the surface of the polymer matrix become filled with dissolution medium, thus the initial drug diffusion is controlled by the dissolution of drug within the pores (Ahuja and Pathak, 2009). Therefore, the formation of pores within the xerogel system involves the initial penetration of dissolution medium into the pores followed by swelling of the xerogel-pore boundaries thereby further prolonging release of drug.

Swelling also depends largely on the extent of crosslinking. As seen from Figure 4.12, xerogel formulations F1, F7 and F9 have similar swelling characteristics with a uniform delayed swelling behavior ranging between 450-500%. Whereas PEO-GG blend shows a constant exponential increase in water uptake and swelling up to and beyond the 24 hour test period. Thus the following observation was made based on swelling test results, the greater the amount of water uptake the greater the degree of erosion due mostly to gellan gum as seen in Figure 4.13. Therefore tablets having a high degree of water uptake were found to erode at a faster rate and thus undergo complete disintegration at an accelerated rate, although water uptake also encouraged the degree of swelling which mostly relied on the properties of PEO and related to a delayed dissolution and disintegration process.

Previous studies have shown that the amount of water uptake is directly proportional to the degree of polymeric erosion; and swelling is controlled by the rate of hydration within dissolution medium. Therefore, extent of matrix swelling and erosion determines drug release kinetics (Sriamornsak et al., 2007). Visual observations showed that xerogel matrices swell in contact with dissolution medium to form a viscous gel barrier around the core of the tablet. Drug release occurred via this hydrophilic gel barrier; therefore the rate of release from the matrix is dependent on the viscosity, swelling rate and erosion of the gel layer. It was also noted within the study that the swelling of the s-IPN xerogel was increased with a corresponding increase in crosslinker concentration, due to the formation of polymer networks between PEO and GG. Therefore the Equation 4.19 substantiates this theory.

$$C_c = \frac{1}{Sw}$$

Equation 4.20

Where, *Sw* is the percentage swelling and *Cc* is the concentration of crosslinker.

Hence by extension a reduction in crosslinker concentration leads to the formation of looser polymer networks or IPNs which thus entails the existence of greater hydrodynamic free volume allowing for the absorption of a greater amount of solvent in turn creating a greater swelling capacity (Kulkarni et al., 2011 (1); Kulkarni et al., 2011 (2). In theory, from the equation of Fick's law of diffusion and the equation for dynamic swelling we can deduce the relationships shown in Equations 4.21-4.23 (Kulkarni et al., 2011 (1).

$$\frac{Mt}{M\infty} = Kt^n$$

Equation 4.21

Where $\frac{Mt}{M\infty}$=fraction of drug released per unit time, *k*=release constant and *n*=release index.

$$\frac{Dt}{D\infty} = Kt^n$$

Equation 4.22

Where $\frac{Dt}{D\infty}$=dynamic swelling, k=release constant and *n*=release index (Rokhade et al., 2006). By equating Equations 4.20 and 4.21, we find that,

$$\frac{Mt}{M\infty} \propto \frac{Dt}{D\infty}$$

Equation 4.23

Therefore, it can be further deduced that the amount of drug released has a strong correlation with the extent of swelling. The amount of drug released at time t is inversely proportional to the overall swelling; hence with an increase in swelling the drug release at time t, will be reduced, because the drug molecule has to traverse the gel layer before coming into contact with the dissolution medium

(a) (b)

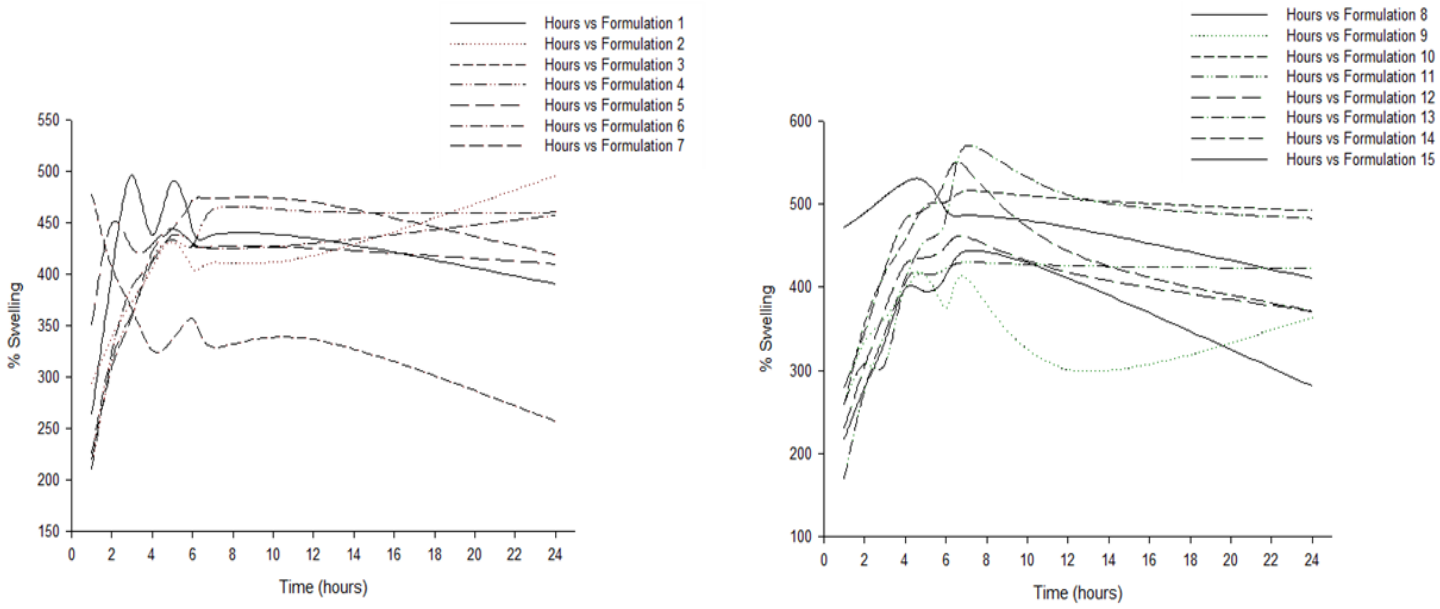


Figure 4.12: Graphical representation of Swelling characteristics (a and b) of crosslinked xerogel formulations vs. a non-crosslinked blend to assist in identification of the influence of polymer ratio as well as crosslinker density on the swelling and erosion capabilities of formulations based on chemical variations on exposure to an aqueous environment (pH 6.8).

4.3.9. *In vitro* drug release analysis

In order to determine the release profiles of the drug from the hydrophilic matrix tablets, dissolution experiments were performed in accordance with simulated intestinal parameters. The plots of Fractional Drug Release vs. Time for the crosslinked s-IPN xerogel matrix tablet F1-15 as well as the PEO-GG blend are depicted in Figure 4.13 a, b respectively.

In the case of the crosslinked s-IPN xerogel formulations, drug release was sustained over a period of 24 hours, the variation in concentration of polymers and crosslinker did generate a noticeable deviation in drug release, however all crosslinked xerogel formulations showed a sustained release over the 24 hour study period. Drug delivery from hydrophilic matrix based systems is controlled by surface erosion of the polymers as well as diffusion of the drug out of the porous matrix network. Furthermore, erosion is based on factors such as water uptake and polymer chain lengths (Toti and Aminabhavi, 2004).

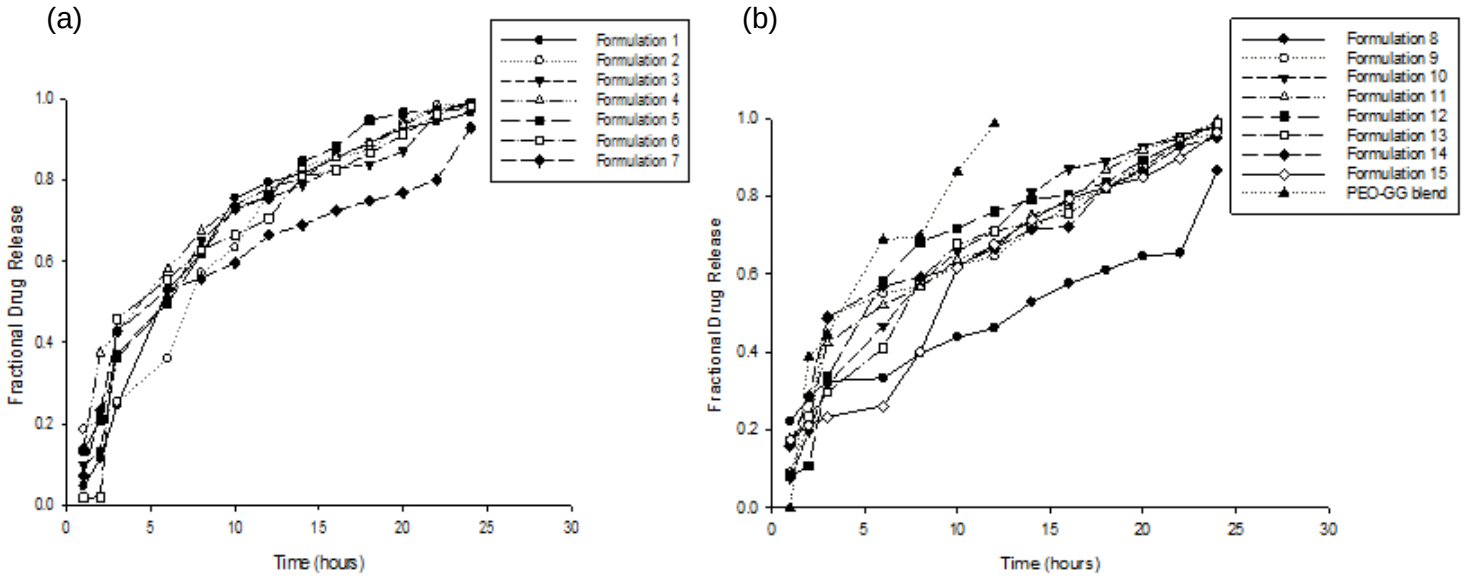


Figure 4.13: Graphical illustration of the *in vitro* fractional drug release vs. time of sustained release s-IPN xerogel matrix tablets in comparison to release profiles of PEO-GG blend formulations.

Polymers forming hydrophilic matrices that come into contact with water are known to undergo prompt ‘gelification’ which is due to the increased size of polymer molecules. There are mainly two mechanisms by which drug release occurs within hydrophilic matrix systems; namely, release by ‘controlled swelling’, whereby drug undergoes the process of diffusion through the gel layer which is formed as stated above by the swelling or increase in size if polymer chains owing to entry of water, and secondly release by ‘controlled dissolution’ in which the water gains entry into the system thereby causing ‘gelification’ of the polymer chains that it comes into contact with, on the other hand; in addition to the conversion of polymer chains to a gel it also causes the polymer to be dissolved, this involves dissolution or erosion of the polymer.

PEO-GG blends showed drug release behavior with characteristics of both the above mentioned mechanisms, GG was subject to controlled dissolution and thus together with swelling it showed an increase tendency to disintegrate and dissolve thus leading to the initial burst effect in drug release, whereas the following controlled release behavior was mainly based on the properties of PEO which follows controlled swelling mechanisms of drug release, in that polymer chains undergo swelling on contact with aqueous phase due to the vitreous-elastic transition of the polymer been activated, thus the gel layer becomes thicker therefore making the drug release slower, because the drug molecule has to now pass through the thickened gel layer formed by swelling of polymer chains which is at a greater distance from the surface of the dosage form, this creates a greater resistance to the diffusion of drug out of the gel layer (Maderuelo et al., 2011). Thus drug release from the PEO-GG blend indicated an initial burst effect followed by a rhythmic sustained release above the desired study period of 24 hours.

Crosslinked PEO-GG s-IPN xerogels F1-F15 displayed constant sustained release during the 24 hour period with 100% drug being released by the end of 24 hours, with slight variations in release rate due to the fact that the swelling and erosion properties of both PEO and GG where modified via the crosslinking reaction, thus these formulations showed a combined mechanism of drug release in terms of 'controlled erosion' and 'controlled dissolution'. From these results it can be deduced that the higher the crosslinker concentration the greater the modification in drug release, as can be seen in F1 and F9 where a concentration of crosslinker between 0.6-0.8mLis correlated to a greater extent of sustained release, whereas F7, 11, 14, and 15 which has a lower concentration of crosslinker depicts irregular drug release kinetics. It can be proven that the boundary layer thickness is directly proportional to the diffusion of the drug; in addition the tortuosity of the matrix is inversely proportional to the boundary layer thickness. In theory, this can be explicated according to the Levenberg Marquardt method and Equations 4.24-4.27 (Siepmann et al., 1999).

$$G = \frac{L \times h}{D}$$

Equation 4.24

Where, *G*='Sherwood number', *D*=diffusion coefficient of the drug, *h*=coefficient of the boundary layer and *L*=thickness of delivery system.

$$D' = \left(\frac{D}{\hat{\delta}}\right)$$

Equation 4.25

Where, *D*=diffusion coefficient of the drug, $\hat{\delta}$=tortuosity of the diffusion matrix and *D'*=effective diffusion coefficient (Siepmann and Peppas, 2012).). By equating Equations 4.24 and 4.25 the relations shown in Equations 4.25 and 4.27 can be deduced.

$$h \propto \frac{1}{D'}$$

Equation 4.26

$$\frac{1}{\hat{\delta}} \propto h$$

Equation 4.27

To determine the mechanism of drug release from the xerogel matrix tablet formulations, the data obtained from *in vitro* release studies were applied to the zero-order (cumulative amount of drug released vs. time) (Shoaib et al., 2006) and Higuchi's (cumulative % of drug released vs. square root of time) (Shah et al., 2008) equation patterns. Release kinetic data for both equations can be seen in Table 4.5.

Table 4.5: Design formulations and their corresponding R^2 values fitted into the zero-order and higuchi model equations.

Formulation Code	Zero-order Kinetics Regression Coefficient (R^2)	Higuchi Model Kinetics Regression Coefficient (R^2)
Formulation 1	0.9879	0.9955
Formulation 2	0.9924	0.989
Formulation 3	0.9927	0.9928
Formulation 4	0.9964	0.9887
Formulation 5	0.9943	0.9952
Formulation 6	0.9969	0.9981
Formulation 7	0.9902	0.9977
Formulation 8	0.9918	0.9991
Formulation 9	0.9965	0.9901
Formulation 10	0.9946	0.9918
Formulation 11	0.9971	0.9953
Formulation 12	0.9953	0.9963
Formulation 13	0.9902	0.9905
Formulation 14	0.9927	0.9973
Formulation 15	0.9957	0.9904

Zero order equation, $Q= k_0t$, Higuchi equation, $Q= k_Ht^{1/2}$

Data plotted in accordance with the zero-order equation showed linearity, with corresponding regression values ranging between 0.9902-0.9879. Release of drug from the matrix system comprising hydrophilic polymers encompasses dynamics of diffusion. Diffusion is responsible for drug passage from the matrix of the system to the dissolution medium subject to a concentration gradient. As the gradient fluctuates, drug is released and the distance for diffusion is increased.

Therefore, drug will diffuse at a reduced rate as the distance for diffusion increases, which is denoted as Higuchi kinetics (Reddy et al., 2003).

Within the context of the current study, *in vitro* profiles of drug release can be elucidated by Higuchi kinetics, as plots showed a great degree of linearity R^2 = 0.9887-0.9991. However, the comparative complexity of the formulation and its respective constituents may imply that drug release is controlled via more than one kinetic process.

4.3.10. Response optimization of s-IPN xerogel matrix

Response optimization procedure (MINITAB®, V15, Minitab, USA) was employed to attain the desired levels of the chosen formulation components. An optimal formulation was fabricated subsequent to concurrent constrained optimization of matrix erosion, drug release, and swelling properties. Minimization of matrix erosion, minimization to an intermediate MDT (Mean Dissolution Time) for drug release and maximization of swelling were utilized for response optimization. The optimized levels of the independent variables and their respective predicted responses were determined. The optimal levels of the independent variables as well as the constraint setting used which would accomplish the preferred erosion, drug release and swelling characteristics are listed in Table 4.6. The optimized levels of the independent variables, the aim for the response, the predicted response (y), at the present factor settings, and the individual and composite desirability scores are shown in Figure 4.16

Table 4.6: Formulation constraints employed for response optimization

Responses	Parameters
Mean % Erosion	Minimize
Drug Release (Total MDT)	Minimize (±13)
Mean % Swelling	Maximize

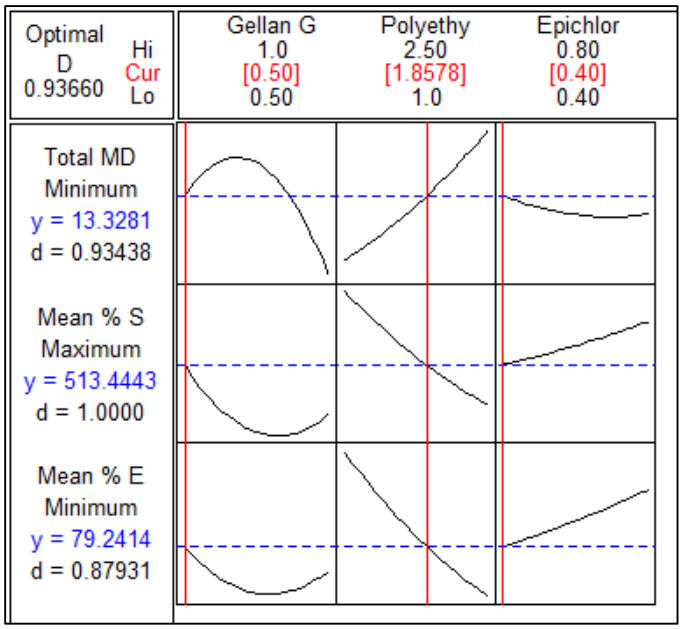


Figure 4.16: Desirability plots representing the levels of GG, PEO and EPI required to synthesize the optimized formulation.

4.4. Concluding Remarks

This chapter detailed the use of a crosslinked PEO: GG polymer solution to formulate an s-IPN xerogel matrix for sustained drug delivery. Results were exhibited employing 3 variables, namely amount of GG, concentration of PEO, and amount of EPI (crosslinker), derived for the measured responses i.e. drug release and degree of swelling and erosion. A ratio of GG: PEO of 0.5g: 1.5%$^{w}/_{v}$ showed desirable drug release in the form of total MDT. A ratio of crosslinker to GG of 0.8 mL: 1g obtained an efficient MDT of 12.5. The concentration of polymers and the ratio of crosslinker influenced drug release, swelling and erosion capabilities of the s-IPN xerogel. Textural profile analysis of the various s-IPN xerogel matrices showed that the crosslinked xerogels were significantly resilient and physically stable. Swelling, erosion and water content studies were consistent with the predicted results from the response surface analyses.

Subsequent to formulation optimization described in the current chapter, additional characterization of the s-IPN xerogel component of the ODLS via physiochemical and physiomechanical characterization studies are described in *Chapter 5* so as to evaluate the efficacy of the design and development of the s-IPN xerogel for ensuing *in vivo* studies.

CHAPTER 5

CHARACTERIZATION AND FURTHER EVALUATION OF THE OPTIMIZED ORAL S-IPN XEROGEL MATRIX FORMULATION

5.1. Introduction

An ultimate dosing regimen in drug therapy of any disease state is one which instantaneously achieves the desired therapeutic concentration of drug in system circulation and maintains a constant plasma concentration for the complete duration of treatment. Comprehensive research efforts have been concentrated on administering drug delivery systems targeted to the site of action for optimum drug bioavailability and minimization of dose related side effects (Bhardwaj et al., 2012).

For drugs administered as a conventional dosage form, such as a tablet, the dosing interval is usually considerably shorter than the half-life of the drug, resulting in restrictions such as poor patient compliance, peak-valley plasma concentration-time profiles, and fluctuations in drug concentration which may lead to the occurrence of adverse effects. So as to overcome these limitations controlled release drug delivery systems are designed and developed (Bhardwaj, et al., 2012).

Sustained release systems include any drug delivery system that achieves slow release of drug over an extended period of time. If the system is successful in maintaining constant drug levels in plasma or target tissue it is considered a sustained release system (Chen et al., 2013; Pundir et al., 2013). Sustained release of drug molecules employing polymers is a deep-rooted proficiency, wherein polymers are rationally selected to encapsulate drug, modify and control its release from the delivery system in a calculated and controllable manner (Angadi et al., 2010). Controlled release formulations can be used to lessen the amount of drug required to illicit the same therapeutic effect. The ease of fewer and more effective doses improves compliance (Huang and Brazel, 2001).

Among the various approaches investigated for attaining sustained release delivery systems, matrix tablets, predominantly those formulated via direct compression methods, are most efficient and remarkable from both the economic and process development perspectives (Marinich et al., 2012). Hydrophilic matrices in particular are been increasingly experimented for controlled drug delivery due to their biocompatibility. Drug release from hydrophilic matrix tablets is governed by the formation of a hydrated viscous polymer layer at the outer boundary of the tablet which acts

as a barrier to drug release by preventing and opposing infiltration of dissolution medium into the tablet and the flow of dissolved solutes out of the matrix tablet (Sriamornsak et al., 2007; Akhgari et al., 2011). The chief drawback to conventional drug delivery systems is their inaptitude to maintain therapeutic concentrations of drugs at the target site. Overcoming this disadvantage by the design and development of sustained release drug delivery systems may offer a great degree of benefit. Sustained release s-IPN xerogel matrices are one example of such drug delivery systems.

An obstacle to the successful treatment of schizophrenia with sulpiride is the reduced patient compliance due to high dosages and therefore, high pill burden; and secondly the low bioavailability observed. A sustained release formulation that would preserve plasma drug levels for 10-12 hours might prove efficient for once-daily dosing of sulpiride. Furthermore, the low bioavailability may be addressed with the incorporation of a P-glycoprotein efflux pump substrate such as lecithin as a formulation excipient, formulation of an s-IPN xerogel matrix system for the delivery of sulpiride, in order to achieve a greater bioavailability; and controlled release will reduce the need for multiple administrations and thus improve patient compliance.

So as to gain insight into the physiomechanical and physiochemical properties of the optimized s-IPN xerogel matrix various studies were conducted. Swelling and erosion were assessed in simulated intestinal conditions; in addition fronts movement studies were performed to evaluate the mechanism of drug release in terms of diffusion and erosion. Fourier Transform Infrared Spectroscopy and Differential Scanning Calorimetry studies were undertaken to assess the chemical composition and thermal characteristics respectively. Porosity analysis, Magnetic Resonance Imaging and Scanning Electron Microscopy were performed to evaluate the surface morphology and physical structure of the matrix system. *In vitro* pharmacokinetic analysis was conducted to decipher the release profile.

5.2. Materials and Methods

5.2.1. Materials

Gellan gum (Gelzan™ CM,1.000kg/mol), poly (ethyleneoxide) (POLYOX™, WSR 303, Average M_v ~ 300.000), (±) sulpiride, epichlorohydrin 99%, carboxymethyl cellulose (disintegrate) , sodium salt, and magnesium stearate (lubricant), were all purchased from Sigma Aldrich (Steinham, Germany), while acetone (Assay 58.08), and sodium hydroxide pearls (Assay min. 97%) were purchased from Merck (Darmstadt, Germany).

5.2.2. Fabrication of optimized s-IPN Gellan Gum- Poly (ethylene) oxide xerogel matrix

For the crosslinked sustained release xerogel, a 1.8578%$^{w}/_{v}$ PEO- 5M sodium hydroxide solution was prepared, in which GG was dissolved subsequently. Thereafter, EPI was added drop wise to facilitate IPN formation by crosslinking of GG. The fabricated gel solution was then placed in acetone for approximately 3 hours to assist solvent removal and pore formation. EPI crosslinking of polysaccharides involves the formation of links via the carbon atoms present, these chemical modifications to the structure of GG allows for characteristic alterations in its mechanical strength, degree of swelling and thus rate of drug release (Gonçalves et al., 2005; Sahin et al., 2011). On the other hand, the presence of PEO during the crosslinking reaction of EPI and GG results in the partial interaction of PEO with the crosslinking agent thus resulting in bonds formed between the ethylene oxide and EPI, resulting in a copolymer (EO-co-EP) (Sanchez et al., 2002). Subsequently, xerogel samples were allowed to dry under ambient conditions, drug was appropriately weighed and added to the powdered xerogel samples (1000mg max. drug loading capacity), and tableted using a hand operated Carver Press tableting press (Model 3851-0, S/N 43000-904, Wabash, IN, USA) employing a compression force of 5 tons.

5.2.3. Characterization of vibrational transitions of optimized s-IPN xerogel

Fourier Transform Infrared Spectroscopy (FTIR) employing a spectrum 100 FTIR spectrometer (Perkin- Elmer, Beaconsfield, BUCKS, UK) was utilized to detect the vibrational individualities of chemical functional groups in the optimized xerogel samples. FTIR analysis was conducted on native polymers incorporated in the xerogel as well as on the optimized s-IPN xerogel as a means of validating the successful crosslinking reaction performed. Samples were placed on a diamond crystal and processed by the universal ATR polarization accessory software for the FTIR spectrum series at a wave number range of 650-4000 cm^{-1}.

5.2.4. Characterization of thermal transitions of the optimized s-IPN xerogel by Differential Scanning Calorimetry and Thermogavimetric Analysis

Differential Scanning Calorimetry (DSC) curves were recorded on a Mettler Toledo, DSC 1, STAR^{e} System (Schwerzenback, Switzerland). The instrument was calibrated with the use of Indium metal (99.99%) with regards to temperature and enthalpy (Kreye et al., 2013). Accurately weighed samples of each (±10mg) were placed into aluminum sample holders covered and a central pin hole made. Samples of crude polymers PEO and GG as well as the optimized s-IPN xerogel were heated in sealed aluminum pans between a temperature range of 25-300˚C under the constant flow of nitrogen gas at a heating rate of 10˚C/minute. Thermogavimetric analysis (TGA) measurements were conducted with a Perkin- Elmer TGA 7 apparatus. Samples of crude PEO

and GG and of optimized s-IPN xerogel, all with an approximate weight of 10mg, were heated in a dynamic nitrogen atmosphere from 30- 700˚C at a heating rate of 10˚C/ min, this was done in order to determine their respective thermal degradation properties.

5.2.5. *In vitro* drug release studies

A calibration curve for sulpiride was constructed as detailed in *Chapter 3, Section 3.3.5.* Dissolution and drug release studies were conducted employing a USP type II apparatus (Caleva, model 7ST, UK) at a rate of 50 rpm and temperature of 37˚C maintained by a thermometer in 900mL of potassium phosphate buffer (pH 6.8) in triplicate. A stainless mesh ring was immersed in to the dissolution bath, secured below the paddle to ensure minimal floating of the sample. 5ml of dissolution medium was withdrawn manually at pre-defined time points during a 24 hour experimental study and an equal volume of drug free dissolution medium was replaced to as to ensure the maintenance of sink conditions. Samples withdrawn were analyzed for drug content by utilizing Ultraviolet Spectrometry at a wavelength of 300nm and drug release profiles were thereby plotted with the use of the generated calibration curve for sulpiride (soluble in phosphate buffer pH 6.8). The conventional system was not tested within this experimental set up due to its rapid dissolution characteristics.

5.2.6. Morphological and surface structure analysis

Scanning Electron Microscopy (SEM) was utilized in determining the surface morphology of crude PEO and GG, as well as providing evidence of the synthesis of s-IPN within the optimized crosslinked xerogel formulation. Samples of native PEO and GG as well as optimized s-IPN xerogel were mounted on steel stubs using double sided adhesive tape and sputter coated with carbon and gold palladium shadowing to ensure increased conduction of the sample employing a sputter coater. The coated samples were observed employing the Phenom G2 Pro SEM (Germany) by utilizing various magnifications at room temperature.

5.2.7. Porositometric analysis

Porosity evaluation was conducted employing the Brunauer- Emmet- Teller (BET) isotherm of nitrogen as a tool to investigate the presence and size of pores within the networked structure of the optimized s-IPN (n=3). An ASAP 2020 Porositometer (Micromeritics Instrument Company (Pty) Ltd., Norcross, GA, USA) equipped with research grade ASAP 2020 V3.01 software was utilized in the determination of the optimized s-IPN xerogel porous structure, such as pore surface area, pore diameter, total pore volume, as well as bulk and absolute densities. Samples were treated with a heat gradient and then evacuated with nitrogen gas (N_2) for the removal of surface

moisture and gas particles preceding analysis. Table 5.1 below lists the parameters and settings used under standard conditions of temperature and pressure (STP: 0˚C and 760 torr). The optimized s-IPN xerogel samples were weighed to (100mg ± 10mg) and placed in a cylindrical sample tube. In order to reduce the total free space and thereby allow for timely degassing, a glass filler rod was inserted within the sample tube. The samples were then covered in an isothermal jacket and degassed for approximately 20 hours. The degassed samples were then transferred to the analysis port and immersed in liquid nitrogen preceding the analysis. The Barrett, Joyner and Halenda (BJH) as well as Brunauer- Emmett- Teller (BET) adsorption and desorption associations were generated.

Table 5.1: Parameters utilized for the evacuation and heating phases in degassing of the optimized s-IPN

Parameter	**Rate/Target**
Heating Phase	
Temperature ramp rate	10˚C/min
Hold Temperature	30˚C
Hold Time	1320 min
Evacuation Phase	
Temperature ramp rate	10˚C/min
Evacuation rate	50.0mmHg/s
Target Temperature	40 ˚C
Unrestricted Evacuation from	30mmHg
Vacuum set point	500μmHg
Evacuation Time	60 min

5.2.8. Assessment of degree of mucoadhesion of the optimized xerogel matrix

Mucoadhesion studies were performed on the optimized matrix tablet to deduce the effect of polymer ratios on the amount of mucoadhesion of the system (n=3). For this study a 0.1%$^{w}/_{v}$ mucin solution prepared in USP intestinal fluid (pH 6.8) was incubated; the optimized xerogel tablet was placed in an orbital shaker maintained at 37˚C and 50 rpm. Concentration of free mucin in the solution, after a 6 hour duration, was determined by a UV spectrophotometer, at wavelength 201

nm(IMPLEN NanophotometerTM, Implen GmbH, München Germany),using a 10 times dilution factor of path-length 0.1 mm. The difference in the concentration of the mucin solution before and after incubation was the indication of the amount crosslinked with the xerogel tablet as seen in Equation 5.1 below, indicating the interaction between particles and mucin (Ping et al., 1998).

$$Mucoadhsion\ \% = \frac{[Mucin\ before] - [Mucin\ after]}{[Mucin\ before]} \times 100$$

Equation 5.1

5.2.9. Elucidation of the pertinent rheological properties of the optimized s-IPN xerogel

The rheological properties of the optimized s-IPN xerogel were evaluated with the use of a Haake Modular Advanced Rheometer System (ThermoFisher, Scientific, Karlsruhe, Germany). Viscosity affects the rate and extent of swelling of polymer agents, thereby imparting vital insight into the drug release behavior within a xerogel based matrix system. Optimized s-IPN samples were analyzed by placing the xerogel solution on the sample stage and then immersing the C35/1˚ titanium rotor on to the xerogel solution while the temperature was maintained at 34˚C, while the shear rate was maintained at $100s^{-1}$ for 360s with viscosity readings being quantified (n=3).

5.2.10. Textural characterization of the optimized s-IPN xerogel matrix tablet

Optimized s-IPN xerogel matrix tablet was analyzed for its physiomechanical properties by performing textural analysis studies (n=3). Results based on hardness, deformation, resilience, and matrix rigidity were obtained from the data generated. Matrix tablets of 3mm thickness were subjected to analysis with the generation of force vs. time and force vs. distance profiles on a TX.XT plus texture analyzer (stable Microsystems, Surrey, UK) equipped with a 2mm flat head cylindrical probe, a 5 kg load cell and texture component V3.2 software for processing data. Tablets were secured on to a raised platform fitted with a central probe with a 5mm diameter central hole. The central probe with a 5kg weight load was lowered on to the tablet surface and measurement conducted. Parameters employed for textural analysis were as follows; test mode was compression, pre-test speed 1mm, test speed 0.5mm, post-test speed 1mm, and the target mode was set as; Distance (0.5mm), Strain(10%), and a trigger force of 0.05N.

5.2.11. Gravimetric swelling and erosion studies

Equilibrium water uptake and swelling studies of the s-IPN xerogel matrix tablets (n=3) loaded with drug was conducted by measuring the extent of swelling of the matrix in Phosphate buffered saline (PBS) (pH 6.8;37˚C). Samples were placed in 20ml PBS and allowed to swell. At pre-determined time intervals over a 24 hour test period, samples were removed from the buffer, surface water was removed with blotting paper and samples weighed. Equations such as, dynamic swelling ratio, equilibrium water content, water uptake and % erosion were employed in characterization of the swelling behavior of the xerogel matrix tablets (Murthy et al., 2006; Reddy et al., 2012).

$$Dynamic\ Swelling\ Ratio\ (S) = \frac{Wt - Wo}{Wo}$$

Equation 5.2

Where Wt. is the weight at time t, and Wo is the initial weight of the tablet.

$$Equilibrium\ Water\ Content(EWC\%) = \frac{Weq - Wo}{Weq} \times 100$$

Equation 5.3

Where Weq is the weight at equilibrium, and Wo is the weight of the initial tablet.

$$Water\ Uptake\ \% = \frac{Ws - Wo}{Wo} \times 100$$

Equation 5.4

Where Ws is the weight of the swollen tablet, and Wo is the weight of the initial tablet

$$\%\ Erosion = \frac{Wo - We}{We} \times 100$$

Equation 5.5

Where Wo is the initial weight of the tablet, and We is the weight of the test after the erosion test.

5.2.12. Determination of the diffusion, swelling and erosion fronts

The experiment was conducted on the s-IPN xerogel, GG and PEO tablets respectively (n=3) to observe the radial swelling behavior and overall swelling capacity of each. In order to improve the visual detection of the swelling fronts, dyes were added to the PBS buffer (pH 6.8; 20ml). At pre–defined time points, over a 24 hour period the hydrated fronts were measured using a digital caliper and pictures were taken using a camera with a 10X digital zoom. The focal distance was kept constant throughout the study, with the interface between the matrix and the dissolution medium at the start of the study been labeled the initial diameter, with inward movement denoted as negative and outward movement denoted as positive.

5.2.13. Magnetic Resonance Image (MRI) analysis of the swelling behavior of the optimized xerogel matrix tablets

s-IPN xerogel matrix tablets were imaged in phosphate buffered saline of pH 6.8 at 37˚C utilizing a 0.5T open – configuration Magnetic Resonance Imaging (MRI) system (Signa SP,General Electric Medical Systems, Milwaukee, WI, USA). Imaging of samples tested was obtained at 30 minute intervals over a 24 hour test period to evaluate the extent of swelling and erosion over time.

5.3. Results and Discussion

5.3.1. Inter and intra- polymeric interaction validation of the optimized crosslinked xerogel

FTIR spectra of the native polymers employed in the synthesis of the crosslinked s-IPN xerogel were analyzed in relation to the spectrum attained for the optimized formulation, to determine whether any components within the formulation interacted as a result of the polymer crosslinking. GG (Figure 5.1a) demonstrates a characteristic peak at 2850-2960cm^{-1} which corresponds to C-H stretching of alkane functional groups (Krishnaraj et al., 2012; Coates, 2000); this is observed within the optimized formulation as a characteristic GG absorption band. The FTIR spectra of crude PEO depicted the functional groups present within its chemical structure, with characteristic bands being the O-H functional groups characteristic of alcohols in the range of 3200-3600cm^{-1} and C≡C stretching depicted at a wavelength range of 2100-2260cm^{-1} (Figure 5.1c) (Krishnaraj et al., 2012;Coates, 2000).

Due to the existence of NaOH within the crosslinking reaction, there is a breakdown of the O-H bonds, thereby leading to an interaction of the hydrogen and oxygen molecules respectively with other molecules, thus forming new functional groups (Durig and Fassihi, 2002).This chemical occurrence causes the addition of alkene groups with characteristic C-H stretching at wavenumbers of approximately 3276cm^{-1} as shown by the highlighted peak in Figure 5.1b. This particular phenomenon relates to a higher level of conjugation and improved stability of the polymer network (Coates, 2000; Krishnaraj et al., 2012). In addition, the strong O-H band at 3200-3600cm^{-1} is observed within the optimized xerogel relating to the presence of alcohols or phenols (Coates, 2000; Krishnaraj et al., 2012).

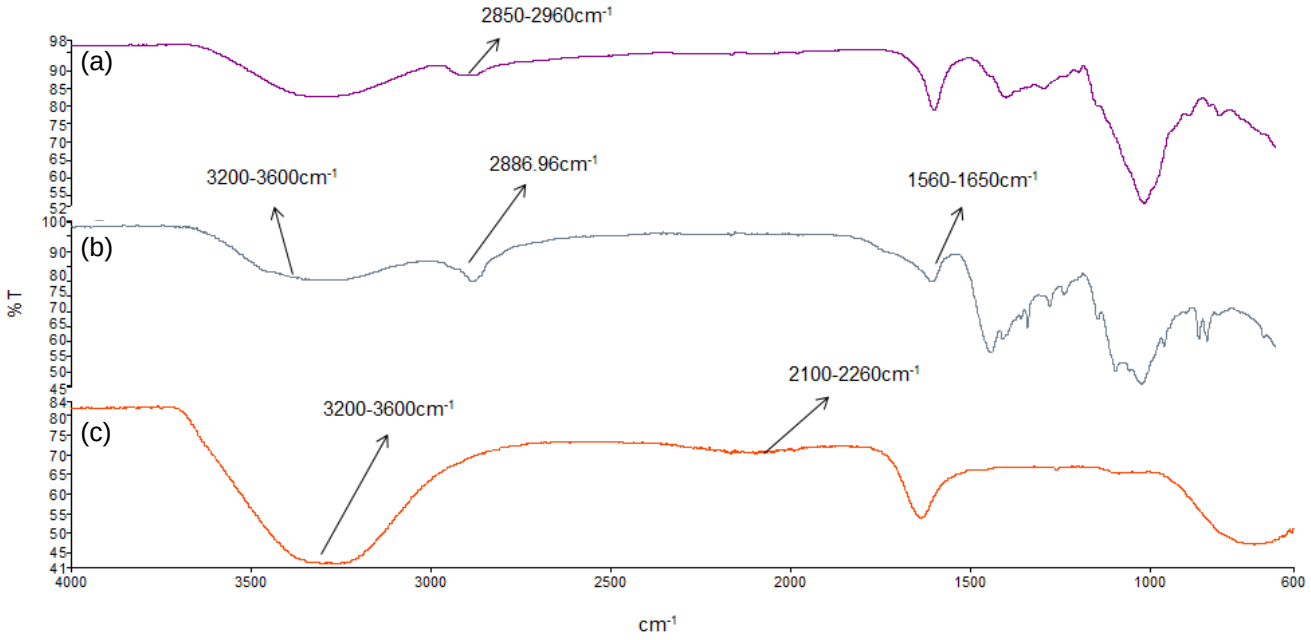


Figure 5.1: FTIR spectra of (a) crude GG; (b) optimized s-IPN xerogel and (c) PEO.

C-N amine stretching occurred at 1560-1650cm^{-1} shown in Figure 5.1b, these peaks tend to occur at higher vibrational frequencies and are known to be associated with the degree of crosslinking and polymer network formation resulting in a change within the structural configuration of molecules (Durig and Fassihi, 2002).The prominent peak at 1606.88cm^{-1} is characteristic of aromatic ring conjugation, thus confirming the presence of an aromatic ring structure within the

optimized formulation. C-H stretching at 2886.96cm^{-1} in Figure 5.1b within the aromatic ring structure, is derived from the chemical structure of crude GG, resulting in the incorporation of C-O functional group within the aromatic structure at 1080-1300cm^{-1} (Coates, 2000; Krishnaraj et al., 2012).

Furthermore, methyl and methylene groups at 1430-1470cm^{-1} were introduced within the structure of the optimized xerogel with the addition of RCH=CH_2 bridges extending from the aromatic ring backbone. A shifting of the aromatic ether occurs at 1240cm^{-1} as compared to 1200cm^{-1} in the spectrum of GG. In addition, the optimized xerogel displays characteristically new bands, such as the addition of a methyl and methylene group at 1430-1470cm^{-1}, alkyl ethers at 1060-1150cm^{-1} and C-H out of plane bending at 800-1000cm^{-1}. Based on the FTIR spectra the optimized xerogel may be characterized as an organic compound due to the presence of C-H stretch and the presence of aromatic bands. In addition the broad O-H alcoholic band is characteristic of the crystalline structure of the xerogel (Coates, 2000).

Chemical crosslinking reactions are associated with the addition of new functional groups and molecular interactions between polymer chains thereby resulting in crosslinked chains (Adel et al., 2010). This theoretical description explains the additional functional groups observed within the chemical structure of the optimized xerogel as compared to the crude polymers utilized.

5.3.2. Thermal analysis of the optimized crosslinked PEO-GG based xerogel by Differential Scanning Calorimetry and Thermogavimetric Analysis

Thermal characterization was conducted to identify any irregularities or damaging alterations to the sample after the crosslinking reaction as well as to determine the thermal stability of the potential drug delivery system. In crosslinked systems, the glass transition temperature (T_g) is dependent on the degree of crosslinking. The relationship between T_g and crosslinking is a proportional one, with an increase in crosslinking degree there is a corresponding increase in the T_g temperature (Mettler Toledo, 2001). Differential Scanning Calorimetry (DSC) results shown in Figure 5.2a depict that the T_g for the optimized formulation was 67.74˚C with a crosslinking concentration of 4%$^{v}/_{v}$. Furthermore, DSC data for the optimized formulation showed an endothermic melting peak at a temperature of 101.65˚C thus indicating the melting temperature of the crosslinked polymer. The optimized xerogel displays a larger relaxation peak when compared to the crude polymers as seen in Figure 5.2a. This is defined by the lower integral value of PEO the crude polymer compared to the higher -274.90mJ of the optimal xerogel thus indicating that more energy was required from the heating system (for the optimized) to allow for melting to occur. An additional exothermic peak at a temperature of 224.59˚C is identified within the DSC

results, corresponding to crystallization on decomposition. This represents the phase change of the sample from a melted (liquid) state to a solid crystalline solid.

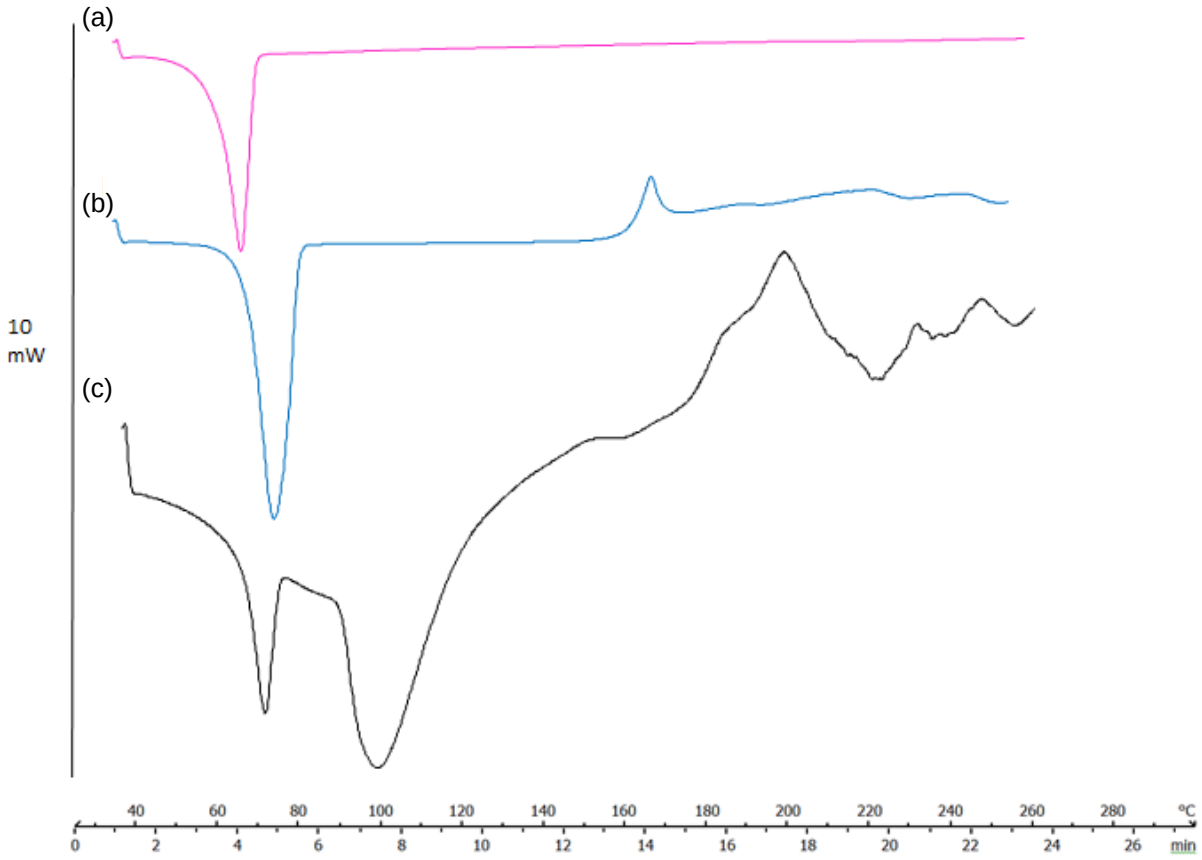


Figure 5.2: DSC Thermograms of a) Gellan Gum b) Optimized s-IPN xerogel c) Polyethylene Oxide

Thus DSC shows that the crosslinking reaction does affect the thermal properties of the optimized formulation yet maintains its stability. Tg is defined as the temperature at which a large variety of coordinated molecular motions occur. Therefore below 67.74˚C the amorphous polymer chains are stationary with only vibrational motion and short range rotations occurring. As the temperature increases to 67.74˚C and above the polymer chains gain mobility and relaxation. At 67.74˚C the sample begins to soften and is described as the melting of the amorphous region of a semi-crystalline sample. As the temperature reaches 101.65˚C the sample undergoes melting and then proceeds to crystallization of the polymer at 224.59˚C.

Thermogavimetric analysis (TGA) was employed to further assist in the interpretation of thermal properties of the optimized xerogel sample by utilizing heat and stoichiometric ratios to determine the percentage by mass of solute. The optimized xerogel displayed weight loss in the region showing an extrapolated onset of 250˚C and an endset of 350˚C which is described as the decomposition temperature (Figure 5.3). The first derivative on a TGA curve (Figure 5.3) designates the point of highest rate change in weight loss (inflection point). The inflection point within the optimized s-IPN xerogel sample was observed at a temperature of 240.33˚C. The observed inflection point may be attributed to chemical reactions such as decomposition, crystallization or physical transitions due to reactions such as evaporation desorption or drying.

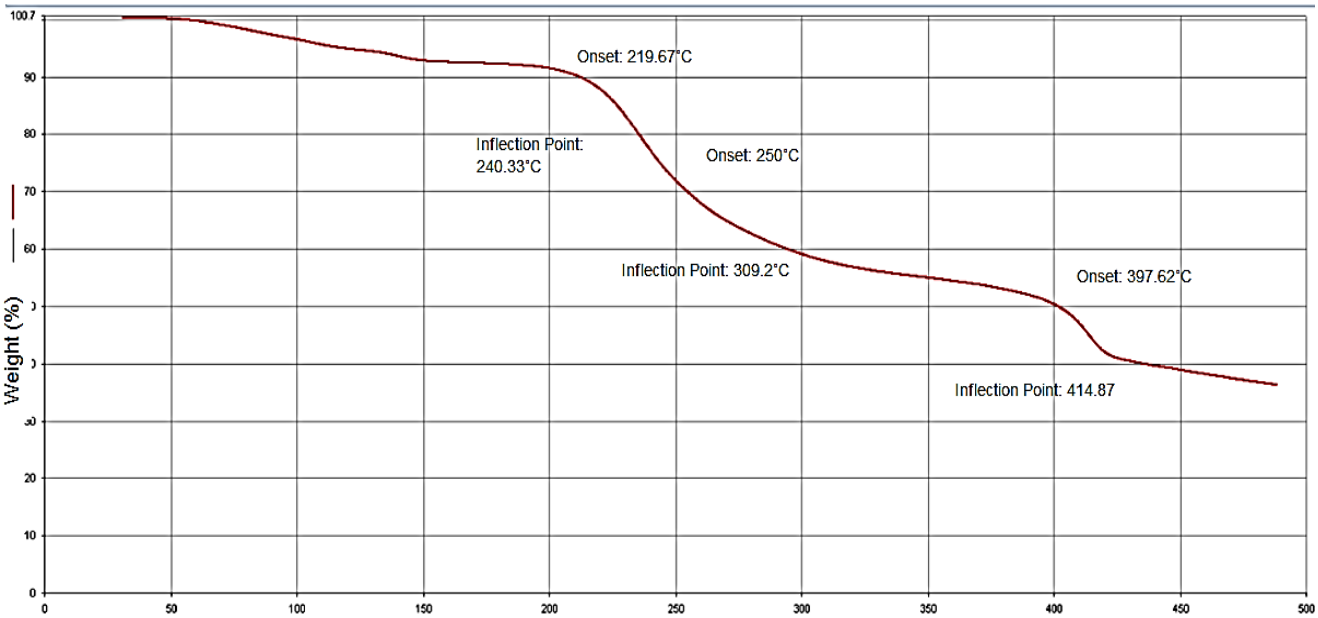


Figure 5.3: TGA thermogram of optimized s-IPN xerogel.

The resulting TGA curve illustrates a multistep decomposition process with two distinct weight loss steps. The first weight loss step occurs at an onset temperature of 219.67˚C (Figure 5.3) due to drying of residual moisture within the sample. The second weight loss step is at an onset temperature of 414.87˚C indicating decomposition of the sample on melting (Figure 5.3). On removal of the sample after TGA testing the sample presented black in color, this change in sample appearance can be explained by the pyrolysis of organic samples under the influence of nitrogen. Polymers present within the sample turns a carbon black upon pyrolysis and when exposed to an air environment it burns (Mettler Toledo, 2001).

5.3.3. Construction of calibration curve for ultraviolet spectrophotometric determination of bioactive release from optimized s-IPN xerogel matrix

A calibration curve for sulpiride was constructed in PBS (pH6.8; 37˚C) using a known series of concentrations of sulpiride as detailed in *Chapter 3, Section 3.2.9 and 3.3.5.*

5.3.4. *In vitro* drug release determination of optimized s-IPN xerogel matrix tablets

Drug release from hydrophilic based matrix systems is considered a multifaceted interaction between dissolution, diffusion, and erosion. Generally, drug release from controlled release matrix tablets encompassing a bioactive and hydrophilic polymer, as is the case in the current research; release ought to ideally follow three steps. i) Dissolution medium penetration into the tablet matrix. ii) Swelling in conjunction with dissolution or erosion of the matrix. iii) Passage of the dissolved bioactive agent, either via the hydrated matrix or from the eroded fragments of the tablet, into the dissolution medium (Shoaib et al., 2006).

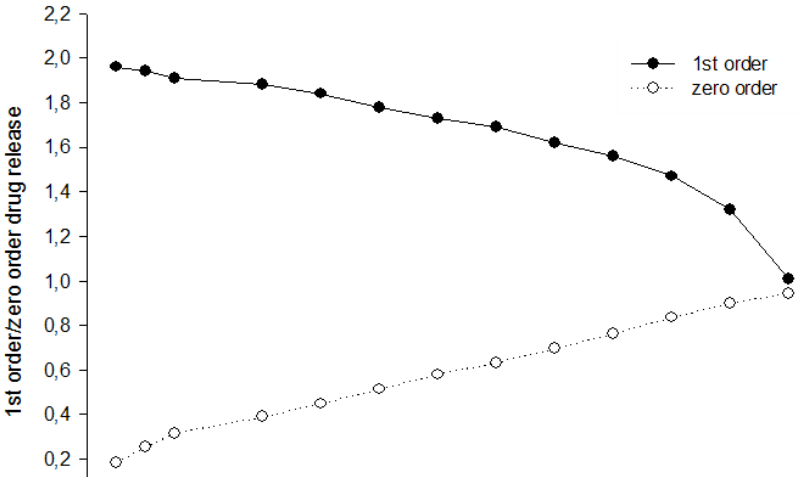
In order to investigate the *in vitro* drug release various kinetic models were employed to describe the mechanism of release kinetics. Therefore, to investigate the mechanism of drug release, release data obtained via *in vitro* dissolution studies were analyzed utilizing zero order, first order, Higuchi, Korsmeyer, and Hixson-Crowell mathematical models. The following plots were made: *cumulative % drug release vs. time* (zero order); *log cumulative % drug remaining vs. time* (first order); *cumulative % drug release vs. square root time* (higuchi); *log cumulative % drug release vs. log time* (Korsmeyer- Peppas) and *cube root of % drug remaining vs. time* (hixson-crowell) as seen in Figure 5.4.

For analytical completion of drug release, release data of sulpiride obtained via dissolution studies was plotted as fractional release vs. time. The resulting straight line specifies zero order release kinetics in accord with the zero order equation ($Q=Q_0+k_0t$). Linear regression analysis of the data produces the equation; c = 0.1136t and an R^2 value of 0.9956. Thus, the rate of dissolution is k_0= 0.115 $mgL^{-1}h^{-1}$.

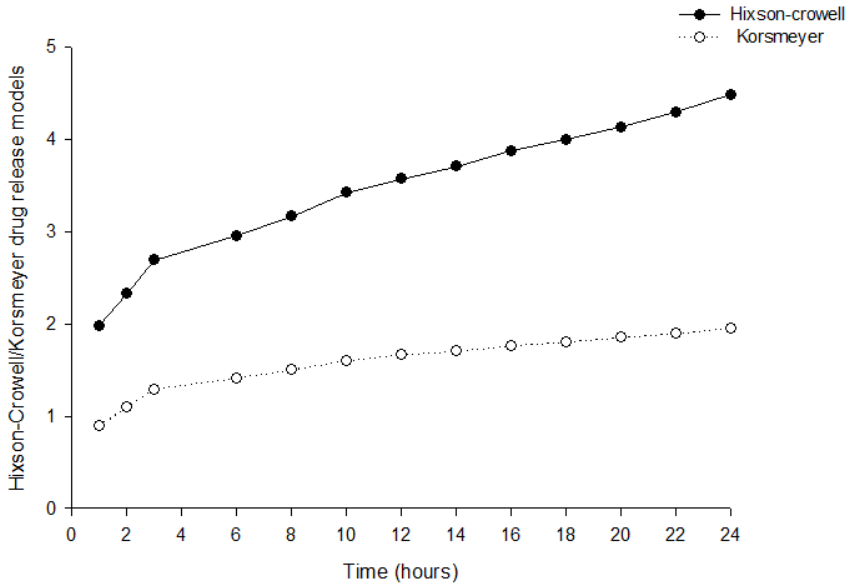
Table 5.2: Zero-order kinetic data.

Linear regression analysis of zero-order release plot ($Q=Q_0+k_0t$)
c = 0.1136t
R^2= 0.9956.
k_0= 0.115 $mgL^{-1}h^{-1}$

(a)



(b)



(c)

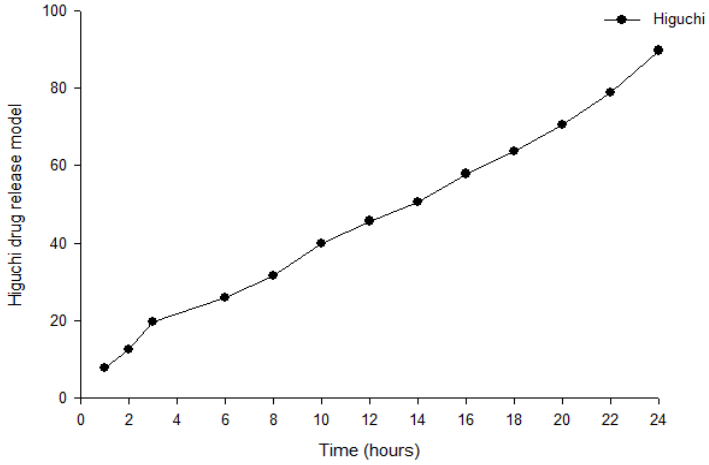


Figure 5.4: Plots of drug release based on the respective mathematical models (n=3).

Hence, the optimized formulation allows for steady sustained release of the bioactive with the drug release rate being independent of concentration, from within the gel matrix. Sulpiride diffuses

through the outer gel layer, which in turn undergoes erosion permitting additional dissolution medium penetration into the matrix core. Within the zero order and first order plots, the obtained R^2 value was 0.99 and 0.64 respectively, thereby confirming drug release as zero order, independent of drug concentration. The Higuchi equation plot was linear with an R^2 value of 0.996 (Figure 5.4) demonstrating the release of bioactive from the matrix as a square root of time. The dissolution data was also plotted into the Hixson-Crowell cube root law equation applicability of the data (R^2 0.9703) which indicates an alteration in surface area and diameter of the matrix tablets via the progressive dissolution as a function of time.

By means of integrating release data into the Korsmeyer equation the mechanism of release can be obtained, where n is the release exponent, indicative of mechanism of drug release. For the Korsmeyer equation an R^2 value of 0.9943 and the value of the release exponent in sulpiride sustained release obtained as 0.85 which follows anomalous transport ($0.45<n<0.89$). However, the power law can only provide restricted understanding into the precise release mechanism of the bioactive (Dash et al., 2010; Sharma, et al., 2014).

5.3.5. Assessment of the surface morphology of the optimized crosslinked xerogel

Scanning Electron Microscopy (SEM) was employed to evaluate the surface morphology of the optimized xerogel formulation. This evaluation was utilized to assess the difference in porosity and surface morphology of the optimal xerogel before and after swelling in phosphate buffered saline of pH 6.8. SEM images for the optimized xerogel (Figure 5.5) revealed a consistently porous crystalline surface morphology with noticeable crevices cracks and pores.

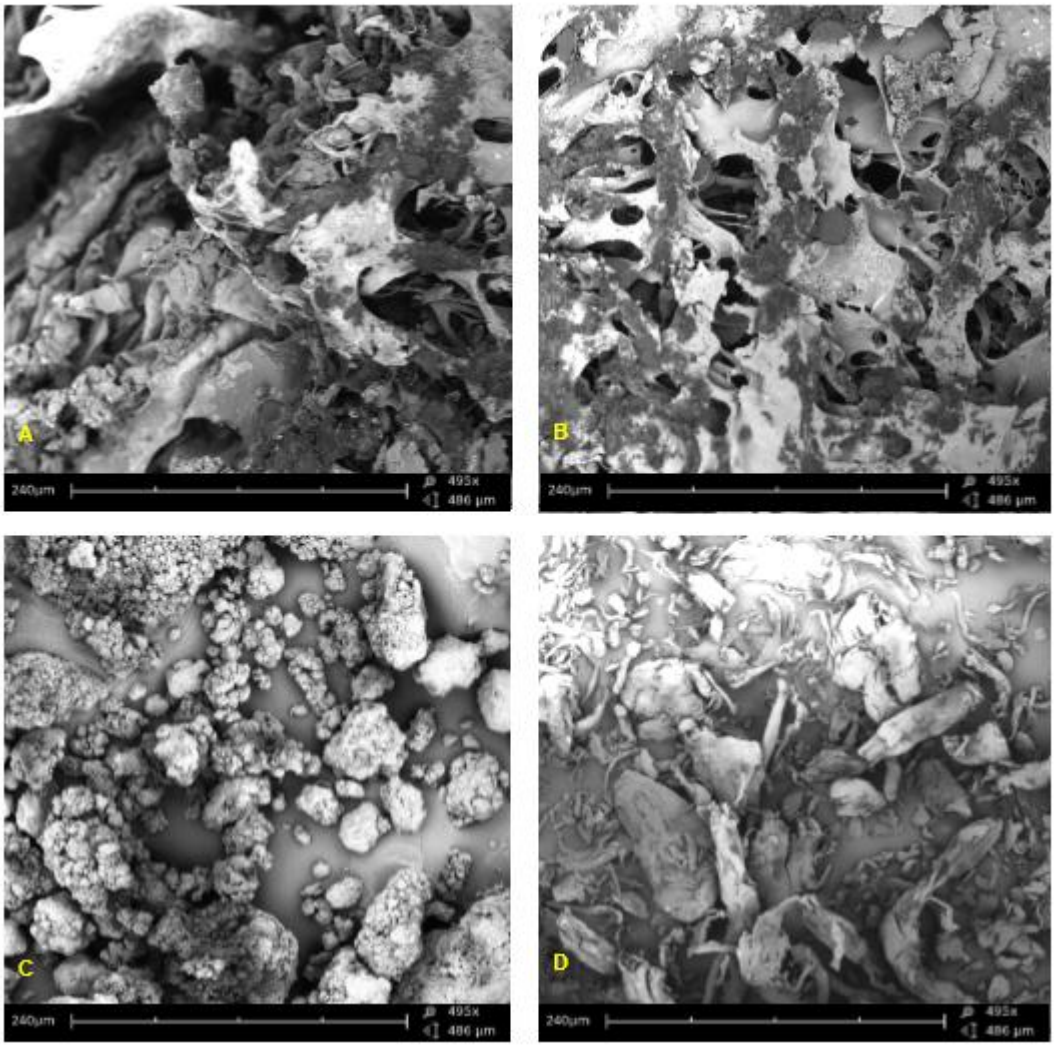


Figure 5.5: SEM images of A) optimized xerogel before swelling B) optimized xerogel after swelling C) pure polyethylene oxide D) pure gellan gum.

The results obtained from SEM imagery showed, as expected, a semi- porous solid matrix. The matrix appeared to have a solid surface with interconnecting networks as well as the presence of interspersed pores (Figure 5.5b). The observed pores are generally circular or asymmetrical through the matrix surface area. Entry of aqueous medium into these pores allowed for the swelling of the polymer chains and thus entrapment of drug within the porous structures.

SEM imagery of the optimized xerogel post swelling show a prominent increase in pore size and a visible increase in the polymer density. The xerogel forms structured pores surrounded by thin folds of polymer. This further ascertains the effect of swelling and pore formation on the resulting

s-IPN xerogel for controlled release of drug from the system. The comprehensive crosslinking of the crude polymers indicated by the lack of excess polymeric residue indicates a high degree of inter-polymeric structure and thus suggests a compact structural integrity.

5.3.6. Determination of xerogel porosity

Porosity analysis was conducted in order to determine the volume of distribution of pores present within the optimized xerogel as observed in surface morphology evaluation studies. Pore size was also investigated. It was determined that pores contained in the s-IPN xerogel were essentially microporous. Pores ranged between the sizes of 67.448 - 70.390Å in diameter. The total pore volume extended between 3.368 - 3.5402m^2/g indicating an increased pore volume which was anticipated. As discussed above, the presence of pores within the matrix system allows for entrapment of drug within the porous structures upon swelling. Therefore, the presence of microporous sized pores is beneficial so as to permit controlled drug release behavior. Table 5.3 summarizes derived porosity data.

Table 5.3: Summary of porosity data obtained for the optimized xerogel.

Measured Characteristic	***Optimized s-IPN xerogel formulation***
Single Point Surface area	1.9952 m^2/g
BJH: Cumulative surface area of pores	Adsorption: 3.368 m^2/g
	Desorption: 3.5402 m^2/g
BJH: Cumulative volume of pores	Adsorption: 0.005926 cm^2/g
	Desorption: 0.005970 cm^2/g
BJH Adsorption average pore diameter (4V/A)	Adsorption: 70.390 Å
	Desorption: 67.448 Å

5.3.7. Determination of degree of mucoadhesion

Mucoadhesive drug delivery structures employ the attractive forces present between mucus and polymeric drug molecule carriers. Mucoadhesive structures allow for localization of the drug delivery system within a specified target site thereby prolonging residence time. This particular mechanism greatly enhances the bioavailability of drugs. Hence, understanding the interactions between mucin and respective polymers within the physiological environment is vital for the rational design and development of mucoadhesive delivery systems (Peppas and Huang, 2004).

Mucoadhesive experimentation of the optimized tablet displayed a mucoadhesion of 74.2%. The observed degree of mucoadhesion may be attributed to the excipients utilized during the formulation process. GG and PEO are known for their excellent mucoadhesive characteristics (Gaikwad and Bhatia, 2012).Thus the resulting mucoadhesion can be attributed to the additive mucoadhesive properties of each of the above mentioned polymers.

5.3.8. Rheological characterization of non-drug loaded xerogel polymeric solution employed in matrix formation

Rheological characteristics, in particular the viscosity of polymeric solutions regulates whether the formulated solution may undergo precipitation, in addition it influences the quality and degree of swelling once formulated into a solid matrix system. The solution parameters for the non-drug loaded formulation was 0.5%$^{w}/_{v}$ GG, 1.858%$^{w}/_{v}$ PEO, and 0.4mL EPI, the drug loaded formulation comprised of the same solution parameters with 50mg sulpiride included. The resulting viscosity at shear rate of 100/s (mPas) standard derivative was 2938.1 and 1815 respectively. As observed the addition of drug into the xerogel solution results in an increased viscosity.

The shear rate (γ) is directly related to the applied stress (σ), the resulting proportionality is the coefficient of dynamic viscosity (η). With a high degree of viscosity and a corresponding low flow rate a thick boundary layer is formed which becomes thinner as the viscosity drops and the flow rate increases (Schnaare et al., 2005). The resulting rheological data indicates non-Newtonian behavior of the s-IPN xerogel solution. This deduction was made on the basis that the xerogel begins to flow as soon as the shear stress is applied, with the slope progressively decreasing with a consistent increase in shear rate. A degree of thixotropy is also observed, after the xerogel is exposed to a particular shear rate, the shear stress and viscosity will decrease with time. When the applied shear stress is removed, even if the structure has been disrupted it is reversible; as thixotropy is defined as a reversible time-dependent decrease in apparent viscosity.

Samples that depict thixotropic behavior are commonly composed of asymmetric macromolecules capable of interacting by numerous secondary bonds so as to produce a loosely linked three-dimensional structure. Thus the sample is gel- like when un-sheared. Upon shearing these bonds become disrupted, so flowing elements align and the viscosity decreases (Schnaare et al., 2005).

5.3.9. Mechanical evaluation and validation of structural integrity of the optimized xerogel matrix

Mechanical evaluation of the matrix system, PEO-GG blend was conducted. For all formulations, a typical force-distance and force-time profile was generated to evaluate deformation energy,

rigidity, resilience, Brinell hardness number (BHN). The force vs time profiles for the optimized xerogel matrix tablet and the PEO-GG blend tablet are depicted in Figures 5.6 and 5.7 respectively. In the textural analysis profile, the gradient represents the matrix flexibility (rigidity), while the area under the curve depicts the deformation energy. Data obtained suggests that the optimized formulation has superior mechanical properties.

Values of resilience and deformation for the optimized tablet and the PEO-GG blend tablet were found to be 46.78%, 54.16%, 0.008J, and 0.013J respectively. Notably both formulations allowed for very high matrix resilience. This is due to the high degree of saturated ionic bonding present in both. The matrix rigidity values obtained varied greatly. The PEO-GG blend tablet displayed a rigidity of 83.119 N.mm as compared to the 104.730N.mm of the optimized matrix tablet. This phenomenon is attributed to the crosslinking present within the optimized formulation thus allowing for greater inter-polymeric bonding thereby forming a greater polymeric network. The resulting BHN showed that the optimized formulation is characterized by a more rigid and solid structural integrity.

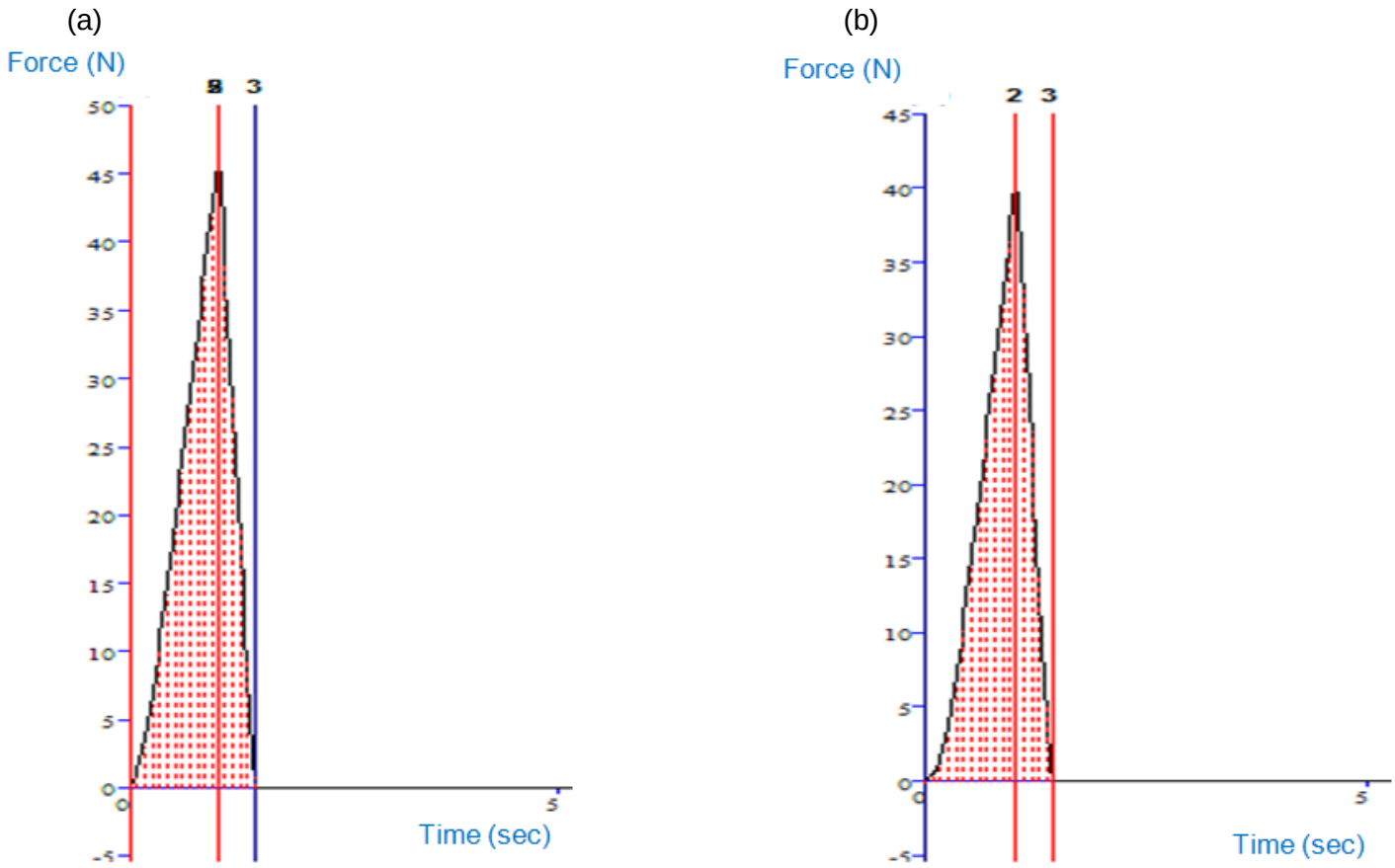


Figure 5.6: (a) Textural analysis Force vs. Time profile for the optimized xerogel matrix tablet and (b) Textural analysis Force vs. Time profile for the PEO-GG blend tablet.

5.3.10. Gravimetric swelling and erosion analysis

Hydrophilic matrix systems are being progressively investigated for their utility within controlled release drug delivery systems. Hypothetically, drug release from hydrophilic matrix tablets were controlled by the formation of a hydrated viscous barrier layer around the tablet which acts by opposing penetration of aqueous medium into the tablet as well as limiting the transport of dissolved solutes out of the matrix. The characteristic hydration of the polymer and the ensuing physical properties of the hydrated gel layer may significantly impact drug release (Sriamornsak et al., 2007). Swelling data obtained for the optimized xerogel matrix tablet via gravimetric analysis indicated the rate at which the formulation absorbed water from the surrounding dissolution media and the degree to which swelling occurred (Figure 5.7). Alterations in weight and an increase in the degree of swelling began when the sample was placed in the dissolution media and continued up to eight hours into the experiment. The percentage of remaining matrices reflects the amount

of polymer dissolved and the erosion of the polymer matrix within dissolution medium during the course of dissolution testing. Weight loss from the matrix tablets increased gradually with the swelling time, as depicted by the percentage remaining tablet mass.

(a)

(b)

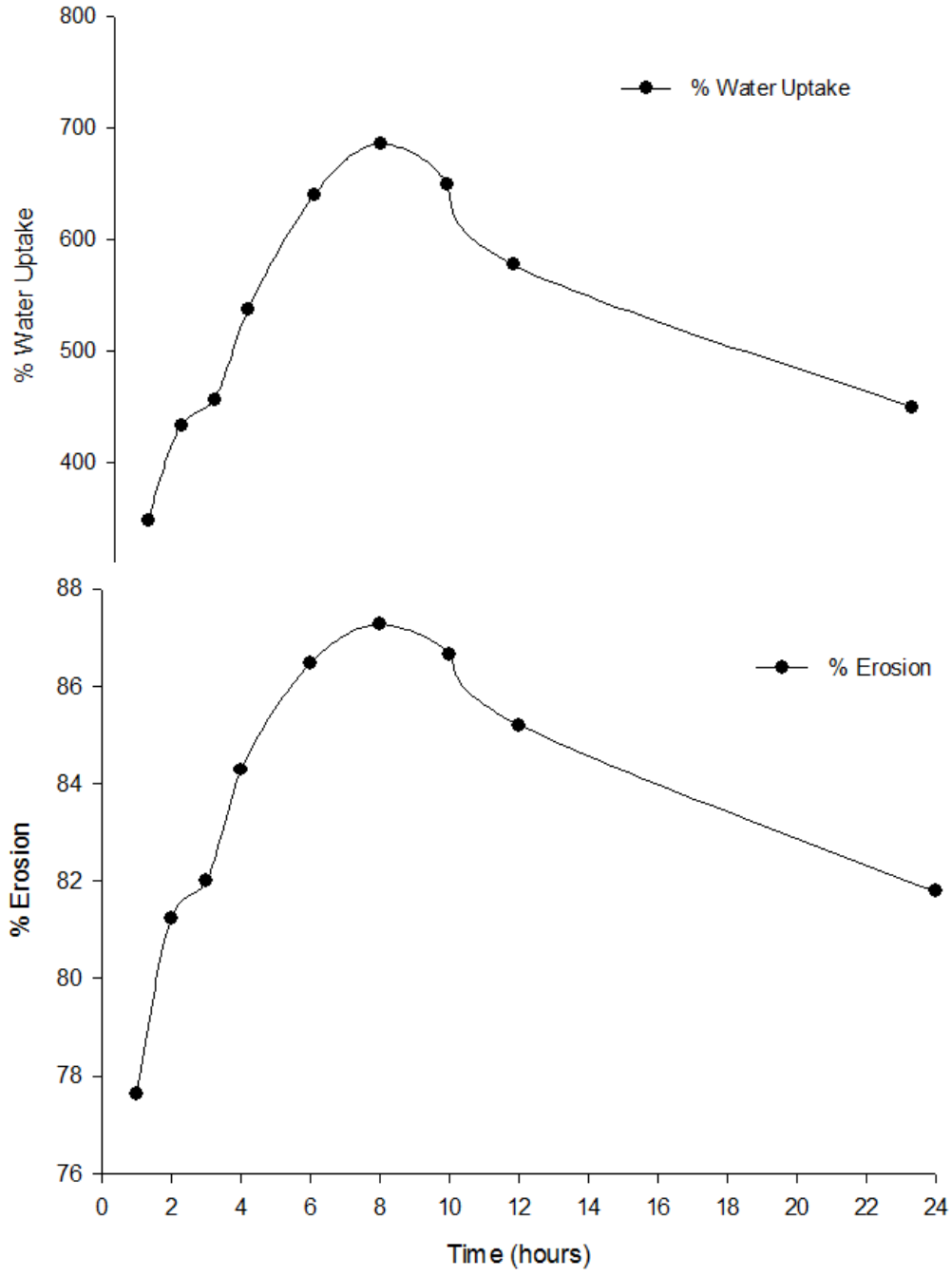


Figure 5.7: (a) % water uptake vs. time and (b) % erosion vs. time of the optimized xerogel matrix tablet.

Swelling ranged between 346.85 - 685.76% over the 24 hour experimental time period. Erosion of the matrix was observed to range from 77.62 - 87.27%; both swelling and erosion displayed paralleled patterns over the test period, with an increase in percentage swelling and erosion observed for the first 8 hours followed by a gradual reduction in both up until 24 hours. By means of visual observation it was found that the matrices appeared to swell immediately, once in contact with the dissolution medium. A viscous gel layer was formed when they were placed in the reaction vessel in direct contact with dissolution medium. The hydrated surface layer formed a viscous transparent gel as it underwent swelling and disintegrated into large particles of gel upon erosion, in contrast the core of the matrix still untouched by aqueous medium remained intact and non-hydrated (Sriamornsak et al., 2007).

Resulting from research investigation on the swelling and dissolution behavior of polymeric matrix systems, it has been established that the thickness of the continuously forming hydrated viscous barrier layer upon water penetration was proportional to the square root of time, where the swelling front was faster than the eroding front. The constant thickness of the hydrated gel layer and zero order drug release kinetics could be achieved when the swelling and erosion fronts synchronized their movements as observed based on data obtained from the gravimetric analysis of the optimized PEO-GG crosslinked xerogel matrix tablet (Yin et al., 2013).

5.3.11. Evaluation of the diffusion, swelling and erosion fronts of the matrix system

Dissolution medium penetration into a swellable matrix system creates defined boundaries (fronts) which isolate various phases of the matrix upon swelling. Lee and Peppas (Lee and Peppas, 1987) have labelled these boundaries as the dissolution/erosion fronts (Escudero et al., 2010). Front movement studies were conducted with the purpose of obtaining useful information in order to gain a better understanding of the drug release mechanism from the optimized s-IPN xerogel matrix. According to Kiil and Dam-Johansen (Kiil and Dam-Johansen, 2003), for swellable matrices there are three proposed fronts observed during front movement studies. They are i) Swelling front, located between the immobile glassy polymer and its rubbery gel layer, ii) Diffusion front, between the undissolved drug and the dissolved drug within the gel layer, and iii) Erosion front, which is located between the matrix and the dissolution medium as depicted in Figure 5.8 below (Escudero et al., 2010).

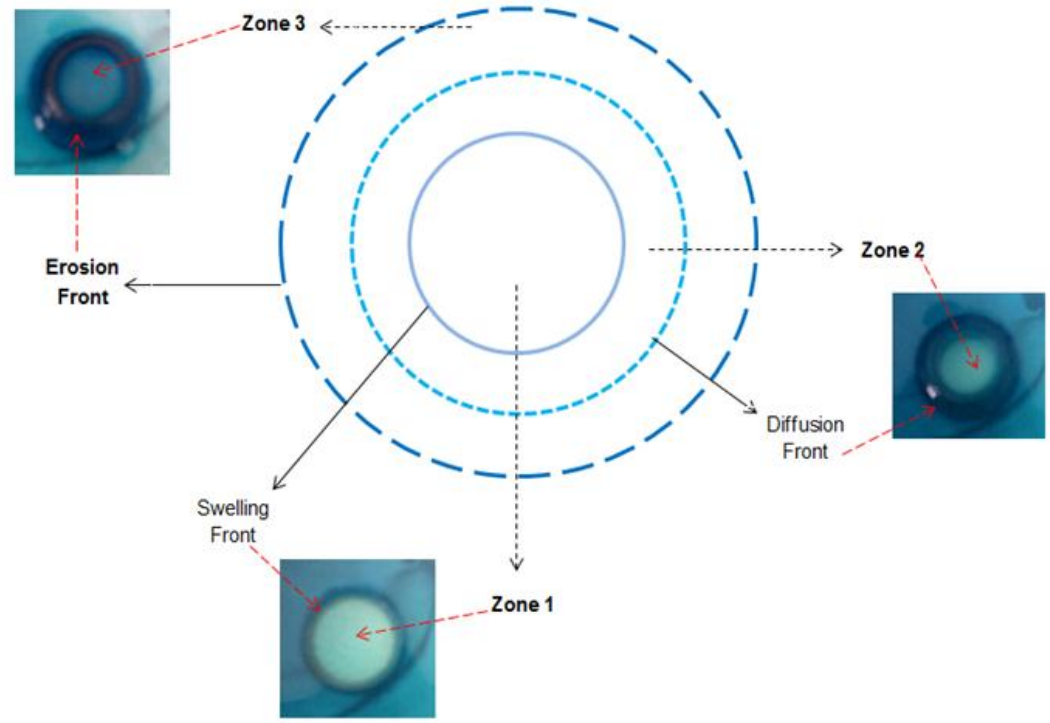


Figure 5.8: The theoretical fronts observed for s-IPN xerogel matrix systems and the respective digital images obtained during the front movement study conducted for the optimized matrix tablet.

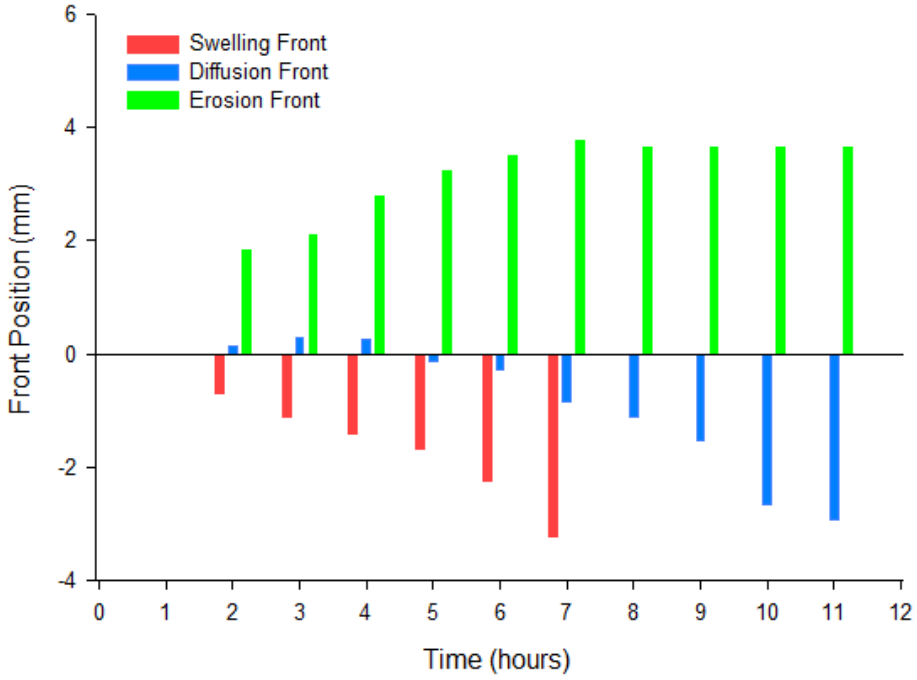


Figure 5.9: Graphical representation of the fronts present and their positions over a 24 hour test period.

Dissolution medium penetration through pores with a greater size regulates the position of the water uptake (swelling) front. As the matrix becomes involved in water uptake; a saturated layer of dye forms. This phenomenon is due to dye diffusion toward the core of the tablet. The crosslinked xerogel present in zone 1 is in its crystalline form since water has not yet infiltrated and plasticised the matrix. The movement of macromolecules within zone 1 is very slow thus leading to a reduction in diffusion rates of dissolution medium. As dissolution medium penetrates the solid matrix (Figure 5.8), it attaches itself between the hydrogen bonds of adjacent polymer chains. As additional dissolution medium becomes inserted between the polymer chains, intermolecular forces weaken. The chains initially begin to inhabit more space, thus resulting in swelling of the polymer. As the dissolution medium penetrates into the matrix it fills voids between the polymer chains and thereby diffuses into denser regions of the polymer matrix (Escudero et al., 2010).

However, the movement of polymer chains in regard to swelling in zones 2 and 3 respectively are greatly increased as compared to zone 1, therefore resulting in higher diffusion rates of dissolution medium into the matrix. The diffusion front is described as the boundary between the undissolved and dissolved drug, along which drug diffusion occurs. Therefore, drug dissolution occurs at the diffusion front allowing dissolved drug to successively diffuse in a radial direction towards the erosion front. A plot of front position against time in hours for the optimized s-IPN xerogel tablet was made. The plot in Figure 5.9 shows the progressive position of the respective fronts over a 24 hour period.

The mobile erosion front is also accurately estimated by the model up to the point at which the swelling front has reached the middle of the matrix which is up to approximately 8 hours of experimentation. The location of the erosion front is a function of the position of the swelling front, as the swelling front disappears; the erosion front becomes immobile and constant. It is clearly evident from the observed experimental data in Figure 5.9 that although the erosion front seems to be immobile once the swelling front disappears, it does continue in a constant fashion to allow for further expansion of the matrix. Once the swelling front reaches the center of the matrix the dissolution medium concentration at all points in the matrix is greater than the threshold concentration for swelling. Therefore, the extended expansion of the matrix is due to polymer chains swelling within the gel layer, most likely due to additional dissolution medium absorption.

Resulting data showed an outward movement of the diffusion front thus indicating the occurrence of the swelling front overcoming drug diffusion. In conclusion, the existence of the distinct swelling and erosion fronts indicate that the optimized matrix can be described as a swellable matrix tablet. Furthermore drug release could be a function of swelling and diffusion mechanisms.

5.3.12. Magnetic Resonance Imaging of the optimized s-IPN xerogel matrix tablet

Magnetic resonance imaging (MRI) has been employed in the study of internal mechanisms underlying *in vitro* drug release behavior in solid dosage forms, so as to observe the events involved in pharmaceutical processes. Hydration of a system reinforces the performance of various solid dosage forms, many studies have utilized MRI to detect the internal events occurring as a result of solvent penetration.

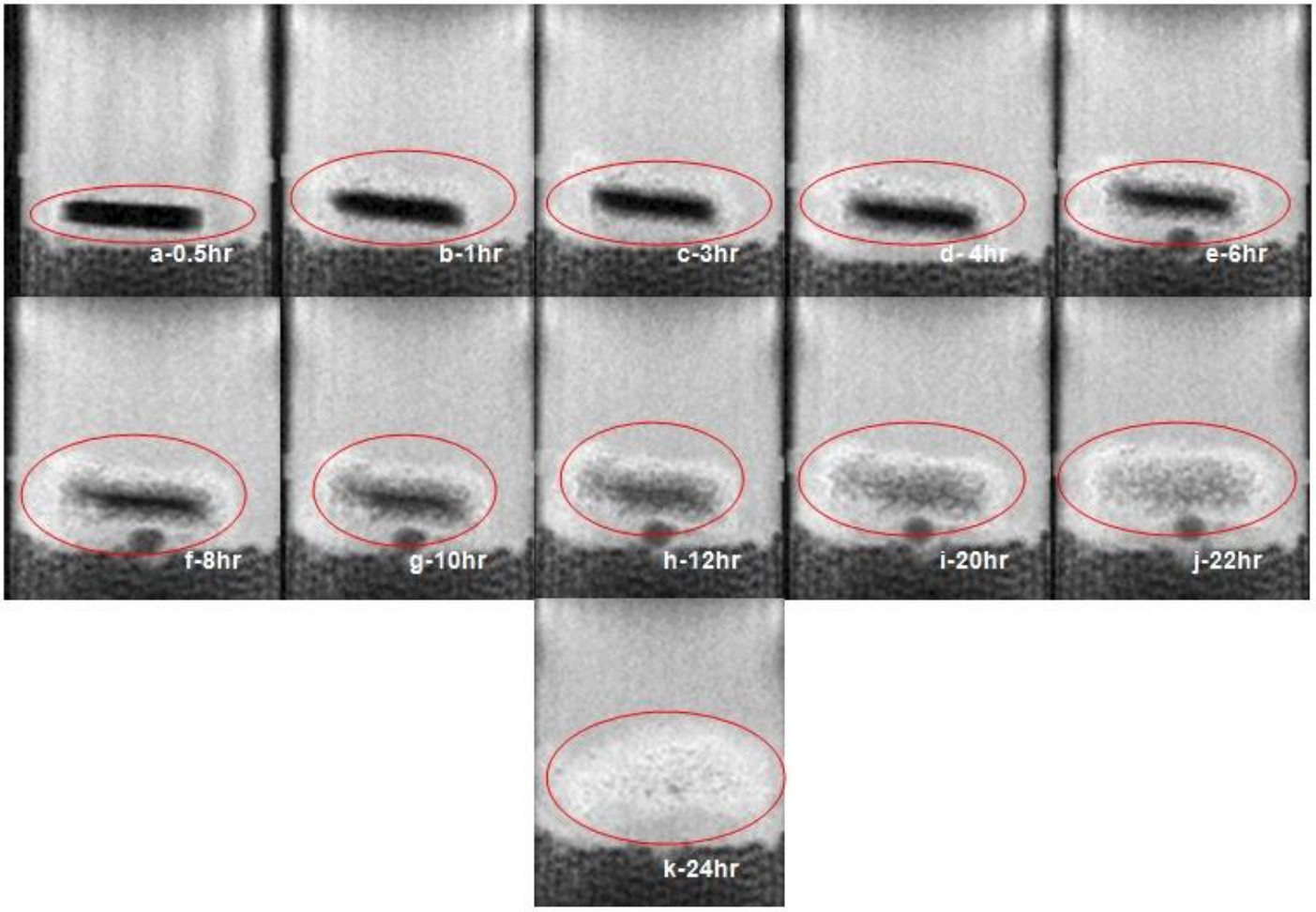


Figure 5.10: MRI imagery of xerogel matrix tablets over 24 hours.

Following ingestion of a solid dosage form surface polymers hydrate and swell to form a viscous gel layer. It is this gel layer that acts as a barrier to bioactive efflux and solvent influx into and out of the solid dosage form, thereby preventing matrix disintegration and prolonging the rate of drug release. Water soluble bioactives seem to endure a diffusion controlled release via the gel layer,

Whereas insoluble bioactive agents are released from the outer surface of the gel layer via surface erosion. MRI may be utilized to evaluate the extent and rate of polymer swelling thus providing evidence of the functionality of hydrophilic matrices (Richardson et al., 2005). It was possible to visually determine the extent of swelling and gel layer thickness of the optimized xerogel matrix tablet. Figure 5.10 shows that upon hydration, the matrix expanded predominantly. This observed phenomenon can be attributed to the release of the tablet compression forces employed during the formulation process.

Based on MRI images, three distinct regions of the matrix system can be observed. These are i) the peripheral region observed as a white hazy area (Figure 5.10i) comprising of freely mobile polymer chains which are undergoing dissolution and diffusing into the bulk dissolution medium ii) the gel layer in which the polymer chain's mobility is reduced attributable to inter-polymeric cohesive forces observed as the grey shaded region (Figure 5.10h), and iii) the core region, within which the mobility of polymer chains is restricted so that it appears to be solid which is seen as the black shaded region (Figure 5.10a).

Determination of the resulting gel structure and the evaluation of the individual constituents are considered vital information due to dissolution medium penetration and polymer swelling directly affects the mechanism and kinetics of drug release. Specifically, the parting of the swollen glassy layer from the gel layer is a critical factor attributing to the understanding of drug release. This is due to polymer chains relaxing within dissolution medium and thereby forming larger voids to allow for drug to diffuse through, thus the drug release rate is directly proportional to the extent and thickness of the swollen gel layer.

As seen in Figure 5.8 the optimized xerogel matrix displayed the formation of a thick gel layer thus creating a barrier to drug release. As time progressed the gel layer became thicker and results in erosion of the surface polymer chains, as this occurs it allows for the penetration of more dissolution medium into the matrix, therefore allowing for dissolution medium to fill the voids and aid in drug diffusion and finally dissolution within the bulk of the dissolution medium. An important observation made from MRI is the presence of air bubbles, seen as minute white spheres with a slightly darker core; this is a characteristic feature of xerogels as they are composed of pores.

It can be deduced that drug release is based on a complex interplay of swelling, erosion and diffusion from the matrix system. Within the context of the current system the bioactive release is sustained due to the fact that the formation of the gel layer acts as a rate limiting step and a barrier to the diffusion and dissolution of the drug in the dissolution medium.

5.4. Concluding Remarks

The use of matrix based systems has been explored and is proven to have the most benefits due to its ease of administration and improved compliance. Modification via crosslinking of hydrophilic polymers to form an s-IPN xerogel matrix is a novel approach; the resulting system displayed desirable release kinetics and physiomechanical properties. The derived optimized formulation showed an admirable swelling capability which is vital to the observed drug release kinetics; in addition, when *in vitro* drug release data was fitted into the various mathematical models the system conformed to zero-order release. Overall, the system has proven to be efficient in prolonging the drug delivery of sulpiride, in addition it displays good physiomechanical characteristics which is vital to maintain the integrity of the system post oral administration.

CHAPTER 6

PRELIMINARY DESIGN OF THE MULTI-LAYERED BIOADHESIVE POLYMERIC INTESTINAL PATCH FOR PULSATILE DRUG DELIVERY (IPRPS)

6.1. Introduction

As previously outlined schizophrenia often presents as schizoaffective disorder which requires the concomitant treatment with antipsychotic and mood stabilizing agents. Valproic acid a well-known mood stabilizing agent also used in the treatment of epilepsy, in particular has been shown to improve behavioral and cognitive performance, suppress neurodegeneration and neuroinflammation (Chiu et al., 2013).

In a study conducted by Suzuki and co-workers atypical antipsychotics were augmented with valproic acid in severely compromised Japanese patients presenting with chronic schizophrenia. The mechanism of valproic acid augmentation of atypical antipsychotics includes the known action on GABAergic neurons, thus potentiating inhibitory neurons and reducing agitation and aggression. Additional mechanisms may be linked to the synergistic increase in dopamine or acetylcholine release in the prefrontal cortex (Suzuki et al., 2009).

Overall the study displayed significant improvement in clinical outcomes, valproic acid augmentation was generally well tolerated, however the few serious side effects observed were thrombocytopenia, anemia, and sedation (Suzuki et al., 2009).

The precipitation of adverse effects in valproic acid augmentation of antipsychotics may lead to a reduction in compliance to therapy and hence treatment resistance and poor clinical outcomes (Belcastro et al., 2013), this may be related to multiple daily administrations required and thus prolonged exposure to the drug.

Efficacy and tolerability of drug therapies could be conspicuously enhanced by the design and development of delivery systems envisioned to timely release drug post administration; thus providing pharmacological protection when necessary while avoiding unnecessary prolonged patient exposure to the bioactive. In addition, when multiple dosing regimens are required repeated pulsatile drug delivery patterns may assist in improving patient compliance when the bioactive agent is not suited for sustained release formulations, one such example would be due to the development of tolerance (Gazzaniga et al., 2008), as is the case with valproic acid.

For this reason pharmaceutical scientists have focused on drug delivery systems that allow for the desired amount of drug to be made available at a predetermined time at the site of action (Gupta et al., 2002). This may be referred to as pulsatile release, generally pulsatile release is meant as the timed release of drugs following programmed lag phases, in this case only system design based mechanisms are operating which is independent of the environmental variables (Gazzaniga et al., 2008).

The current study details a novel drug delivery system that offers numerous advantages. One of the proposed strategies for achieving greater levels of site specific drug absorption at the intestinal epithelium is the use of multilayered intestinal patches. Once the patch is in contact with the mucus; surface drug flows unidirectionally through the intestinal wall into the bloodstream at a rate that is controlled by the rate controlling layer (Tao and Desai, 2005).

For pulsatile delivery of valproic acid in the treatment of schizoaffective disorder, the second component of the ODLS delivery system will be formulated as bioadhesive multilayered intestinal patches. A schematic representation of the proposed patch is shown in Figure 6.1.

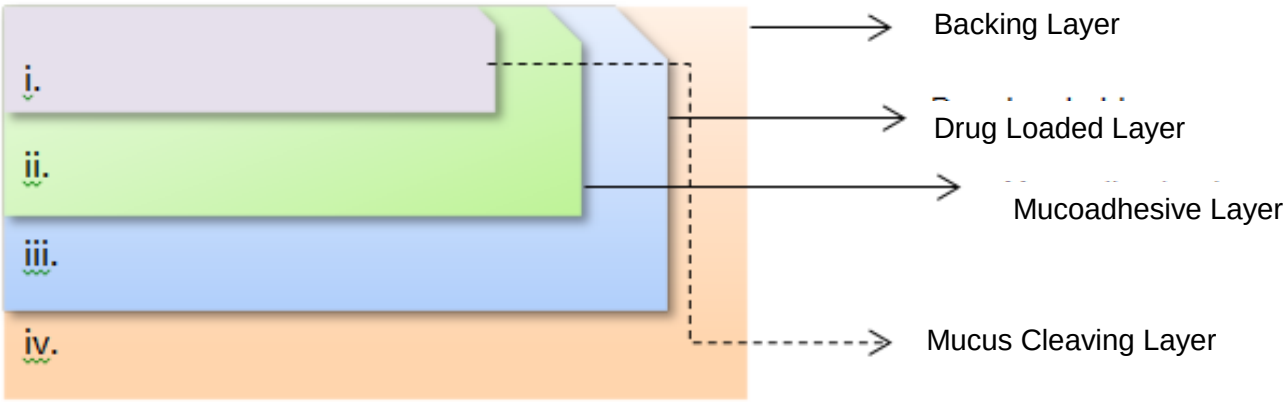


Figure 6.1: Assembly of the bioadhesive multilayered intestinal patches

The current system consists of layers; a backing layer composed of an impermeable ethycellulose polymer; a drug loaded layer comprised of sodium alginate and Poly(ethyl acrylate-co-methyl methacrylate-co-trimethylammonioethyl methacrylate chloride (Eudragit® RS 100); a mucoadhesive layer encompassing chitosan and hypromellose amalgamated with soybean lectin and a mucus cleaving layer comprising an N-acetyl cysteine (NAC): gellan gum: chitosan blend.

Film formation from polymeric solutions is a reasonably forthright procedure as the selected polymer/s is already dissolved as shown in Figure 6.2. The polymeric solution spreads over the film casting surface, and as the solvent evaporates, polymer chains interpenetrate, passing from a gel state to then forming a film with additional drying. Polymer chain interpenetration arises at a particular concentration which is the reciprocal of the intrinsic viscosity of the polymeric solution. Intrinsic viscosity is the rise in viscosity precipitated by the dissolved polymer and thus is an indication of hydrodynamic interaction between the polymer/s and solvent. The rate at which solvent evaporates is vital in the film formation process (Felton, 2013).

If a solvent evaporates too slowly the film casting surface becomes over wetted resulting in the film being unable to be removed easily; conversely, if solvent evaporates too quick the polymer solution begins to dry before impacting onto the casting surface thereby leading to an uneven film being formed with a tendency to form cracks.

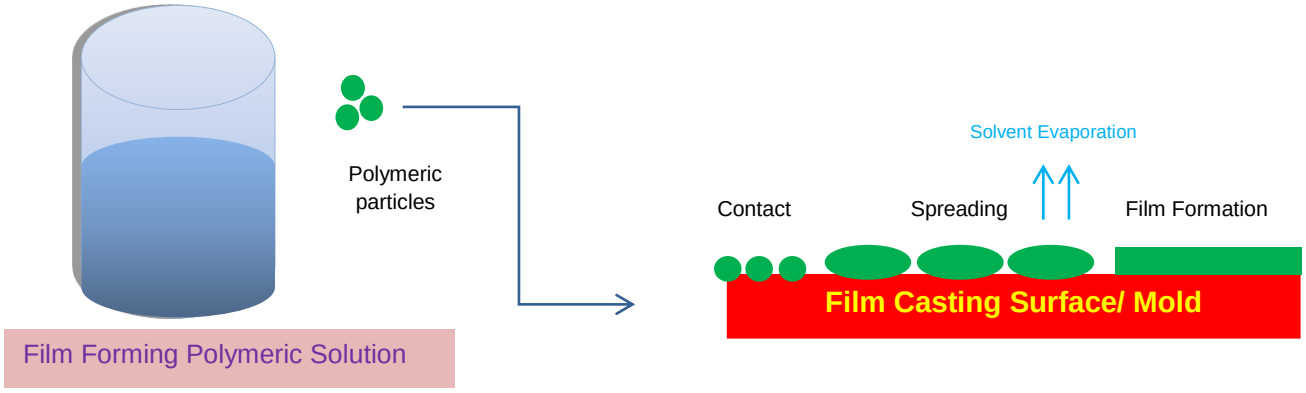


Figure 6.2: Mechanism of polymeric film formation by the film casting method.

6.1.1. Selection of independent variables for input into a Central Composite Design

Based on the preliminary results conducted, the formulation component (input variables) for the bioadhesive layer that influenced the mucoadhesion, swelling and membrane strength of the formulation (measured responses) were identified in conjunction with their upper and lower limits. The same was done for the drug loaded layer with the measured response being drug release kinetics. Factors with their corresponding factor levels were selected for the bioadhesive multilayered intestinal patch component of the ODLS so that a mathematical model was generated. Polymers, crosslinking agents, active formulation excipients and the model drug employed in the respective layers of the system design are outlined below:

Sodium alginate is a water soluble polymer which may be easily crosslinked with the use of other multivalent cations such as calcium. It is the major structural polysaccharide found in brown seaweed. In its crude state alginate exists as calcium, magnesium and sodium salts of alginic acid which provides flexibility and strength to the seaweed. Alginate is a linear copolymer of –d-mannuronic acid and –l-guluronic acid linked residues arranged in homopolymer blocks, alginate is commonly employed in bioencapsulation (Himadri and Samit, 2014; Sellimi et al., 2015).

Poly (ethylacrylate-co-methyl methacrylate-co-trimethylammonioethyl methacrylate chloride (Eudragit® RS 100), is a copolymer synthesized from acrylic and methacrylic acid esters, consisting of a low degree of quaternary ammonium groups. RS100 has a lower consistency of charged groups and is considered less permeable to water. It is capable of swelling and hence controlled drug delivery (Pignatello et al., 2001; Barzegar-Jalali et al., 2012).

Chitosan, derived from crab and shrimp shells has been employed in food and pharmaceutical fields due to its outstanding antimicrobial properties, biocompatibility, and biodegradability (Zhang and Zhao, 2015). It is derived from chitin a non-starch based material, which is similar in structure to cellulose. It's the second most abundant biopolymer in nature; the partial alkaline deacetylation of chitin produces the cationic polysaccharide, chitosan. Chitosan is soluble in organic solvents such as formic and citric acid. The linear biopolymer is made up of two monosaccharides, namely N-acetyl-glucosamine and D-glucosamine, which are linked by glycosidic bonds (Yang et al., 2015).

Hypromellose, or hydroxypropyl methylcellulose (HPMC) are water soluble cellulose ethers which are synthesized by substituting the hydroxyl group of anhydroglucose with methoxy/ hydroxypropyl groups. The resulting cellulose ethers may undergo thermos reversible sol-gel transitions (Almeida et al., 2014). Hypromellose is a commonly utilized pharmaceutical excipient with low toxicity, easily accessible and cheap.

Soybean Lectin (agglutinin), is a carbohydrate–binding protein, it belongs to a heterogeneous group of proteins that reversibly bind specific mono or oligosaccharides. Lectins have been isolated from various plants, animals and bacteria. They are classified into 5 subgroups based on their respective origins (Guo et al., 2013). Soybean lectin is a legume derived lectin isolated from seeds of soybeans. Soybean lectin displays specificity to N-acetyl-D-galactosamine and D-galactose, it is one of the best characterized lectins, which consists of four 30 kDa sub-units with two polysaccharide binding sites per 120 kDa (Panda et al., 2014).

The focus of this Chapter lies in the development and optimization of the bioadhesive and drug loaded layers of the intestinal patch component of the ODLS through a systematic approach of

experiments, employing a two level, face-centered, randomized Central Composite Design. The optimized formulation will provide the most ideal drug release profile and mucoadhesion.

Subsequent to identification of the polymer combinations for the respective mucoadhesive and drug loaded layers, the upper and lower limit variables of the formulations was determined. The resultant variables are illustrated in Table 6.1. The limits were determined via ensuring that the fabricated formulations met the criteria required for appropriate mucoadhesion and drug release respectively.

Table 6.1: The identified variables and their corresponding upper and lower limits for input into the Central Composite Design.

Polymer employed	Lower Limit (%w/v)	Upper Limit (%w/v)
Mucoadhesive Layer		
Chitosan	0.05g - Anything <0.05g did not demonstrate satisfactory film forming properties. These formulations tended to stick to the mold surface and could not be peeled off. There was also an observed reduction in mucoadhesion.	0.25g- Formulations containing >0.25g resulted in solutions that were too viscous for appropriate film-casting and films formed were not uniform and consistent in surface structure.
Hypromellose	0.05g- Formulations containing <0.05g demonstrate poor mucoadhesion properties and not form good films, films formed were too thin and prone to tearing.	0.15g- Formulations containing > 0.15gdid not form viable films, the resulting polymeric solution was too viscous and stick to work with.
Citric Acid	0.15g- Formulations containing <0.15g did not dissolve the chitosan sufficiently. Solutions remained murky	0.3g- Formulations containing >0.3g resulted in solutions that had a residue of citric acid and chitosan.
Drug Loaded Layer		
Eudragit® RS100	0.1g- Formulations with <0.1g did not form viscous solutions and were unable to form films and thus could not allow for the required drug release.	1g - Formulations comprising >1gformed relatively viscous solutions that were capable of film-casting, however, they formed brittle films that were prone to cracking and breakage.
Calcium Chloride	0.01g- Formulations containing <0.01g did not sufficiently crosslink the sodium alginate: Eudragit RS100 blend and thus could not control drug release.	0.1g- Formulations of >0.1g crosslinked the blend successfully, however the resulting solution was far too viscous and could not undergo film-casting methodology.

6.2. Materials and Methods

6.2.1. Materials

Chitosan (deacetylated chitin) medium molecular weight, Citric acid ACS reagent ≥ 99.5 %Mw 192.12 g/mol, sodium valproate ≥ 98% Mw 166.19 g/mol, hypromellose (hydroxypropyl)methyl cellulose 2910, sodium alginate, glycerin Mw 92.09g/mol, potassium phosphate monobasic Mw 136.09 g/mol, Mucin, from porcine stomach were all procured from Sigma-Aldrich® (St. Louis, USA). Lectins (Bio-Research products (Cherry St. North Liberty, USA), Methacrylic acid copolymer (Eudragit RS 100) (Degussa, Röhm GMbH, Pharma Polymers, Germany) and calcium chloride dihydrate 99% was purchased from Rochelle Chemicals (Johannesburg, South Africa) . All other reagents were of analytical grade and are used as received.

6.2.2. Construction of a Randomized Central Composite Design for optimization of the bioadhesive multilayered intestinal patch component of the ODLS

A model independent approach (Minitab® V15, Minitab Inc. PA, USA) was employed for optimization of the intestinal patches. The input factors or independent variables were the concentration of chitosan, citric acid and hypromellose for the mucoadhesive layer and the concentration of Eudragit®RS100 and calcium chloride for the drug loaded layer. These were studied at two levels each, and the DoE generated twenty and thirteen experimental runs (formulations) for the mucoadhesive and drug loaded layers respectively. Statistical optimization was employed to ascertain the ideal combination of polymers and crosslinker required to achieve the desired drug release profile, swelling, and mucoadhesive efficacies amongst others. Tables 6.2 and 6.3 summarize the derived factor combinations for the mucoadhesive and drug loaded layer respectively of the experimental runs studied and their conversion of the coded levels to the experimental units utilized during the study. The coded variables chosen for the statistical design were; total mean dissolution time (MDT), mean % swelling, Young's Modulus and % mucoadhesion. Whereas, parameters for the design were set as the concentrations of hypromellose (g), citric acid (g) and chitosan (g) for the mucoadhesive layer and concentrations of Eudragit® RS100 (g) and calcium chloride (g) for the drug loaded layer.

Table 6.2: Mucoadhesive layer Central Composite statistical design.

Mucoadhesive Film	[Chitosan] (g)	[Hypromellose] (g)	[Citric Acid] (g)
F1	0.15	0.1	0.225
F2	0.15	0.1	0.225
F3	0.15	0.05	0.225
F4	0.15	0.1	0.225
F5	0.15	0.1	0.225
F6	0.05	0.05	0.15
F7	0.05	0.05	0.3
F8	0.15	0.1	0.225
F9	0.05	0.15	0.15
F10	0.25	0.1	0.225
F11	0.25	0.15	0.15
F12	0.15	0.15	0.225
F13	0.05	0.15	0.3
F14	0.05	0.1	0.225
F15	0.25	0.05	0.3
F16	0.25	0.15	0.3
F17	0.15	0.1	0.15
F18	0.25	0.05	0.15
F19	0.15	0.1	0.3
F20	0.15	0.1	0.225

Table 6.3: Drug loaded layer Central Composite statistical design.

Drug Loaded Film	[Eudragit® RS 100] (g)	[Calcium Chloride] (g)
F1	0.55	0.055
F2	0.55	0.1
F3	0.1	0.055
F4	1	0.1
F5	1	0.055
F6	1	0.01
F7	0.55	0.055
F8	0.55	0.01
F9	0.55	0.055
F10	0.55	0.055
F11	0.55	0.055
F12	0.1	0.1
F13	0.1	0.01

6.2.3. Fabrication of mucoadhesive lectin fused hypromellose-chitosan blend and drug loaded layer

Bioadhesive multilayered intestinal patch layers were prepared by solvent casting method (Gungor et al., 2008). A chitosan aqueous solution was prepared by dissolving the chitosan powder into distilled water containing varying concentrations of citric acid until the chitosan was completely dissolved and a clear solution was formed. Subsequently, the chitosan solution was added into aqueous solutions of varying concentrations of hypromellose. Once the blend formed a homogenous solution soybean lectin (0.25mg/mL) was added and allowed to undergo amalgamation for 2 hours.

Eudragit® RS100 in varying concentrations was dissolved in a 60:40 $\%^{w}/_{v}$ isopropyl alcohol, acetone mixture. A $2\%^{w}/_{v}$ sodium alginate solution was added to the above mentioned solution

until homogenous. Thereafter, varying concentrations of calcium chloride solution was added to the blend and allowed to crosslink for 3 hours.

Glycerin (1mL) was added to both film forming solutions as a plasticizer, the use of a plasticizer aims to i) providing easily removable films from the casting surface (mechanical stability and drug permeability, and ii) ensuring the polymer particles coalesce during film formation (Siepmann and Siepmann, 2013). A thin layer of the respective polymer solutions were casted onto individual molds and allowed to dry under the influence of a fumehood at room temperature for 24 hours. The resulting polymeric films were then carefully lifted off the mold surface and layered into the final intestinal patch with the assistance of compression employing the Carver Press tableting press (Model 3851-0, S/N 43000-904, Wabash, IN, USA) employing a pressure of 5 tons.

PART I: Preliminary Mucoadhesive Layer Characterization

6.3. Physiomechanical and Physiochemical Characterization of the Mucoadhesive Layer

6.3.1. Chemical transitional characterization of the lectin amalgamated mucoadhesive layer of the intestinal patches

Fourier Transform Infrared Spectroscopy (FTIR) employing a spectrum 100 FTIR spectrometer (Perkin- Elmer, Beaconsfield, BUCKS, UK) was utilized to detect the vibrational frequencies of chemical functional groups in the design formulations. FTIR analysis was conducted on native polymers incorporated in the mucoadhesive layer as a means of validating the successful lectin amalgamation. Samples were placed on a diamond crystal and processed by the universal ATR polarization accessory software for the FTIR spectrum series at a wave number range of 650-4000cm^{-1}.

6.3.2. Thermal analysis of polymeric material employed in the formulation of the mucoadhesive layer of the intestinal patch

Differential Scanning Calorimetry (DSC) was conducted on the mucoadhesive layers. Obtained DSC thermograms provided information regarding the thermal stability of the formulations. With the further intention of ascertaining the melting points, phase transitions and glass transitions (Tg) of the formulated lectin amalgamated hypromellose, DSC studies employing a Temperature Modulated DSC (Mettler Toledo DSC- 1 STAR^{e} System , Schwerzenback, ZH, Switzerland) was conducted.

6.3.3. Mucoadhesive analysis of the mucoadhesive layer

Mucoadhesion studies were performed on all Box–Behnken design mucoadhesive layer formulations to deduce the effect of the change in variable concentration on the amount of mucoadhesion of the polymeric film. For this study a 0.1%$^{w}/_{v}$ mucin solution prepared in USP intestinal fluid (pH 6.8) was used to incubate mucoadhesive films in an orbital shaker maintained at 37˚C and 50 rpm. Concentration of free mucin in the solution, after 6h duration, was determined by a UV spectrophotometer, at 201nm (IMPLEN NanophotometerTM, Implen GmbH, München Germany), using a 10 times dilution factor of path-length 0.1 mm. The difference in the concentration of the mucin solution before and after incubation was the indication of the amount crosslinked with the mucoadhesive films as seen in Equation 6.1, indicating the interaction between particles and mucin (He et al., 1998).

$$Mucoadhesion\,\% = \frac{[Mucin\ before] - [Mucin\ after]}{[Mucin\ before]} \times 100$$

Equation 6.1

6.3.4. Evaluation of the swelling behavior of the mucoadhesive layer

Mucoadhesive films were analyzed for water content and swelling by gravimetric analysis utilizing the weight of the sample. Gravimetric analysis was performed as follows: the film sample was weighed before submersion in 20 ml PBS (pH 6.8, 37˚C) and then again after 24 hours. The film was then removed and surface water removed by blotching on dry laboratory paper, followed by the determination of the equilibrium swelling ratio by use of the following Equation 6.2 (Murthy et al., 2006; Reddy et al., 2012):

$$ESR=W_1\text{-}W_0\ )/W_0$$

Equation 6.2

Where W0 is the initial weight of the film and W1 is the weight after the 24 hour swelling time.

6.3.5. Textural analysis of formulated mucoadhesive film layer

Mechanical properties of the mucoadhesive layers were evaluated via textural analysis using the TX.XTplus Texture Analyzer. Films were cut into approximately 0.55× 2.55 mm^2 strips and

secured within the grips, textural analysis was conducted with a pre-test and test speed of 0.5, post-test speed of 5, with the target mode being distance, and the force applied being 5N. The Young's Modulus or ratio of stress over strain of the mucoadhesive film was determined by the Equation 6.3 via utilization of data obtained from textural analysis;

$$E = \frac{Tensile\ stress}{Extensional\ strain} = \frac{FL_0}{A_0 \Delta L}$$

Equation 6.3

Where;

E is the Young's modulus

F is the force exerted on an object under tension;

A0 is the original cross-sectional area through which the force is applied;

ΔL is the amount by which the length of the object changes;

L0 is the original length of the object.

6.3.5.1. *Determination of the tensile properties and Young's modulus of the intestinal mucoadhesive films via NanoTensile analysis*

The tensile characteristics and Young's modulus were determined further employing the NanoTensile® 5000 (Hysitron Inc. Nanomechanical Test Instrument, Minneapolis, MN, USA). NanoTensile (NT) system was calibrated prior to sample testing to ensure accurate analysis. Samples cut into approximately 0.55 x 2.55 mm^2 strips were mounted on the specially designed mounting brackets. Brackets were held together with a rigid cardboard frame, enabling ease of sample alignment, samples were attached to the brackets using double sided adhesive tape, thus keeping the sample in place during evaluation. Accurate measurements of the sample width, thickness and length were recorded utilizing a digital caliper. Thereafter, the upper sample bracket was attached to the upper sample holder of the NT head and the mass recorded. The NT head was then lowered and aligned to the lower NT stage; the lower sample bracket was then secured to the lower sample holder on the NT stage. Sample mounting brackets were pulled apart at a constant rate of displacement; 100µm/s^{-1} whereby tensile characteristics of the mucoadhesive formulation sample was measured and recorded.

6.3.6. Elucidation of the pertinent rheological properties

Using a Modular Advanced Rheometer system (ThermoHaake MARS Rheometer, Thermo Fischer Scientific, Karlsuhe, Germany) equipped with a T-type spindle sensor (C35/1˚Ti) set at a sample gap of 1mm and Thermo controller (UTC-MARS II) utilized for viscosity measurements. Viscosity is a vital parameter in the formation of polymeric films or membranes. For this reason viscosity measurements were carried out on the mucoadhesive layer polymeric solution.

6.3.7. Response surface analysis of the employed responses

Minitab® statistical software (V15, Minitab Inc., PA, USA) was utilized to perform the response surface analysis of the various response variables. The results were demonstrated employing response surface and contour plots which were derived for the measured responses (Young's Modulus, and % mucoadhesion), based on the experimental model.

6.4. Results and Discussion

6.4.1. Chemical composition elucidation of the mucoadhesive layer of the intestinal patches

Analysis of all design formulations (Figure 6.3) revealed that all characteristic peaks present within the FTIR spectra of the native polymers were altered proving that covalent interactions between polymers occurred, thereby resulting in improved mucoadhesion. Fourier Transform Infrared Spectroscopy (FTIR) of the native excipients employed in the formulation of the mucoadhesive layer displayed characteristic functional groups; chitosan displayed a peak at 3493cm^{-1} (Figure 6.3a) relating to a normal O-H polymeric stretch (Krishnaraj et al., 2012), a second distinct peak is observed at 1697.14cm^{-1} illustrative of a C=O carboxylic acid group, a third distinct peak is seen at 1388.02cm^{-1} representative of C-H alkanes, a peak at approximately 1140cm^{-1} is depictive of C-O phenol functional groups, and a peak at 771.69cm^{-1} is descriptive of an o-substituted C-H functional group (Figure 6.3a).

Hypromellose FTIR spectra showed peaks at 3497cm^{-1} relating to a normal O-H polymeric stretch, 3354cm^{-1} N-H amine groups, 2911cm^{-1} depictive of a O-H carbon, 1670cm^{-1} C=O aldehyde, 1138cm^{-1} is related to C-O phenol functional groups, and a peak at 780.56cm^{-1} characteristic of substituted aromatic C-H bending (Figure 6.3b). Citric acid displayed FTIR peaks at 2635.93cm^{-1} related to carboxylic acid functional group, 766.94cm^{-1} depictive of a C-H alkene (Figure 6.3c). Lectin FTIR spectra exhibited peaks at 3253.65cm^{-1} hydrogen bonded alcohol O-H, 1639.46cm^{-1} representative of C=C alkyl stretch, a peak at 1518.09cm^{-1} related to NO_2 nitro functional groups, 1237.22cm^{-1} aryl/vinyl ethers (Figure 6.3d).

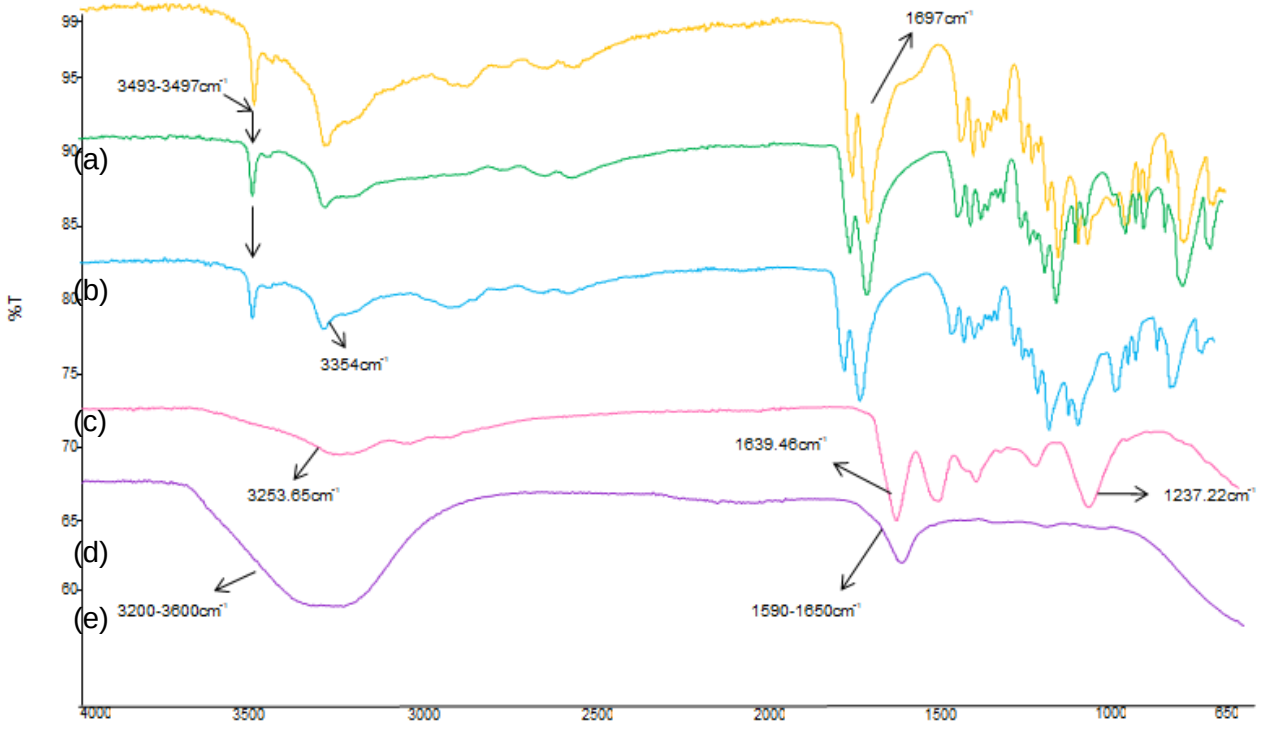


Figure 6.3: FTIR spectra of native polymers a) chitosan, b) hypromellose, c) citric acid and d) lectin employed in the fabrication of the mucoadhesive films and e) a representative design formulation.

Spectra of the mucoadhesive design formulations exhibited peaks in the range of 3200-3600cm^{1} relating to a broad hydrogen bonded alcohol which is also known as a normal polymeric O-H stretch observed within all native polymer FTIR spectra, a peak in a range of 3200-3570cm^{-1} linked to C-H stretching for diagonal carbon alkyls displaying a shift in peak intensity of the polymeric O-H stretch which is attributed to the formation of intermolecular and intra-molecular hydrogen bonds (Wang et al., 2014), an additional peak in the region of 2100-2260cm^{-1} was observed which

represents C≡C terminal alkyne, an additional peak in the range of 1590-1650cm^{-1}corresponding to C=C aromatic double bond was noted (Figure 6.3e).The presence of a peak at ±1730cm^{-1} corresponds to ester C=O stretching (Krishnaraj et al., 2012). In addition, it was observed that a reduction in hypromellose and an increase in citric acid concentration within formulations led to a shift into the lower region of the FTIR spectra, whereas an increase in chitosan concentration led to a corresponding shift of the spectra to higher frequencies. The manifestation of two additional peaks demonstrates the successful lectin amalgamation to the chitosan: hypromellose blend. In addition, the known amine groups on the chitosan molecule provide polycationic electrolytes when dissolved in acid solutions, such as citric acid. These electrolytes are able to bind with other hydrophilic compounds, in this case the hydroxyl group of hypromellose.

6.4.2. Thermal appraisal of polymeric components of the mucoadhesive film layer

DSC thermal analysis of native polymers utilized in the formulation process of the mucoadhesive layer displayed the following thermal events: chitosan presented with a Tg of 26.21˚C, an endothermic peak at 65.42˚C related to solid-solid phase interactions, an exothermic peak at 211.56˚C representative of crystallinity, and an exothermic peak at 275.34˚C illustrative of decomposition (Figure 6.4a). Citric acid exhibited a Tg of 26.24˚C, an endothermic event at 128.19˚C relating to sublimation or solid-solid transitions, an endothermic peak at 212.97˚C representing melting with decomposition followed by an exothermic peak at 259.31˚C illustrating melting along with eutectic impurities present (Figure 6.4b). Hypromellose revealed a Tg of 26.12˚C, an endothermic thermal event at 77.36˚C representing solid-solid phase sample transitions, followed by an endothermic peak at 261.98˚C descriptive of melting along with decomposition (Figure 6.4c). Thermogram of lectin WGA displayed a Tg of 25.71˚C, an exothermic peak at 238.57˚C illustrating crystallinity, and an endothermic peak at 255.48˚C signifying melting upon stable modification (Figure 6.4d) (Mettler Toledo, 2001).

Mucoadhesive layer design formulations showed four characteristic thermal peaks. The first event representing the Tg occurred in a range within 83.99˚C- 138.72˚C, it was noted that with an increase in crosslinker density, the Tg was shifted to higher values. The second thermal peak ranges between 139.03˚C- 178.95˚C relating to crystallinity and solid-solid transitional peaks (Figure 6.4e). The third observed thermal event constituted an endothermic peak representative of the beginning of the melting phase. The fourth thermal event was an exothermic peak associated with decomposition.

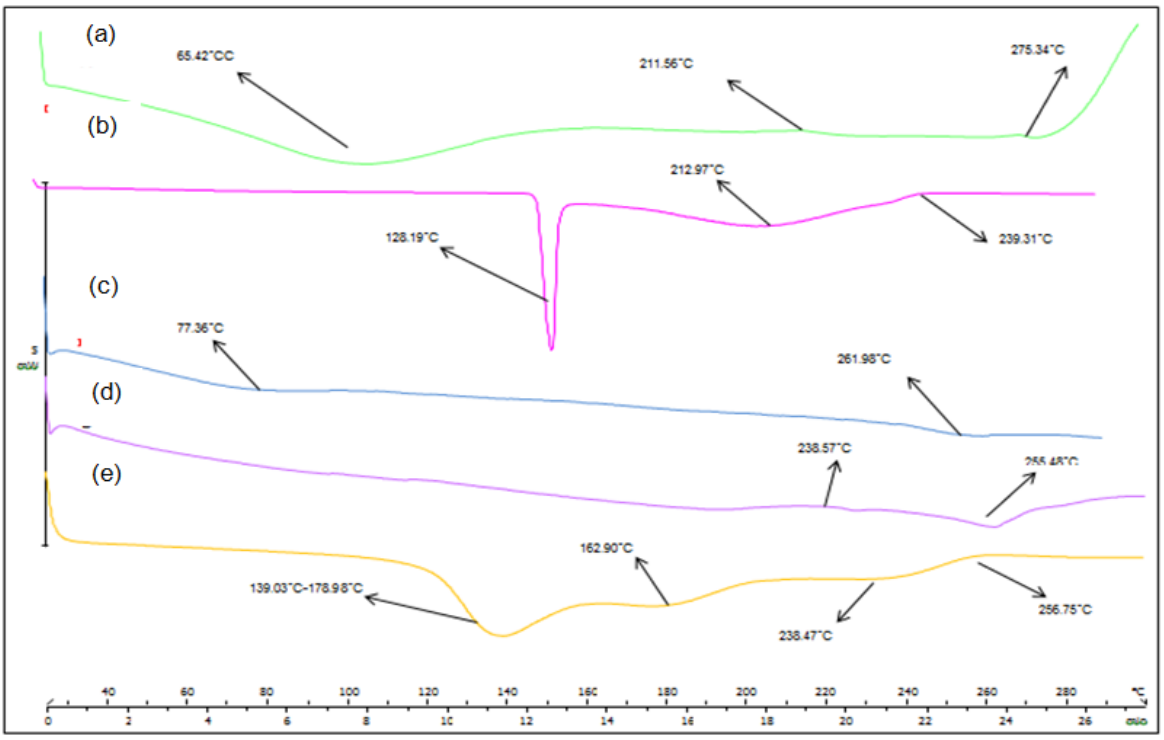


Figure 6.4: DSC thermograms of the native polymers a) chitosan, b) citric acid, c) hypromellose and d) lectin employed in the fabrication of the mucoadhesive layer and e) a representative design formulation.

6.4.3. Clarification of the mucoadhesive properties of the mucoadhesive layer

Mucoadhesive properties of the statistically derived mucoadhesive film formulations were evaluated to screen their ability to adhere to the intestinal surface lining, to increase the retention time and enhance absorption of the drug through the mucosal lining of the small intestine. Figure 6.5 summarizes the mucoadhesion results for the mucoadhesive film design layers via mucin cleavage, yielding the average percentage crosslinking values of the mucus solution.

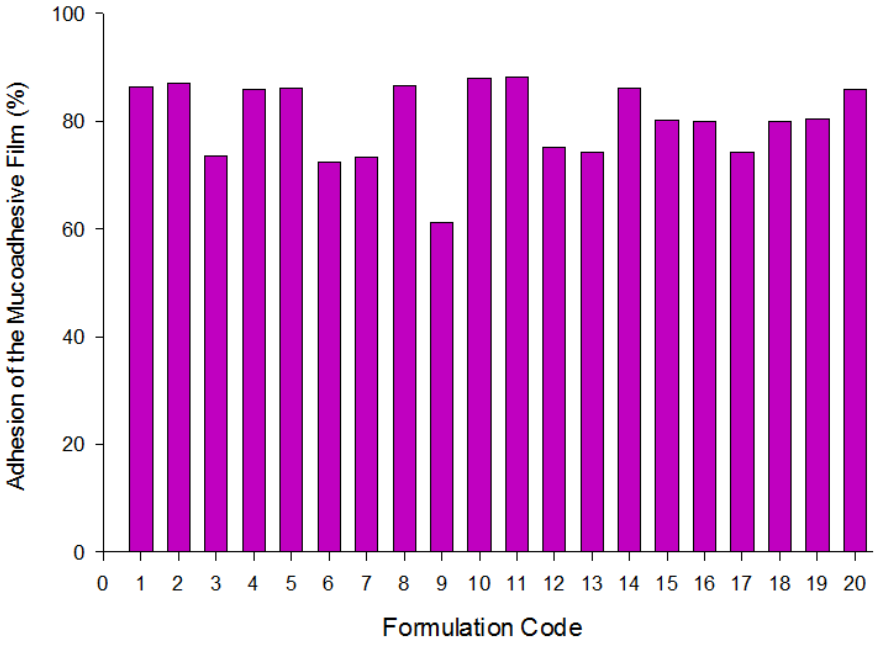


Figure 6.5: Percentage adhesion of mucoadhesive films to mucus for all 20 design formulations.

Formulations displayed mucoadhesion in the range of 61.2 to 88.1%, it was observed that % mucoadhesion increased with a corresponding increase in polymer concentration (HPMC and CHT) thus allowing for greater interaction between the polymeric chains and mucus. Lectin, a highly heterogeneous group of proteins and glycoproteins of non-immune origin that bind to carbohydrates in biological tissue specifically and non-covalently (Gavrovic-Jankulovic and Prodanovic, 2011) was amalgamated to the solutions forming polymeric films at a constant concentration, thus resulting in the high level of mucoadhesion observed in all formulations. However, it was also noted that an increase in citric acid concentration (0.3%) lead to a reduction in the percentage mucoadhesion possibly due to a reduced amount of polymer chains available for crosslinking to the mucin. Generally, all formulations exhibited satisfactory mucoadhesive abilities and thus would function efficiently in prolonging residence time and thus improving drug absorption through the intestinal mucosal surface.

6.4.4. Assessment of the gravimetric swelling characteristics of the mucoadhesive layer

Through gravimetrical analysis it was shown that with an increased exposure to simulated intestinal conditions design formulations of the mucoadhesive layer tended to swell, resulting in a corresponding increase in weight. The hydrated and thus expanded nature of the polymeric network allows for mutual interpenetration between the mucoadhesive layer with mucin molecules, subsequently forming stabilized interactions and thereby strengthening the mucoadhesive characteristics of the formulations (Salamat-Miller et al., 2005; Roy et al., 2009).

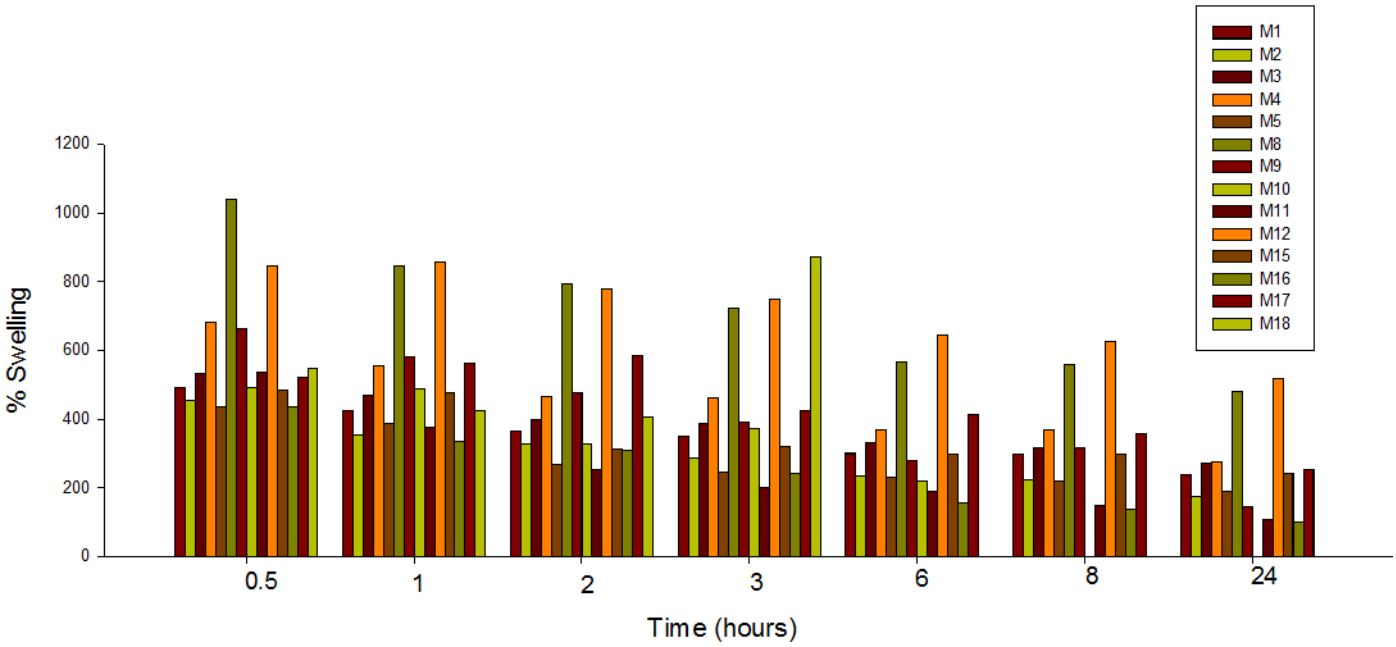


Figure 6.6: Percentage swelling of mucoadhesive layer design formulations over 24 hours.

With exposure of the surface layer of the mucoadhesive films to simulated intestinal conditions, polymeric chains present on the surface, underwent swelling, thus promoting both mucoadhesion and weight gain. Upon continuous exposure the surface layer ultimately disintegrates and erodes out of the film, resulting in a decrease in both the swelling (weight gain) and mucoadhesion. The underlying polymeric chains consequently become exposed to the surrounding fluid and undergo swelling, and hence mucoadhesion. As a result, a fluctuating degree of swelling was observed at differing time points, leading to the resultant variations in mucoadhesion among design formulations. Formulations 6, 7, 13 and 14 of the mucoadhesive layer design (Figure 6.6) were excluded from the gravimetrical swelling study as they were shown to disintegrate before the 0.5 hour time interval. This is attributed to the reduced concentration of chitosan among these formulations, with a corresponding low concentration of hypromellose. The high percentage of

swelling observed within the range of design formulations could be attributed to the high polydispersity index and solubility parameter of hypromellose and chitosan. The degree of swelling is also affected by citric acid content, with a higher ratio of citric acid to chitosan the percentage swelling was lower, and this is attributed to the ester bonds formed between citric acid and the polysaccharide, thus producing a dense structure (Azeredo et al., 2015).

6.4.5. Mechanical strength appraisal of the mucoadhesive film layer

Tensile properties determine the mechanical response and flexibility of the produced films to forces it may be subjected to. Young's Modulus and other tensile properties of the design mucoadhesive layer were determined utilizing the NanoTensile® 5000 and Texture Analyzer as described in *Chapter 6, Sections* 6.3.5 and 6.3.5.1 respectively. The stress-strain relationship of a material is greatly reliant on the flexibility of the polymer chains and the strength of the material. When a small degree of stress is requisite to produce a large degree of strain, the test material is considered to be flexible and the Young's Modulus, which is the slope of the linear portion of the stress-strain curve will be comparatively small (Leung and Ko, 2011). Tensile properties were determined as the mucoadhesive layer would eventually be compressed to form an intestinal patch which would further be incorporated into a layered tablet to ease oral administration.

The average experimental values of Young's Modulus (E), yield stress (Q_Y) (extent of stress on the stress-strain curve at which considerable deformation occurs without any considerable increase in stress), ultimate strength (Q_U) (the maximum stress a material can withstand), ultimate strain (ε_u) and toughness (U_f) are outlined in Table 6.4 .

Table 6.4: Experimental average values obtained from NanoTensile (NT) and Textural analysis (TA) of mucoadhesive layer design formulations.

Formulation	E(MPa) NT	E(MPa) TA	Q_Y (MPa)	Q_U(MPa)	ε_u	U_f(J/cm^{-3})
Mucoadhesive Layer	0.48	0.15	0.09	0.1	0.53	0.002

The observed Young's Modulus values were relatively low indicating that the films demonstrated good elasticity. The mucoadhesive films, containing chitosan and hypromellose, displayed high elasticity values (a low Young's Modulus). The films demonstrated suitable strength and toughness to be able to withstand compression and incorporation into tablets.

6.4.6. Assessment of Rheological characteristics of the mucoadhesive polymeric solutions of the multi-layered intestinal patch

The rheological characteristics, and in particular the viscosity, of polymeric solutions determines whether the solution can satisfactorily form a polymeric film, and further influences the casted film's surface morphology and quality. A low viscosity polymer solution leads to the formation of thin films that easily undergo tearing, on the other hand a polymer solution with a high viscosity leads to the formation of casted films which are brittle and display a reduced quality of surface morphology. The respective viscosities, determined through rheological analysis of the mucoadhesive layer polymeric solutions, are listed in Table 6.5. As illustrated in the table, an increase in % concentration of polymeric material increases the viscosity of the solutions.

Table 6.5: Effect of polymer concentration on viscosity for the mucoadhesive layers.

Intestinal Patch Layer	*Solution Parameters*	*Viscosity at shear rate of 100 m/s (mPas)*
Mucoadhesive Layer	5%$^{w}/_{v}$CHT+2%$^{w}/_{v}$HPMC+0.225%$^{w}/_{v}$ CA	1071.3
	5%$^{w}/_{v}$ CHT+3%$^{w}/_{v}$ HPMC+0.15%$^{w}/_{v}$ CA	2597.5
	5%$^{w}/_{v}$ CHT+3%$^{w}/_{v}$ HPMC+0.3%$^{w}/_{v}$ CA	4974.6

- CHT (Chitosan), HPMC (Hypromellose), CA (Citric Acid).

As shown in the Table 6.5, for the mucoadhesive layer polymeric solution there is evidence that an increase in hypromellose and citric acid concentrations leads to a corresponding rise in solution viscosity. Mucoadhesive film solutions with a viscosity in the range of 1071.3 to 2253 mPas formed satisfactory polymeric films that had a durable structure with good surface morphology and tensile strength. However, as the concentration of polymers increased so did the viscosity which resulted in the formation of polymeric films with a greater film thickness and brittleness with a related reduction in tensile strength; solution viscosity also influences droplet spreading, thus with more viscous solutions they are not able to readily spread across the film casting surface before solvent evaporation occurs (Felton, 2013). The thickening capacity of some formulations is greater than others, which may be attributed to the significant differences in their polymer chain arrangement (Xuaet al., 2015).

6.4.7. Response surface analysis of the Central Composite design

With the purpose of determining the relationship between the response variables and predictor variables, a complete ANOVA analysis was performed of the measured formulation responses (Figure 6.7, Table 6.6), mucoadhesion and Young's Modulus. The aptness of the multiple regression models are accessed via residual analysis. Residual plots for mucoadhesion (%) and Young's Modulus are depicted in Figure 6.7. The hypotheses of a multiple linear regression model is that the response variables are independent and ordinarily distributed, arbitrary variables with constant variance and means depending linearly on the explanatory variables (Larsen and McCleary, 1972; Huynh, 2000). Resilient linear relationships were observed for all response variables as indicated by the restrained grouping of the partial residuals. The scatter plot of the residual, in which the residuals were plotted against the model predictions, is empirically uniform and radiate around zero.

The exhibited asymmetrical scatter demonstrated that none of the fundamental hypotheses of the multiple regression analysis were visibly breached; some deviations and some broadly spread points were observed revealing of a degree of non-constant variance (du Toit et al., 2013). The normal probability plots of the residuals fell on a straight line signifying the data to be ordinarily distributed with no assertion of unknown variables. Deviations could have resulted from experimental error. The histograms for Young's Modulus were largely symmetrical thus supporting the probability plots of constant and uniform distribution. The attained histogram for % mucoadhesion depicted an absence of symmetry suggestive of a random error of the data set. The scatter plot, which is the residual vs. observation order, depicts the performance of the model. Scatter plots stayed within constant scale indicating non-arbitrary error. A full ANOVA was conducted and shown in Table 6.6.

Table 6.6: ANOVA analysis for the measured responses.

Response Variables	***p-values***	
	Young's Modulus	*Mucoadhesion (%)*
[CHT]	0.202	0.476
[HPM]	0.110	0.205
[CA]	0.819	0.420

The complete regression equations generated for Young's Modulus and % mucoadhesion are indicated below;

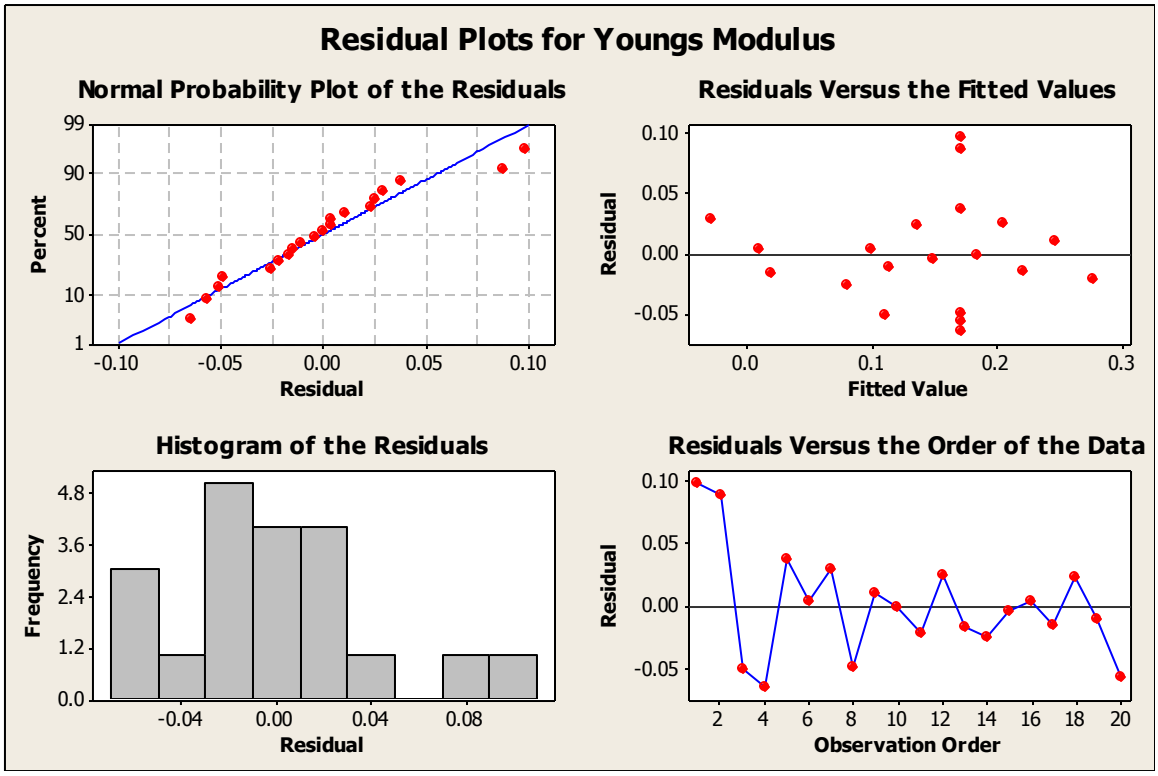
$$Young's\ Modulus = -0.3279 + 1.8093[CHT] + 5.6234[HPM] + 0.6961[CA]$$

Equation 6.4

$$\%\ Mucoadhesion = 43.40 - 177.50[CHT] + 787.10[HPM] - 450.22[CA]$$

Equation 6.5

(a)



(b)

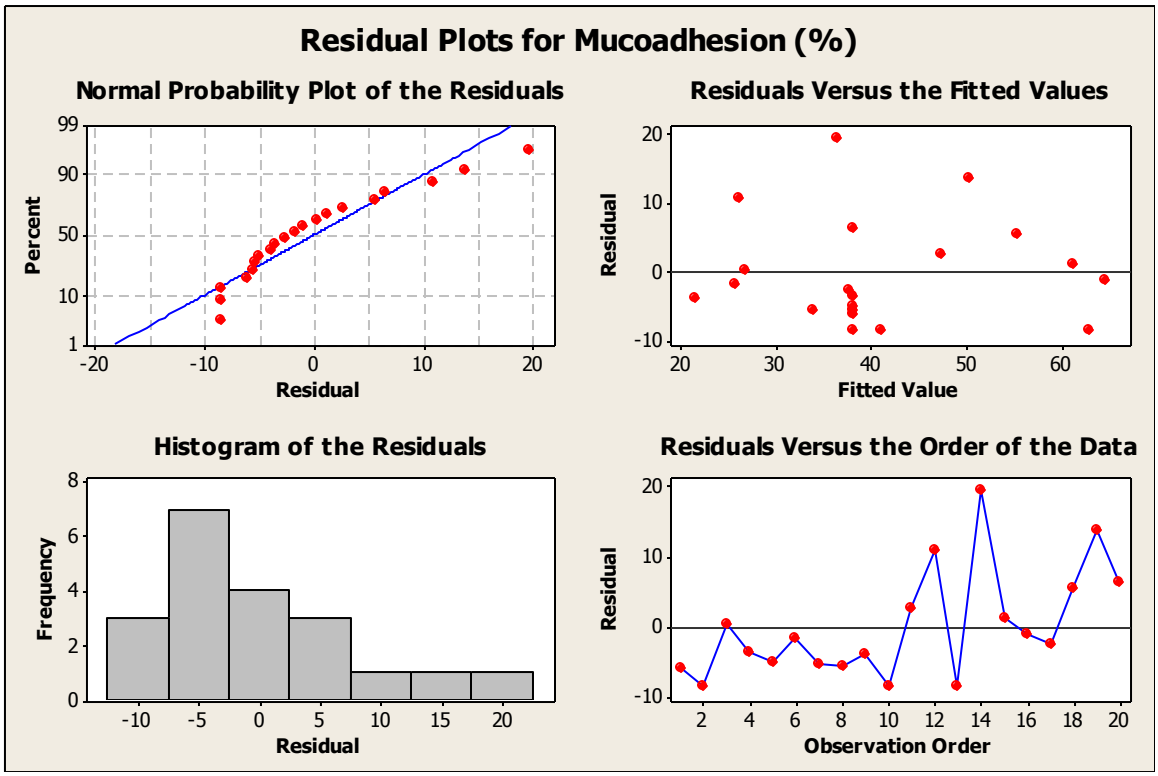


Figure 6.7: Residual plots for the responses a) Young's Modulus b) % Mucoadhesion

Young’s Modulus and mucoadhesion of the mucoadhesive layer are important factors influencing the degree of gastric retention and capability of the system to endure gastric transit post oral dosing. Data plots depicted in Figure 6.8 were utilized to illustrate the purposeful relationship between the experimental variables and achieved responses. The effects of CHT, CA and HPM on the tensile strength via Young's Modulus and % mucoadhesion; the desired Young's Modulus was within the range of 0.1-0.3, formulations having chitosan: hypromellose: citric acid ratios of approximately 0.25: 0.15: 0.3 were found to display the anticipated Young's Modulus. It was observed that an increase in polymer and crosslinker concentrations lead to a lower Young's Modulus and thereby better polymeric film flexibility. It was noted that none of the factors were significant.

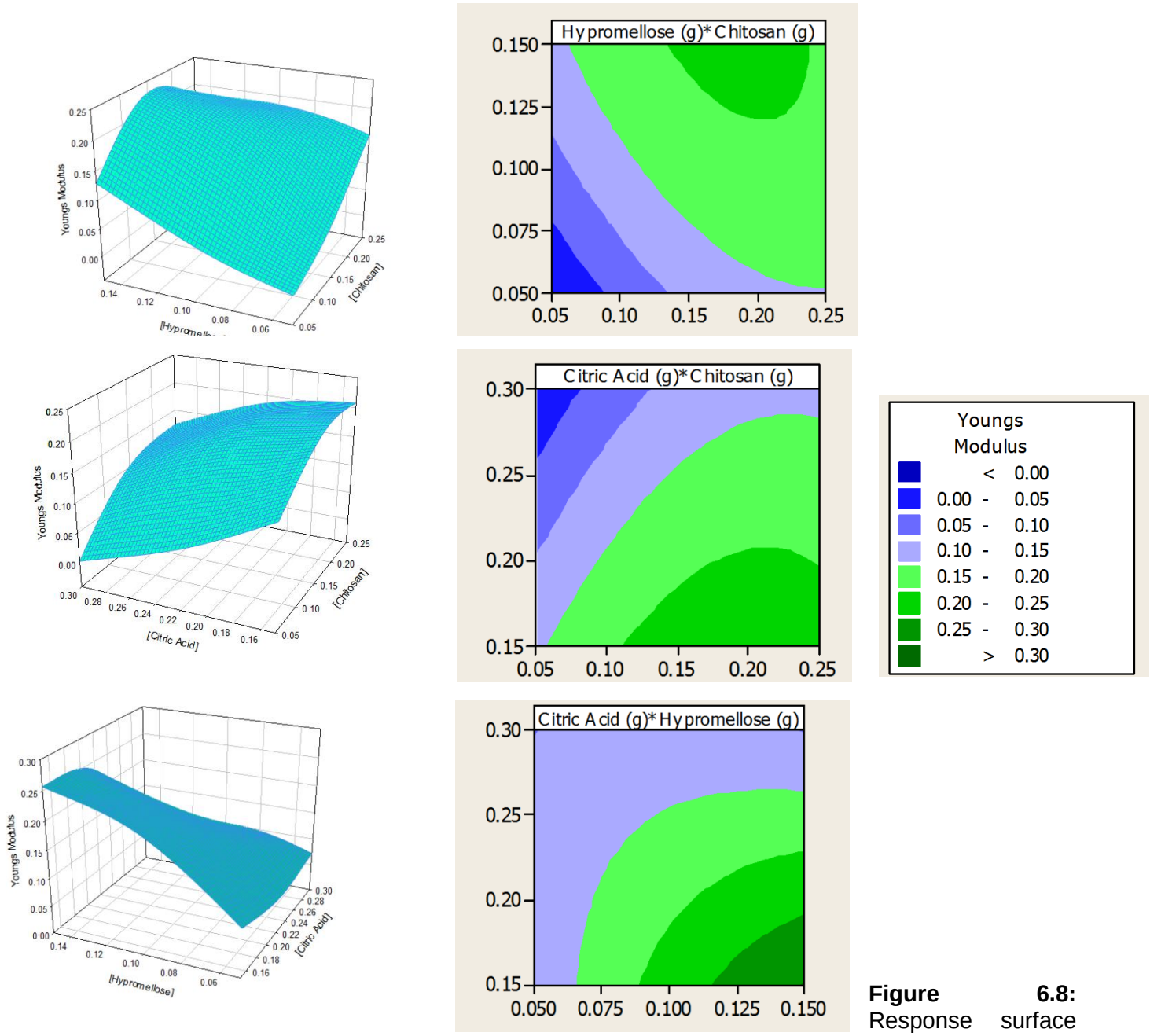


Figure 6.8: Response surface and contour plots depicting the effects of citric acid (CA), chitosan (CHT) and hypromellose (HPM) on Young's Modulus.

From the obtained surface plots for the % mucoadhesion shown in Figure 6.9 it was observed that mucoadhesion was shown to increase with a corresponding increase in the respective formulation constituents. This can be attributed to the additive mucoadhesive properties of the respective polymers. The highest % mucoadhesion ranged from 60-65% and showed the most desirable mucoadhesive capabilities, formulations having chitosan: hypromellose: citric acid ratios of approximately 0.20:0.10:0.26 were found to exhibit the predicted mucoadhesion.

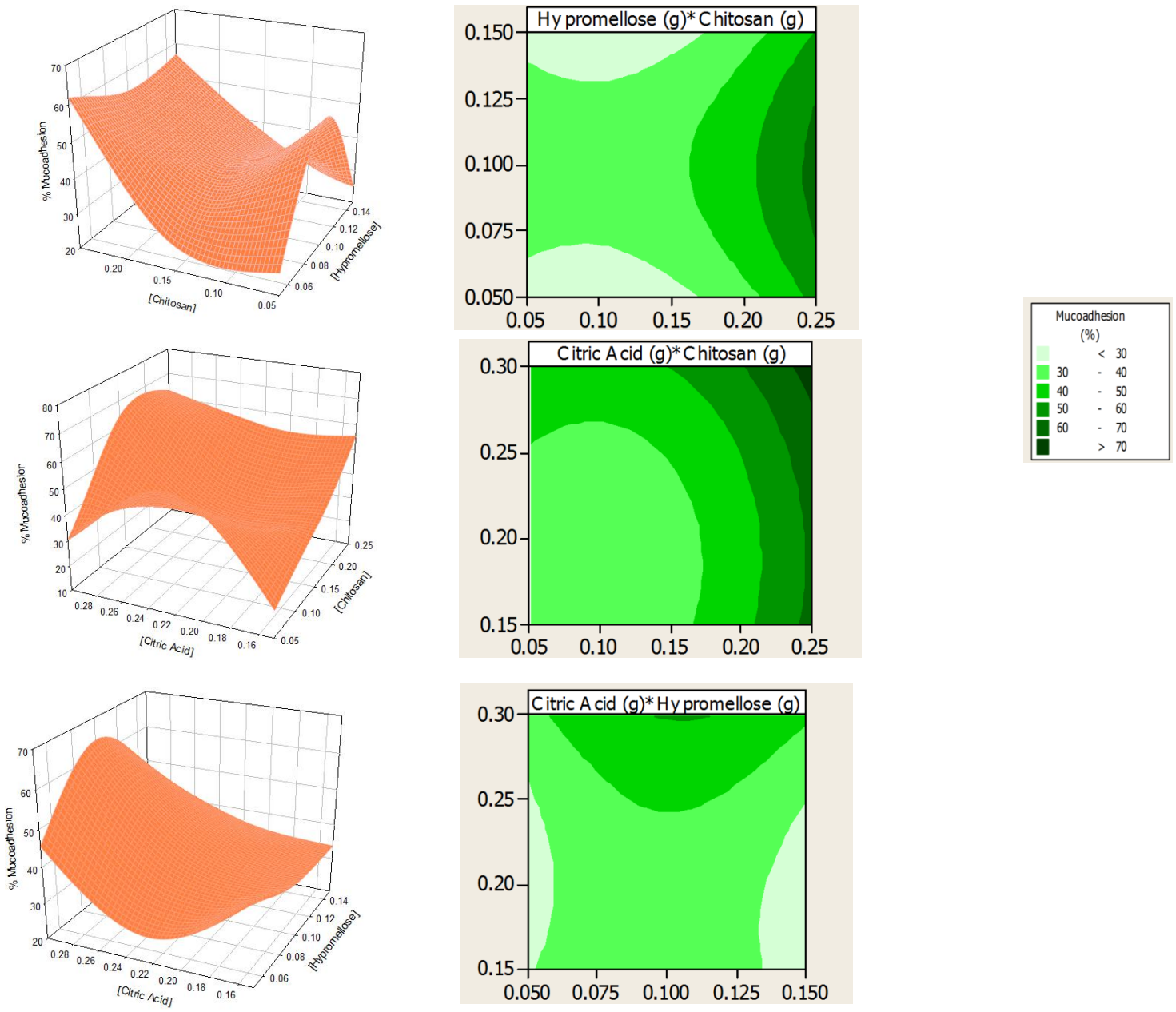


Figure 6.9: Response surface and contour plots depicting the effects of citric acid (CA), chitosan (CHT) and hypromellose (HPM) on % mucoadhesion.

PART II: Preliminary Drug Loaded Layer Characterization

6.5. Physiomechanical and Physiochemical Characterization of the Drug Loaded Layer

6.5.1. Determination of the chemical vibrational transition of the crosslinked drug loaded layer of the bioadhesive multilayered intestinal patch

Fourier Transform Infrared Spectroscopy (FTIR) was utilized to determine the chemical structural composition of the design formulations as well as native polymers incorporated in the drug loaded layer. FTIR analysis was conducted as outlined earlier in *Chapter 6, Section 6.3.1.*

6.5.2. Thermal event analysis of the drug loaded layer of the bioadhesive multilayered intestinal patch

Differential Scanning Calorimetry (DSC) was conducted on the drug loaded layer design formulations. DSC studies provided information regarding the thermal stability of the formulations. DSC analysis was performed as detailed in *Chapter 6, Section 6.3.2* for the mucoadhesive layer.

6.5.3. Textural analysis of the drug loaded layer

The mechanical strength of the drug loaded layer of the intestinal patch system is vital as it is required to endure the peristaltic motion and remain attached to the intestinal wall for a prolonged period. Mechanical strength of the drug loaded layer was evaluated via textural and NanoTensile® analysis as described in *Chapter 6, Section 6.3.5* for the mucoadhesive layer. The Young's Modulus was calculated as per Equation 6.6.

6.5.4. Appraisal of swelling behavior of the drug loaded layer

The degree of swelling of the drug loaded layer was analyzed via gravimetric analysis; gravimetric analysis was carried out in accordance to the method and equation detailed in *Chapter 6, Section 6.3.4.*

6.5.5. Determination of the Rheological Properties

Understanding of the rheological properties within a micro structured system is vital in relation to the rate and degree of drug release as well as the mechanical features of the system as a whole. Thus, viscosity analysis was performed for the drug loaded layer polymeric solution as detailed previously in *Chapter 6, Section 6.3.6.*

6.5.6. Construction of a calibration curve for the ultraviolet spectrophotometric determination of valproic acid

Utilizing UV spectroscopy, it was established that valproic acid (sodium valproate) exhibits a maximum wavelength at λ_{215}, consistent with published literature on the absorption peak of valproic acid being at 215nm (Thakkar et al., 2012). Using a series of known concentrations (0.2-1mg/mL) of valproic acid in PBS, a calibration curve at λ_{215} was conducted (Figure 6.10). The linear curve was plotted with the observed absorbance of sodium valproate as the dependent variable and the concentration of sodium valproate as the independent variable (Figure 6.10). The obtained R^2 value of the calibration curve was 0.99 (Figure 6.10), indicating a perfect correlation.

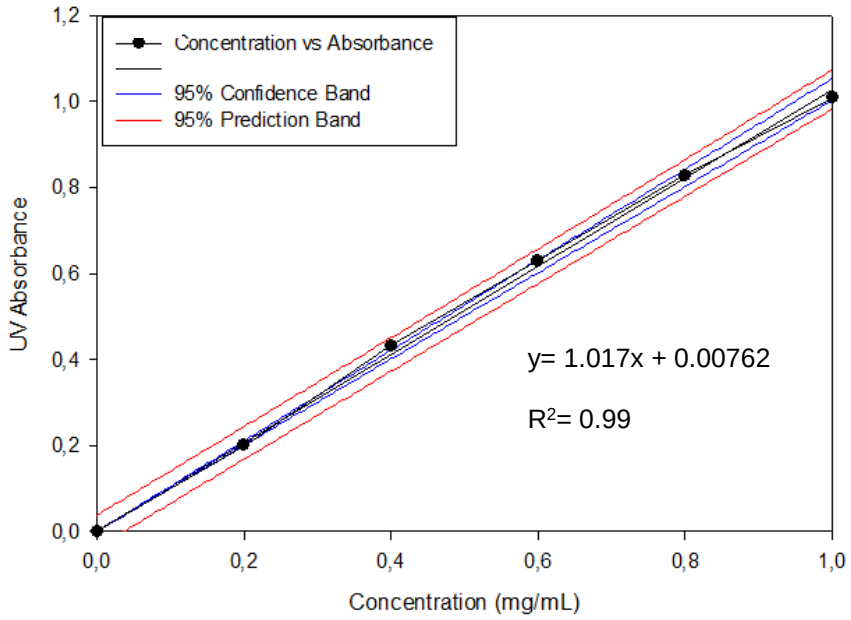


Figure 6.10: Calibration curve of sodium valproate in PBS at λ_{215}.

6.5.7. *In vitro* drug release from the drug loaded layer of the bioadhesive multilayered intestinal patch

Release kinetics was evaluated using the USP type II apparatus (Caleva, model 7ST) at 50rpm. Dissolution vessels were filled with 900mL dissolution medium and samples were placed within dissolution vessels employing mesh rings placed into the lower part of the standard dissolution vessel to allow for intestinal drug loaded layer film attachment. Dissolution medium aliquots of 5mL were withdrawn manually at predetermined time intervals during the 12 hour study and replaced with an equal volume of fresh dissolution medium to ensure sink conditions were maintained. The samples were then filtered and analyzed for drug release via Ultraviolet spectrometry (WinAspect Spectro-analytical software, Analytik Jena AG), at a wavelength of 215

nm employing a calibration curve obtained for the drug as detailed in *Chapter 6, Section 6.5.6.* (Thakkar et al., 2012).

6.5.8. Response surface analysis of the employed responses

Minitab® statistical software (V15, Minitab Inc., PA, USA) was utilized to perform the response surface analysis of the various response variables for the drug loaded layer. Results were established employing response surface and contour plots which were derived for the measured response (drug release) based on the experimental model.

6.6. Results and Discussion

6.6.1. Elucidation of chemical vibrational transitions of the drug loaded layer

Crosslinking of sodium alginate with the use of calcium chloride in the direct presence of Eudragit® RS100 results in the formation of a polymer complex capable of controlling drug release. An increase in calcium chloride concentration results in a decrease in drug release rate. Calcium chloride at low concentrations reduces the tortuosity of the diffusion path thereby increasing drug release rates. At higher concentrations there is a greater quantity of calcium ions available to bind, thus forming an efficiently crosslinked strong gel that prevents excessive dissolution medium penetration leading to a reduction in release rates (Nokhodchi and Tailor, 2004).

Analysis of crosslinking efficiency therefore becomes apparent, all design formulations (Figure 6.11) displayed that distinguishing peaks existent within the FTIR spectra of the natural polymers were altered verifying that covalent interfaces between polymers ensued, thereby subsequent enhancement of drug release properties. FTIR investigation of the crude polymers employed in the formulation of drug loaded layers displayed the following characteristic peaks: all crude polymers displayed an O-H stretch related to normal polymeric stretching ranging between 2349.84cm^{-1}-3212.92cm^{-1}. Alginate displayed additional peaks at 1404.87cm^{-1} descriptive of carbonyl ions, and a peak at 878.18cm^{-1} C-H aromatic ring (Figure 6.11a). Eudragit RS100 exhibited peaks at 1722.54cm^{-1} representative of aldehydes, 1383.28cm^{-1} C-H alkanes, 1142.86cm^{-1} C-O phenols and a peak at 847.95cm^{-1} C-H aromatic ring (Figure 6.11b). Spectra of calcium chloride dihydrate presented with peaks at 3362.84cm^{-1} illustrative of N-H amines,

1742.62cm^{-1} representative of an alkyl carbonate, 1139.67cm^{-1} expressive of C-O phenols, and a peak at 763.71cm^{-1} C-H alkene functional group (Figure 6.11d) (Krishnaraj et al., 2012).

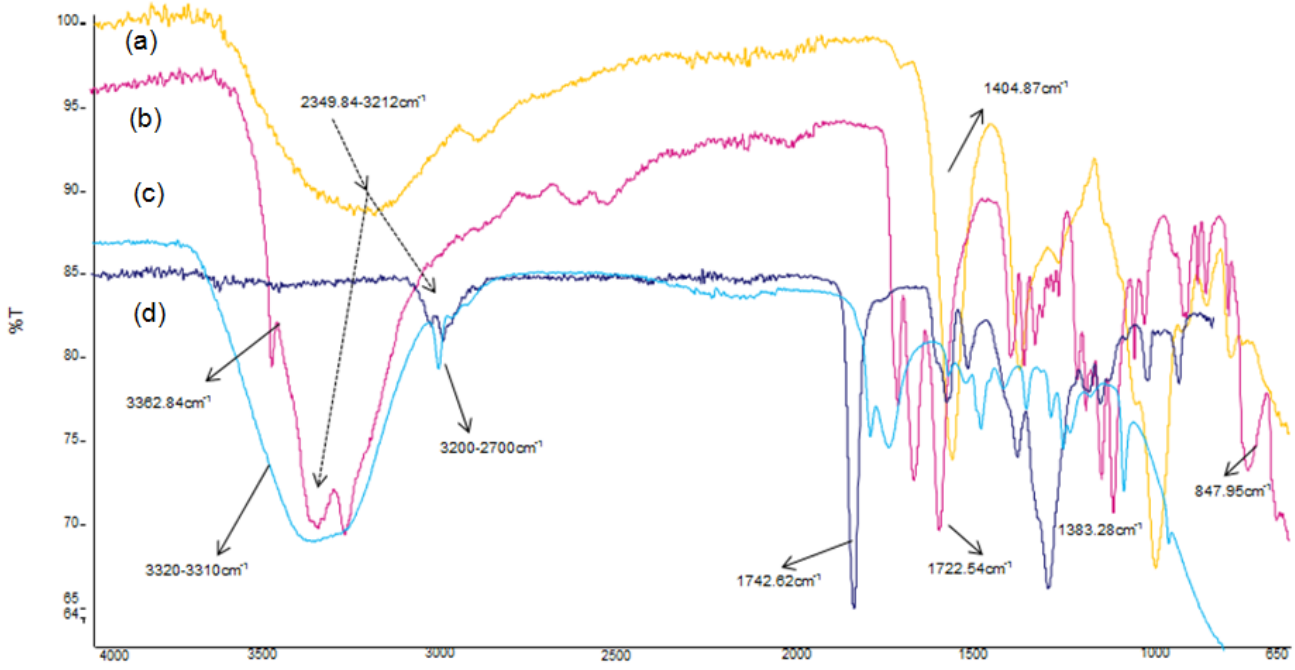


Figure 6.11: FTIR spectra of native polymers a) alginate, b) Eudragit RS 100 and d) calcium chloride employed in fabrication of drug loaded layer and c) a representative design formulation.

FTIR spectra of drug loaded design formulations displayed characteristic peaks at a range of 3320-3310cm^{-1} which is representative of alkyne related C-H stretching, a peak in the region of 3200-2700cm^{-1} related to tetrahedral carbon hybridization as well aliphatic C-H stretching, followed by a peak within the range of 1675-1725cm^{-1} associated with C=O conjugated carboxylic acid stretch characteristic of native polymers, a peak between the range of 1640-1680cm^{-1} is representative of C=C alkene stretch, an additional peak at 1470-1430cm^{-1} illustrative of C-H methyl stretching, a modified peak at 1370cm^{-1} displaying strong tert-butyl unsymmetrical doublet, 1270-1230cm^{-1} O-H aromatic ether, 1130-1190 C-N secondary amine (Durig and Fassihi, 2002) and a peak in the region of 800-1000cm^{-1} alkene out of plane C-H bending (Figure 6.11c). It was noted that an increase in polymer and crosslinker concentration led to a proportional higher shift of FTIR spectra wavelength. The additional and modified peaks verify the crosslinking of sodium alginate and Eudragit RS100 via calcium chloride.

6.6.2. Thermal characteristics of the drug loaded layer

Crude polymers employed in the formulation of the drug loaded layer displayed DSC thermograms as follows: alginate displayed a Tg of 26.34˚C, an endothermic peak at 124.52˚ relating to solid-solid transitions, an exothermic peak at 240.76˚C representative of crystallinity, endothermic peak at 260.58˚C relating to solid-solid transitions, and a peak at 281.16˚C showing melting with stable modification (Figure 6.12a) (Mettler Toledo, 2001). Calcium chloride dihydrate with a Tg of 27.41˚C presented with two distinct peaks, an exothermic peak at 146.28˚C descriptive of sample crystallinity, and an endothermic peak at 124.37˚C descriptive of melting with stable modification (Figure 6.12b) (Mettler Toledo, 2001). Eudragit RS100 displayed thermal events at 28.61˚C relating to its Tg, 200.48˚C relating to sample crystallinity and an exothermic peak at 231.65˚C demonstrative of melting with decomposition (6.12c) (Mettler Toledo, 2001).

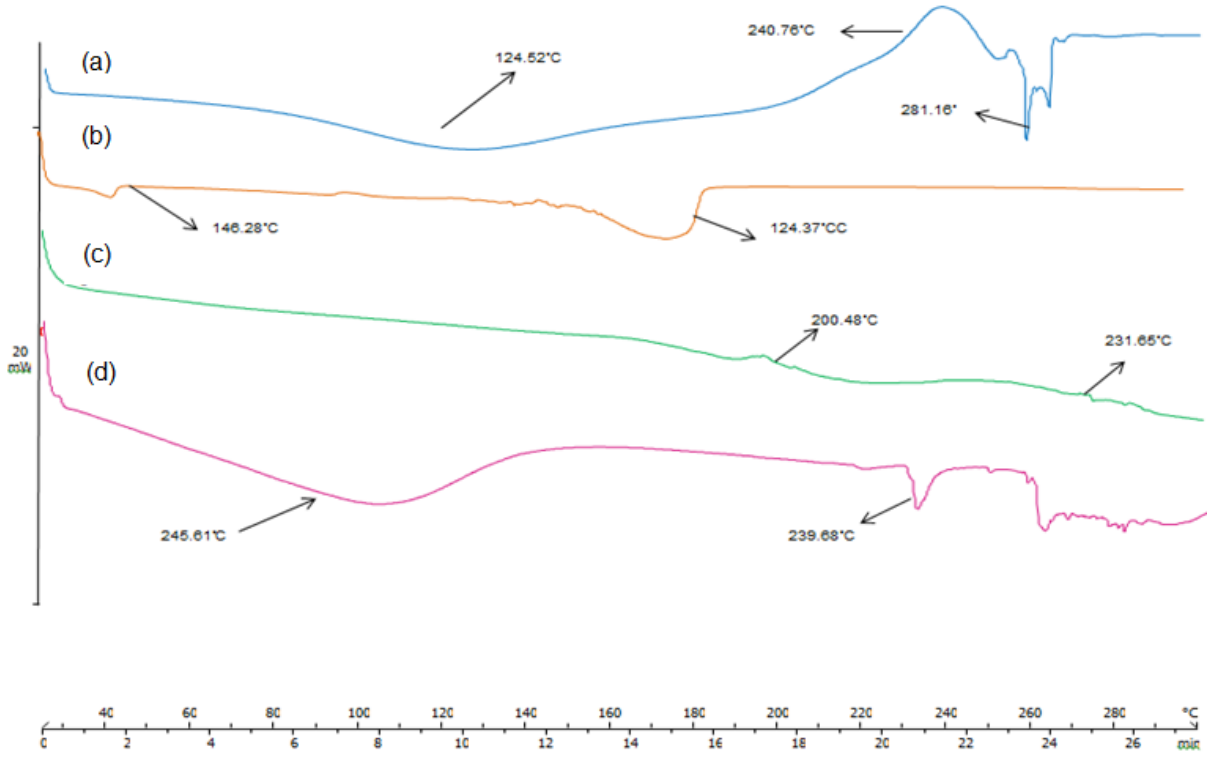


Figure 6.12: DSC thermograms of the native polymers a) alginate, b) calcium chloride and c) Eudragit RS100 employed in the fabrication of drug loaded layers and d) a representative design formulations.

Design formulations of the drug loaded layer displayed two distinct thermal events. The first being the glass transition (Tg) temperature which ranged between 25.67˚C -37.41˚C with a corresponding increase in Tg as the degree of crosslinking increased (Mettler Toledo, 2001). The second thermal observed was that of melting of stable modification which occurred at 245.61˚C-284.15˚C (Figure 6.12d). However, formulations 4 and 6 showed an additional melting peak at 239.68˚C- 261.55˚C respectively, attributable to an increase in polymer concentration thus leading to a prolonged stable modification melting.

6.6.3. Tensile assessment of the drug loaded layer

In fabricating polymeric films that are intended as a dosage form for oral drug delivery, films should have adequate strength and flexibility to endure mechanical manipulation during production and administration. Young's Modulus of the design drug loaded layers were determined utilizing the NanoTensile® 5000 and Texture Analyzer as described in *Chapter 6, Sections* 6.3.5 and 6.3.5.1. Young's Modulus, which is the slope of the linear portion of the stress-strain curve, will be comparatively small for flexible materials (Leung and Ko, 2011).

The average experimental values of Young's Modulus (E), yield stress (Q_Y) (extent of stress on the stress-strain curve at which considerable deformation occurs without any considerable increase in stress), ultimate strength (Q_U) (the maximum stress a material can withstand), ultimate strain (ε_u) and toughness (U_f) are outlined in Table 6.7.

Table 6.7: Experimental average values obtained from NanoTensile (NT) and Textural analysis (TA) for the drug loaded design formulations.

Formulation	***E(MPa) NT***	***E(MPa) TA***	***Q_Y (MPa)***	***Q_U(MPa)***	***ε_u***	***U_f(J/cm^{-3})***
Drug Loaded Layer	11	0.09	0.24	0.4	0.11	0.03

The average Young's Modulus for design formulations was relatively low indicating that the films demonstrated satisfactory elasticity and flexibility. It was noted that tensile strength decreased with greater concentration ratios of the employed polymers and crosslinker. As the concentration of Eudragit® RS100 increased the measured tensile strength decreased, this may be attributed to the formation of brittle films as there is not sufficient polymer entanglement upon solvent evaporation.

6.6.4. Appraisal of swelling behavior of the drug loaded layer

Swelling characteristics of a film influences its bioadhesive properties and drug release pattern; it also assists in ascertaining whether the formulation is able to maintain its integrity after moisture absorption (Kaur et al., 2014). Swelling is defined as a process of dissolution of a polymer in a specified solvent. Initially, solvent molecules slowly diffuse into the polymeric system to yield a swollen gel; this process holds true for polymer-polymer intermolecular forces that are strong due to crosslinking or strong hydrogen bonding. However, if these intermolecular forces are overcome by polymer-solvent interactions dissolution of the polymeric system may occur (Izák et al., 2007).

Polymeric film swelling has been defined by two standpoints namely; 'macroscopic swelling' which is a bulk growth of polymer membranes; in the region of at least 1mm^2 and 'microscopic swelling' where the alterations in film dimensions are measured from small-angle X-ray scattering. Macroscopic swelling is most commonly measured gravimetrically (Izák et al., 2007). Via gravimetrical swelling analysis it was revealed that drug loaded film layers gained in weight on exposure to intestinal simulated dissolution medium. This phenomenon allows for interpenetration of polymer chains thereby stabilizing interactions of the multiple layers as mentioned in *Chapter 6, Section 6.4.4* (Salamat-Miller et al., 2005; Roy et al., 2009).

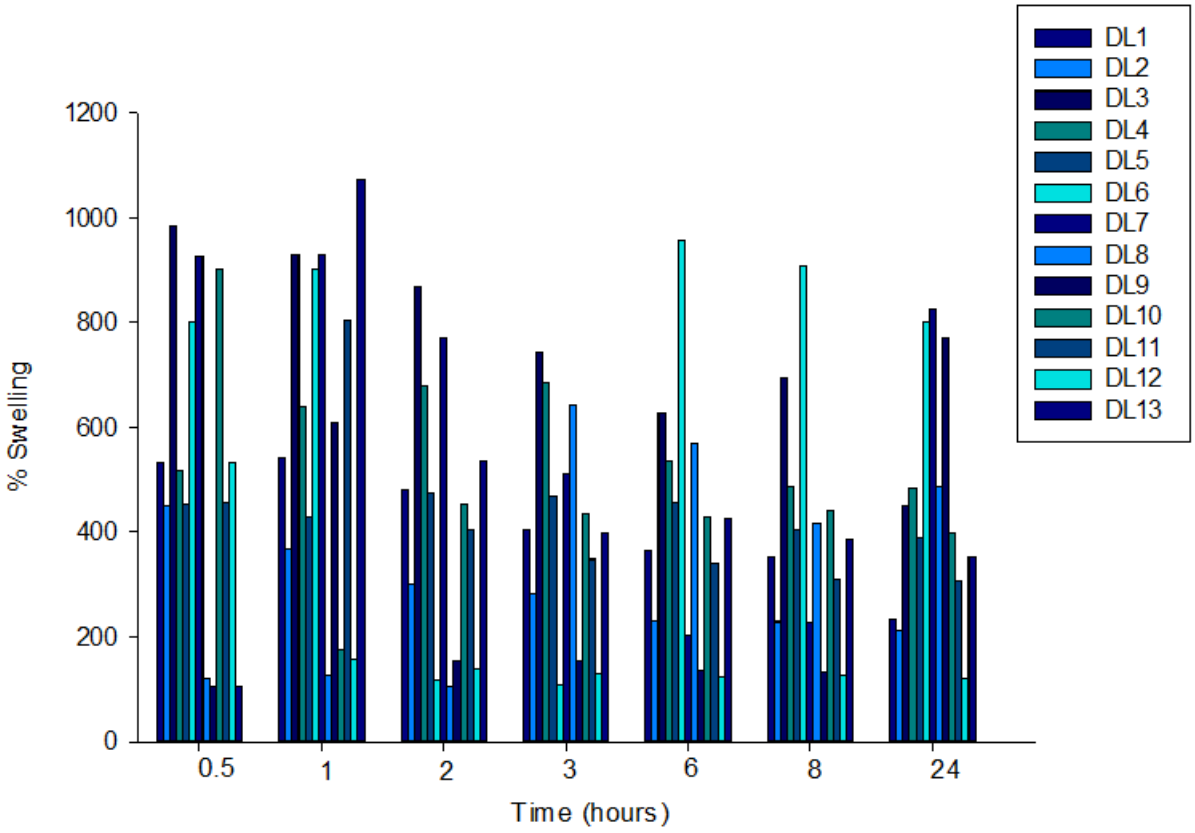


Figure 6.13: Percentage swelling of the drug loaded design formulations over 24 hours.

On exposure of the drug loaded layer to dissolution medium, polymer chains underwent swelling which is illustrated as percentage swelling over 24 hours in Figure 6.13. Films maintained their shape and macrostructure indicating that the cohesiveness of the polymers is proficient in affording the system stability to sustain pulsatile release. There was an observed rise in degree of swelling with a consistent increase in calcium chloride concentration. Calcium chloride in the current context is employed as a crosslinking agent; it is thus expected to retain water and thereby enhances the water uptake capability of the system as a whole.

Once the system is exposed to dissolution medium, surface polymer chains absorb the surrounding medium and undergo swelling, with constant exposure to dissolution medium the surface layers eventually undergo dissolution and erosion, with underlying polymer chains subsequently being exposed to the same process. This results in the observed variations and fluctuations in degree of swelling over the experimental period.

6.6.5 Assessment of rheological characteristics

Viscosity analysis is a quick and simple method to evaluate the effectiveness of the homogeneity process. It characterizes the degree of solids and level of hydrolysis of solutions and its respective ability to form polymeric films. The degree of viscosity is a vital parameter that influences the fabrication and manufacturing process of polymeric films. Higher viscosities maintain stability of a solution by preserving homogeneity. However, viscosity that is too high will adversely affects the mixing, spreading and transferring process of the solution to the film casting surface (Lin and Pascall, 2014). The respective viscosities, determined through rheological analysis of the drug loaded layer polymeric solutions, are listed in Table 6.8. As illustrated in the table, an increase in % concentration of polymeric material increases the viscosity of the solutions.

Table 6.8: Effect of polymer concentration on viscosity.

Intestinal Patch Layer	***Solution Parameters***	***Viscosity at shear rate of 100 m/s (mPas)***
Drug Loaded Layer	2% EUD+0.055% CaCl2	261.9
	2% EUD+0.01% CaCl2	488.8
	1.1% EUD+0.055 CaCl2	1066.9

As shown in the table 6.8 the drug loaded layer displays an increase in solution viscosity when there is a related reduction in Eudragit: $CaCl_2$ ratio. However, as the concentration of polymers

increased so did the viscosity which resulted in the formation of polymeric films with a greater film thickness and brittleness with a related reduction in tensile strength. Drug loaded layer films displayed a relatively constant surface morphology and tensile properties, with little variations among design formulations. The thickening capacity of some formulations is greater than others, which may be attributed to the significant differences in their polymer chain arrangement (Xuaet al., 2015). .

6.6.6. *In vitro* drug release from the drug loaded layer

In general, pulsatile release is termed as the timed release of drugs subsequent to programmable lag phases. Within the context of time-based pulsatile drug delivery systems inner mechanisms are responsible for the desired release which are expected to be independent of physiological and environmental markers (pH, enzymatic activity, intestinal motility and/or stimuli) (Gazzaniga et al., 2008). In order to accomplish drug release that is independent of the environment, the lag phase prior to drug liberation has to be controlled principally by the delivery system (Anal, 2007).

The clinical efficiency and tolerability of drug therapy may possibly be markedly improved by delivery systems projected to timely release drug after administration; thereby providing pharmacological protection without an unnecessary extended period of patient exposure to the active drug molecules and thus not influencing patient compliance to treatment (Gazzaniga et al., 2008). Drug is released from the intestinal patch at two hours as the first pulsed release occurs. The remaining two drug loaded layers, control the rate of drug release via the concentration of polymer and the degree of crosslinking. Ideally, drug release should occur in three pulses over a 24 hour period.

All release profiles as displayed in Figure 6.14 display triphasic release; with an initial lag-phase observed in some formulations. The first pulse provides rapid drug release while the second and third pulses display controlled release. The rate at which drug is released during the second and third pulses are governed by the concentration of polymer and the corresponding degree of crosslinking as well as the interpenetrating mucoadhesive polymers. It was shown that an increase in calcium chloride concentration within the design formulation patches resulted in a corresponding reduction in drug release rate; this phenomenon allowed for the desired pulsatile release kinetics with drug being release at 6 hour intervals.

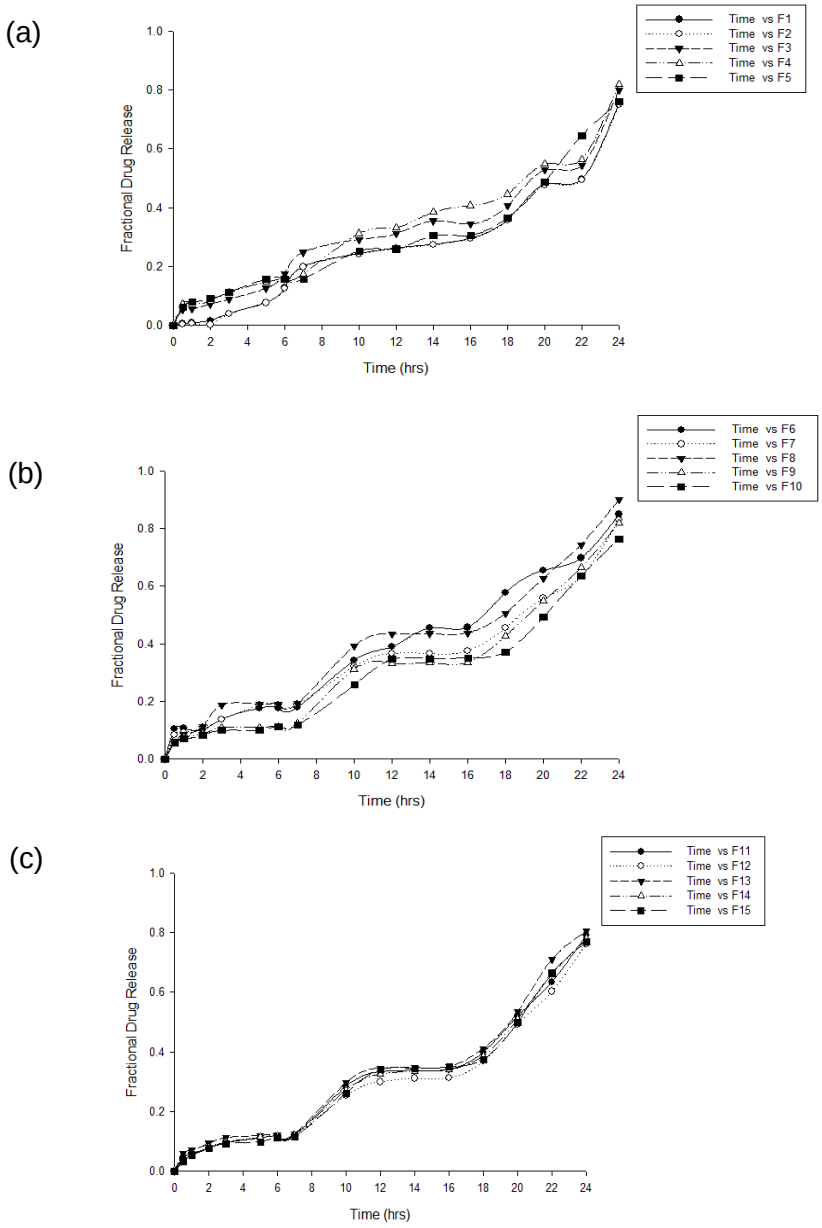


Figure 6.14: *In vitro* fractional drug release profiles for all design formulations.

Formulation 1 displayed an initial lag phase followed by the first pulsed drug release at 2 hours, thereafter showing controlled release until approximately 10 hours when the second pulse release occurred. Drug release plateaued before the third pulse release occurred at approximately 18 hours. Formulation 3 displayed a reduction in lag phase, with drug being released from the first hour; there was also an erratic and undesired drug release pattern over the 24 hour period this could be attributed to the low polymer and crosslinker concentration. Formulations 10 to 15 show the most efficient drug release profiles with distinct triphasic pulsatile release of drug as seen in Figure 6.14c.

6.6.7. Response surface analysis of the Central Composite design

With the purpose of determining the relationship between the response variables and predictor variables, a complete ANOVA analysis was performed of the measured formulation responses (Figure 6.15, Table 6.9), drug release (MDT). The aptness of the multiple regression models are assessed via residual analysis. Residual plot for MDT is depicted in Figure 6.15. Resilient linear relationships were observed for the response variable as indicated by the restrained grouping of the partial residuals. The scatter plot of the residual, in which the residuals were plotted against the model predictions, is empirically uniform and radiate around zero.

Asymmetrical scatter was observed thus indicating that the fundamental hypothesis of multiple regression analysis was breached; some deviations and widely spread points were shown, revealing a degree of non-constant variance (du Toit et al., 2013). The normal probability plot of the residuals fell on a straight line indicating the data to be normally distributed with no affirmation of unknown variables. Distinctive patterning was not observed in any of the variable plots, showing non-contravention of the assumptions of zero means and constant variance of the regression model apart from the occurrence of a few outlying points in these plots. Deviations could have resulted from experimental error. The histogram for MDT was mostly symmetrical thus supporting the probability plots of constant and uniform distribution. The scatter plot, which is the residual vs. observation order, depicts the performance of the model. Scatter plots stayed within constant scale indicating non-arbitrary error. A full ANOVA was conducted and shown in Table 6.9.

Table 6.9: ANOVA analysis for the measured responses.

Response Variables	***p-values***
	MDT
[Eudragit® RS100]	0.281
[Calcium Chloride]	0.152

The complete regression equation generated for MDT is indicated below;

$$MDT = 3.719 + 2.790\left[Eudragit^{®}\right] - 38.315\,[Calcium\ Chloride]$$

Equation 6.6

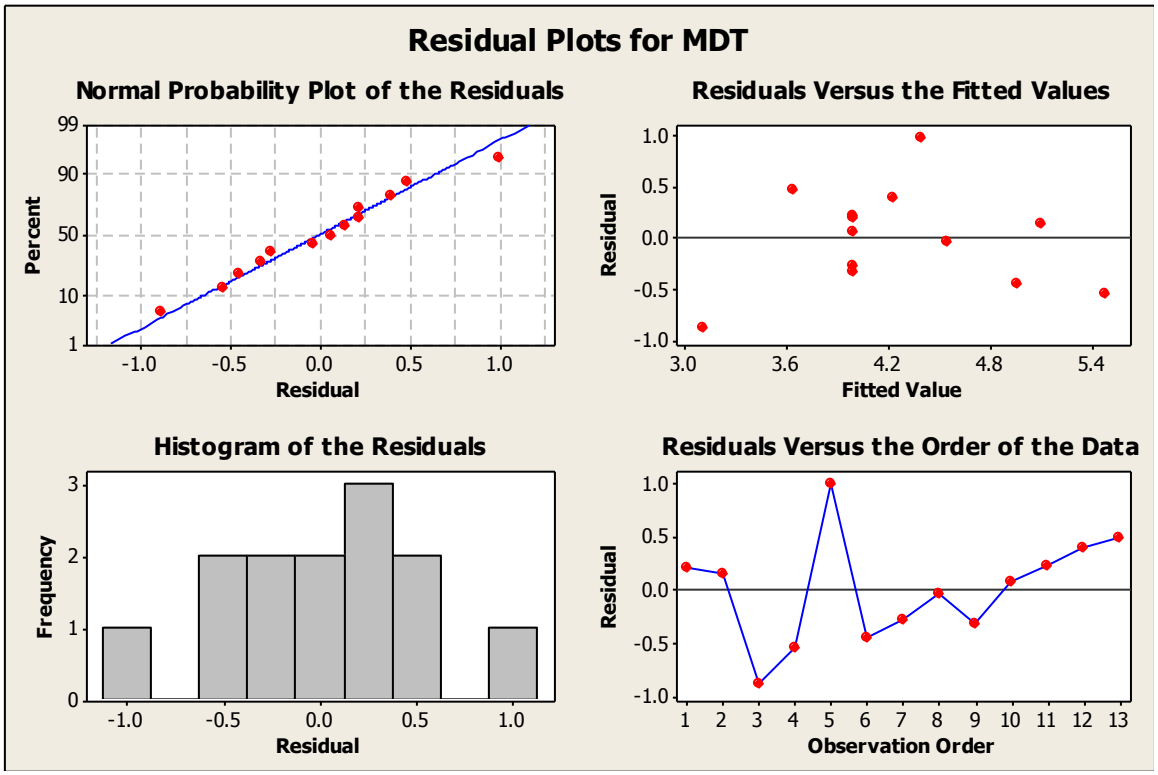


Figure 6.15: Residual plot for the response MDT.

MDT of the drug loaded layer is a vital factor affecting the drug release kinetics of the bioadhesive multilayered intestinal patch. A data plot as shown in Figure 6.16 was employed to depict the decisive relationship between the experimental variables and the achieved response. The effects of Eudragit® RS100 and $CaCl_2$ on the MDT were illustrated with the help of surface and contour plots. From the results it was shown that with an increase in concentration of the respective variables there was a corresponding increase in MDT. It was found that formulations with a ratio of Eudragit® RS100: calcium chloride of (0.5-1) :(0.05-0.1) resulted in the desired MDT.

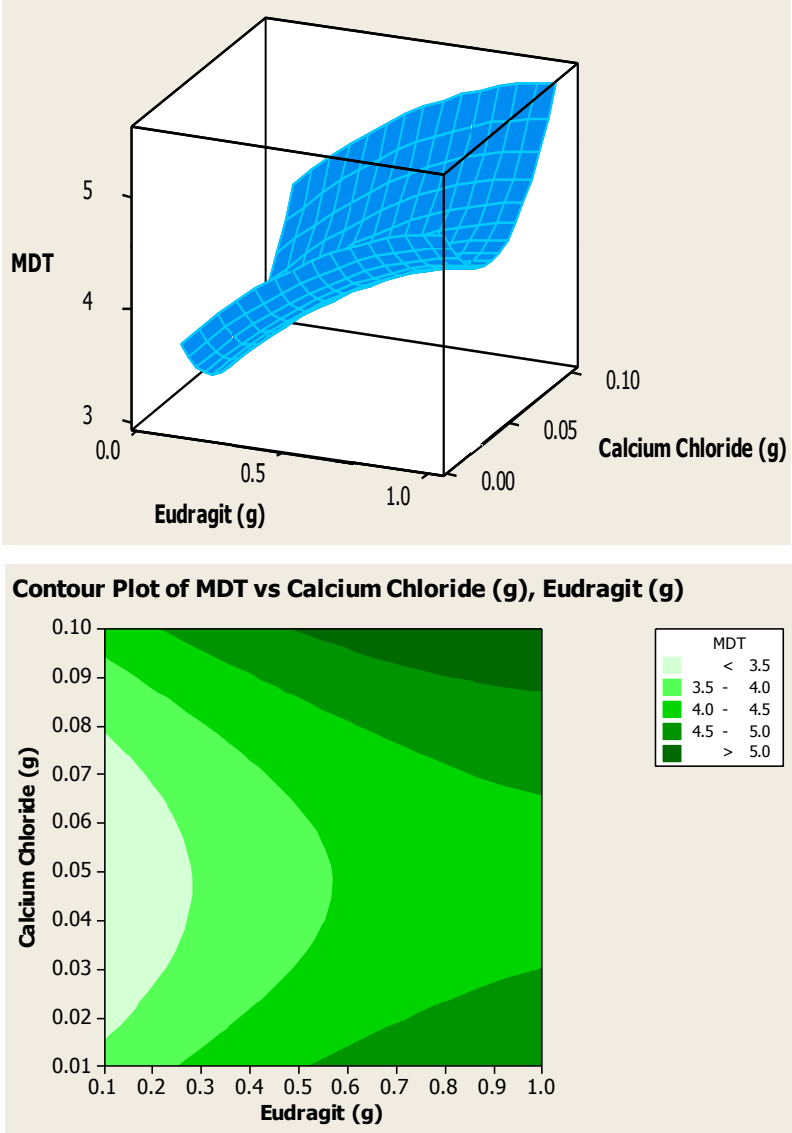


Figure 6.16: Response surface and contour plots depicting the effects of Eudragit® RS100 and $CaCl_2$ on the MDT.

6.6.8. Response optimization of the mucoadhesive and drug loaded layer of the bioadhesive multilayered intestinal patch

Response optimization procedure (MINITAB®, V15, Minitab, USA) was employed to attain the desired levels of the chosen formulation components. An optimal formulation was fabricated subsequent to concurrent constrained optimization of mucoadhesion, Young's Modulus (mucoadhesive layer) and MDT (drug loaded layer) characteristics. Maximization of mucoadhesion, minimization of Young's Modulus (mucoadhesive layer) and maximization of MDT (drug loaded layer) to the appropriate levels for each patch so as to achieve pulsatile release were employed for response optimization. The optimized levels of the independent variables and their respective predicted responses were determined. The optimal levels of the independent variables as well as the constraint setting used which would accomplish the preferred mucoadhesion, Young's Modulus and MDT characteristics are listed in Table 6.10. The optimized levels of the independent variables, the aim for the responses, the predicted responses (y), at the present factor settings, and the individual and composite desirability scores are shown in Figure 6.17

Table 6.10: Formulation constraints employed for response optimization.

Responses	Parameters
% Mucoadhesion	Maximize
Young's Modulus	Minimize
Drug Release (Total MDT)	Maximize (according to pulses required)

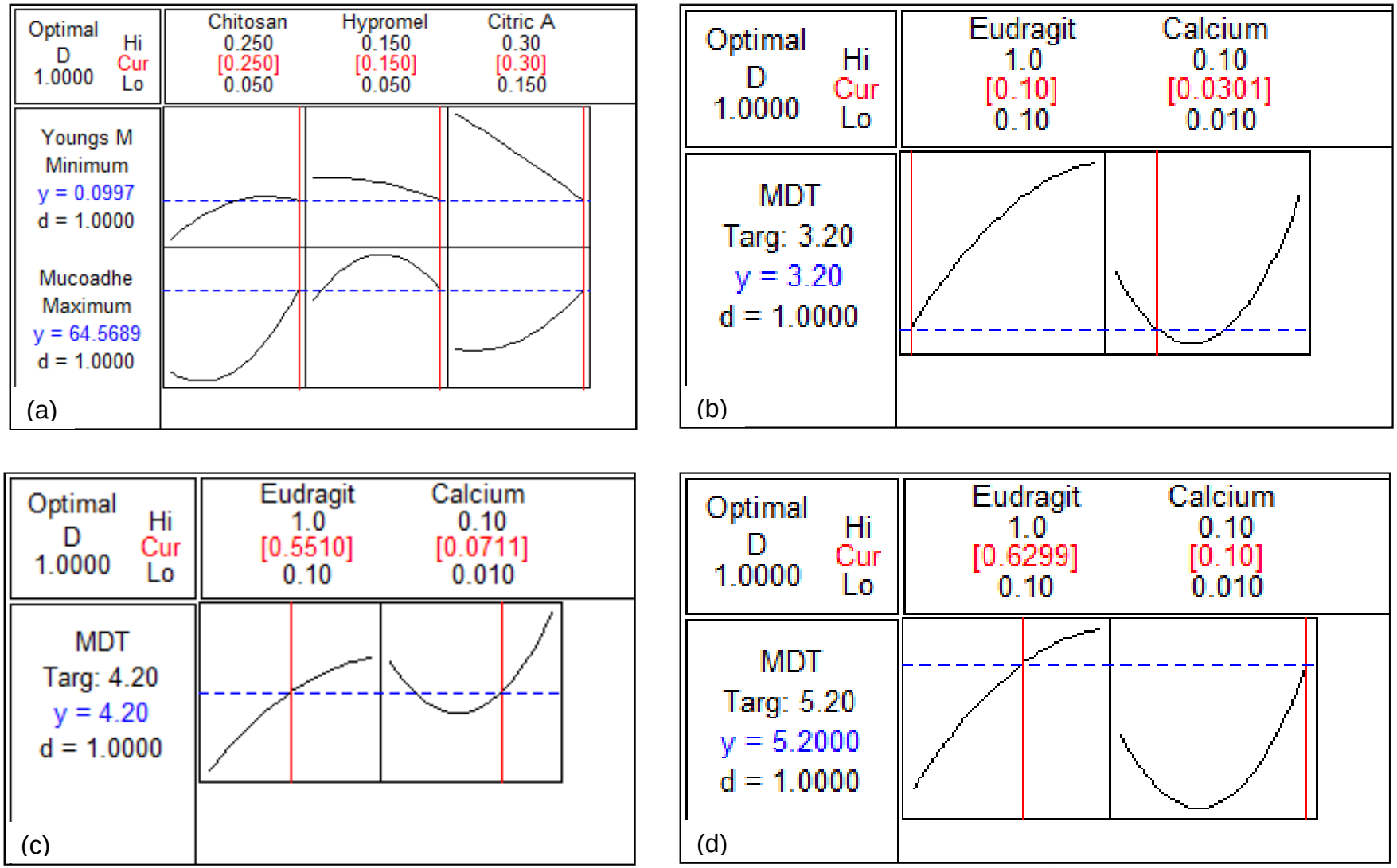


Figure 6.17: Desirability plots representing the levels of chitosan, hypromellose, citric acid, Eudragit® RS100 and calcium chloride required to synthesize the respective optimized bioadhesive multilayered patch layers, a) bioadhesive layer and drug loaded layers b) 2h, c) 10h and d) 18h.

6.7. Concluding Remarks

The mucoadhesive and drug loaded layers of the bioadhesive multilayered intestinal patch component of the ODLS were successfully developed via statistical analysis and characterized. The Face- centered Central Composite Experimental Design generated 20 and 13 formulations for the mucoadhesive and drug loaded layer, respectively; of which the effects of independent variables on the dependent response variables was analyzed. The experimental and fitted values achieved good correlation, demonstrating a good fit of the design model. Analysis of Variance (ANOVA), correlation analysis and regression analysis was used to analyze the dataset, proving the statistical acceptability of the models proposed. Both mucoadhesive and drug loaded layer design formulations provided necessary mucoadhesive and drug release characteristics. Furthermore, this chapter demonstrated the manner in which the mucoadhesive and drug loaded layer formulations would behave on exposure to simulated intestinal conditions, providing vital information requisite to predict the formulation's *in vivo* performance. Tensile analysis showed that design formulations of both layers possess satisfactory elasticity and flexibility required for oral administration targeted to the intestine for pulsatile release which in turn required prolonged residence time. The variations observed from gravimetric swelling studies are related to the physical alterations i.e. swelling and erosion of the system occurring upon exposure to simulated intestinal conditions.

CHAPTER 7

FABRICATION AND CHARACTERIZATION OF THE STATISTICALLY OPTIMIZED MULTI-LAYERED BIOADHESIVE INTESTINAL PATCH FOR PULSATILE BIOACTIVE RELEASE

7.1. Introduction

The importance of developing controlled-release drug delivery systems has been outlined previously, this allows for the maintenance of desired blood plasma levels of the selected drug for prolonged time periods without reaching toxic levels or falling below the minimum effective concentration (Gavrovic-Jankulovic and Prodanovic, 2011). Mucoadhesive drug delivery systems are drug carriers that employ bioadhesive properties of particular polymers that become adhesive upon hydration and may thus be utilized for targeted drug delivery to a specific region of the body for prolonged periods of time, as is the case in sustained and pulsatile drug release, mucoadhesive patches and microparticles have been commonly used for this purpose (Gavrovic-Jankulovic and Prodanovic, 2011). The use of mucoadhesive polymers within pharmaceutical formulations may alter the permeability of mucosal tissue and thus aid the adsorption of drug molecules. In addition the interaction between mucoadhesive systems and mucosal surfaces allows for prolonged residence time of the dosage forms at the target site, thereby decreasing the dosing frequency and improving patient compliance (Yu, et al., 2014), which is a great concern among the schizophrenic community as the reduction in normal functioning reduces the ability of schizophrenic patients to adhere to therapeutic regimens.

Mucoadhesion is defined as two materials, with at least one being of biological origin, held together for a prolonged period of time via interfacial forces (Yadav, et al., 2010). Polymeric properties required for mucoadhesive interactions at specific sites include hydrophobicity, negative charge and the presence of hydrogen bonding groups. Furthermore, polymers should possess adequate flexibility to penetrate mucus networks and be biocompatible, non-toxic and affordable. Mucoadhesive polymers are categorized as; polymers that are bioadhesive due to their stickiness upon hydration; polymers that adhere via non-specific, non-covalent, primary electrostatic interactions and polymers that bind to specific receptors on the cell surface. To improve bioadhesive characteristics of drug delivery systems it is requisite to divulge structural features of epithelial surfaces for which the delivery system is targeted. Mucus is a composite viscous secretion synthesized by specialized goblet cells in columnar epithelium that lines organs such as

the GIT. The mucus blanket lining these organs are highly hydrated (95% water content), with the principle component; glycoprotein mucin being responsible for it viscosity (Gavrovic-Jankulovic and Prodanovic, 2011). Mucins are large (0.5-20 MDa) membrane bound, extracellular glycoproteins. They are glycosylated and compose of 80% carbohydrates, primary N-acetyl-D-galactosamine, N-acetyl-D-glucosamine, fructose, galactose and sialic acid. The oligosaccharide chains, comprising of 5-15 monomers, display moderate branching and are attached to the protein core by O-glycoside bonds via hydroxyl side chains of serine and threonine (Perez-Vilar and Hill, 1999; Gavrovic-Jankulovic and Prodanovic, 2011). Bioadhesion is also known to improve bioavailability of drugs via various functions such as i) higher bioactive concentration at the site of adhesion and absorption, ii) a decrease in the diffusion path from the drug delivery system to absorbing biological membrane, iii) prolonged GIT residence time, thus enhancing absorption and iv) absorption from the drug delivery system without preceding degradation or dilution of drug in luminal fluids.

The phenomena of bioadhesion occur via a multifaceted mechanism. Six mucoadhesion theories have been proposed which can detail the mechanism of bioadhesion. Theories include: i) the wetting theory which describes bonding between the formulation and the mucosal surface tissue as intermolecular interaction and interfacial tension (Figure 7.1). This theory applies to liquid or low viscosity mucoadhesive systems and is primarily a measure if ‘spreadability’ of the system across the biological substrate tissue. Adhesive forces between a liquid and solid allow a liquid droplet to spread across the surface, while cohesive forces within the liquid lead to the droplet to ball up and avoid contact the surface. Contact angles less than 90˚ show that the wetting of the surface is favorable and the liquid can spread across a large surface area. Contact angles greater than 90˚ indicates the wetting of the surface is unfavorable; interactions between liquid molecules preserves the droplet shape and thereby minimizes contact with the substrate surface. (Dodou, et al., 2005; Khutoryanskiy, 2011; Mythri, et al., 2011*;* Yu, et al., 2014). Contact angles may be experimentally calculated.

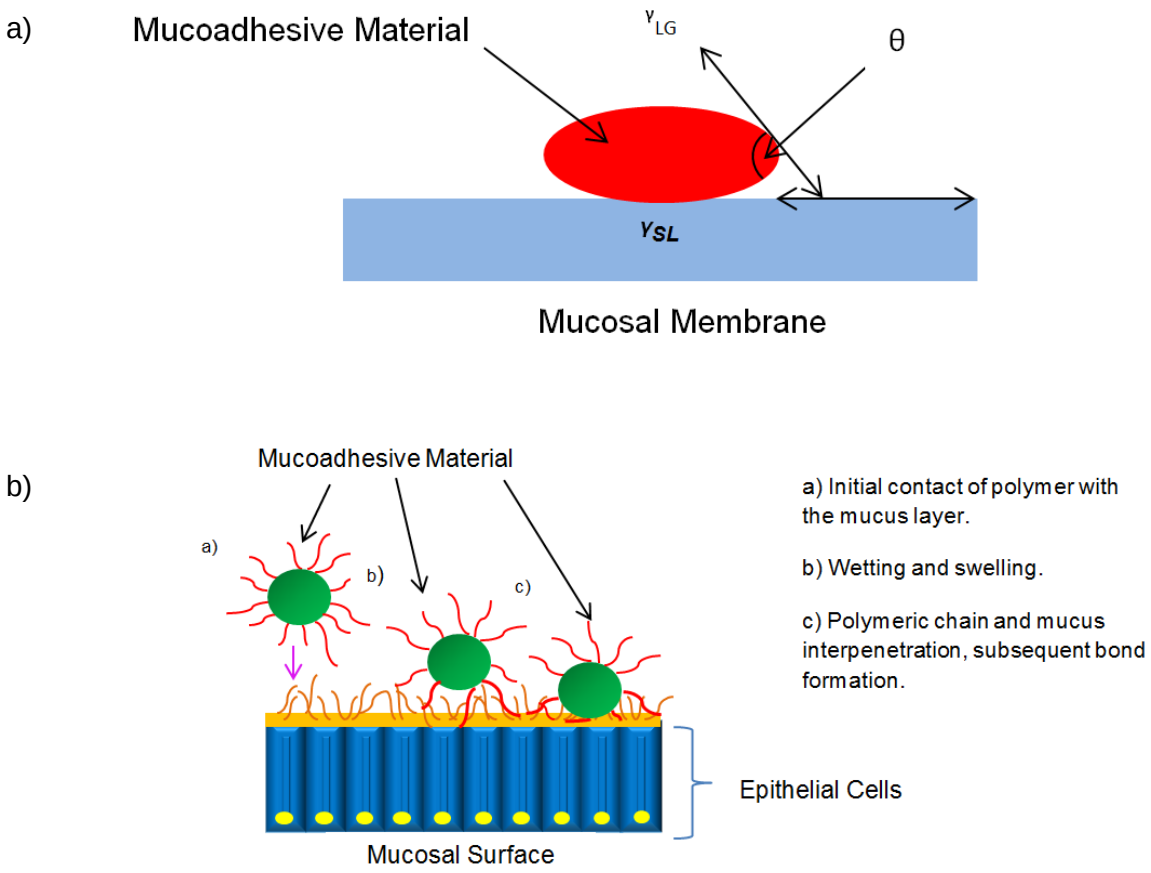


Figure 7.1: Illustration of a) the wetting theory and b) the diffusion theory of mucoadhesion.

Where γ_{SG} is the interfacial tension between solid and gas; γ_{SL} is interfacial tension between solid and liquid; γ_{LG} is the interfacial tension; and θ is the contact angle between solid and liquid interface; (Yu, et al., 2014); ii) Electronic theory where mucoadhesion occurs due to transfer of electrons between mucus and the mucoadhesive system, leading to the formation of double-layered electronic charge at the interface (Khutoryanskiy, 2011; Mythri, et al., 2011; Yu, et al., 2014); iii) the adsorption theory offers that intermolecular forces such as hydrogen bonding, Van der Waals forces and covalent bonds, provide the adhesive attraction between mucus and mucoadhesive polymers (Khutoryanskiy, 2011; Yu, et al., T., 2014); iv) the diffusion theory is the most commonly used to describe mucoadhesion and describes the interpenetrative entanglement between polymer and mucus chains (Figure 7.1b). The initial step involves the contact between bioadhesive polymer chains and mucus chains. In this initial step, weak physical forces (attractive and electronic forces) control the mobility of polymer chains. The subsequent step involves the interpenetration of polymer chains from the delivery system into the mucus lining to allow for

mucoadhesion via extensive bond formation (Khutoryanskiy, 2011; Mythri, et al., 2011*;* Yu, et al., 2014). The process of the diffusion theory is shown in Figure 7.2b; v) the mechanical theory considers only the adhesion between liquid and a rough or porous surface.

The theory proposes that adhesion between the substrates is due to mechanical meshing/ interlocking of the adhesive into irregularities on the substrate surface (Dodou, et al., 2005; Khutoryanskiy, 2011; Mythri, et al., 2011*;* Yu, et al. 2014); and the fracture theory in which adhesive strength (fracture strength) is interrelated to the force necessary to separate the platform and mucosal surface. Fracture theory is considered the most widely accepted theory of mucoadhesion. The equation of Young's modulus of elasticity is used to determine the fracture strength (Dodou, et al., 2005; Khutoryanskiy, 2011; Mythri, et al., 2011*;* Yu, et al., 2014). The mucoadhesive ability and adhesive strength can be influenced by the polar functional groups. The most commonly employed polymers are composed of polar functional groups such as hydroxyl (-OH), amide ($-NH_2$), and carboxyl (-COOH) that are capable of interaction with mucin glycoprotein's. Interactions of polymers with mucin involve physical entanglement and secondary interactions such as hydrogen bonds, these aids in the formation of strong crosslinked networks and thus mucoadhesion.

Lectins are a highly heterogeneous group of proteins and glycoprotein's of non-immune origin that bind to carbohydrates specifically and non-covalently. Lectins are involved in cell to cell recognition and communication, adhesion and attack of infectious agents and clearance of glycoproteins from general circulation. The use of lectin facilitated drug delivery system targeting is based on the knowledge that cell surface proteins and lipids within the plasma membrane are glycosylated and these glycans act as ligands for lectins. Plant derived lectins are key candidates in targeting drug to the GIT epithelium due to their capability to bind with specificity to epithelial cells (Gabor, et al., 2004). In addition, the viscous mucosal lining of the epithelium may prevent absorption. Hence the need for bioadhesive delivery systems becomes apparent.

7.2. Materials and Methods

7.2.1. Materials

The materials employed were as described in *Chapter 6, Section 6.2.1* for the optimized mucoadhesive and drug loaded layers. For preparation of the mucus cleaving layer; Gellan Gum (Gelzan™ CM), N-acetylcysteine (≥99%) and chitosan (deacylated chitin) medium molecular weight were procured from Sigma-Aldrich® (St. Louis, USA). Ethylcellulose (EC, 10 cP) was used to prepare the backing layer; procured from Sigma-Aldrich® (St. Louis, USA). All other reagents were of analytical grade and are used as received.

Ethical Clearance

This study had received the approval of the Animal Ethics Screening Committee of the University of the Witwatersrand with ethics clearance number 2013/23/04 (Appendix 11.3). The ethics clearance was granted for both the ex vivo and in vivo studies.

7.2.2. Preparation of the respective layers of the optimized bioadhesive intestinal patches

The preparation methods utilized were as described in *Chapter 6, Section 6.2.3* for the optimized mucoadhesive and drug loaded layers. The drug loaded layer for the three patches were optimized in accordance with timed release, hence the optimized formulation compositions varied between the 2, 10 and 18 hour patches; optimized mucoadhesive and drug loaded layers compositions are outlined in Table 7.1. The backing layer was prepared by the solvent casting technique from a plasticizer-containing ethylcellulose solution. Elasticized polymer solution (11%$^{w}/_{v}$) was prepared by dissolving the required amount of ethylcellulose in a 5mL mixture of methylene chloride and methanol (4:1) and subsequently adding glycerin as a plasticizer. The mucus cleaving layer was prepared from a polymer blend of gellan gum: chitosan incorporated with N-acetyl-cysteine. A 1%$^{w}/_{v}$ gellan gum solution was prepared to which an equal concentration of chitosan was added, the polymer blend was allowed to homogenize after which N-acetyl-cysteine was incorporated (200mg).

Table 7.1: Outline of optimized patch layer compositions.

Multilayered Intestinal Patch Layer	***Polymeric Composition***
Mucus Cleaving Layer	- Gellan Gum 1% $^{w}/_{v}$ - Chitosan 1% $^{w}/_{v}$ - N-acetyl-cysteine
Mucoadhesive Layer	- Chitosan 0.25 - Hypromellose 0.15 - Citric Acid 0.30
Time controlled Drug Loaded Layers	**2 hour** - Eudragit® RS100 0.10 - Calcium Chloride 0.0301 - Alginate 1% $^{w}/_{v}$ **10 hour** - Eudragit® RS100 0.5510 - Calcium Chloride 0.0711 - Alginate 1% $^{w}/_{v}$ **18 hour** - Eudragit® RS100 0.6299 - Calcium Chloride 0.10 - Alginate 1% $^{w}/_{v}$
Backing Layer	- Ethylcellulose 11% $^{w}/_{v}$

7.2.3. Physiomechanical and Physiochemical Characterization of the layers of the Optimized Multilayered Bioadhesive Intestinal Patches

7.2.3.1. Evaluation of membrane uniformity

The uniformity of the respective patch layers was determined by accurately weighing a number of samples (n=10) on a calibrated Mettler Toledo Balance (Model AB104-S, Mettler Toledo, Switzerland). The average weight was calculated followed by determination of the standard deviation. In addition, the thickness of the polymeric films was determined utilizing an Electronic Vernier Digital Fractional 150mm caliper (n=10). Various regions within a single film were also measured for thickness so as to determine the consistency of individual films; the average thickness was determined and the standard deviation calculated. All samples were for this purpose cut into 10x20mm dimensions. The polymeric films were visually evaluated for color, presence of air bubbles and transparency.

7.2.3.2. Determination of the tensile properties and Young's Modulus of the respective layers of the optimized bioadhesive multilayered intestinal patch

Young's Modulus and other tensile properties of the layer of the optimized intestinal patch layers (n=3) were determined using the NanoTensile® 5000 (Hysitron Inc. Nanomechanical Test Instrument, Minneapolis, MN, USA). The NanoTensile® (NT) apparatus was calibrated prior to testing to ensure accuracy. Samples were cut into 2x15mm strips and then mounted onto NT mounting brackets, as demonstrated in Figure 7.2. The mounting brackets were held together with a cardboard frame to allow for sample placement, samples were attached to the brackets using cyanoacrylate based adhesive, thereby holding the samples in place during the experiment. Samples were allowed to cure; subsequently they were accurately measured for their width, thickness and length utilizing a digital caliper. The upper sample bracket was attached to the upper sample holder of the NT head, the cardboard frame was cut at the yellow points illustrated in Figure 7.2 to prevent interference during testing, and thereafter the mass was measured. The NT head was then lowered and the lower sample bracket attached to the lower sample holder on the NT platform. The mounting brackets were pulled apart at a constant rate of displacement of 100µm/sec and the tensile properties of the sample were measured.

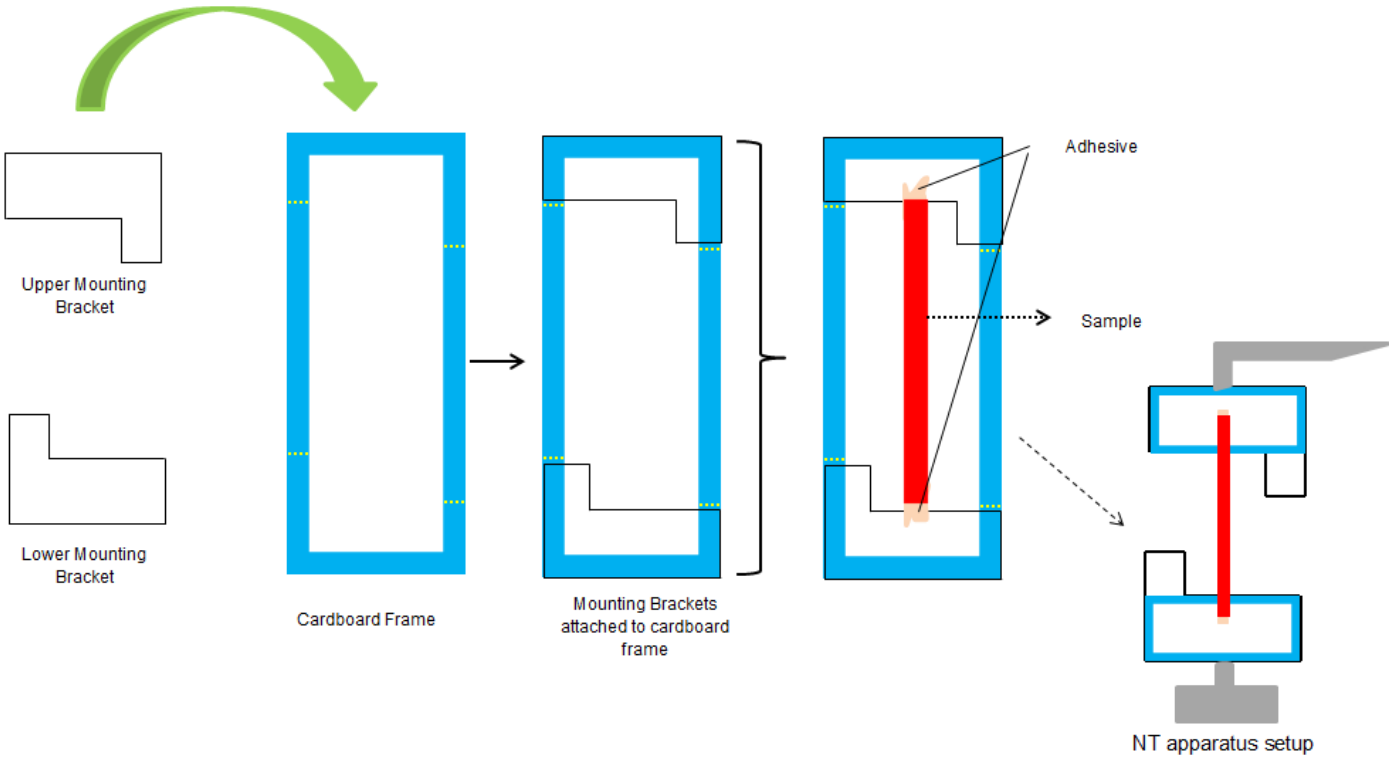


Figure 7.2: Illustration of NanoTensile® sample preparation and set-up.

For comparative analysis the Young's Modulus of the optimized intestinal patch layers were determined using the Texture Analyser TA.XT*plus* (Stable Microsystems, England). Samples were cut into strips of approximately 12x5mm and were then mounted onto the tensile apparatus of the texture analyzer. The upper and lower ends of the polymeric film strip were secured into the upper and lower sample grips respectively. Samples were accurately measured in respect to their width, thickness and length using a digital caliper. Sample grips were moved apart at a constant speed and distance according to the test parameters. Test parameters were as follows: pre-test speed 0.5mm/sec, test speed 0.5mm/sec, post-test speed 5mm/sec, trigger force 0.05N and distance 20mm.

7.2.3.3. Analysis of surface morphology of the optimized mucoadhesive and drug loaded layers

Surface morphology of the optimized mucoadhesive and drug loaded layers were analyzed on a Phenom™ Scanning Electron Microscope (SEM) (FEI Company, Hillsboro, Oregon, USA). To qualitatively interpret the surface morphology of the respective layers in relation to surface area. Samples were firmly mounted onto aluminum stubs with carbon tape. They were then subjected to gold sputter coating under the influence of a vacuum of 0.1Torr with argon gas in a SPI-Module™ Sputter Coater and SPI-Module™ Control (SPI Supplies, Division of Structure Probe Inc., West Chester, PA, USA). Individual samples underwent 90 seconds of coating to allow for

sufficient coverage of the sample. Microscopic imaging was then conducted on the Phenom™ SEM.

7.2.3.4. Evaluation of the polymeric structural and vibrational frequency vibrations of the optimized mucoadhesive and drug loaded layers

The vibrational molecular transitions of the optimized mucoadhesive and drug loaded layers upon conjugation and crosslinking reactions was characterized to attain vital micro-structural information via the use of an Attenuated Total Reflectance Fourier-Transform Infrared (ATR-FTIR) spectroscopy, recorded on a PerkinElmer® Spectrum 100 series fitted with a universal ATR polarization accessory (PerkinElmer® Ltd., Beaconsfield,UK). Samples were placed directly on the ATR crystal and FTIR spectra were recorded in the range of 4000-650cm^{-1}.

7.2.3.5. Evaluation of the degree of swelling and its effect on mucoadhesive characteristics of the optimized patch layers upon intestinal environment exposure

The differences in the swelling of the optimized formulation layers with the exception of the backing layer (due to minimal swelling of the impermeable layer) were evaluated by exposing the respective layers to simulated intestinal conditions as described in *Chapter 6, Section 6.3.4* (n=3). The degree of swelling and its effect on mucoadhesive characteristics were determined at 0, 2, 4, 6, 8, 10, and 12 hours; fresh samples were assessed at each time point. The degree of swelling promotes polymer chain entanglement with the mucin on the intestinal epithelium, thus swelling affects the mucoadhesive characteristics of a drug delivery system; as a system undergoes erosion preceding swelling additional surface area is exposed for mucoadhesion to occur. Hence, gravimetric swelling analysis was conducted, where the respective optimized patch layers were subjected to the exact experimental conditions outlined in *Chapter 6, Section 6.3.4*. Each patch layer was removed from the dissolution apparatus at predetermined time points (0, 2, 4, 6, 8, 10 and 12 hours). Excess dissolution medium (phosphate buffered saline (PBS) pH 6.8) was removed by placing the polymeric films on laboratory blotting paper for 1 minute prior to gravimetric analysis. The degree of swelling at each time point, stated as a percentage of PBS uptake was calculated based on the increase or decrease in weight of the formulation, Equation 7.1 was employed for this purpose;

$$Swelling\ \%_{(PBSuptake)} = \left(\frac{Wt - W0}{W0}\right) \times 100$$

Equation 7.1

Where swelling % is the percentage of PBS uptake by the respective polymeric patch layer at the specified time point, Wt. is the weight of the layer at the specified time point, and W0 is the initial weight prior to gravimetric analysis.

7.2.3.6. Characterization of thermal transitions employing Differential Scanning Calorimetry

With the intention of ascertaining chemical reaction and phase temperatures, as well as melting points (T_m) and glass transitions (T_g) of the optimized intestinal patch layers, the optimized mucoadhesive and drug loaded layers underwent thermal analysis employing a Temperature Modulated or Advanced DSC (TMDSC/ADSC) (Mettler Toledo DSC-1 STARe System, Schwerzenback, ZH, Switzerland) to assess the thermal characteristics of the statistically optimized system layers.

Thermal transitions were analyzed in accordance with the measured T_g temperature in reaction to differences in crystallization (T_c) and melting temperatures (T_m). The instrument was calibrated in terms of temperature and enthalpy using indium. Thermal transitions of native polymers employed in the formulation of the respective optimized layers; namely hypromellose, chitosan, citric acid, Eudragit® RS100, calcium chloride and sodium alginate were compared to their related optimized formulation layers. Samples (±10mg) were accurately weighed into standardized 40µL aluminum sample pans which were then perforated and hermetically sealed. Samples were then heated from 25-100˚C and held at 100˚C for 2 minutes so as to evaporate excess moisture present in the sample. The sample pans were then heated at 10˚C/minute between a temperature range of 25-300˚C under constant purge of an inert nitrogen (N_2) atmosphere (100mL/minute) do minimize oxidation.

7.2.3.7. *Ex vivo* determination of mucoadhesive properties via textural analysis

So as to evaluate the mucoadhesive properties of the optimized intestinal patch layers, the Work of Adhesion (WA) and the Maximum Detachment Force (MDF) needed to detach a hydrated polymeric film layer from an appropriately sized fragment of pig intestinal epithelial tissue was determined, employing a Texture Analyzer TA.XT*plus* (Stable Microsystems, England), utilizing the parameters as follows: pre-test speed of 0.5mm/sec, test speed of 0.5mm/sec, post-test speed of 10mm/sec, applied force of 5N, contact time of 10 seconds and trigger force of 0.05N (n=3). A portion of the pig intestinal epithelial was secured to a cylindrical flat tip TA probe, while a hydrated piece of the respective optimized polymeric layer was secured to the TA sample platform. Polymeric film layers were pre-impregnated with PBS; pH 6.8 prior to mucoadhesive testing for simulation of intestinal conditions. The probe was lowered to make contact with the mounted

polymeric patch layer inducing a test force, and consequently raised, while simultaneously measuring the MDF. Required data was captured textural profiles of Force: Distance curves.

The WA (mJ) was derived from the Area Under the Curve of the force: distance curve (AUC_{FD}) and the MDF (N) needed to detach the intestinal tissue from the polymeric patch layer was determined by measuring the maximum peak force from the force: distance curve. The Work of Adhesion per unit area (WA αβδ), was described by the work used on the matrices when the two contact phases i.e. the tissue (α) and the polymeric layer (β), formed an interface of unit area were then separated to form unit areas of each of the αδ and βδ interfaces. This is mathematically characterized by Equation 7.2.

$$WA\alpha\beta\delta = \gamma\alpha\delta + \gamma\beta\delta - \gamma\alpha\beta$$

Equation 7.2

Where, γαβ, γαδ and γβδ are surface tensions between the phases comprising the intestinal tissue and polymeric film layers, α, β; α, δ and β, δ respectively.

The *ex vivo* tensile mucoadhesive test outlined is adept to emulate *in vivo* processes to a certain degree. This method of testing provides information on the mucoadhesiveness of a delivery system and allows for characterization of mucoadhesive properties based on their respective performance. It is indicated that detachment of the dosage form from the biological tissue or substrate is a complex physical process, dependent on deformation and mechanical characteristics of the individual phases (Khutoryanskiy, 2011).

7.2.3.8. *In vitro* perfusion studies

In vitro perfusion tests were conducted to discern the dissolution process of the tablet encased mini gastrointestinal films as well adhesion of the films after dissolution of the encasing tablet (n=3). During the experiment, an excised portion of the porcine intestine was placed horizontally in a Franz Diffusion Cell and the lumen was connected to tubing so that it could be perfused with phosphate buffered saline (pH 6.8). A longitudinal incision was made along the intestinal surface for observation. A tablet encapsulating 3 mini intestinal films was placed in the intestine and periodically observed so as to note the release, attachment and residence time of the optimized intestinal patches (Whitehead, et al., 2004).

7.2.3.9. *Ex vivo* drug permeation studies

Ex vivo permeation studies were conducted to ascertain the effectiveness of the optimized intestinal patch as well as permeability of porcine intestinal mucosal tissue to sodium valproate. Studies were performed utilizing a Franz Diffusion Cell apparatus (PermeGear Inc., Bethlehem, PA, USA) equipped with a 12mL receptor compartment, clamp, stirrer bar and thermostat maintained water jacket (Figure 7.3). Porcine intestinal tissue which was excised following euthanasia of the animal subsequent to ethics approval was employed; the adhering fat and visceral debris was removed and the excised intestinal tissue washed with saline.

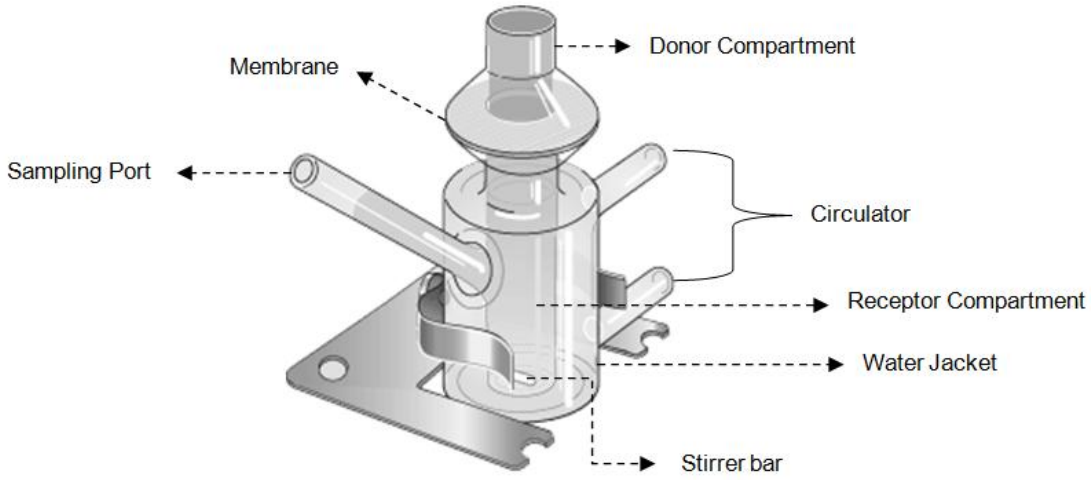


Figure 7.3: Pictorial illustration of the Franz diffusion cell set up.

Excised porcine samples with a thickness of 1mm were clamped to the membrane platform of the Franz diffusion cell with the outside wall of the tissue facing the donor chamber, the receptor chamber equipped with a magnetic stirrer and sampling port was filled with simulated plasma (PBS; 12mL; pH 7.4; 37°C). A known concentration of sodium valproate (2.5mg/mL) was placed in the donor compartment and permeation was determined via analysis of sodium valproate concentration in the receptor compartment by withdrawal of samples (100μL) over a period of 8 hours (Dureja, et al., 2001; Patel, et al., 2010). All samples were analyzed using UV Spectroscopy (IMPLEN Nanophotometric™ Implen GmbH, München Germany) and the concentration of sodium valproate determined via utilizing the calibration curve constructed in *Chapter 6, Section 6.5.6* (n=3). The flux ($mg.cm^{-2}.hr^{-1}$) of sodium valproate across the intestinal mucosa was calculated per

unit area at steady state concentration by linear regression analysis of permeation data employing Equation 7.3:

$$J_{d=\frac{Cr}{A\times t}}$$

Equation 7.3

Where, *Jd* is the flux; *Cr* is the quantity of sodium valproate that diffused through the intestinal mucosa into the receptor compartment (mg); *A* is the cross-sectional area accessible for drug permeation (1.466 cm^2) and *t* is the time of drug contact with the intestinal mucosa (hours).

The permeability coefficient (*P*), subsequent to use of Fick's law, can be calculated with the use of Equation 7.4:

$$P = \frac{Jd}{Cdonor}$$

Equation 7.4

Where *P* is the permeability coefficient; *Jd* is the flux and *Cdonor* is the drug concentration in the donor compartment.

7.2.3.9.1. *Integrity evaluation of the intestinal mucosal tissue*

Substantiation of tissue integrity is a crucial element for *ex vivo* analysis, as compromised tissue integrity for the duration of any preliminary tissue handling may misrepresent permeation results (Roberts, 1991). Tissue integrity was evaluated via ionic conductivity using a SevenMulti S40 pH/electrical conductivity meter (Mettler-Toledo, Zurich, Switzerland) prior to and subsequent to experimental procedures. The resistance Reduction Factor (RF) was calculated. RF is defined as the ratio of the initial resistance value at time 0 to the resistance value of the sample obtained at time t (Lavon, et al., 2005). The; as depicted by Equation 7.5:

$$RF = \frac{R_0}{R_t}$$

Equation 7.5

Where R_0/R_t is the ratio of the initial mucosal resistance to the mucosal resistance at time t.

7.2.3.10. In vitro drug release analysis

The *in vitro* drug release studies on the optimized bioadhesive intestinal patches were carried out in a USP type II apparatus (Caleva, model 7ST) at 50rpm as described in *Chapter 6, Section 6.5.7* (n=3). Drug release samples were removed at predetermined time intervals over 24 hours with sink conditions being maintained with replacement of fresh dissolution medium. Samples were analyzed via UV spectroscopy as detailed in *Chapter 6, Sections 6.2.7.*

7.3. Results and Discussion

7.3.1. Physical characterization of optimized patch layers: Analysis of membrane uniformity

Membrane uniformity evaluation of the optimized patch layers provided insight into the inter and intra formulation variability. Uniformity and constancy of the respective intestinal patch layers were important features to assess, as these parameters influence the mucoadhesive properties. The mean weight and thickness as well as the corresponding standard deviations of the respective intestinal patch layers are provided in Table 7.2. The standard deviations for tested parameters were<10% for all intestinal patch layers, thus indicating that all patch layers were consistent and uniform with a limited variability index. Upon visual examination the mucoadhesive and mucus cleaving layers displayed a yellow tint, with the mucus cleaving layer presenting a darker yellow. The drug loaded and backing layers were clear and translucent; all patch layers showed minimal bubble formation.

Table 7.2: Optimized patch layers and their respective average weight and thickness.

Optimized Multilayered Intestinal Patch Layer	***Physical Parameters (Mean ± s.d, n=3)***
Mucus Cleaving Layer	• *Average weight: 10.19±0.6* • *Average thickness: 0.14±0.03*
Mucoadhesive layer	• *Average weight: 20.8±2.5* • *Average thickness: 0.18±0.04*
Drug Loaded Layer	• *Average weight: 16.53±5.5* • *Average thickness: 0.14±0.05*
Backing Layer	• *Average weight: 10.3±0.52* • *Average thickness: 0.15±0.02*

7.3.2. Assessment of the tensile properties and Young's Modulus of the optimized intestinal patch layers

The stress-strain correlation of a particular material is greatly reliant on the flexibility of the respective compositional polymer chains and corresponding strength of the material as a whole. When a minor extent of stress is necessary to create a great amount of strain, the material is understood to be flexible and the analogous Young's Modulus, highlighted in Figure 7.4a-d (which is the linear segment of the stress-strain curve) will be comparatively small (Leung and Ko, 2011).Tensile characterization was performed as the bioadhesive intestinal patches are to be placed within an oral dosage form, which requires good tensile properties so as to withstand oral delivery. The average experimental values of Young's Modulus (E), yield stress (σ_y) (magnitude of stress on stress-strain curve at which deformation occurs without significant increase in stress), ultimate strength (σ_u) (maximum stress endurable), ultimate strain (ε_u) and toughness (u_f) are outlined in Table 7.3.

Table 7.3: Experimental values obtained from NanoTensile® and Textural Analysis of optimized patch layers *(Mean ± s.d, n=3).*

Formulation	E(MPa)	E(MPa) NT	σ_y (MPa)	σ_u (MPa)	ε_u	U_f (J/cm^{-3})
Mucus Cleaving Layer	0.27±0.249412	0.17±0.06321	0.01±0.05694	0.10±0.1251	0.629±0.2132	0.02±1.2460
Optimized Mucoadhesive Layer	0.05±1.512697	0.11±0.02346	0.01±0.06141	0.02±0.1121	0.391±0.1371	0
Optimized Drug Loaded Layer	13.09±0.42113	0.07±0.162133	0.31±0.15128	0.50±0.0043	0.100±0.1154	0.04±1.1170
Backing Layer	0.26±0.349033	0.15±0.04211	0.07±0.04549	0.07±0.1261	0.350±0.1224	0.01±0.11

The Young's Modulus values were low indicating that the optimized patch layers demonstrated excellent elasticity and flexibility. The optimized Mucoadhesive layer containing CHT and HPM displayed higher elasticity (lower Young's Modulus values), as compared to the drug loaded layer containing Eudragit®RS 100 and alginate. Both the mucus cleaving and backing layers revealed good elasticity indicated by low Young's Modulus values. All polymeric film layers exhibited satisfactory degrees of strength and toughness to be able to endure/withstand placement within a tablet core and the process of oral drug delivery.

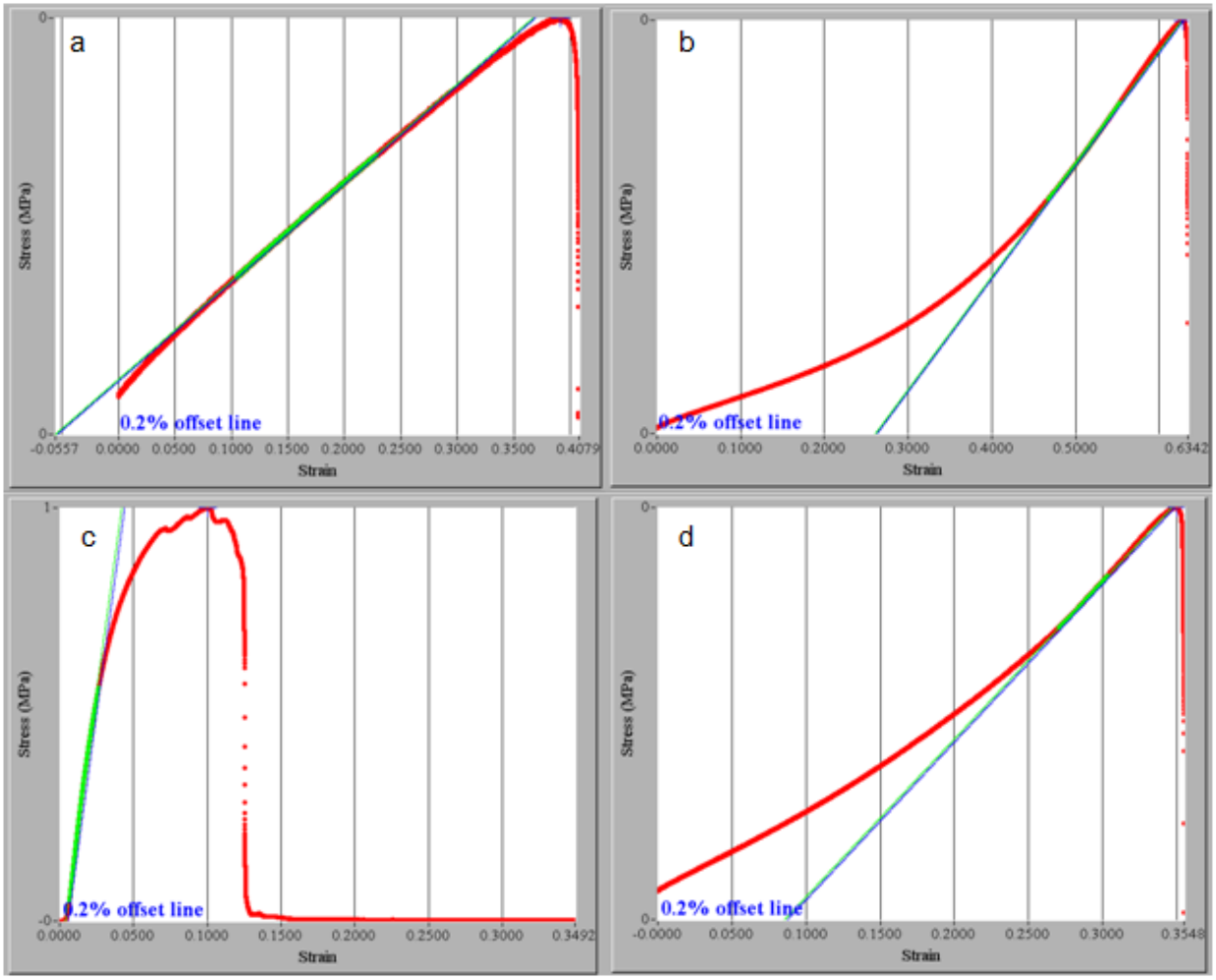


Figure 7.4: Typical stress-strain NanoTensile® profile of a) mucus cleaving layer b) optimized mucoadhesive layer c) optimized drug loaded layer and d) backing layer.

7.3.3. Evaluation of surface morphology of the optimized mucoadhesive and drug loaded layers

Scanning electron microscopy (SEM) studies were conducted to appraise the surface structural characteristics of the optimized patch layers (mucoadhesive and drug loaded layers). As previously discussed, micro-cracks and pores within a system promote mucoadhesion via the formation of an interlocking network thereby enhancing adhesion (Dodou, et al., 2005; Harsulkar, et al., 2011; Tangri and Madav, 2011).

The mechanical premise of mucoadhesion as outlined in *Chapter 7, Section 7.1* theorizes that surface irregularities and asymmetry promotes mucoadhesion via an increase in contact area. As

illustrated by the SEM images at a magnification of x4000 (Figure 7.5), both the mucoadhesive and drug loaded optimized formulations possess surface morphology idyllic for promotion of mucoadhesion. The optimized drug loaded layers (2,10 and 18 hours) formulations showed similar surface structures, the surface structure was noted to be smooth prior to exposure to simulated intestinal conditions (Figure 7.5a); however once exposed to intestinal conditions majority of the surface morphology remained smooth with the occurrence of small pores as illustrated with red circles in Figure 7.5c. The observed pores can be attributed to polymer erosion out of the film, with concurrent drug release. Conversely, the optimized mucoadhesive layer displayed micro-cracks or fissure-like surface structure as shown by yellow arrows in Figure 7.5d. Due to these fissures not being present prior to swelling studies and taking into consideration that it is the focal physical variation upon exposure to simulated intestinal conditions, it may concluded that the observed fissuring is as a result of slower swelling areas forming the ridges illustrated by the yellow arrows in Figure 7.5d as compared to the smooth surface morphology of the optimized mucoadhesive film before swelling in Figure 7.5b. In addition, it was observed that there were no significant deviations in surface structure or morphology that would result in exorbitant differences in the comprehensive polymeric film performance, both within an individual film layer or between differing films.

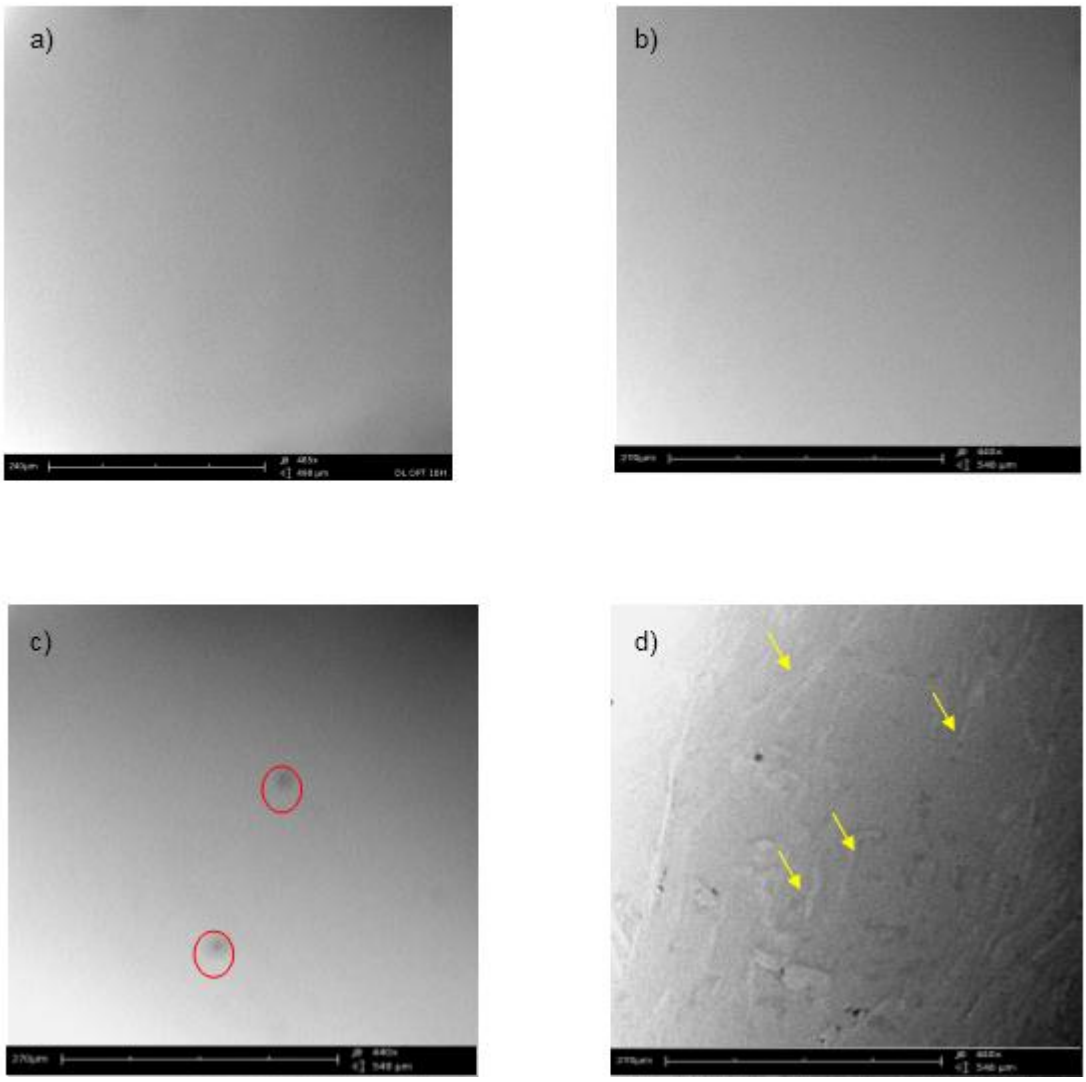


Figure 7.5: Scanning electron micrographs depicting the surface morphology of a) optimized drug loaded layer and b) the optimized mucoadhesive layer c) optimized drug loaded layer after swelling and d) optimized mucoadhesive layer after swelling.

7.3.4. Appraisal of the polymeric structural and vibrational frequency variations of the optimized mucoadhesive and drug loaded layers

Fourier Infrared Spectroscopy (FT-IR) studies were performed for the optimized mucoadhesive and drug loaded layers due to the crosslinking and amalgamation reactions involved in their formulation processes. FT-IR spectra of the native polymers employed in the respective polymeric film layers were analysed in relation to the spectrum of the optimized formulations; to determine whether any constituents within the formulation interacted as a result of the polymer blending, crosslinking and film-casting procedures.

CHT (Figure 7.6a) demonstrates a characteristic peak at 1697.08cm^{-1} corresponding to the amide group; the hydroxyl group at 3443.28cm^{-1} and the C-O stretching at 1053.30cm^{-1}. The FT-IR spectra of hypromellose (Figure 7.6b) depicts characteristic C=O aldehyde band at 1670cm^{-1} (1690-1760cm^{-1}), a strong transmittance band at 3497cm^{-1} relating to a normal O-H polymeric stretch; the transmittance band at 1138cm^{-1} is related to C-O phenol functional groups; N-H amine groups at 3354cm^{-1}. In the FT-IR spectra of citric acid (Figure 7.6c) carboxylic acid functional group at 2635.93cm^{-1} and C-H alkene functional group at 766.94cm^{-1}. The spectra of lectin (Figure 7.6d) displayed characteristic bands at 3253.65cm^{-1} descriptive of hydrogen bonded alcohols O-H, 1639.46cm^{-1} representative of C=C alkyl stretch, an absorption band at 1518.09cm^{-1} related to NO_2 nitro functional groups, and aryl/vinyl ethers at 1237.22cm^{-1}. Analysis of the optimized mucoadhesive formulation (Figure 7.6e) revealed that all characteristic peaks present in the spectra of the native polymers were unaltered thus providing evidence that no covalent interactions between the polymers occurred; eliminating any detrimental effects on the mucoadhesive properties of the system. However, additional peaks in the region of 2100-2260cm^{-1} was observed which represents C≡C terminal alkyne and 1590-1650cm^{-1}corresponding to C=C aromatic double bond was noted. The appearance of two additional peaks demonstrates the successful lectin amalgamation to the chitosan: hypromellose blend.

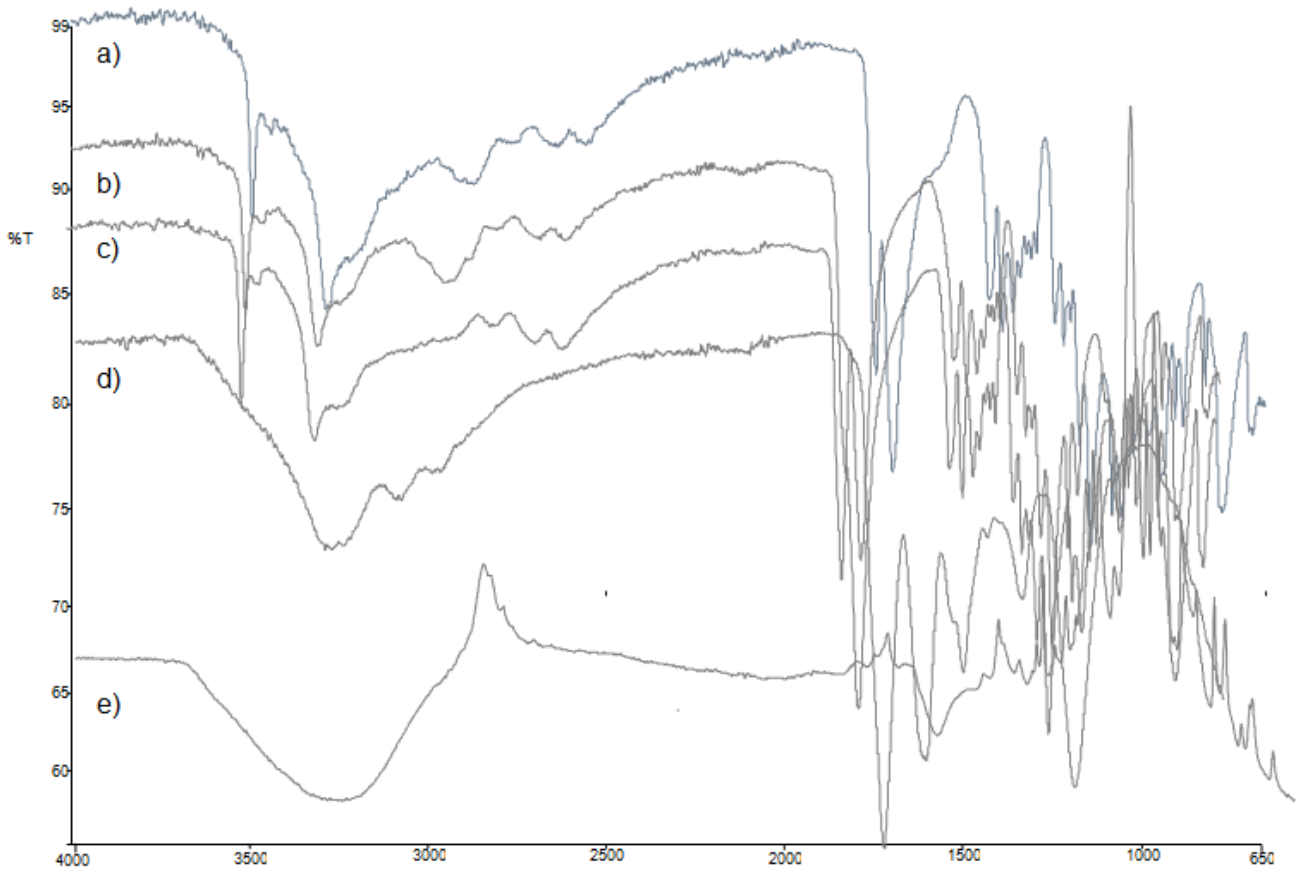


Figure 7.6: FT-IR spectra of native polymers a) chitosan; b) hypromellose; c) citric acid; and d) lectin employed in fabrication of e) the optimized mucoadhesive layer.

Figure 7.7a illustrated the FT-IR spectra of Eudragit® RS100, the characteristic peaks associated with Eudragit® RS100 includes an aldehyde functional group at 1722.54cm^{-1}; 1383.28cm^{-1} C-H alkanes, and a peak at 1142.86cm^{-1} representative of C-O phenols. Alginate (Figure 7.7b) displayed characteristic absorption bands at 1404.87cm^{-1} descriptive of carbonyl ions, and a peak at 878.18cm^{-1} C-H stretch. N-H amine at a transmittance band of 3362.84cm^{-1} is characteristic of calcium chloride (Figure 7.7c); a peak at 1742.62cm^{-1} is representative of an alkyl carbonate; 1139.67cm^{-1} expressive of C-O phenols, and a peak at 763.71cm^{-1} is descriptive of C-H an alkene functional group. Similarly, analysis of the native polymer spectra (Figure 7.7a-c) along with the optimized drug loaded layers (2, 10 and 18 hour) formulations (Figure 7.7d-f) revealed there were additional modified absorption bands that were indicative of the successful crosslinking reaction. Additional peaks at 1470-1430cm^{-1} illustrative of C-H methyl stretching, O-H aromatic ether at 1270-1230cm^{-1}; a transmittance absorption band at 1130-1190 representing C-N secondary

amine; a modified peak at 1370cm^{-1} displaying strong tert-butyl unsymmetrical doublet and a peak in the region of 800-1000cm^{-1} alkene out of plane C-H bending (Durig and Fassihi, 2002). The three optimized drug loaded formulations did not show any significant variations in spectra aside from the slight shift to higher frequencies as the crosslinking density increased.

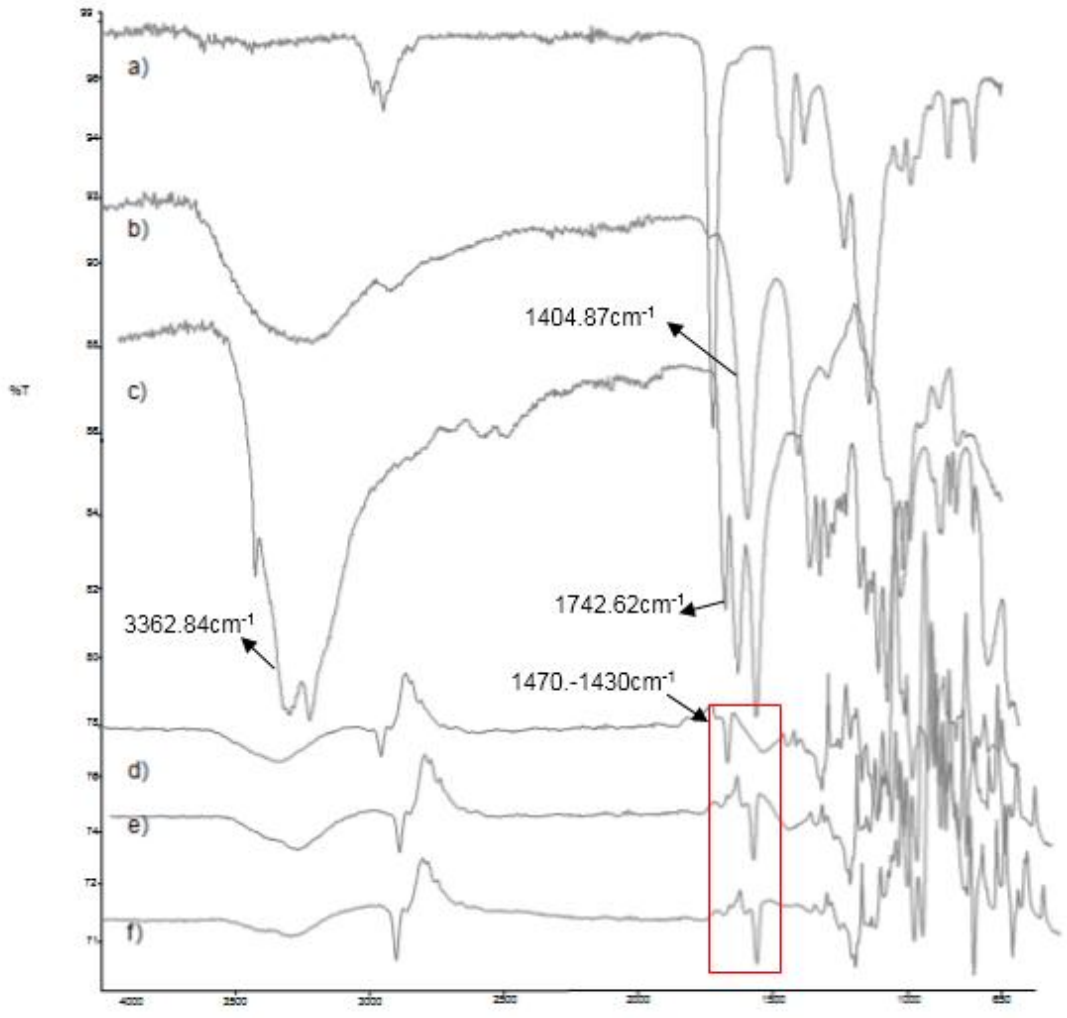


Figure 7.7: FT-IR spectra of native polymers a) Eudragit®RS100; b) alginate and c) calcium chloride employed in the fabrication of d) optimized 2hour; e) optimized 10hour and f) optimized 18hour drug loaded layer formulations.

7.3.5. Elucidation of the degree of swelling and its effect on mucoadhesive characteristics of the optimized patch layers upon intestinal environment exposure

The average degree of swelling and erosion of the drug loaded layers (2, 10 and 18 hour) was employed. Through gravimetrical analysis it was illustrated that with an increased exposure to simulated intestinal fluids, the optimized formulations swelled, resulting in a corresponding increase in weight of the polymeric films (Figure 7.9). The hydration of the polymeric chains allows reciprocal interpenetration between the polymeric film and mucin molecules, consequently creating stabilized interactions and thus strengthening the mucoadhesive characteristics of the optimized formulations (Salamat-Miller, et al., 2005; Roy, et al., 2009). Upon contact of the surface layer of the polymeric films to simulated intestinal conditions, surface occurring polymeric chains swelled permitting both mucoadhesion and weight gain (swelling) (Figure 7.8a). With constant exposure, the surface layer disintegrates and undergoes erosion out of the film, resulting in a decrease in weight (erosion) (Figure 7.8b). The underlying polymeric chains subsequently become exposed to the surrounding dissolution medium and experience supplementary swelling, promoting mucoadhesion. Hence, fluctuating degrees of swelling was observed at various time points resulting in variations in percentage mucoadhesion over time.

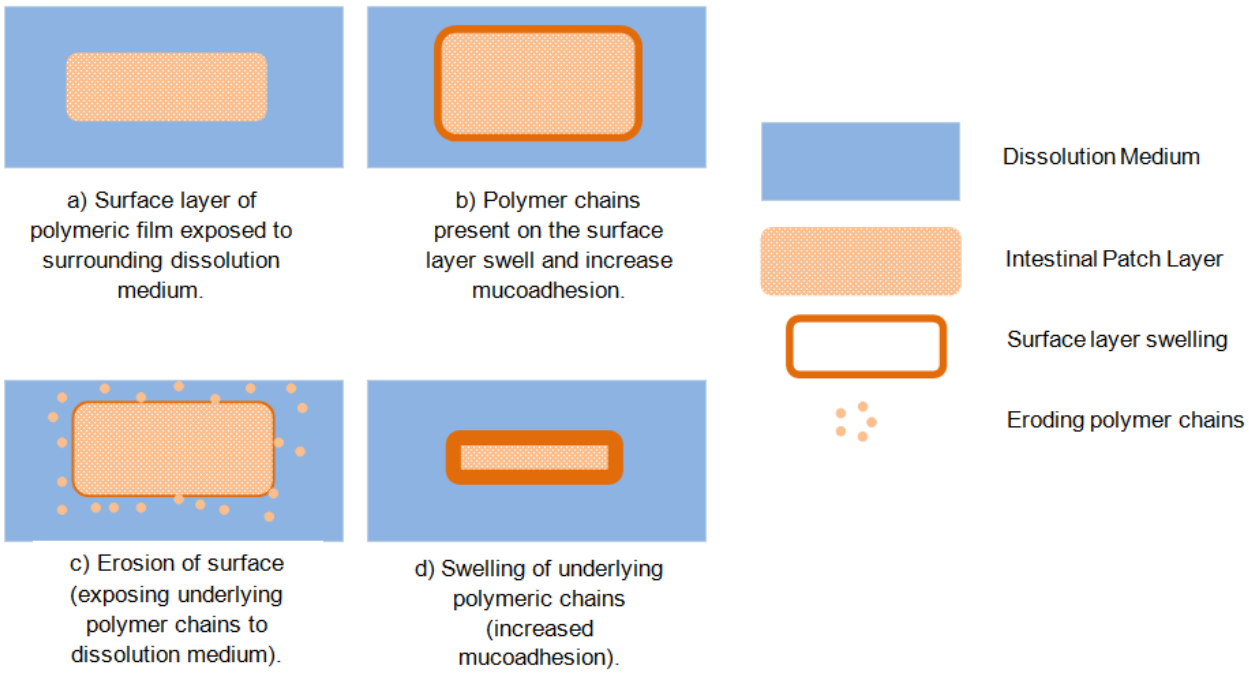


Figure 7.8: Schematic illustration of the proposed process resulting in the fluctuations observed in swelling and hence in mucoadhesion characteristics of the optimized formulations.

All system layers gravimetrically studied displayed relatively intermediate rates of erosion (Figure 7.9). As a result, fluctuations in the degree of swelling as a function of time was observed. However, the reduction in percentage swelling did not significantly hinder the mucoadhesive characteristics of the formulations, as seen in mucoadhesion results in *Chapter 7, Section 7.3.7.* It may thus be deduced that the polymeric patch layers displayed satisfactory swelling properties over the specified test period and thus promoted and maintained adequate mucoadhesion over a prolonged period of time, allowing for a greater residence time necessary for pulsatile drug delivery.

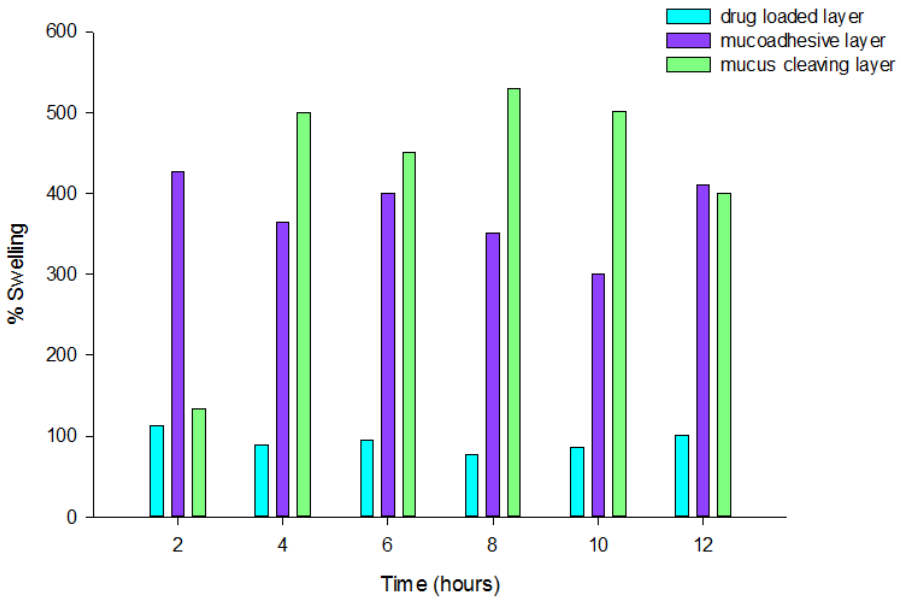


Figure 7.9: Graphical illustration of the variations in degree of swelling and erosion of a) optimized mucoadhesive layer b) optimized drug loaded layers and c) the mucus cleaving layer.

7.3.6. Analysis of thermal transitions

Thermal evaluation was conducted for the optimized mucoadhesive and drug loaded layers so as to ascertain the effect of crosslinking and amalgamation reactions on the thermal characteristics of the respective layers. DSC thermograms of native polymers used in the formulation process of the optimized mucoadhesive (Figure 7.10A; a-d) and drug loaded (Figure 7.10B; a-c) layers were evaluated in comparison to the thermogram of the optimized formulations.

Thermal analysis of the optimized mucoadhesive formulation displayed a single small T_g related to enthalpy relaxation at 25.07˚C; this indicates that the native polymer components employed have exceptional miscibility and there exists strong hydrogen bonding interactions between the respective polymer networks (Figure 7.10A; e). In the case of native polymer components being immiscible there would be two T_g peaks observed within the thermograms corresponding to the respective native polymers (Zhang *et al*., 2004; Yue *et al*., 2008). A crystallization peak is observed at 117.62˚C, this crystallization peak is reciprocated in the thermograms of CHT (Figure 7.10A; a) and lectin WGA (Figure 7.10A; d) at higher temperatures of 211.56 and 238.57˚C respectively, this represents shift of the polymers to a more ordered state. These thermal events are followed by sample melting at 192.02˚C which illustrates the return of the polymer system to a less ordered form, this is followed by decomposition of the sample at 242.82˚C. Solvent evaporation from the optimized formulation occurs at 261.05˚C thus resulting in complete dehydration of the system.

DSC evaluation of the optimized drug loaded layers (2, 10 and 18 hour formulations) (Figure 7.10B; d-f) all displayed T_g in the range of 86.36-101.15˚C; it was noted that as the degree of crosslinking was increased the T_g shifted to higher temperatures. The optimized drug loaded layer formulations (2, 10 and 18 hour) displayed crystallization peaks at 144.47˚C; 146.25˚C and 143.82˚C respectively, which may be attributed to the crystallization of the system with the emergence of nuclei of calcium chloride. The optimized 18 hour drug loaded formulation illustrated a peak at 283.00˚C representative of partial oxidation of samples with residual oxygen within the hermetically sealed pan. All formulations then displayed melting peaks between a temperature ranges of 210.19-283.34, this indicates that they undergo a transition from an ordered to an amorphous state and approximately 200˚C.

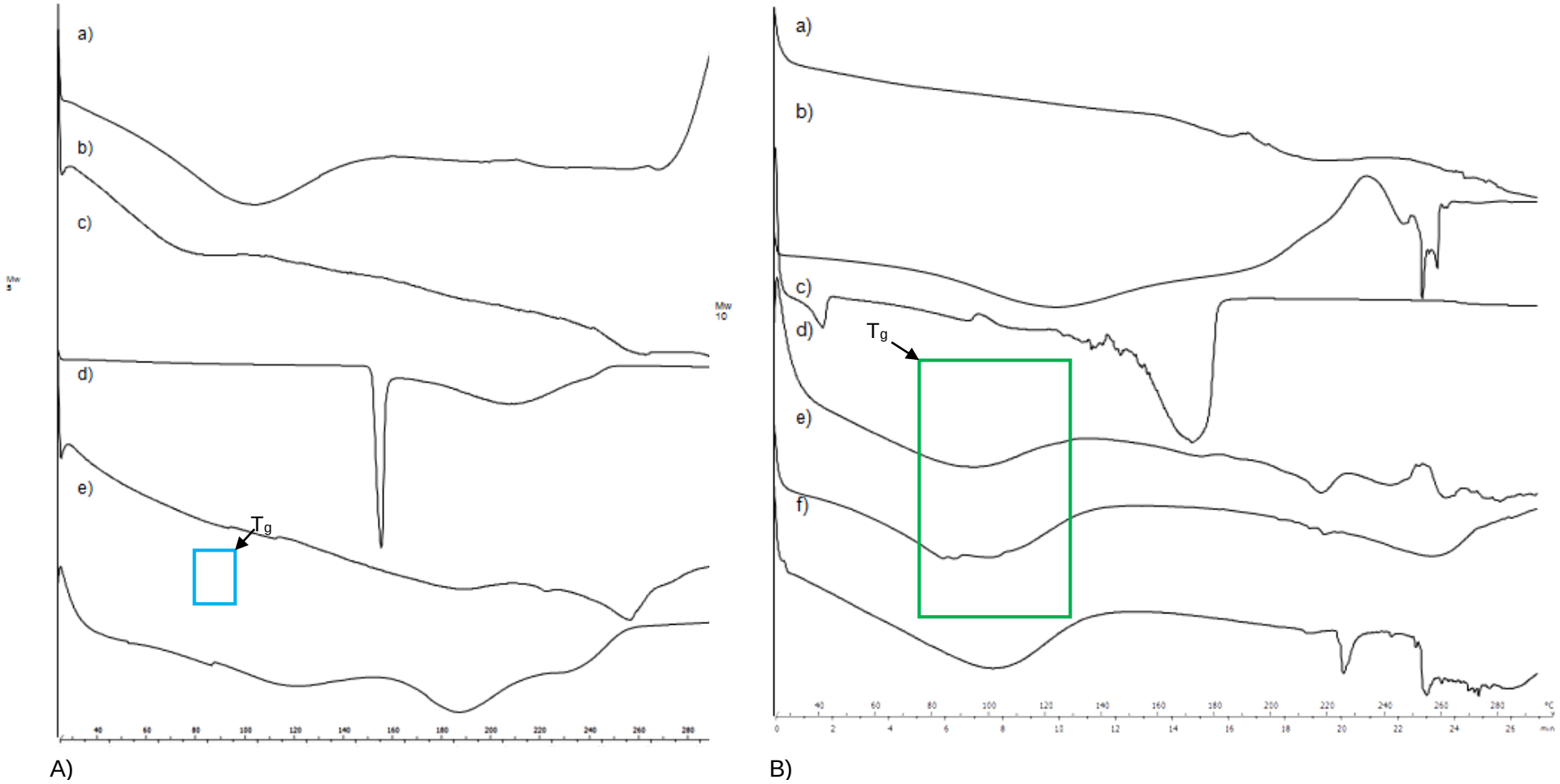


Figure 7.10: DSC thermograms of A) the optimized mucoadhesive layer (e); and native polymers a) CHT; b) hypromellose; c)citric acid; d) lectin WGA and B) the optimized drug loaded layers 2,10 and 18 hours (d-f); and the native polymers a) Eudragit®RS100; b) alginate and c) calcium chloride.

7.3.7. *Ex vivo* determination of mucoadhesive properties via textural analysis and a comparative evaluation via *ex vivo* perfusion

Film-casting formed polymeric films that were uniform, clear, and flexible all through its structure for the drug loaded and backing layers; whereas in addition to these properties the mucoadhesive and mucus cleaving layers displayed a yellow tint. Figure 7.11 illustrates a typical force: distance curve obtained via mucoadhesive textural analysis. The MDF (N) (highlighted with a blue arrow) and the WA (mJ) (area highlighted in pink) are related to mucoadhesive properties, where the higher the MDF and WA the stronger the mucoadhesive properties.

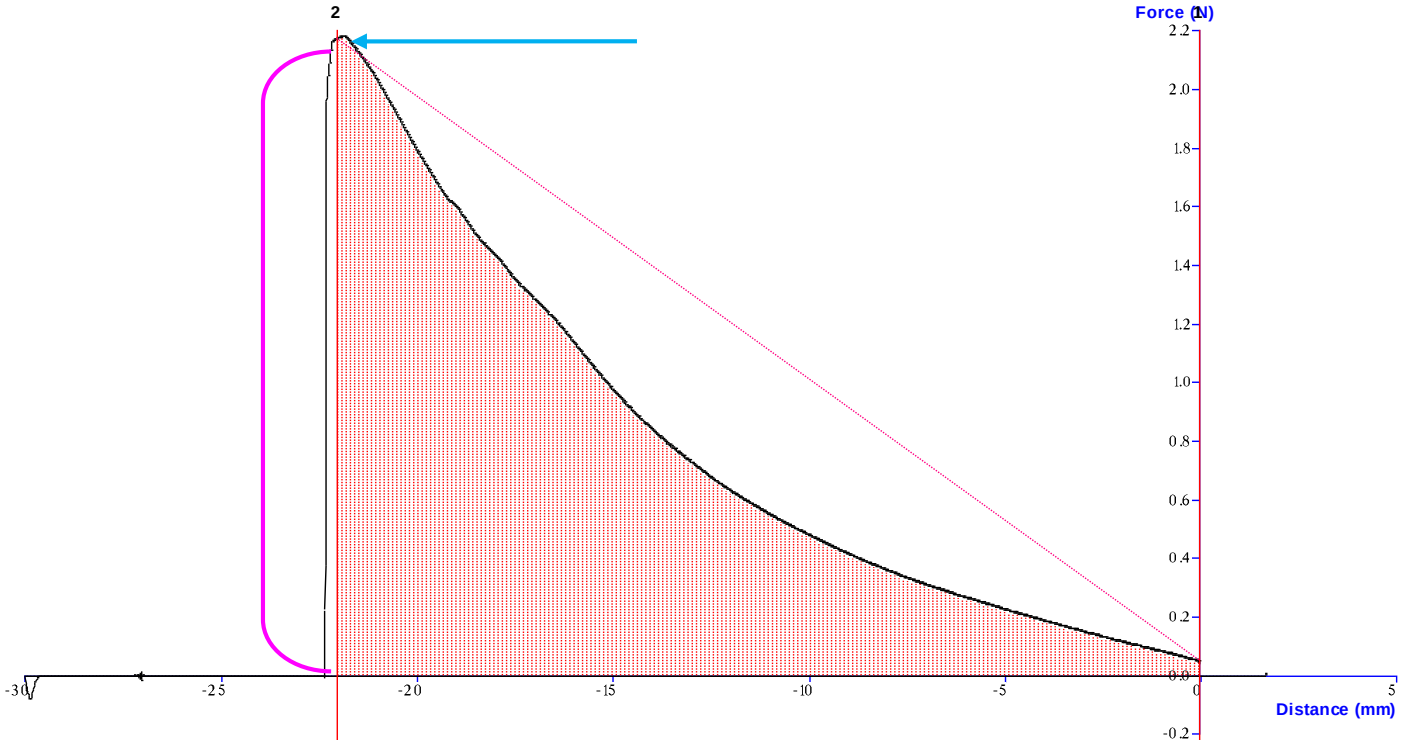


Figure 7.11: Typical textural profile demonstrating the MDF (N) and WA (AUC_{FD}) (mJ).

Mucoadhesion was achieved from the mucoadhesive, drug loaded, mucus cleaving and backing layers respectively (Figure 7.12). All intestinal patches displayed satisfactory mucoadhesion in respect to their individual functionalities within the system.

Mucoadhesive analysis revealed that the mucoadhesive and mucus cleaving layers displayed the highest levels of mucoadhesion (MDF=5.9±0.0015; AUC_{FD}= 6.179±0.001mJ) and (MDF=4.5±0.004; AUC_{FD}=4.779±0.002mJ) respectively (Figure 7.12). The greater degree of mucoadhesion observed may be attributed to the presence of CHT, hypromellose and lectin WGA N-acetyl-cysteine and all known for their mucoadhesive characteristics. However, the fact that

CHT and hypromellose are cationic and non-ionic polymers respectively it is most likely that the mucoadhesive characteristics observed are attributable to lectin WGA and N-acetyl-cysteine. The mucoadhesion observed by the presence of hypromellose is related to the diffusion theory; where polymeric chains interpenetrate with the mucin layer thus promoting mucoadhesion. The drug loaded and backing layers demonstrated intermediate mucoadhesion (MDF=3.5±0.002; AUCFD=3.761±0.001mJ) and (MDF=2.121±0.004; AUC_{FD}=2.4±0.003mJ) this may be associated with the mucoadhesive characteristics of alginate and ethyl cellulose.

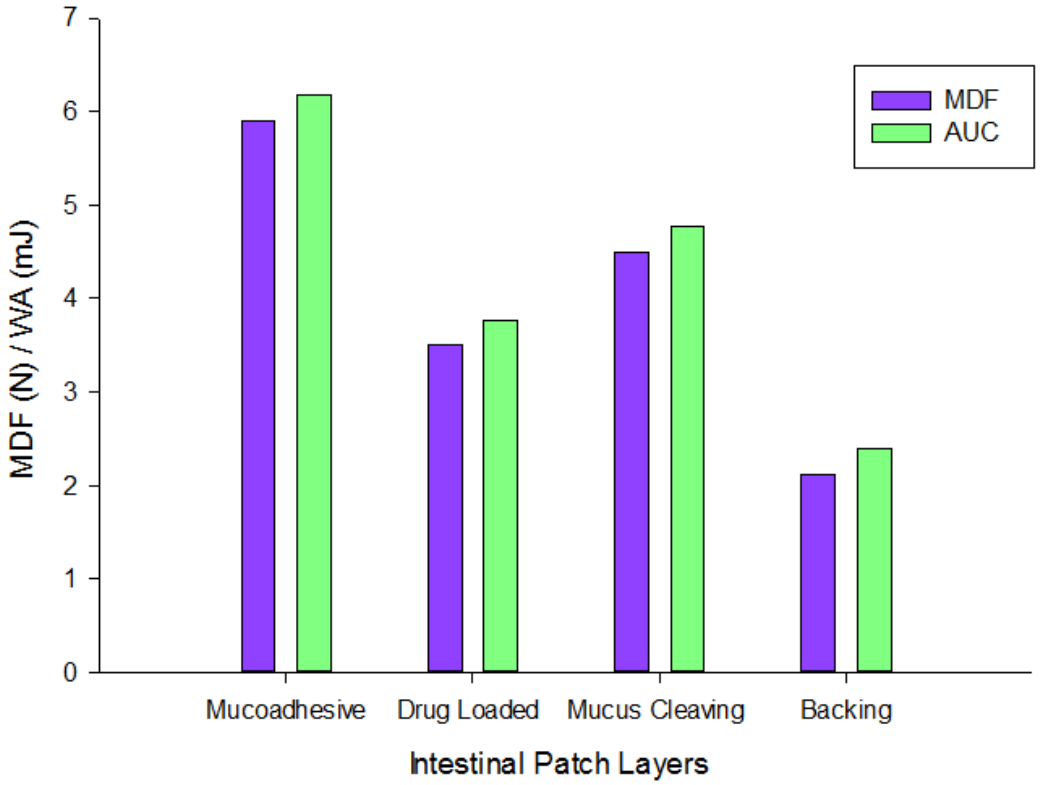


Figure 7.12: A comparison of a) Maximum Displacement Force (MDF)(N) and b) Work of Adhesion (AUC_{FD}) (mJ) of intestinal patch layers in phosphate buffered saline (pH 6.8) (n=3; SD < 0.025).

As the proposed drug delivery system requires mucoadhesion to ensure site-specific prolonged drug delivery, it was thought necessary to study the release, adhesion and dissolution of the intestinal patches. The prolonged contact of patches with the mucosa was confirmed by *ex vivo* perfusion studies; the results were documented via images (for clear illustration of the observations they have been schematically presented). Perfusion studies demonstrated that the patches adhered to the luminal wall by the most mucoadhesive surface exposed i.e. mucus cleaving layer. There were no patches that adhered via their backing layer region. When delivered in a tablet, the patches exited the tablet upon dissolution and adhered to the mucosa within ± 10

minutes (Figure 7.13a and b); thereafter the patches remained attached to the intestinal mucosa for the residual duration of the study with slow dissolution (Figure 7.13c).

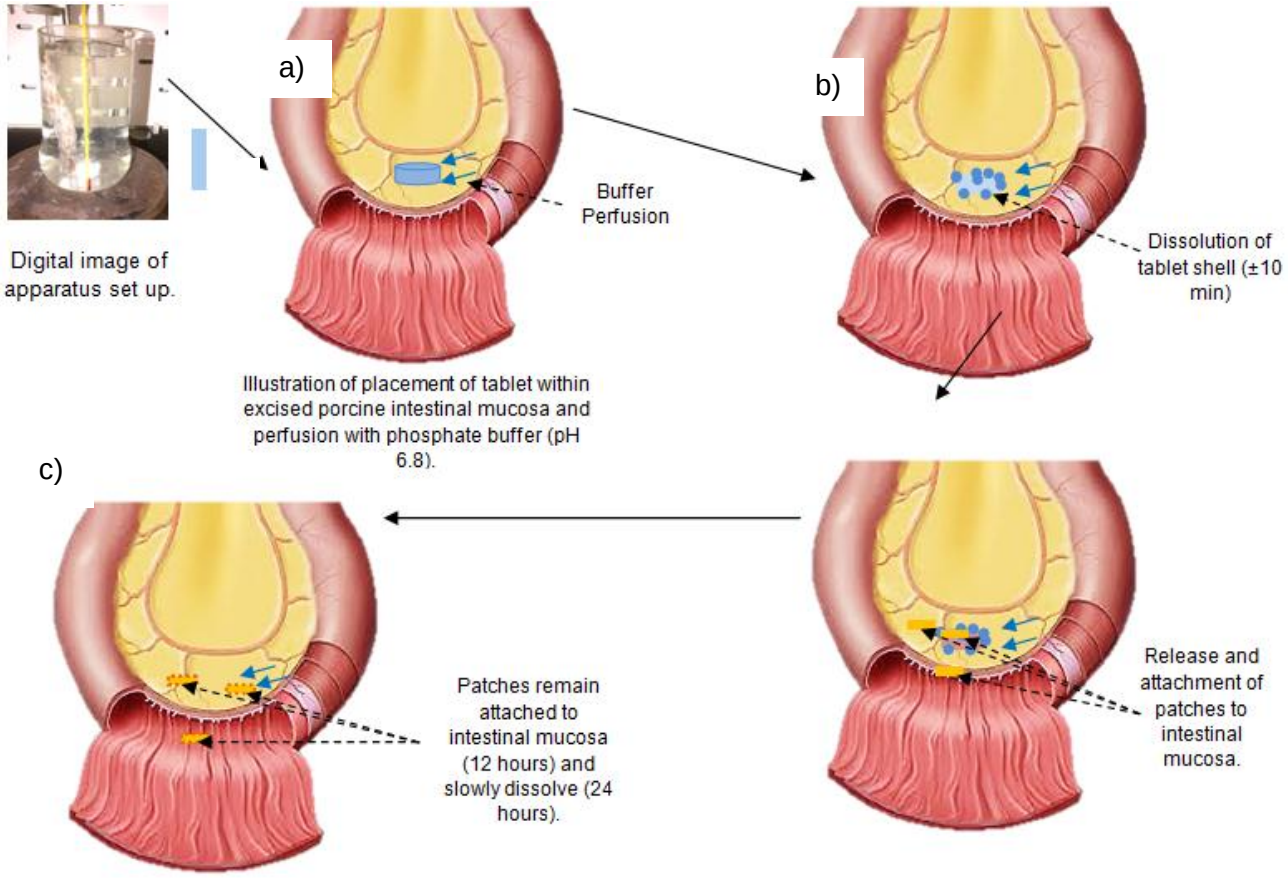


Figure 7.13: Schematic illustration of perfusion study observations.

7.3.8. *Ex vivo* drug permeation studies

Permeability studies of sodium valproate demonstrated a constant increase in the rate of flux over a period of 3, 4 and 5 hours respectively for the optimized drug loaded formulations (2, 10 and 18 hours) to steady state concentration (Figure 7.14). At this particular point a plateau was reached due to saturation of the intestinal mucosa, and thus no additional molecules entered the receptor compartment of the FDC apparatus. This assessment illustrates the high degree of permeability of sodium valproate, which may be accredited to its solubility characteristics resulting in increased dissolution. There was an observed variation in diffusion amongst the optimized drug loaded layers this is attributed to the difference in composition; with an increase in polymer and

crosslinking concentration so as to prolong drug release respective to the times chosen. It was shown that the flux was minimally reduced as the polymer concentration and crosslinking density increased; while permeability was satisfactory among all optimized drug loaded layers despite the variations in their composition so as to enable time controlled drug release.

The flux at the plateau was determined to be 0.6116 $mg.cm^{-2}.hr^{-1}$; 0.6122 $mg.cm^{-2}.hr^{-1}$ and 0.5593 $mg.cm^{-2}.hr^{-1}$ respectively for the optimized drug loaded formulations (2, 10 and 18 hours) with the permeability coefficient determined to be 1.1366; 1.136 and 1.0831 respectively (Table 7.4). The data obtained determined that in the pig model, sodium valproate would undergo relatively quick absorption.

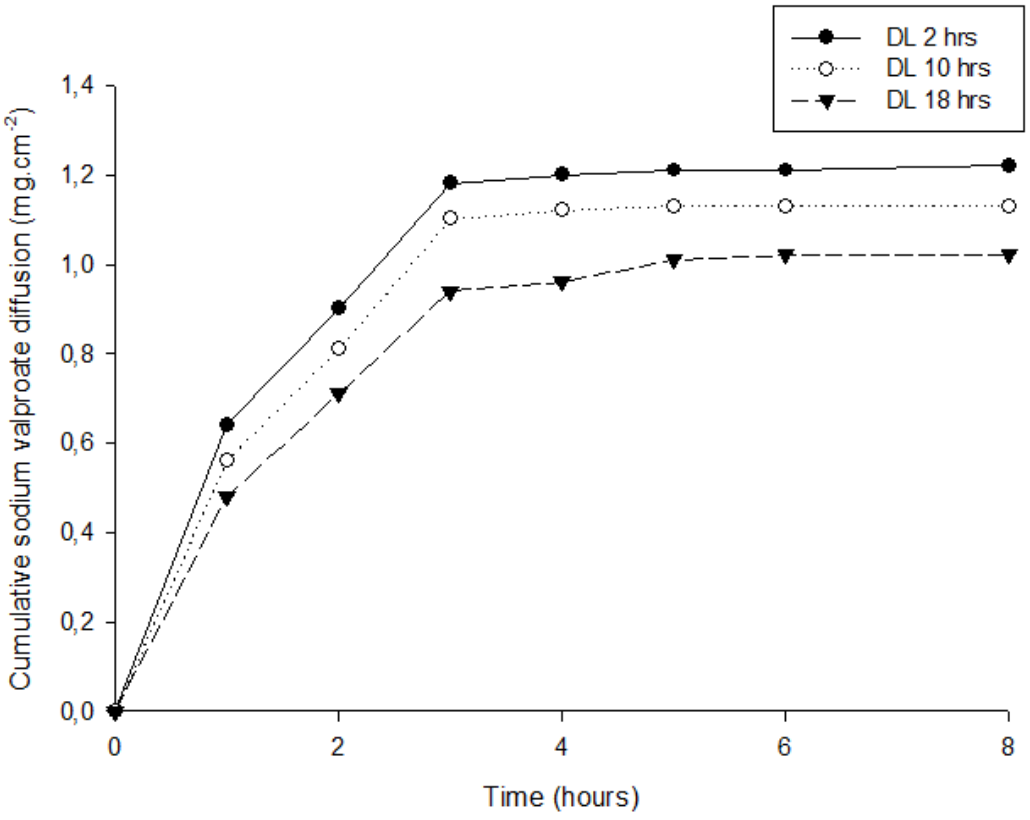


Figure 7.14: *Ex vivo* permeation profile of sodium valproate across excised porcine intestinal mucosa (n=3; SD ≤0.02 in all cases).

Table 7.3: Sodium valproate flux and permeability coefficient as determined via *ex vivo* permeability analysis.

Drug Loaded Layer	***Flux (Jd;mg.cm^{-2}.hr^{-1})***	***Permeability Coefficient***
DL 2hr	0.6116±0.004	1.1366±0.012
DL 10hr	0.6122±0.002	1.136±0.011
DL 18hr	0.5593±0.004	1.0831±0.011

7.3.8.1. *Porcine intestinal mucosa integrity evaluation*

Evaluation of the porcine intestinal mucosa displayed a RF of 1±0.03. This analysis thereby elucidated that the intestinal mucosa had maintained its integrity with negligible variation in resistance factor notwithstanding its delicate structure. The RF calculated validates the sodium valproate permeation results.

7.3.9. *In vitro* drug release analysis

Drug release occurs after a short lag-phase (due to the dissolution of enteric coating and tableting excipients) from patch 1 (DL 2hr) corresponding to the first pulse release. The concentration of polymer and degree of crosslinking within the patch 2 (DL 10hr) and patch 3 (DL 18hr) govern and control the rate of release from these respective layers. The optimized patches protect drug from release for approximately 6 hours respectively to allow for the "switch-off" phase. Theoretically release should not occur from any two patches at the same time. A schematic of this process is outlined in Figure 7.15.

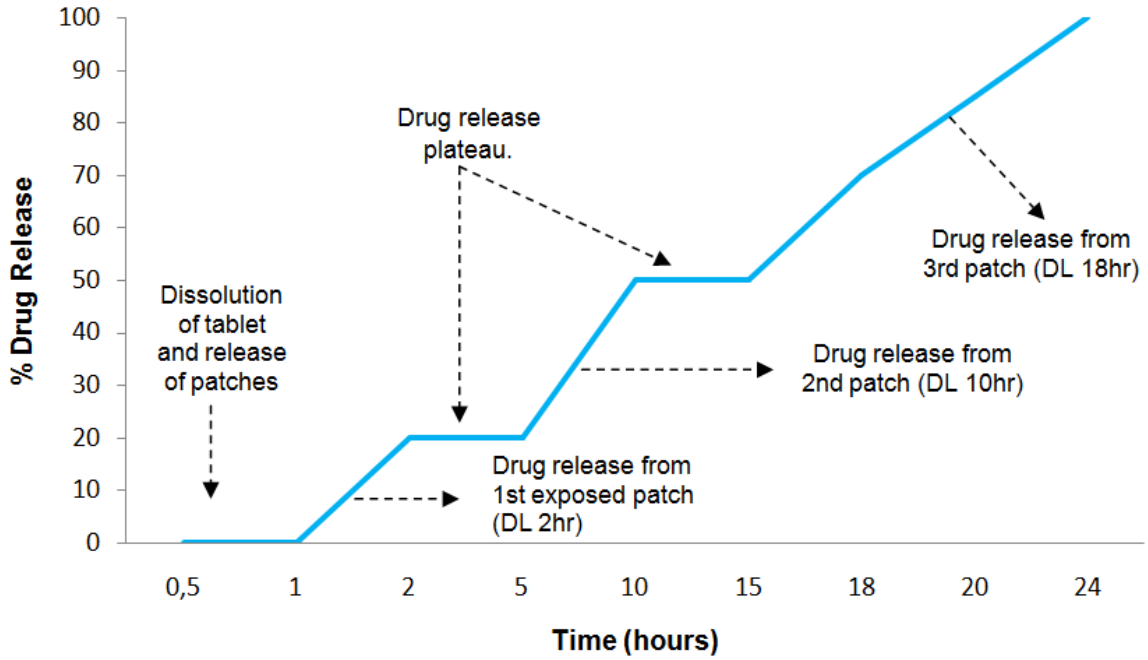


Figure 7.15: Schematic illustrating ideal drug release profile requisite for the bioadhesive multilayered intestinal patch system.

In vitro performance studies demonstrated that bioactive release from the optimized device is a complex interplay of system structure and composition of excipients employed in the formulation process. Figure 7.16 depicts the drug release profile of the optimized bioadhesive multilayered intestinal patch formulation. The observed release profile mirrors triphasic release with an initial lag-phase attributed to the tablet dissolution process and attachment of the patch to the intestinal wall via the mucus cleaving and mucoadhesive layers as well as swelling of these respective layers. The initial pulse provides rapid drug release with 40% of loaded drug (DL 2hr) being released within approximately 3 hours; while the second and third patches allow for controlled drug release. The rate of drug release during the second and third pulses are governed by the concentration of polymer, degree of crosslinking, and interpenetrating polymer networks present between patches and patch layers. The system displayed >70% bioactive release over 24 hours.

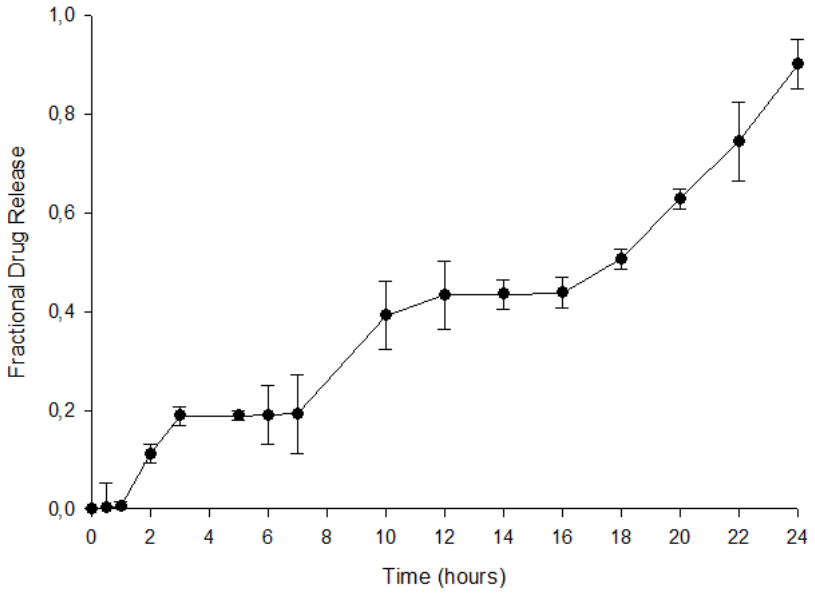


Figure 7.16: Drug release profile of the optimized bioadhesive multilayered intestinal patch device.

For analytical conclusion of drug release, *in vitro* release data obtained via dissolution studies were plotted as a function of fractional release vs. time (Figure 7.16). Linear regression analysis of the data provides an R^2= 0.9568 (t0-24). Hence, the optimized formulation does not follow zero-order kinetics as predicted. When drug release data was plotted employing the Higuchi model, the resulting plot demonstrated release of bioactive from the optimized system as a square root of time.

7.4. Concluding Remarks

Both optimized layers (mucoadhesive and drug loaded) formulations achieved a high desirability with optimization. This chapter demonstrated the manner in which the optimized formulation layers would react upon exposure to simulated intestinal conditions, providing constructive information required to predict the formulation's *in vivo* performance. Tensile analysis revealed that the optimized formulation layers possesses suitable elasticity and flexibility, necessary for embedding within a tablet and for oral drug delivery. SEM displayed that physical structure of the polymeric film layers were satisfactory and in line with interactions upon swelling. Variations observed in the mucoadhesive characteristics were related to the physical alterations (concurrent swelling and erosion) of the optimized system upon exposure to simulated intestinal conditions. Drug release studies displayed ideal triphasic release over 24 hours.

CHAPTER 8

IN VIVO ANALYSIS OF THE DUAL LAYERED ORAL DRUG DELIVERY SYSTEM COMPONENTS IN RELATION TO MARKETED GOLD STANDARD FORUMULATIONS

This study had received the approval of the Animal Ethics Screening Committee of the University of the Witwatersrand with ethics clearance number 2013/23/04 (Appendix 11.3). Ethics clearance was granted for the ex vivo and in vivo studies.

8.1. Introduction

A fundamental step in the design and fabrication of a new drug delivery system is performing *in vivo* animal studies. Information generated can be used to assess the safety and efficacy of a dosage form and mostly to predict the pharmacokinetics and pharmacodynamics of the system in humans (Dali et al., 2006). Selection of an applicable/appropriate animal model depends greatly on the specified dosage form and frequency of dosing (Hildebrand, 1991).

The Large White Pig model is assuredly expedient over other animal models such as rabbits and dogs for more accurate validation and correlation of data with human doses. As the use of rabbits and rodents are excluded due to the size of oral dosage forms and the multiple samples required; the use of dogs is limited due to their restricted availability and high costs (Kostewicz et al., 1996). The pig (*Sus scrofa domestics)* has attained acclaim as an animal model in biomedical research fields mostly due to the anatomical similarities it shares with humans. In addition, they are large animals thereby allowing for multiple blood sampling and have similarities to humans in terms of metabolism, biotransformation (CYP450) and dietary habits amongst others (Brunet et al., 2006).

With frequent blood sampling the comprehensive identification and quantification of drug release is achievable. The explicit prevalent utilization of the pig model for *in vivo* drug delivery studies on an ethical level adds supplementary validity to the use of the Large White Pig model for assessment of the optimized dual-layered xerogel-bioadhesive intestinal patch tablet components. Thus this Chapter involves the *in vivo* administration of the conventional drug products and the optimized dual- layered xerogel-bioadhesive intestinal patch tablet components containing sulpiride (xerogel component) and sodium valproate (bioadhesive intestinal patches component), for assessment of the performance, safety and tolerability of the optimized formulations in the Large White Pig model.

The purpose of this study was the development of an innovative 'smart' dual-layered oral delivery system intended to deliver multiple drugs individualistically within the intestine. The preceding Chapters of the current thesis identified and detailed the various formulation variables employed in fabrication of the drug delivery system and are further summarized in Figure 8.1. The system is composed of two components, intended for delivery of sulpiride and sodium valproate respectively. Layer one of the dual-layered tablet comprises an s-IPN xerogel for sustained release of sulpiride; whereas Layer two comprises bioadhesive multilayered intestinal patches (n=3) for the pulsatile delivery of sodium valproate, each patch includes; a mucus cleaving layer, a mucoadhesive layer, a drug loaded layer and a backing layer.

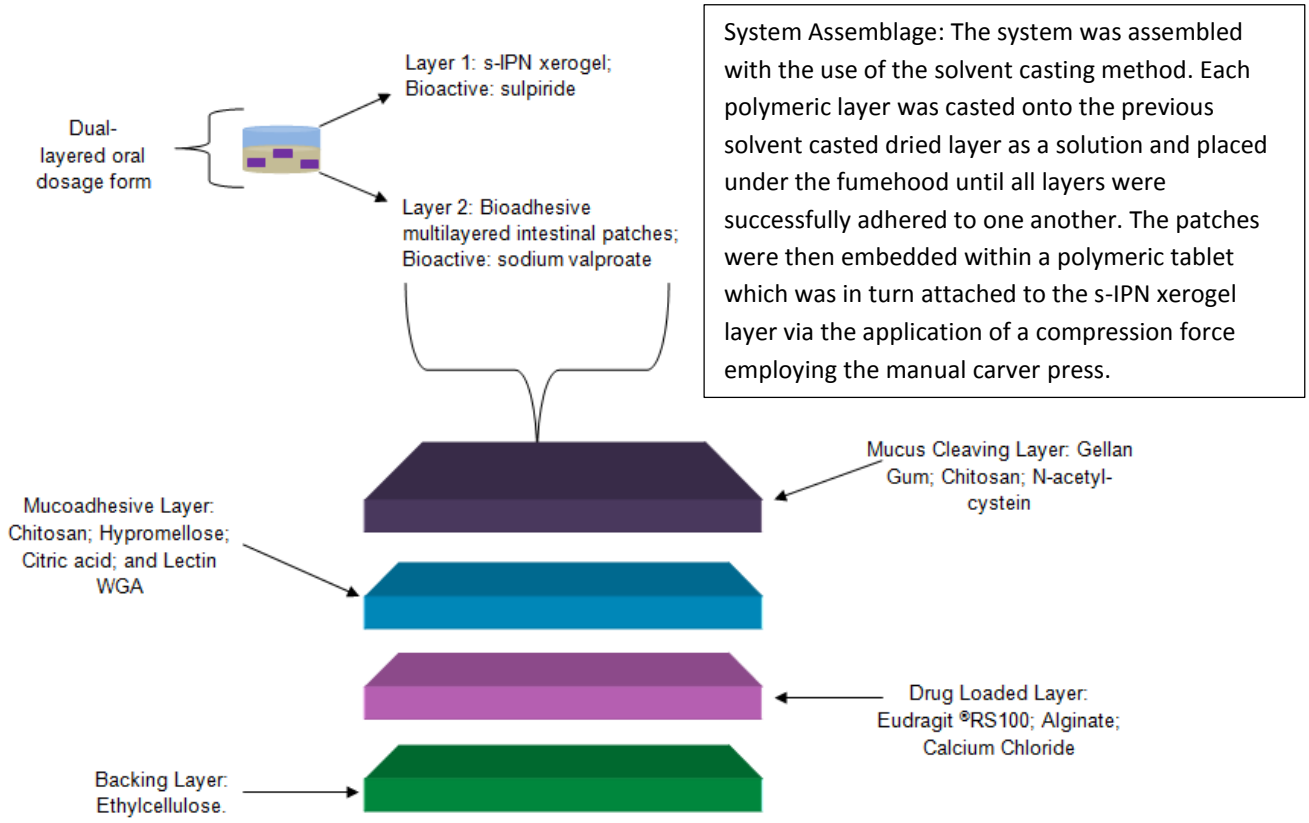


Figure 8.1: Summary of system assembly.

8.2. Materials and Methods

8.2.1. Materials

The materials described in *Chapter 5, Section 5.2.1* were employed in the fabrication of the s-IPN xerogel component (Layer 1 of the dual-layered system), while the bioadhesive multilayered intestinal patches (Layer 2 of the dual-layered system) were fabricated employing the materials described in *Chapter 7, Section 7.2.1*. Carboxymethylcellulose sodium (CMC) and magnesium stearate purchased from Sigma Aldrich (Sigma Aldrich (Pty) Ltd., St. Louis, MO, USA) were

utilized to assemble the dual-layered tablet. Solvents employed for UPLC-MS/MS measurements were of UPLC grade and all other reagents were of analytical grade. Double deionized water was obtained from a Mili-Q water purification system (Mili-Q, Millipore, Bedford, MF, USA).

For UPLC analysis of sulpiride: UPLC grade solvents employed for UPLC measurements included Acetonitrile (ACN) 200 (ROMIL- SpS™ Super Purity Solvent (CH_3CN), Assay >99.9%), Acetone purchased from Merck (Darmstadt, Germany), Dichloromethane, Triethylamine and Metocloperamide, utilized as an internal standard were all purchased from Sigma Aldrich (Sigma Aldrich (Pty) Ltd., St. Louis, MO, USA), all of which were of analytical grade and employed without any further purification. A marketed gold standard formulation was obtained from Sanofi-Aventis (Sanofi-Aventis (Pty) Ltd., Paris, France).

UPLC analysis of sodium valproate: UPLC grade solvents employed for UPLC measurements included Acetonitrile (ACN) 200 (ROMIL- SpS™ Super Purity Solvent (CH_3CN), Assay >99.9%), Methanol purchased from Merck (Darmstadt, Germany), Orthophosphoric acid, Ammonium acetate, and hydrochlorothiazide (internal standard) all of analytical grade were purchased and from Sigma Aldrich (Sigma Aldrich (Pty) Ltd., St. Louis, MO, USA). A marketed gold standard formulation was obtained from Sanofi-Aventis (Sanofi-Aventis (Pty) Ltd., Paris, France). A total of 10 female Large White Pigs were employed in the study, each healthy and of an average weight of 35kg. Fresh blank (control) plasma was routinely withdrawn via catheterized pigs. The acquity UPLC® BEH Shield C_{18} RP 1.7μm column (2.1x100mm) was utilized to separate analytes. The sample vials used were 2mL ANSI48 vials which were LCMC certified and clear, pre-slit silicone screw-top vial.

8.2.2. Preparation of system components

The ODLS components (s-IPN xerogel and bioadhesive intestinal patches) were prepared in accordance with the methodologies detailed in *Chapters 5 and 7, Sections 5.2.2 and 7.2.2* respectively.

8.2.3. Habituation of pigs prior to drug study commencement

Pigs were housed in a farm unit maintained under a 12 hour light and dark cycle and fed a commercial diet. Figure 8.2 is a digital photograph showing the farm unit and housing of the pigs and the daily habituation process. Habituation was necessary prior to dosage form administration so as to reduce the challenges associated with handling the animals for administration of formulations and blood sampling. The habituation involved visiting the animals twice daily and during these visits feeding them ''treats' such as raisins as well as patting and brushing them.



Figure 8.2: Farm unit, housing, daily habituation (feeding and behavioral learning) of the Large White Pig.

8.4.4 Surgical implantation of a chronic catheter into the left jugular vein

It was decided that the most efficient way to sample blood from the pig was via insertion of a jugular catheter due to it resulting in the least distress to the animal as compared to the drawing of blood via a marginal ear vein. The surgical procedure was performed by the chief veterinarian and supporting staff of the Central Animal Services (CAS) at the University of the Witwatersrand. Prior to catheterization the pigs were anaesthetized (using Ketamine (11mg/kg I.M; Midazolam (0.3mg/kg I.M)) and then transported to the operating room for preparation for surgery. The preparation prior to surgery included the administration of antibiotics and analgesics (Buprenorphine 0.05mg/kg I.M; Carpofen 4mg/kg I.M).

The surgical area (left neck and shoulder) of the pigs were prepared by shaving and sterilization of the area. Once intubated, anesthesia was maintained with 2% isoflurane in 100% oxygen as shown in Figure 8.3.

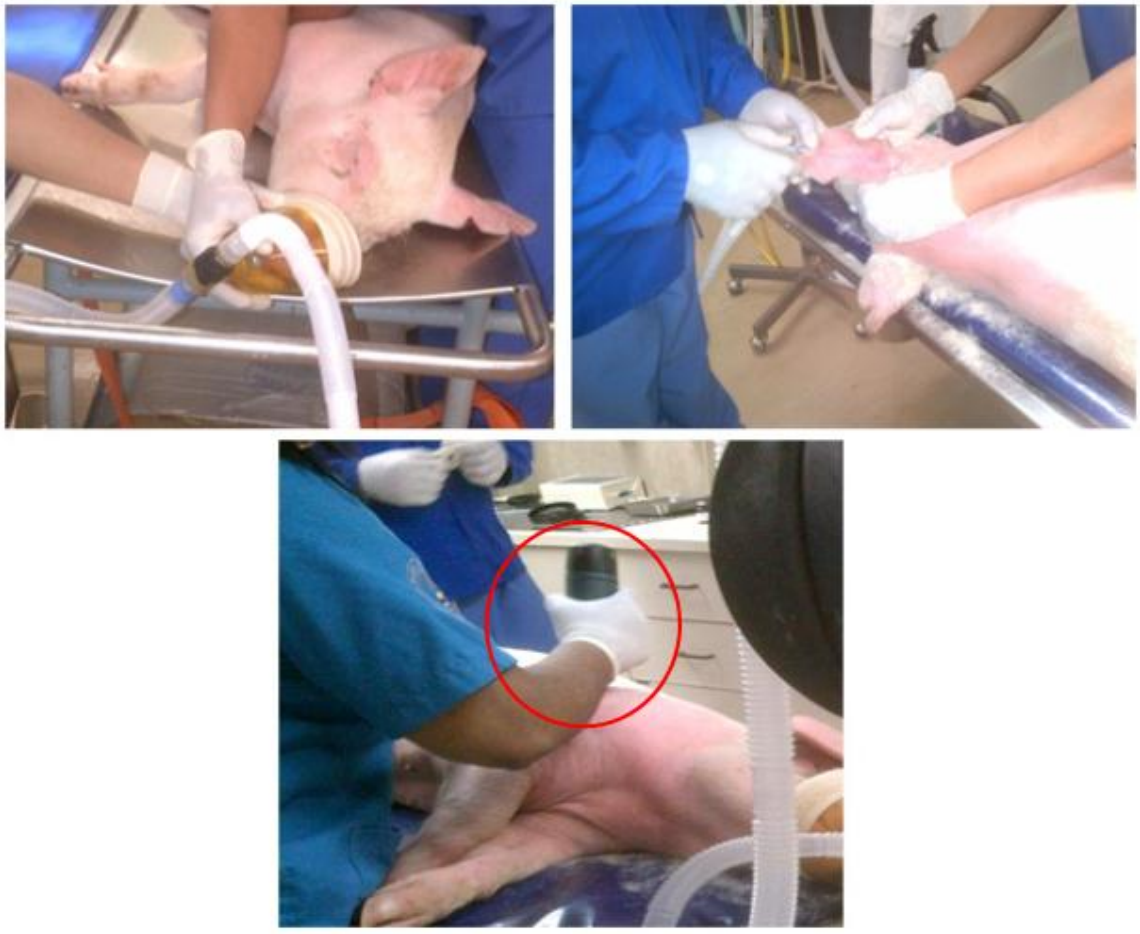


Figure 8.3: Digital images demonstrating a) oxygen supply to animal after anesthesia; b) administration of injections and c) shaving of the surgical area (indicated by red circle).

Figure 8.4 a-d are digital images demonstrating the preparation for surgery. Within an aseptic environment, the left jugular vein was exposed by an incision made dorsal to the jugular groove on the left lateral aspect of the neck. To prevent jugular vein collapse during surgery the catheter (a 7 French gauge double lumen 35cm catheter (CS-28702) obtained from Arrow Deutschland GmdH, Erding, Germany) was first tunneled subcutaneously to the exit point located on the cranial aspect of the scapular. The external ports of the catheter were sutured to the skin of the pig to limit displacement and bending. Subsequently, the catheter was surgically inserted approximately 10cm into the left jugular vein as shown in Figure 8.4. The lumen of the catheter was fastened to the wall of the vein employing a purse suture. To evaluate the functionality of the catheter, blood was withdrawn from the catheter after which the catheter was flushed with heparinized saline (1000i.u of heparin in 1L of 0.9% saline). Throughout the period of surgery, the pigs' vital signs (i.e. heart rate, blood pressure, respiratory rate, body temperature) were constantly monitored. Following surgery, the pigs underwent a 10 day recovery period. For the duration of this time the

habituation process facilitated blood sampling and flushing of the catheters three times daily with heparinized saline. In addition, the surgical entry and exit points were continuously observed for any sign of infection.

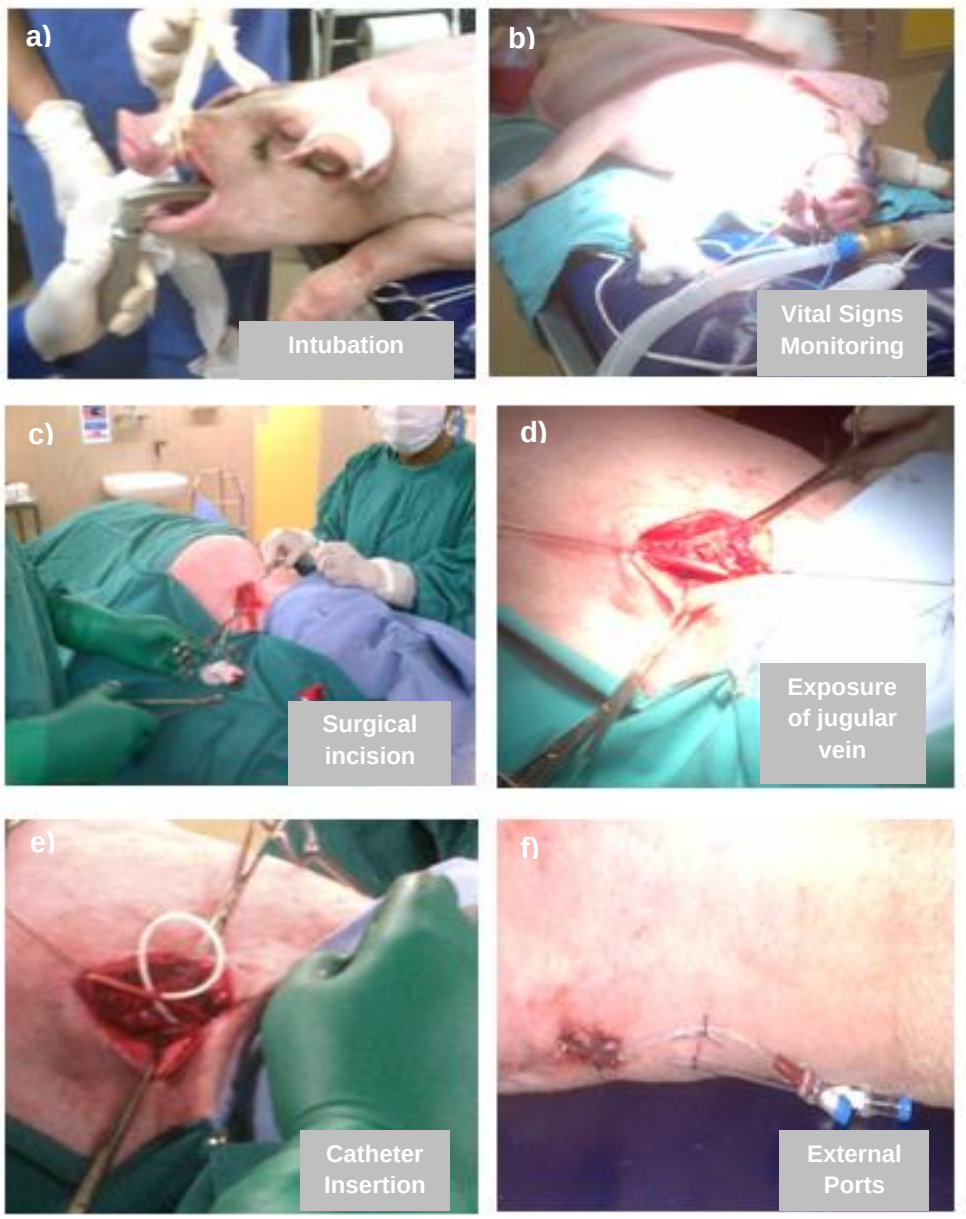


Figure 8.4: Digital images of surgical implantation of the jugular catheter.

8.4.5 Administration of the marketed gold standards and the optimized system formulations to the Large White Pig model

The dosing procedure was performed in conjunction with the animal technicians at the CAS. To assist dosage administration, pigs were sedated to allow for insertion of an intra-gastric tube. A

total of 5 pigs (n=5) were orally dosed with either the optimized formulation components (as the dual-layered system as whole would not be able to be administered to the pig due to size restrictions; in addition, the system components act independently of each other and separate upon exposure to intestinal conditions) or the respective marketed gold standard formulation via an intra-gastric tube as illustrated in Figure 8.5. This aided in averting physical alteration or damage to the system which may arise from mastication by the pigs. For anesthesia Dormicum® and Anaket® were administered directly into the jugular vein catheter. Sedation was maintained with 2% isoflurane and 100% oxygen with the pigs' vital signs being continuously monitored. Subsequently, the intra-gastric tube was inserted into the stomach of the pig while being held upright. To make certain that the drug delivery system was not lodged in the intra-gastric tube, 50mL of water was poured down the tube before removal of the intra-gastric tube. Whilst still under sedation, all surgical sites were examined for infection or injury. Thereafter, the animal was returned to its housing unit for recovery under observation.



Figure 8.5: Sequential digital images depicting the process of dosage administration.

8.2.6. Blood sampling protocol from the surgically implanted jugular vein catheter

Administration of the respective dosage forms were performed with the use of 5 pigs at a time, which were dosed separately with a 3 day wash out period between each dosing in accordance with the half-life of the respective drugs. Dosage administration was divided into six groups (Figure 8.6). Following administration of the respective dosage forms and the wearing off of anesthesia, blood sampling occurred at pre-determined time intervals over a 24 hour test period (0 ,2, 4, 6, 8, 10, 12, 16, 20, and 24 hours). Animals were preoccupied with food which allowed for effortless blood sampling. The surgically implanted jugular catheter external ports were disinfected, flushed with heparinized saline to remove any blood cloths and then 10mL of blood was withdrawn and placed in a lithium heparin vacutainer®. Thereafter, the external jugular ports were again flushed to clear away any residual blood in the ports so as to prevent clotting and hence blockage of the catheter. Withdrawn blood samples were centrifuged at 5000rpm for 15 minutes to aid in the extrication of red blood cells, the plasma supernatant was removed and frozen at -70°C until analysis.

.

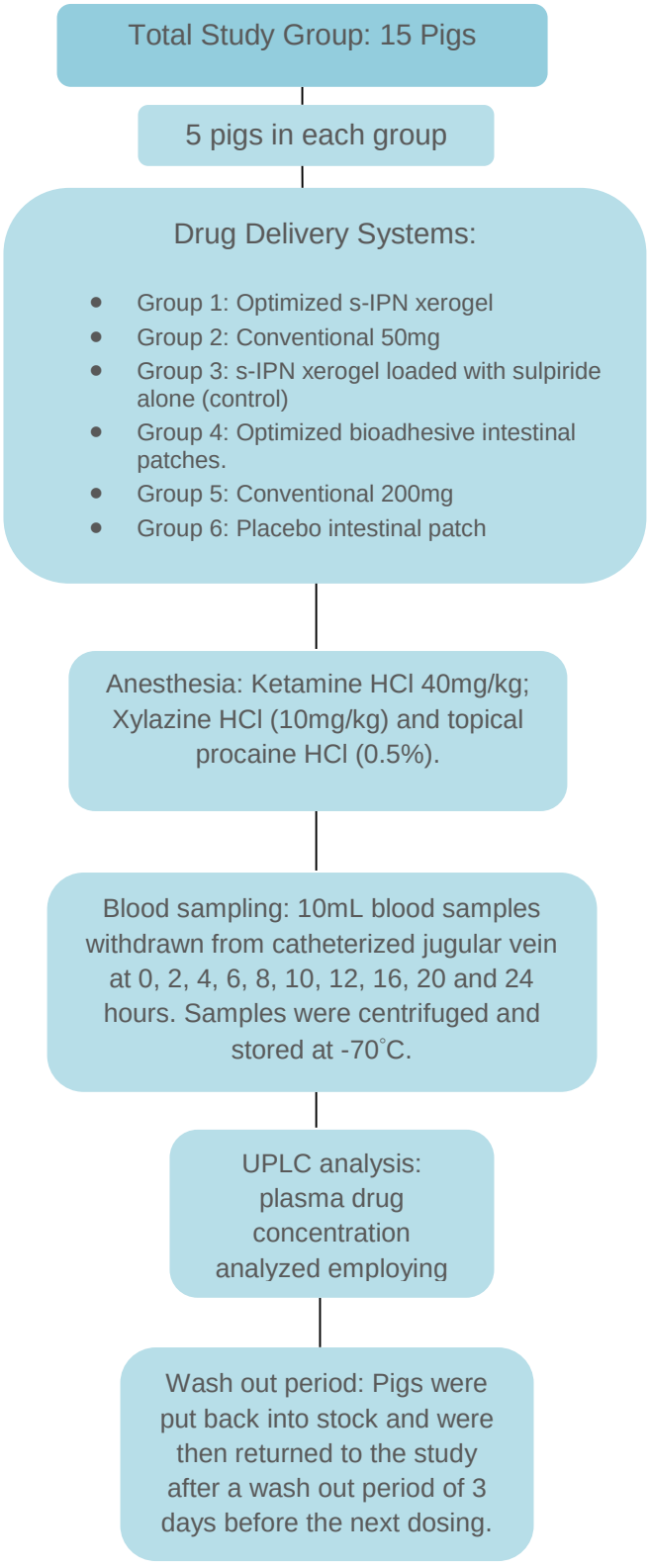


Figure 8.6: Schematic illustrating the quantity of pigs required and the procedural steps involved during *in vivo* studies

8.3. Quantification of *In Vivo* Release of the Model Drugs Employed Utilizing Ultra-Performance Liquid Chromatography Analysis

The optimized dosage form encompassing both the s-IPN xerogel layer and the bioadhesive multilayered intestinal patch layer resulted in a dosage form that exceeded the size restrictions of the CAS's ethical protocol as dosage forms that are above the intra-gastric tube size restrictions specific to animal weight and size may result in esophageal hemorrhage and ultimately death of the animal (Tablet size specifications: Thickness= 0.7cm and width= 0.8cm). The animals employed in the study had an average weight of 45kg's, for this reason a smaller intra-gastric tube is utilized. Therefore, due to the respective layers detaching from each other upon contact with dissolution medium and thus functioning independently of each other it was not deemed necessary to dose them together. For this reason the respective system layers were dosed separately and analysis was conducted independently.

An Ultra-Performance Liquid Chromatography (UPLC) method was employed using a Waters® ACQUITY™ LC system (Waters®, Milford, MA, USA) coupled with a photodiode array detector (PDA), and Empower® Pro Software (Waters®, Milford, MA,USA). The UPLC apparatus was fitted with an Acquity UPLC® BEH Shield C_{18} RP column (2.1x100mm), with a particle size of 1.7μm. For analysis of sulpiride from the s-IPN xerogel layer an isocratic method with a run time of 1 minute was used employing triethylamine (0.5%): acetonitrile: methanol [10:5:85 v/v/v] (solvent A) and acetonitrile 100% (solvent B) as the mobile phase in a 50:50 ratio. The flow rate was 0.3mL/minute with an injection volume of 10μL. The PDA detector was set at 300nm. Metocloperamide was used as the internal standard (IS) (Giorgi, et al., 2015).

For UPLC analysis of sodium valproate from the pulsatile release bioadhesive multilayered intestinal patches the mobile phase was ammonium acetate 10mM (solvent A) and acetonitrile 100% (solvent B) at a run time if 3 minutes employing an isocratic method (50:50 ratio). The flow rate was set at 0.15mL/minute with an injection volume of 10μL. The PDA detector was set at 215nm; hydrochlorothiazide was utilized as the IS. The analysis was conducted at room temperature (21˚C) (Proença et al., 2011). Table 8.1 details the mobile phases/solvents used during UPLC analysis:

Table 8.1: Mobile phases and priming solvents used for determination of sulpiride and sodium valproate in plasma samples.

Solvent/ Mobile phase	Solvent Concentrations	
	Sulpiride	**Sodium Valproate**
Strong wash	Acetonitrile (ACN) (90%): Double de-ionized water (10%).	Acetonitrile (ACN) (90%): Double de-ionized water (10%).
Weak wash	Acetonitrile (ACN) (10%): Double de-ionized water (90%).	Acetonitrile (ACN) (10%): Double de-ionized water (90%).
Solvent A line	Triethylamine (0.5%): ACN: Methanol [10:5:85]	Ammonium acetate 10mM
Solvent B_1 line	Acetonitrile (ACN) (100%)	Acetonitrile (ACN) (100%)
Solvent B_2 line	Methanol (100%)	Methanol (100%)

8.3.1. Preparation of calibration standards

Standard stock solutions of sulpiride and sodium valproate, as well as their respective IS's metocloperamide and hydrochlorothiazide were prepared in ultra-pure double de-ionized water (Milli-Q, Millipore, Johannesburg). A working standard solution of sulpiride and sodium valproate (0.25mg/50mL) was used to prepare the calibration standards with concentrations ranging between 0.2-100μg/mL via dilution of appropriate quantities of the stock solution with de-ionized water prior to injection into the UPLC.

8.3.2. Calibration sample preparation of plasma employing liquid-liquid extraction

In vivo frozen blank plasma samples were allowed to thaw at room temperature (±25°C). Extraction of plasma containing sulpiride: aliquots of plasma (1000μL) was transferred to polypropylene tubes. A 1000μL aliquot of drug stock solution; 1N sodium hydroxide (1000μL) and ethyacetate: methanol (5:1$^{v}/_{v}$) (6000μL) was then added to the tube and vortexed for 2 minutes. Thereafter the mixture was centrifuged at 5000rpm for 10 minutes. The supernatant was collected and placed in a polytop bottle, to which 200μL of mobile phase was added; subsequently the mixture was dried

under the influence of liquid nitrogen. To the dried residue 1000μL of mobile phase was added for dilution of the drug residue. To a 500μL aliquot of plasma, the IS standard solution (0.25mg/50mL, 1000μl) was added and vortexed for 1 minute prior to injection.

For analysis of sodium valproate containing plasma: aliquots of frozen blank plasma samples (500μL) were transferred to polypropylene tubes. The IS solution (0.25mg/50mL; 1000μl); 10% ortho-phosphoric acid ($^{v}/_{v}$) (1000μL) and 2000μL of double de-ionized water was added to the tube. The mixture was vortexed for 2 minutes, followed by centrifugation at 5000rpm for 10 minutes. The sodium valproate was then eluted with the addition of 2000μL methanol, after which the mixture was dried with the use of liquid nitrogen. The dried extract was then reconstituted with 2000μL mobile phase. Solutions after completion of extraction were transferred to Waters® certified UPLC vials (ANSI48) for analysis. UPLC measurements were conducted in triplicate.

8.3.3. Validation of liquid-liquid extraction methodologies

The meticulousness and accuracy of the extraction procedures was determined via repetition of the extractions mentioned in *Chapter 8, Section 8.5.2* on three consecutive days so as to establish the inter-day precision and accuracy, and intra-day variability which involved numerous UPLC analysis runs of samples within a 24 hour period. A measure of accuracy was achieved by employing the mean percentage error, which is centered on the variances between actual and predicted concentrations. The percentage yield of extraction was calculated by comparison of the peak areas when extracted from plasma (AUC_{plasma}) and when extracted from standard solutions ($AUC_{standard\ solution}$) at an equal concentration using Equation 8.1:

$$\%\ Extraction\ Yield = \frac{AUC_{plasma}}{AUC_{standard\ solution}} \times 100$$

Equation 8.1

8.3.4. Construction of calibration curves for the quantification of sulpiride and sodium valproate release from the dual-layered oral device

Blank plasma samples were thawed at room temperature (±25°C). Aliquots (100μL) of blank plasma were transferred to polypropylene tubes and was then spiked with standard solutions of the model drugs (sulpiride/sodium valproate) and IS's (metocloperamide/ hydrochlorothiazide) at varying concentrations. The mixture was then vortexed for 2 minutes and the respective extraction procedure was performed described in *Chapter 8, Section 8.5.2*. The drug/IS peak area ratios were plotted against the corresponding drug concentration (ng/mL) and the statistical R^2 value was derived for the obtained curve.

8.4. Pharmacokinetic Modeling Employing Non-compartmental and Compartmental Algorithms

Based on the *in vitro* and *in vivo* release dynamics of sulpiride and sodium valproate from the respective components of the dual-layered oral device, compartmental analysis was performed utilizing pharmacokinetic data analysis and the use of PKSolver, a menu-driven add-in program for Microsoft Excel (Zhang et al., 2010). Polynomial regression analysis was employed for correlation of the observed and predicted values.

Compartmental analysis was applied so as to quantitatively evaluate and predict *in vivo* outcome of sulpiride and sodium valproate from the dual-layered oral device via modeling of the concentration-time data by means of an appropriate pharmacokinetic compartmental model. The dual-layered oral device was considered a single extravascular dose with the bioadhesive multilayered intestinal patch component instituting an absorption lag. For this purpose four pharmacokinetic algorithms were employed as follows:

- Non-compartmental
- One compartmental
- One compartmental with T_{lag}
- Two compartmental with T_{lag}

8.4.1. Pharmacokinetic analysis: *in vitro-in vivo* correlation establishment

WinNonLin® software (V5.3 with IVIVC Toolkit Build 20091211139, Pharsight Software, Statistical Consultants Inc., Apex, NC, USA) was used for the development of a level A IVIVC; where the input data included *in vitro* sulpiride and sodium valproate release data and *in vivo* plasma drug release data. A requirement for the evaluation of IVIVC data is development and validation. Thus, the development of a level A IVIVC model follows a two-stage process:

a) Deconvolution- where the observed fraction of drug absorbed is estimated based on the Wagner-Nelson method (Wang and Nedelam, 2002). After which the IVIVC model is developed utilizing the observed fraction of drug absorbed and the fraction of drug dissolved. Depending on the IVIVC model employed, the predicted fraction of drug absorbed is then calculated from the observed fraction of drug dissolved.

b) Convolution- where the predicted fraction of drug absorbed is then convolved/intertwine with the predicted concentrations initiating the convolution method. The predictability of a level a

correlation's focal point is estimation of the percentage prediction error (%PE) between the observed and predicted concentration profiles.

8.5. Results and Discussion

8.5.1. Behavioral evaluation of pig's post-surgical implantation of the jugular vein catheter and administration of the optimized formulations

Post-surgical implantation of the jugular catheter (day 1), the pigs were slightly lethargic due to the effects of the anesthesia. Once the anesthesia wore off the animals displayed their usual levels of activity and appetite comparative to behavior monitoring prior to surgery. Blood sampling proved to be non-complex and time efficient thus demonstrating the feasibility of using jugular catheters for this purpose. Administration of both the components of the dual-layered oral device to the animals showed no adverse effects thus substantiating their biocompatibilities; in addition the dosing procedure employed i.e. dosing of the respective layers of the dual-layered oral device separately, and not as part of a single dosing proved to be advantageous as there was a 100% survival rate amongst both study groups therefore eliminating the likely harm to the animal upon intra-gastric dosing of large doses.

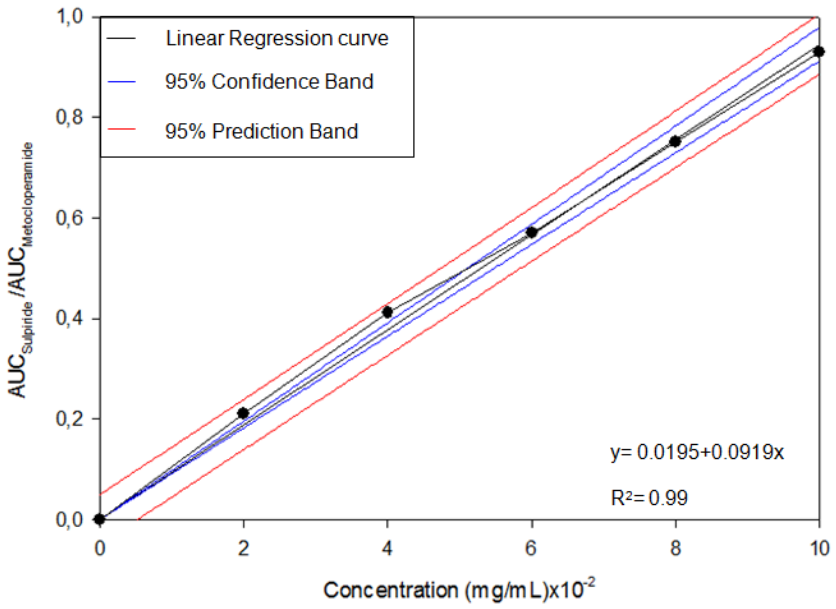
8.5.2. Validation of the extraction procedure

The mean variation of the intra-day and inter-day precision validation studies was determined to be 0.19% and 0.22% (sulpiride extraction) and 0.21% and 0.15% (sodium valproate extraction). Mean extraction yield of sulpiride and sodium valproate respectively from plasma was determined to be 93.5% and 91.3% (SD≤3.35 and 4.15 respectively). The liquid-liquid extraction procedures employed were thus verified as the optimum methodologies that provided a high degree of recovery of sulpiride and sodium valproate respectively.

8.5.3. *In vivo* release of sulpiride and sodium valproate in the Large White Pig model from the dual-layered oral device components

The UPLC calibration curves for plasma sulpiride and sodium valproate are depicted in Figure 8.7a and b. The typical chromatograms (Figure 8.8a and b) displays retention times of s 0.6 and 0.539 minutes for sulpiride and sodium valproate respectively.

a)



b)

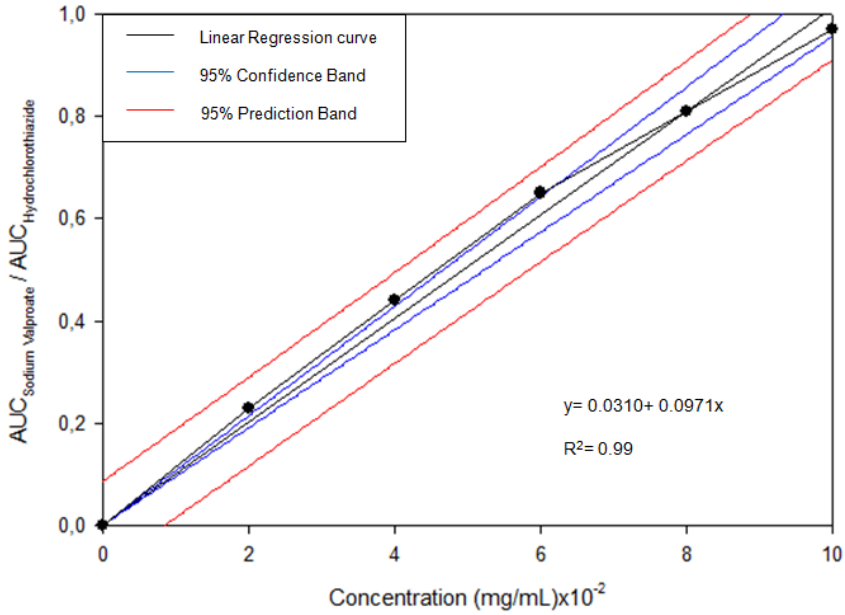
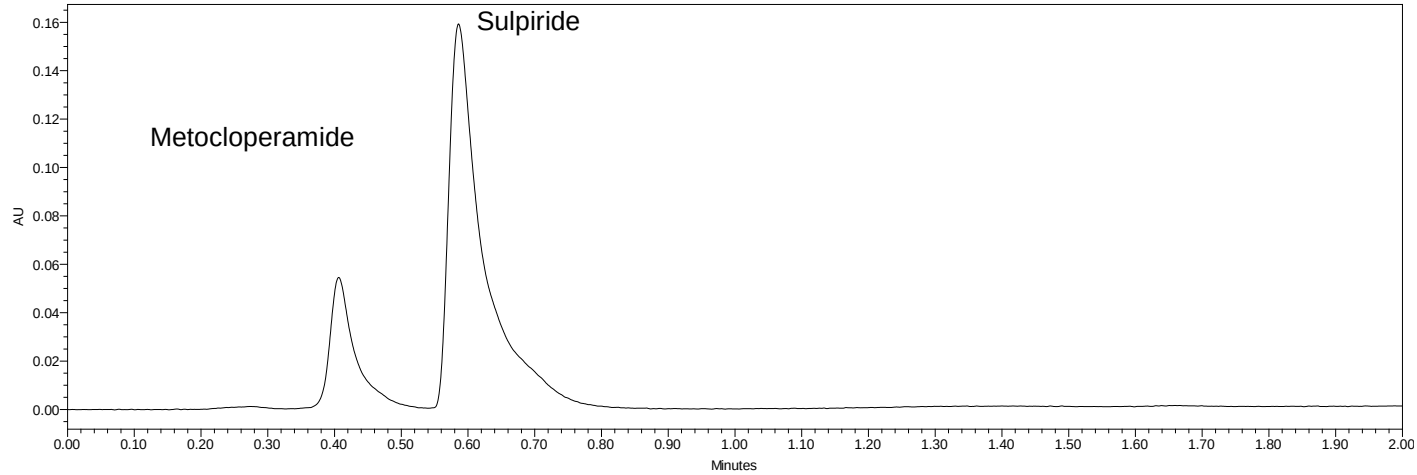


Figure 8.7: Calibration curves of a) sulpiride at 300nm and b) sodium valproate at 215nm.

(a)



(b)

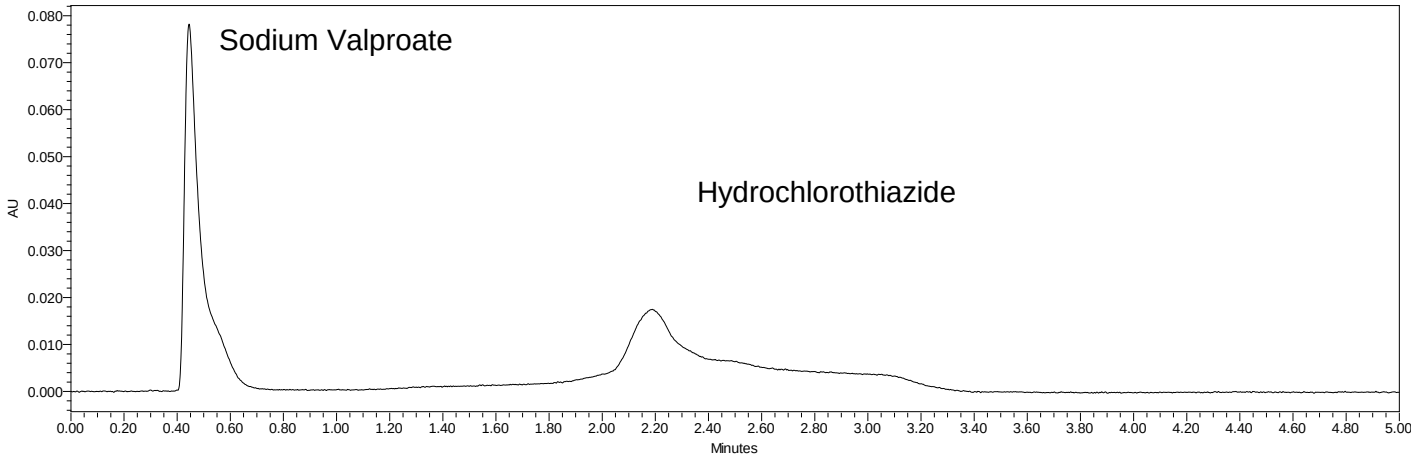


Figure 8.8: Typical chromatograms of a) sulpiride in plasma and b) sodium valproate in plasma; with their respective internal standards.

The comparative plasma concentration profiles of sulpiride display discernible differences when administered as the optimized s-IPN xerogel matrix oral device or as the conventional capsules as illustrated in Figure 8.9. Although conventional capsules achieved a higher maximum plasma concentration (C_{max}) of sulpiride (C_{max}= 842ng/mL) as compared to the optimized device, where a C_{max} of 830.58ng/mL was achieved, only the optimized device was able to achieve consistent or steady state plasma concentrations throughout the duration of the study (Figure 8.9). As a result, side effects experienced due to high drug concentrations are able to be avoided, ultimately greatly improving patient compliance. In order to achieve steady state concentrations, conventional capsules are most typically administered multiple times in the day, resulting in complicated treatment regimens. The optimized device is able to overcome the need for multiple doses, thus eliminating the need for complex treatment regimens.

For the conventional capsules it was noted that there was an initial ascension of plasma concentration after 0.5 hours, with a peak plasma concentration (C_{max} = 842ng/mL) being reached at approximately 6 hours. This was followed by a swift reduction in plasma concentration for a further 8 hours. Thus it can be confirmed that for the conventional system, most of the drug was released by an initial burst before 6 hours after administration. This may be due to the lack of controlling mechanisms present within the conventional systems, which are compressed powders of sulpiride coupled with formulation excipients embedded in a capsule.

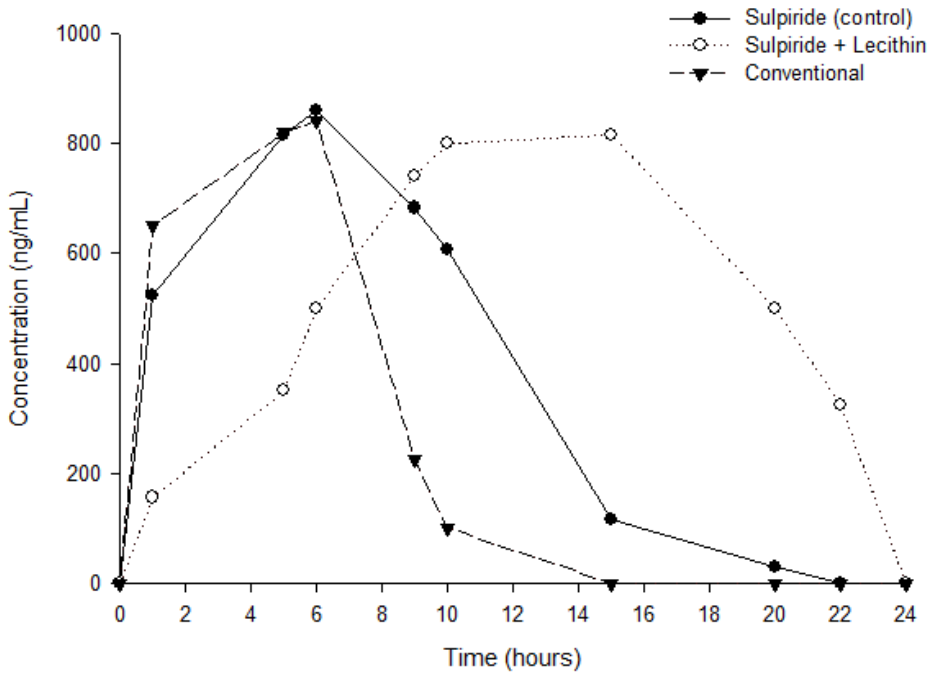


Figure 8.9: Plasma drug concentration profile depicting the release behavior over 24 hours of Control (Sulpiride alone), optimized s-IPN xerogel matrix oral device and, Conventional.

The control system tested comprised of the optimized s-IPN xerogel and sulpiride alone; a gradual release of drug was noted at the onset. The observed steady increase in drug release reached a C_{max} of 859ng/mL after 6 hours. The plasma levels decreased thereafter till the end of the 24 hour period. The control system displayed steady state drug release over the duration of the study, however, it did show release in the initial two hours similar to that of the conventional system.

The *in vivo* plasma concentration profiles of the optimized device and conventional capsules shown in Figure 8.9 shows that for the initial two hours post dosing, minimal sulpiride is released from the optimized device (211.09ng/mL) whereas a concentration of 700ng/mL is achieved from

conventional capsule within the same time period. The results obtained in the initial two hours subsequent to oral dosing provide the ultimate evidence of the efficiency of the optimized device in terms of site-specific drug delivery. Owing to enhanced site-specific drug delivery, a greater quantity of sulpiride is released in the intestine where a higher degree of absorption is attained. This can be seen from a comparison of the two hour blood sample; where the plasma concentration of sulpiride was noticeably lower (211.09ng/mL) from the optimized device, consistent with the time when the drug delivery system is yet to pass through the gastric region of the GIT, as opposed to the four hour blood sample (300ng/mL) corresponding to when the drug delivery system has entered the intestine.

Furthermore, the reduced quantity of sulpiride release in the gastric region allows for greater absorption and thus improved bioavailability. As illustrated in Figure 8.9, the optimized device achieved consistent plasma levels of sulpiride throughout the duration of the study as compared to conventional capsules, therefore demonstrating desirable release behavior of the optimized device in the large pig model. The low therapeutic levels of drug that were reached may be due to the *in vivo* absorption and distribution characteristics of the drug. According to literature, sulpiride has an overall low systemic bioavailability (Chitneni, et al., 2011) which is confirmable with the low C_{max} of sulpiride obtained. However, compared to the C_{max} observed for the conventional, the optimized device displayed an increase in bioavailability as well as prolonged release over the 24 hour test period.

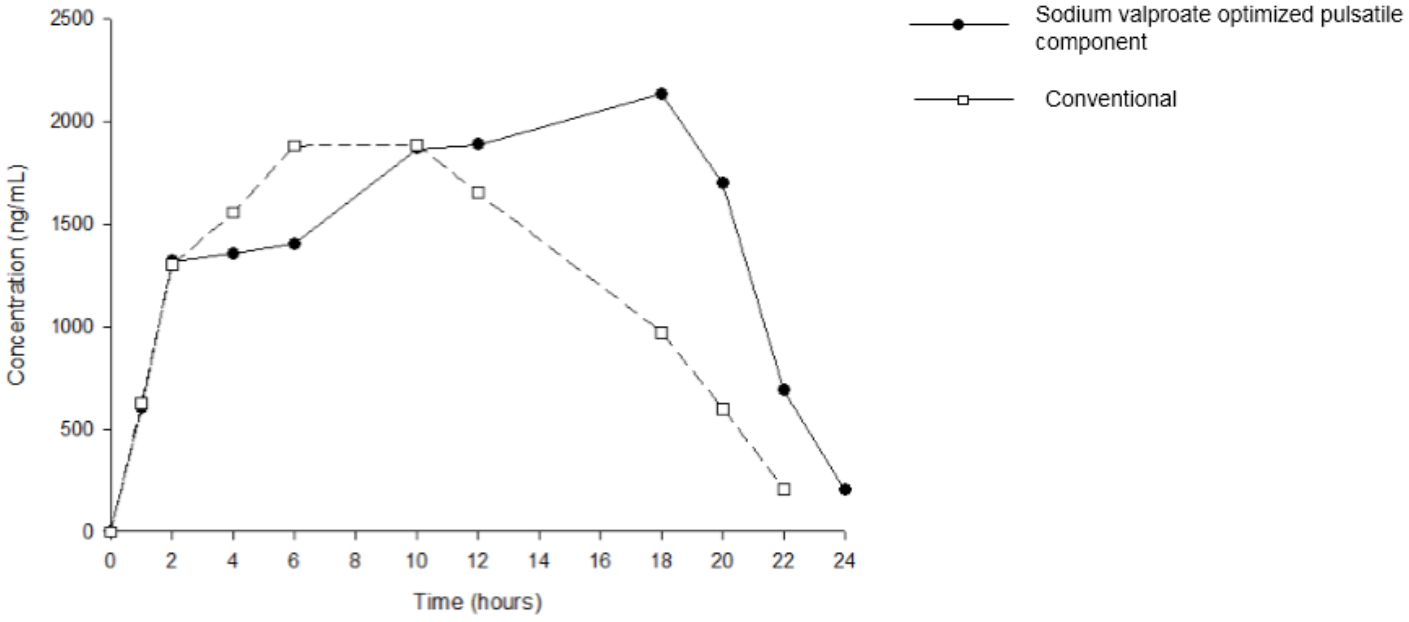


Figure 8.10: Plasma drug concentration profile depicting the release behavior over 24 hours of the optimized bioadhesive multilayered intestinal patch oral device pulsatile component and conventional 200mg.

The relative plasma concentration profiles of sodium valproate exhibit distinct differences when administered as the optimized bioadhesive multilayered intestinal patch oral pulsatile device component or as the conventional capsules as illustrated in Figure 8.10.

Conventional capsules achieved C_{max} of 1886.4ng/mL at 6.25 hours, whereas the optimized pulsatile release component reached a C_{max} of 2371.8ngmL at approximately 15.5 hours. The conventional system allowed for sustained release of sodium valproate over the 24 hour period. The efficiency and ability of the optimized system to release drug in a pulsatile, time controlled manner is advantageous and is made evident by the *in vivo* release profile shown in Figure 8.10. Pulsatile drug release differs from sustained release due to drug release occurring in a step wise manner in accordance with a time controlled system design, there is no constant level of drug as compared to sustained release, where drug concentrations remain constant. Due to the pattern of drug release achieved by the optimized pulsatile component of the dual-layered oral device the occurrence of adverse drug effects at high drug concentrations may be greatly reduced. Ultimately, the optimized pulsatile component will highly improve patient compliance. In order to achieve adequate therapeutic levels of drug the conventional system characteristically requires multiple administrations in a day, resulting in complicated treatment regimens and resistance. The combination of the optimized s-IPN xerogel matrix and the bioadhesive multilayered patch components into the single dual-layered oral device will significantly increase the therapeutic outcomes of schizoaffective patients, as an assemblage of improved patient compliance by means of the delivery of two bioactives in a single once daily dosage form and increased bioavailability will greatly enhance therapeutic management of schizoaffective disorder.

8.5.4. Interpretation of the extravascular compartmental and non-compartmental pharmacokinetic model analysis

The extravascular pharmacokinetic analysis results of the compartmental analysis for sulpiride and sodium valproate are presented in Tables 8.2 and 8.3 respectively. Evaluation of the pharmacokinetic analysis revealed that sulpiride release was best described by a one compartmental model without Tlag which displayed the most favorable AIC and SBC values determined via this algorithm (Table 8.2). The most idyllic sum of squares (SS) and standard error (SE) values were also determined for the one compartmental model (SS=124344.8; SE=143.95). The minimal values for SS and SE are an indication of a lower fit illustrating a low variability in data points. Assessment of the R^2 values and regression residuals (R observed-predicted) values, displayed a negligible difference of 0.03 between the one compartment model with Tlag and that of the one compartment model without Tlag.

Sodium valproate release was most appropriately by a one compartmental model without Tlag with the corresponding most affirmative AIC and SBC values (Table 8.3). The most ideal SS and SE values were also determined within the one compartmental model (SS=1433611.69; SE=423.32). There was an observed difference of 0.04 between the R^2 values of the compartmental models with and without Tlag.

Table 8.2: Compartmental analysis of plasma sulpiride data after extravascular input without and with lag.

Parameter	Units	Average Value	Diagnostics	Value
		Extravascular Model without Tlag		
A	ng/mL	6780.11	r obs-pre	0.904
k_a	1/h	0.1048	SS	124344.8
K_{10}	1/h	0.0799	WSS	124344.8
$t_{1/2ka}$	h	6.613	R^2	0.95
$t_{1/2k10}$	h	8.668	WR^2	0.95
V/F	(mg)/(ng/mL)	0.0311	SE	143.95
CL/F	(mg)/(ng/mL)/h	0.0024	AIC	111.58
T_{max}	h	10.889	SC	112.16
C_{max}	ng/mL	672.96		
AUC_{0-t}	ng/mL*h	11951.25		
AUC_{0-inf}	ng/mL*h	20103.76		
AUMC	Ng/mL*h^2	443217.75		
MRT	h	22.04		
Parameter	**Units**	**Average Value**	**Diagnostics**	**Value**
		Extravascular Model with Tlag		
A	ng/mL	17162.855	r obs-pre	0.987
k_a	1/h	0.266	SS	38444.2
K_{10}	1/h	0.2298	WSS	38444.2
$t_{1/2ka}$	h	0.000001	R^2	0.984
$t_{1/2k10}$	h	2.6033	WR^2	0.984
V/F	(mg)/(ng/mL)	3.0162	SE	98.03
CL/F	(mg)/(ng/mL)/h	0.0213	AIC	92.455
T_{max}	h	0.0048	SC	92.77
C_{max}	ng/mL	4.039		
AUC_{0-t}	ng/mL*h	928.76		
AUC_{0-inf}	ng/mL*h	9784.2		
AUMC	Ng/mL*h^2	10224.82		
MRT	h	8.1		

Table 8.3: Compartmental analysis of plasma sodium valproate data after extravascular input without and with lag.

Parameter	Units	Average Value	Diagnostics	Value
Extravascular Model without Tlag				
A	ng/mL	31736.1	r obs-pre	0.852
k_a	1/h	0.1209	SS	1433611.69
K_{10}	1/h	0.10029	WSS	1433611.69
$t_{1/2ka}$	h	5.7308	R^2	0.945
$t_{1/2k10}$	h	6.9109	WR^2	0.945
V/F	(mg)/(ng/mL)	0.0369	SE	423.32
CL/F	(mg)/(ng/mL)/h	0.0037	AIC	161.93
T_{max}	h	9.0661	SC	1630126
C_{max}	ng/mL	2182.86		
AUC_{0-t}	ng/mL*h	39926.92		
AUC_{0-inf}	ng/mL*h	54030.86		
AUMC	Ng/mL*h^2	985427.85		
MRT	h	18.23		
Parameter	**Units**	**Average Value**	**Diagnostics**	**Value**
Extravascular Model with Tlag				
A	ng/mL	17162.855	r obs-pre	0.987
k_a	1/h	0.266	SS	38444.2
K_{10}	1/h	0.2298	WSS	38444.2
$t_{1/2ka}$	h	0.000001	R^2	0.984
$t_{1/2k10}$	h	2.6033	WR^2	0.984
V/F	(mg)/(ng/mL)	3.0162	SE	98.03
CL/F	(mg)/(ng/mL)/h	0.0213	AIC	92.455
T_{max}	h	0.0048	SC	92.77
C_{max}	ng/mL	4.039		
AUC_{0-t}	ng/mL*h	928.76		
AUC_{0-inf}	ng/mL*h	9784.2		
AUMC	Ng/mL*h^2	10224.82		
MRT	h	18.2		

A: the zero time intercept associated with the Alpha phase (*an initial phase of rapid decrease in*

Plasma concentration due distribution)

ka: 1st order absorption rate constant

k10: Elimination rate constant

Tlag: Finite time taken for a drug to appear in systemic circulation following

Extravascular administration

$t^1/_2$ka: Absorption half-life rate constant

$t^1/_2$k10: Elimination half-life rate constants

V/F: The volume of distribution of the absorbed fraction

CL/F: The observed total body clearance for extravascular administration

Tmax: Time at which the maximum concentration (Cmax) is observed

Cmax: Maximum observed concentration occurring at Tmax

AUC0-t: Area Under the Curve (AUC) from the dosing time to the last measurable concentration

AUC0-inf: AUC from dosing time extrapolated to infinity

AUMC: Area Under the Moment Curve

MRT: *Mean Residence Time is the average amount of time the drug remains in a compartment or system*

Pharmacokinetic parameters for sulpiride determined by the one compartment model without Tlag depicted, a first order absorption rate constant (k_a) of 0.1048/h, an elimination rate constant of 0.0799/h, and an elimination half-life of 8.668/h. Additionally, the C_{max} was determined to be 672.96ng/mL with Tmax occurring at 10.889 hours. The indicated first order absorption rate constant confirmed the rapid transit of the oral device into the intestine, followed by fast absorption. The effectiveness of the optimized s-IPN xerogel component to provide the required concentration of sulpiride to exert effective antipsychotic effects was proved by the observed C_{max} and the MRT of 22.04 hours. The determined AUC_{0-t} and AUC_{0-inf} values also exhibited a difference of 8152.51 ng/mL*h, thus sulpiride clearance is relatively swift.

Pharmacokinetic compartmental analysis of the sodium valproate *in vivo* release determined by the one compartmental model without Tlag was found to be the best fit. This algorithm displayed a first order absorption rate constant of 1.209/h. A Cmax of 2182.86ng/mL was observed with a Tmax of 9.0661 hours. The effectiveness of the intestinal patch component of the dual-layered oral device to provide pulsatile drug release over a 24 hour period was shown by the observed MRT of 18.23 hours; thereby allowing for sufficient time for pulsatile release from the delivery system. The elimination half-life was noted to be approximately 6.9109/h. The AUC_{0-t} and AUC_{0-inf} (AUC_{0-t}=39926.92ng/mL/h^{-1}; AUC_{0-inf}=54030.80 ng/mL/h^{-1}) indicates elevated plasma drug levels, hence providing enhanced therapeutic efficacy. Results obtained via *in vivo* pharmacokinetic compartmental analysis of the dual-layered oral device components provided pertinent information on the gastric-emptying and transit time of the Large White Pigs used in the

study as well as absorption and elimination characteristics of sulpiride and sodium valproate respectively. Therapeutic levels of sulpiride for the Large White Pig was attained and maintained, whereas the therapeutic levels of sodium valproate were attained based on a time controlled design, with three pulses over 24 hours, ultimately proving the therapeutic efficiency and capability of the dual-layered oral device.

Table 8.4: Results of the non-compartmental analysis of plasma sulpiride and sodium valproate data after extravascular input.

Parameter	Unit	Value
Sulpiride Extravascular non-compartmental model		
λ_z	1/h	0.1251
$t_{1/2}$	h	5.536
T_{max}	h	15
C_{max}	ng/mL	816.34
T_{lag}	h	0
$C_{last\ obs}/C_{max}$		0.3979
AUC_{0-t}	ng/mL*h	12303.26
$AUC_{0-inf-obs}$	ng/mL*h	14898.35
$AUC_{0-t/0-inf-obs}$		0.825
$AUMC_{0-inf-obs}$	ng/mL*h^2	229288.5
$MRT_{0-inf-obs}$	h	15.390
Parameter	Unit	Value
Sodium Valproate Extravascular non-compartmental model		
λ_z	1/h	0.1426
$t_{1/2}$	h	4.8617
T_{max}	h	12
C_{max}	ng/mL	2156.64
T_{lag}	h	0
$C_{last\ obs}/C_{max}$		0.4177
AUC_{0-t}	ng/mL*h	40882.6
$AUC_{0-inf-obs}$	ng/mL*h	47701.45
$AUC_{0-t/0-inf-obs}$		0.8661
$AUMC_{0-inf-obs}$	ng/mL*h^2	688218.6
$MRT_{0-inf-obs}$	h	14.58

λz: *1st order rate constant of the terminal (log-linear) portion of the curve terminal elimination rate constant*

$t^1/_2$: Terminal phase half-life. The time it takes for the concentration levels to fall to 50% of their value.

Clast: The last quantifiable concentration following dosing

AUC0-inf obs: AUC from dosing time extrapolated to infinity based on the last observed concentration

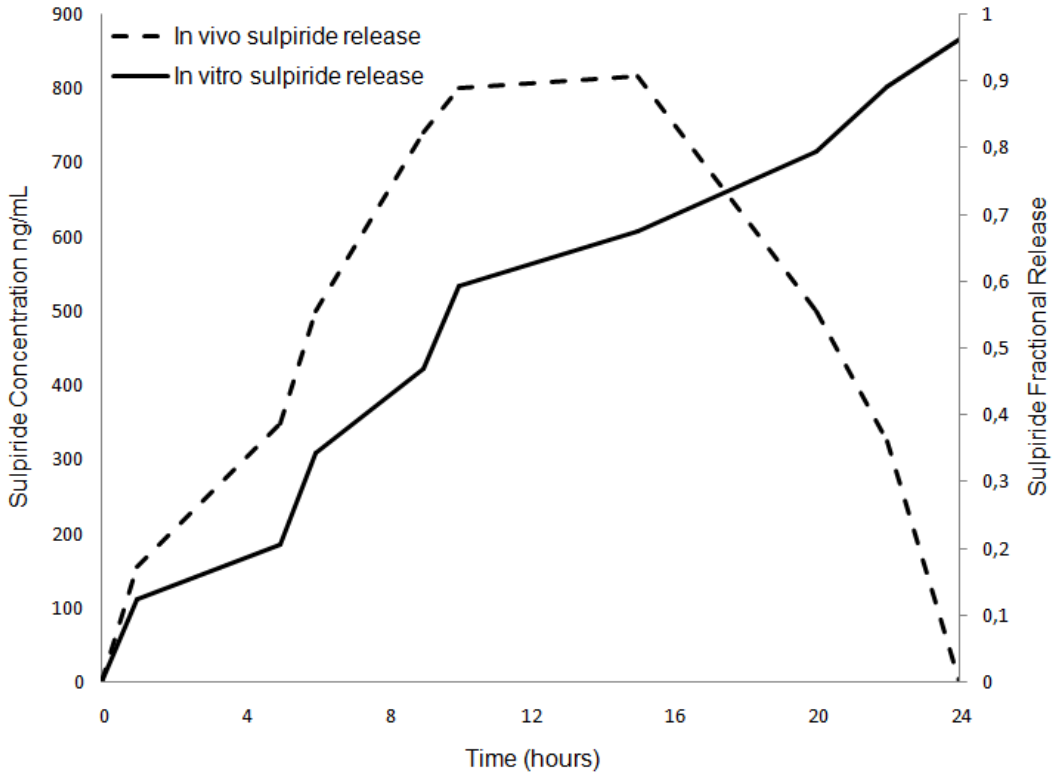
AUMC0-inf obs: AUMC extrapolated to infinity based on the last observed concentration

MRT0-inf obs: *MRT extrapolated to infinity*

8.5.5. Establishment of an *in vitro-in vivo* correlation

A level A IVIVC was established for the evaluation of sulpiride and sodium valproate release, which utilizes the data provided via the *in vitro* dissolution and *in vivo* absorption curves. The amount of sulpiride and sodium valproate absorbed following administration of the respective ODLS layers were calculated by employing the Wagner Nelson method by means of the linear trapezoidal rule. For the construction of a Level A IVIVC, the concentration of drug absorbed up to time t was plotted against the fractional release of drug *in vitro* (Figure 8.11a and b; Figure 8.12a and b).

(a)



(b)

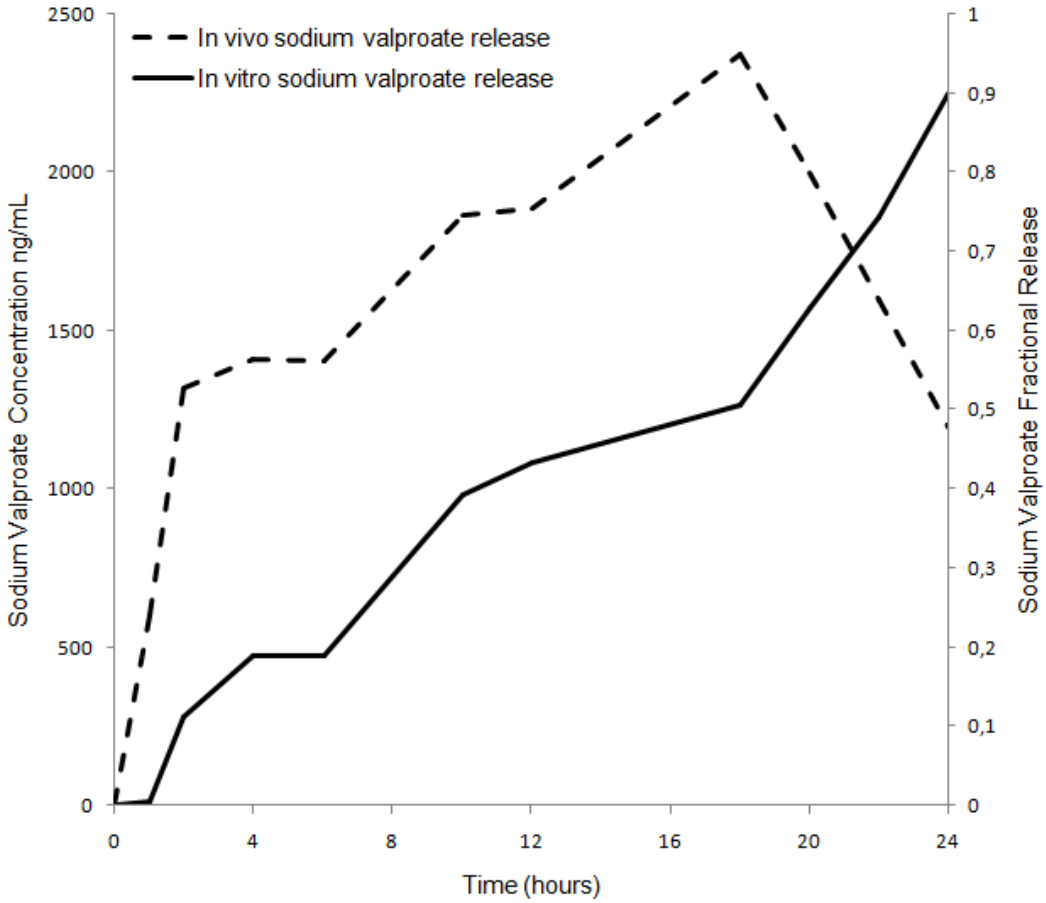
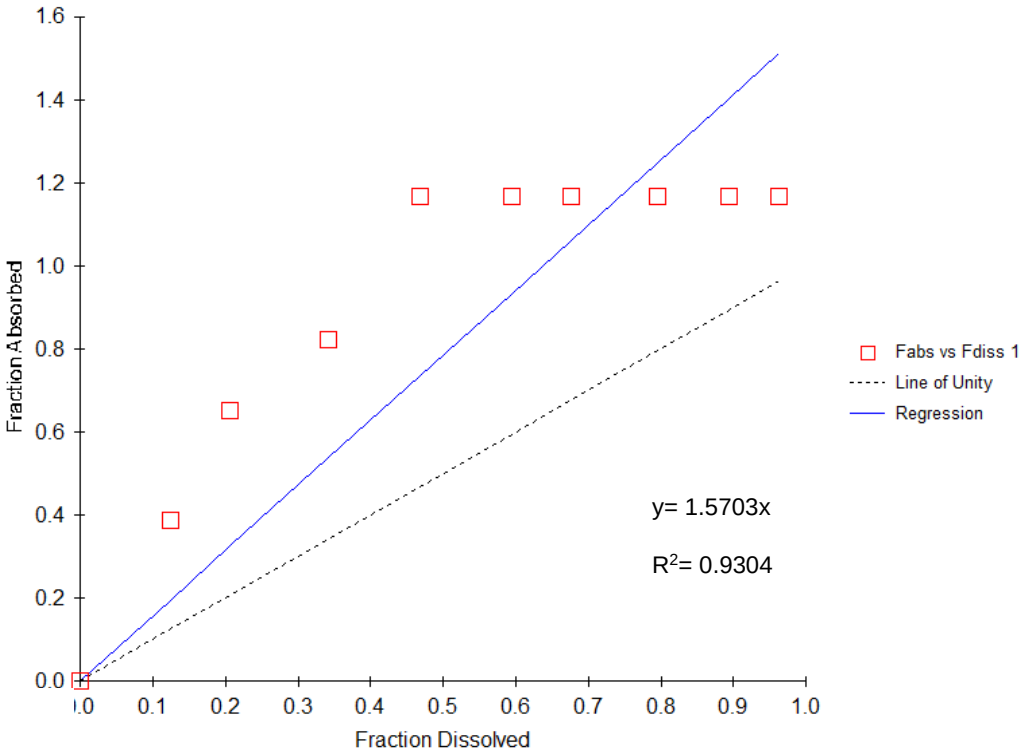


Figure 8.11: Drug release profiles of the *in vitro* and *in vivo* a) sulpiride and b) sodium valproate release from the Dual-layered oral system obtained via deconvolution analysis.

(a)



(b)

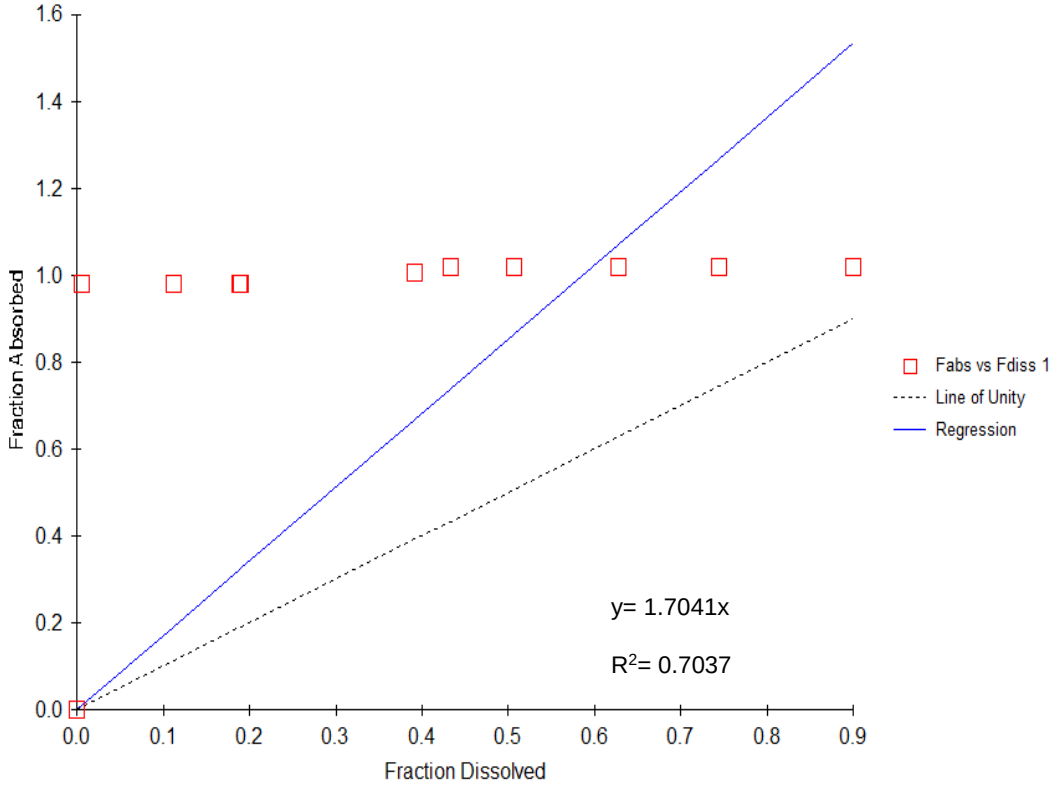


Figure 8.12: Regression plot showing the relationship between the fraction of (a) sulpiride and (b) sodium valproate absorbed *in vivo* and the fraction released *in vitro.*

The pharmacokinetic data obtained from this analysis complies with the requirements of deconvolution via convolution, as sulpiride and sodium valproate release from the Dual-layered oral system was determined to via a one-compartmental pharmacokinetic model without T_{lag}.

Level A IVIVC analysis for sulpiride and sodium valproate yielded levy plots with an R^2 values of 0.9486 and 0.9843 respectively. Thus *in vitro* data was predictive of *in vivo* data with 94.86 % and 98.43% accuracy respectively for sulpiride and sodium valproate. Although the plots determined were not precisely superimposable, based on qualitative parameters, a Level A correlation was utilized. The observed results show a quicker *in vivo* absorption compared to the *in vitro* dissolution, this may be attributed to the gastrointestinal transit time (simulated intestinal conditions) employed during *in vitro* studies which did not directly translate to release *in vivo.* It was also noted that the enteric polymer coating of the Dual-layered oral system displayed a faster rate of swelling and dissolution within the context of *ex vivo* studies compared to *in vitro* analysis. The high protein binding capacity and bioavailability of sodium valproate could also be a contributing factor, with display of a steeper gradient in the sodium valproate *in vivo* profile, when compared to relative the *in vitro* profile. The prompt absorption of sulpiride may be attributed to the improved permeability as discussed in *Chapter 7, Section 7.3.8*.

8.6. Concluding Remarks

The effectiveness of the Dual-layered oral system was evaluated via the *in vivo* analysis in a Large White pig model. Site-specific delivery was achieved via the use of gastro-resistant enteric tablet coating solution as well bioadhesive polymers. The development of individual system layers ensures individualistic drug release profiles and avoidance of drug interactions. Evaluation of the Dual-layered oral system thus accurately proved that the formulation is effective in delivering sulpiride in a sustained pattern with an improvement in bioavailability with the use of P-gp efflux pump inhibitory excipients; and the pulsatile release of sodium valproate in a time controlled manner. Ultimately, the formulation allows for the combination treatment of an antipsychotic and mood stabilizing agent in a single dosage form with individually therapeutic suited release profiles.

CHAPTER 9

CONCLUSIONS, RECOMMENDATIONS AND FUTURE OUTLOOK

9.1. Conclusions

The design and development of an innovative and novel drug delivery system by combining a myriad of pharmaceutical and scientific techniques has been demonstrated within the context of this study with the objective of overcoming the current limitations in clinical practices with the eventual aim of improving patient compliance and therapeutic outcomes in the treatment of schizoaffective disorder.

Poor patient compliance has been acknowledged as a foremost cause of drug resistance in many disease states. The basis of poor patient compliance can principally be accredited to complex dosing and treatment regimens made obligatory on patients as an element of a standard therapeutic intervention as is the case in the treatment of schizoaffective disorder. This creates a greater obstacle to clinical outcomes as patients suffering from schizophrenia are already limited in the performance of normal daily skills.

The dual-layered oral device formulated in this study has been developed and comprehensively analysed with the intention of overcoming the issues of complex regimens and poor bioavailability in the treatment of schizoaffective disorder. This has been undertaken via development of an optimized Dual-layered system with individualistic mechanisms and drug release kinetics for 2 bioactive agents. The s-IPN xerogel layer incorporated polymers known for P-glycoprotein efflux transporter inhibition so as to increase bioavailability of sulpiride and allow for sustained drug release; in addition the pulsatile release layer of the Dual-layered system encompassed lectins and N-acetyl-cysteine to allow for superior bioadhesion and allow for enhanced residence time for pulsatile delivery of sodium valproate.

The dual-layered oral device components were proven effective via advanced and progressive *in vitro*, *ex vivo* and *in vivo* analyses. *In vitro* release studies performed determined that the dual-layered oral device components acted independently of each other once exposed to intestinal conditions (the respective system layers detach from each other). *In vitro* characterization was additionally utilized to ascertain pharmaceutical stability. *Ex vivo* studies were performed to determine the permeation and adhesion properties of the bioadhesive intestinal patch component of the dual-layered oral device.

Furthermore, *in vivo* studies were undertaken on the optimized dual-layered oral system components. The optimized components were individually administered to pigs and drug release

profiles were generated according to the concentration of drugs in plasma. *In vivo* results showed a definite difference in plasma profiles between the respective conventional and optimized component formulations. For sulpiride, release was noticeably more controlled and provided zero-order release as compared to the conventional. Thus, the optimized s-IPN xerogel component provided sustained release of sulpiride. Release of sodium valproate was distinctly different from that of the conventional system, as the optimized intestinal patches were intended for pulsatile delivery of sodium valproate. The release profile of sodium valproate followed an ideal triphasic release pattern, with maintenance of plasma concentrations within the required therapeutic levels with the added benefit of avoiding resistance to therapy.

Pharmacokinetic modelling of *in vivo* results determined that sulpiride and sodium valproate release were best described by a one compartmental model without T_{lag}, with IVIVC displaying an ideal relation.

This thesis thus focused on the fabrication through to preclinical analyses of a Dual-layered oral system for the concurrent and idiosyncratic administration of sulpiride and sodium valproate. In concise terms, via this research study a novel Dual-layered oral system has been developed and extensively characterized, with the prospect of the system clinically enhancing therapeutic outcomes associated with schizoaffective therapeutic regimens.

9.2. Recommendations

Amid the design and development all the way through to the analysis of the dual-layered oral system components, many points of interest and challenges in regard to schizophrenia therapy were considered and overcome. Although the efficacy and accomplishment of the dual-layered oral device components have been extensively analysed up till a preclinical standpoint, other factors will have to be considered for production advancement. Despite the dual-layered system being relatively cost-effective to formulate, the array of pharmaceutical steps required for the final system assemblage would necessitate specialized equipment for manufacture and general use to the public. The use of commercial tablet compressors and dyes would be greatly useful and advantageous in the assembly of the dual-layered tablet, as with the use of more specialized machinery the dual-layered device may be reduced in size and thus be made more acceptable to the patient.

With the success of the dual-layered system detailed in this study, the adaptability to scaling of the system can be evaluated. Sulpiride and sodium valproate were selected as model drugs due to their common use in schizoaffective disorder treatment regimens and the limitations associated with them, which has been addressed. However, alternative drug agents may be incorporated into

the dual-layered system with variations in drug combinations, provided they require the drug release kinetics the respective layers were designed for i.e. sustained and pulsatile release.

9.3. Future Outlook

- While the drug delivery system has been developed for the use in treatment of schizoaffective disorder, it is not exclusive to this specific disease state as the system may be loaded with drugs of varying solubility.

- The system also permits the versatility of combining two bioactives in a single dosage form, this may be applied to treatment of a single disease state requiring multiple drugs or to the treatment of 2 different disease states or disorders.

- The system may also be applied to combine two drugs that are pharmaceutically incompatible within a single dosage form due to the functionality of the drug delivery system (i.e. respective system layers detach upon contact with intestinal environment and act independently of each other).

- The addition of patches within the intestinal patch layer of the system may be explored, additional patches may be incorporated with crosslinking agents so as to allow for in situ crosslinking to further regulate drug release rate or for protection of incorporated drugs such as proteins.

- The system may be modified to release drug based on varying stimuli so as to further monitor and control the drug release kinetics, such as hormonal levels, pH, and thermal variations and based on the circadian rhythms of a specific disease state.

- Furthermore, the individualistic action of the device components allows the flexibility of employing either of the optimized system layers separately for their respective functions.

Therefore, the research generated within the current study will provide crucial techniques, data and concepts that can be tailored and modified to fit various pharmaceutical research endeavours.

10. REFERENCES

Adel, A.M., Abou-Youssef, H., El Gendy, A.A., Nada, A.M., (2010). Carboxymethylated cellulose hydrogel sorption, behavior, and characterization. *Journal of Natural Science*, **8**, 8.

Agarwal, A., Lariya, N., Saraogi, G., Dubey, N., Agrawal, H., and Agrawal, G. P., (2009). Nanoparticles as novel carrier for brain delivery: a review. *Current Pharmaceutical Design*, **15 (8)**, 917– 925.

Ahuja, G and Pathak, K., (2009). Porous carriers for controlled/modulated drug delivery. *Indian Journal of Pharmaceutical sciences*, **71**, 599-607.

Akhgari, A., Abbaspour, M.R., Rezaee, S., Kuchak, A., (2011). Evaluation of the swelling, Erosion, and Drug release from polysaccharide matrix tablets based on Pectin and Inulin. *Jundishopur Journal of Natural Pharmaceutical Products*, **6(1)**, 51-58.

Aller, S. G., Yu, J., Ward, A., et al., (2009). Structure of P-glycoprotein reveals a molecular basis for poly-specific drug binding. *Science*, **323 (5922)**, 1718–1722.

Almeida, N., Rakesh, L., Zhao, J., (2014). Monovalent and divalent salt effects on thermogelation of aqueous hypromellose solutions. *Food Hydrocolloids*, **36**, 323-331.

Al-Mohizea, A. M., (2010). Influence of intestinal efflux pumps on the absorption and transport of furosemide. *Saudi Pharmaceutical Journal*, **18 (2)**, 97–101.

American Psychiatric Association, (1994). *Diagnostic and Statistical Manual of Mental Disorders*, American Psychiatric Association, Washington, DC, USA, 4th edition.

Anal, A.K., (2007). Time-Controlled pulsatile delivery systems for bioactive compounds. *Recent patents on drug delivery and formulation*, **1**, 73-79.

Angadi, S.C., Manjeshwar, L.S., Aminabhavi, T.M., (2010). Interpenetrating polymer network blend microspheres of chitosan and hydroxyethyl cellulose for controlled release of isoniazid. *International Journal of Biological Macromolecules,* **47**, 171-179.

Aouali, N., Eddabra, L., Macadr´e, J., and Morjani, H., (2005). Immunosuppressors and reversion of multidrug-resistance. *Critical Reviews in Oncology/Hematology*, **56 (1)**, 61–70.

Azeredo, H.M.C., Kontou-Vrettou, C. Moates, G.K., Wellner, N., Cross, K., Pereira, P.H.F., Waldron, K.W., (2015). Wheat straw hemicellulose films as affected by citric acid. *Food Hydrocolloids*, **50**, 1-6.

B´eduneau, A., Saulnier, P., Anton, N., et al., (2006). PEGylated nanocapsules produced by an organic solvent-free method: evaluation of their stealth properties. *Pharmaceutical Research*, **23(9)**, 2190–2199.

Bakde, B.V., Channawar, M., Chandewar, A.V., Mishra, B., (2012). Gastric retentive controlled drug delivery: an overview. *International Journal of Pharmaceutical and Chemical Sciences,* **1(1)**, 156-163.

Banerjee, S., Ray, S., Maiti, S., Sen, K.K., Bhattacharyya, U.K., Kaity, S., Ghosh, A., (2010). Interpenetrating Polymer Network (IPN): A novel biomaterial. *International Journal of Applied Pharmaceutics*, **2(1)**, 28-34.

Bansal, T., Akhtar, N., Jaggi, M., Khar, R. K., and Talegaonkar, S., (2009). Novel formulation approaches for optimizing delivery of anticancer drugs based on *P*-glycoprotein modulation. *Drug Discovery Today*, **14 (21-22)**, 1067–1074.

Barnes, T.R.E., Davison, S., Ferrier, I.N., et al., (2006). Consensus Statement on High Dose Anti-Psychotic Medication.

Bartels, A. L., Kortekaas, R., Bart J., et al., (2009). Blood-brain barrier P-glycoprotein function decreases in specific brain regions with aging: a possible role in progressive neurodegeneration. *Neurobiology of Aging*, **30 (11)**, 1818–1824.

Bartels, A. L., Willemsen, A. T.M., Kortekaas, R., et al., (2008). Decreased blood-brain barrier P-glycoprotein function in the progression of Parkinson's disease, PSP and MSA. *Journal of Neural Transmission*, **115 (7)**, 1001–1009.

Barzegar-Jalali, M., Alaei-Beirami, M., Javadzadeh, Y., Mohammadi, G., Hamidi, A., Andalib, S., Adibkia, K., (2012). Comparison of physicochemical characteristics and drug release of diclofenac sodium–eudragit® RS100 nanoparticles and solid dispersions. *Powder Technology*, **219**, 211–216.

Bassett, D.R., Hamilec, E., (2009). Process Bulletin, Emulsion Polymerization, APV, Emulsion polymers and Emulsion Polymerization. *ACS Symposium Series,* **165**.

Batrakova, E. V., Li, S., Vinogradov, S. V., Alakhov, V. Y., Miller, D. W., and Kabanov, A. V., (2001). Mechanism of pluronic effect on Pglycoprotein efflux system in blood brain barrier: contributions of energy depletion and membrane fluidization. *Journal of Pharmacology and Experimental Therapeutics*, **299 (2)**, 483–493.

Batrakova, E. V., Li, S., Li, Y., Alakhov, V. Y., and Kabanov, A. V., (2004). Effect of pluronic P85 on ATPase activity of drug efflux transporters. *Pharmaceutical Research*, **21 (12)**, 2226– 2233.

Batrakova, E. V., Miller, D. W., Li, S., Alakhov, V. Y., Kabanov, A. V., and Elmquist, W. F., (2001). Pluronic P85 enhances the delivery of digoxin to the brain: in vitro and in vivo studies. *The Journal of Pharmacology and Experimental Therapeutics*, **296 (2)**, 551–557.

Bebawy, M. And Chetty, M., (2008). Differential pharmacological regulation of drug efflux and pharmacoresistant schizophrenia. *BioEssays*, **3 (2)**, 183–188.

Belcastro, V., D'Egidio, C., Striano, P., Verrotti, A., (2013). Metabolic and endocrine effects of valproic acid chronic treatment. *Epilepsy Research*, **107**, 1-8.

Beloqui, A., Solinís, M.Á., Gascón, A.R., del Pozo-Rodríguez, A., des Rieux, A., Préat, V., (2013). Mechanism of transport of saquinavir-loaded nanostructured lipid carriers across the intestinal barrier. *Journal of Controlled Release*, **166**, 115–123.

Bernkop-Schnurch, A., Hornof, M., and Zoidl, T., (2003). Thiolated polymers— thiomers: synthesis and in vitro evaluation of chitosan- 2-iminothiolane conjugates. *International Journal of Pharmaceutics*, **260 (2)**, 229–237.

Bhadwaj, V., Harit, G., Kumar, S., (2012). Interpenetrating Polymer Network (IPN): Novel Approach in Drug Delivery. *International Journal of Drug Development and Research*, **4(3)**, 41-54.

Blasi, P., Giovagnoli, S., Schoubben, A., Ricci, M., and Rossi, C., (2007). Solid lipid nanoparticles for targeted brain drug delivery. *Advanced Drug Delivery Reviews*, **59 (6)**, 454–477.

Boulton, D.W., DeVane, C. L., Liston, H. L., and Markowitz, J. S., (2002). In vitro P-glycoprotein affinity for atypical and conventional antipsychotics. *Life Sciences*, **71 (2)**, 163–169.

Brunet, B., Doucet, C., Venisse, N., Hauet, T., Hébrard, W., Papet, Y., Mauco, G. and Mura, P., Validation of large white pig as an animal model for the study of cannabinoids metabolism: application to the study of the distribution in tissues. *Forensic Science International,* **161**, 169-174.

Cappello, B., DeRosa, G., Giannini, L., (2006). Cyclodextrin containing polyethylene oxide tablets for the delivery of poorly soluble drugs: Potential as buccal delivery system. *International Journal of Pharmaceutics,* **319**, 63-70.

Chavanpatil, M. D., Khdair, A., Gerard, B., et al., (2007). Surfactant-polymer nanoparticles overcome P-glycoprotein-mediated drug efflux. *Molecular Pharmaceutics*, **4, (5)**, 730–738.

Chen, Y.C., Ho, H.O., Lee, T.Y., Sheu, M.T., (2013). Physical characteristics and sustained release profiling of gastroretentive drug delivery systems with improved floating and swelling capabilities. *International Journal of Pharmaceutics*, **441**, 162-169.

Chiba, R., Soukura, M., Tatsuta, S., (2011). Liquid Chromatography solid phase extraction and determination of Sulpiride in human serum by high performance liquid chromatography using electro generated chemiluminescence detection. *Analytical* Letters, **44,** 1559-1569.

Chikh, L., Delhorbe, V., Fichet, O., (2011). (Semi-) Interpenetrating polymer networks as fuel cell membranes. *Journal of Membrane Science*, **368**, 1-17.

Chitneni, M., Peh, K.K., Darwis, Y., Abdulkarim, M., Abdullah, G.Z., Qureshi, M.J., (2011). Intestinal Permeability Studies Of Sulpiride Incorporated Into Self-Microemulsifying Drug Delivery System (Smedds). *Pakistan Journal of Pharmaceutical. Sciences,* **24**, 113-121.

Chiu, C.T., Wang, Z., Hunsberger, J.G., Chuang, D.M., (2013). Therapeutic Potential of Mood Stabilizers Lithium and Valproic acid: Beyond Bipolar Disorder. *Pharmacological Reviews,* **65**, 105-142.

Choo, E. F., Kurnik, D., Muszkat, M., et al., (2006). Differential in vivo sensitivity to inhibition of P-glycoprotein located in lymphocytes,] testes, and the blood-brain barrier. *Journal of Pharmacology and Experimental Therapeutics*, **317 (3)**, 1012–1018.

Choonara, Y.E., Pillay, V., Carmichael, T., Danckwerts, M.P., (2006). An in vitro study of the design and development of a novel doughnut-shaped Minitab let for intraocular implantation. *International Journal of Pharmaceutics*, **310**, 15–24.

Coates, J., (2000). Interpretation of Infrared Spectra, a Practical Approach. *Encyclopedia of Analytical Chemistry*, 10815–10837.

Constantinides, P. P., and Wasan, K. M., (2007). Lipid formulation strategies for enhancing intestinal transport and absorption of Pglycoprotein (P-gp) substrate drugs: In vitro/in vivo case studies. *Journal of Pharmaceutical Sciences*, **96 (2)**, 235– 248.

Coviello, T., Matricardi, P., Marianecci, C., Alhaique, F., (2007). Polysaccharide hydrogels for modified release formulations. *Journal of Controlled Release*, **119**, 5-24.

Covielloa, T., Alhaiquea, F., Parisia, C., Matricardia, P., Bocchinfusob, G., Grassi, M. A., (2005). New polysaccharidic gel matrix for drug delivery: preparation and mechanical properties. *Journal of Controlled Release,* **102**, 643–656.

Cui, D., Xu, Q., GU, S., Shi, J., and Che, X., (2009). PAMAM-drug complex for delivering anticancer drug across blood-brain barrier in-vitro and in-vivo. *African Journal of Pharmacy and Pharmacology*, **3 (5)**, 227–233.

D'Emanuele, A., Jevprasesphant, R., Penny, J., and Attwood, D., (2004). The use of a dendrimer-propranolol prodrug to bypass efflux transporters and enhance oral bioavailability. *Journal of Controlled Release*, **95 (3)**, 447–453.

Da Fonseca, L.S., Silveir, R.P., Debon, A.M., (2008).Nanocapsule@ Xerogel microparticles containing sodium Diclofenac: A new Strategy to control the release of drugs. *International Journal of Pharmaceutics*, **358**, 292-295.

Dali, M.M., Moench, P.A., Mathias, N.R., Stetsko, P.I., Heran, C.L. and Smith, R.L., (2006). A rabbit model for sublingual drug delivery: comparison with human pharmacokinetic studies of propranolol, verapamil and captopril. *Journal of Pharmaceutical Sciences*, **95** 37–44.

Danson, S., Ferry, D., Alakhov, V., et al., (2004). Phase I dose escalation and pharmacokinetic study of pluronic polymer-bound doxorubicin (SP1049C) in patients with advanced cancer. *British Journal of Cancer*, **90 (11)**, 2085–2091.

Dash, S., Murthy, P.N., Nath, L., Chowdhury, P., (2010). Kinetic Modeling on Drug Release from Controlled Drug Delivery Systems. *Acta Poloniae Pharmaceutica ñ Drug Research.,* **67**, 217-223.

Davis, S.S., (2005). Formulation Strategies for absorption windows. *Drug Discovery Today*, **10(4)**, 249-257.

de Klerk, O. L., M. Willemsen, A. T., Bosker, F. J., et al., (2010). Regional increase in P-glycoprotein function in the blood-brain barrier of patients with chronic schizophrenia: a PET study with [11C] verapamil as a probe for P-glycoprotein function. *Psychiatry Research—Neuroimaging*, **183 (2)**, 151–156.

de van Wetering, K., Burkon, A., Feddema, W., et al., (2009). Intestinal breast cancer resistance protein (BCRP)/Bcrp1 and multidrug resistance protein 3 (MRP3)/Mrp3 are involved in the pharmacokinetics of resveratrol. *Molecular Pharmacology*, **75 (4)**, 876–885.

Demeule, M., R´egina, A., Jodoin, J., et al., (2002). Drug transport to the brain: key roles for the efflux pump P-glycoprotein in the blood brain barrier. *Vascular Pharmacology*, **38 (6)**, 339– 348.

Doan, K. M. M., Humphreys, J. E., Webster, L. O., et al., (2002). Passive permeability and P-glycoprotein-mediated efflux differentiate central nervous system (CNS) and non-CNS marketed drugs. *The Journal of Pharmacology and Experimental Therapeutics*, **303 (3)**, 1029–1037.

Dodou, D., Breedveld, P., Wieringa, P, A., (2005). Mucoadhesives in the gastrointestinal tract: revisiting the literature for novel applications. *European Journal of Pharmaceutics and Biopharmaceutics,* **60**, 1-16.

Doran, A., Obach, R. S., Smith, B. J., et al., (2005). The impact of Pglycoprotein on the disposition of drugs targeted for indications of the central nervous system: evaluation using the MDR1A/1B knock out mouse model. *Drug Metabolism and Disposition*, **33 (1)**, 165–174.

Du Toit, L.C. A Bioresponsive Polymeric Implant for Site-Specific Prolonged Drug Delivery. A thesis submitted to the Faculty of Health Sciences, University of the Witwatersrand, in fulfilment of the requirements for the degree of Doctor of Philosophy, 2013.

Du¨rig, T and Fassihi, R., (2002). Guar-based monolithic matrix systems: effect of ionizable and non-ionizable substances and excipients on gel dynamics and release kinetics. *Journal of Controlled Release*, **80**, 45–56.

Dureja H., et al., 2001; Patel, H. J., Patel, J. S., Desai, B. G., Patel, K. D, Permeability studies of anti-hypertensive drug amlodipine besilate for transdermal delivery, Asian *Journal of Pharmaceutical and Clinical Research*, 3(1), 2010, 31-34.

El Ela, A. A., H¨artter, S., Schmitt, U., Hiemke, C., Spahn- Langguth, H., and Langguth, P., (2004). Identification of P-glycoprotein substrates and inhibitors among psychoactive compounds—implications for pharmacokinetics of selected substrates. *Journal of Pharmacy and Pharmacology*, **56 (8)**, 967–975.

El-Kattan, A., and Varma, M., (2012). Oral absorption, intestinal metabolism and human oral bioavailability. In *Topics on Drug Metabolism*, Pharmacokinetics, Dynamics and Metabolism Department, Pfizer, NewYork, NY, USA, 1–34.

Elsinga, P. H., Hendriks, N. H., Bart, J., Vaalburg, W., and Van Waarde, A., (2004). PET studies on P-glycoprotein function in the blood brain barrier: how it affects uptake and binding of drugs within the CNS. *Current Pharmaceutical Design*, **10(13)**, 1493–1503.

Escudero, J.J., Ferrero, C., Jiménez-Castellanos, M.R., (2010). Compaction properties, drug release kinetics and fronts movement studies from matrices combining mixtures of swellable and inert polymers. II. Effect of HPMC with different degrees of methoxy/hydroxypropyl substitution. *International Journal of Pharmaceutics*, **387**, 56–64.

Estudante, M., Morais, J. G., Soveral, G., and Benet, L. Z., (2013). Intestinal drug transporters: an overview. *Advanced Drug Delivery Reviews*, 65 (10), 1340–1356.

Falkai, P., and M¨oller, H.-J., (2012). Neurobiology of schizophrenia: from outcome to pathophysiological insights. *European Archives of Psychiatry and Clinical Neuroscience*, **262 (2)**, 93–94.

Fardel, O., Lecureur, V., and Guillouzo, A., (1996). The P-glycoprotein multidrug transporter. *General Pharmacology: The Vascular System*, 27 **(8)**, 1283–1291.

Felton, L.A., (2013). Mechanisms of polymeric film formation. *International Journal of Pharmaceutics*, **457**, 423-427.

Feng, B., Mills, J. B., Davidson, R. E., et al., (2008). In vitro P-glycoprotein assays to predict the in vivo interactions of P-glycoprotein with drugs in the central nervous system. *Drug Metabolism and Disposition*, **36 (2)**, 268–275.

Ferrero, C., Massuelle, D., Deolker, E., (2010). Towards elucidation of the drug release mechanism from compressed hydrophilic matrices made of cellulose ether. II. Evaluation of a possible swelling-controlled drug release mechanism using dimensionless analysis. *Journal of Controlled Release*, **141**, 223-233.

Fortuna, A., Alves, G., and X Falcao, G., (2011). In vitro and in vivo relevance of the p-glycoprotein probe substrates in drug discovery and development: focus on rhodamine 123, digoxin and talinolol. *Journal of Bioequivalence & Bioavailability*, **1 (2)**.

Gabathuler, R., (2010). Approaches to transport therapeutic drugs across the blood-brain barrier to treat brain diseases. *Neurobiology of Disease*, **37 (1)**, 48–57.

Gabor, F., Bogner, E., Weissenboeck, A., Wirth, M., (2004). The lectin-cell interaction and its implications to intestinal lectin mediated drug delivery. *Advanced Drug Delivery Reviews*, **56(4)**, 459-480.

Gaikwad, V.L., Bhatia, M.S., (2012). Polymers influencing transportability profile of drug. *Saudi Pharmaceutical Journal*. 1-9.

Gaikwad, V.L., Bhatia, M.S., (2013). Polymers influencing transportability profile of drug. *Saudi Pharmaceutical Journal*, **21**, 327–335.

Gan, C. W., and Feng, S.-S., (2010). Transferrin-conjugated nanoparticles of Poly (lactide)-d-*α*-Tocopheryl polyethylene glycol succinate diblock copolymer for targeted drug delivery across the blood-brain barrier. *Biomaterials*, **31 (30)**, 7748–7757.

Gavrovic-Jankulovic, M., Prodanovic, R., (2011). Drug Delivery: Plant Lectins as Bioadhesive Drug Delivery Systems. *Journal of Biomaterials and Nanobiotechnology*, **2**, 614-621.

Gazzaniga, A., Palugan, L., Foppoli, A., Sangalli, M.E., (2008). Oral pulsatile delivery systems based on swellable hydrophilic polymers. *European Journal of Pharmaceutics and Biopharmaceutics*, **68**, 11-18.

Ghada, A.A., Mina, I.T., (2008). Design and in vitro/ in vivo evaluation of novel nicorandil extended release matrix tablets based on hydrophilic interpolymer complexes and a hydrophobic waxy polymer. *European Journal of Pharmaceutics and Biopharmaceutics*, **69**, 1019-1028.

Gillies, E. R., and Fr´echet, J. M. J., (2005). Dendrimers and dendritic polymers in drug delivery. *Drug Discovery Today*, **10 (1)**, 35–43.

Giorgi, M., Vullo, C., De Vito, V., Catone, G., Faillace, V., Laus, F. (2015). Pharmacokinetic Evaluations of Sulpiride after Intravenous, Intramuscular, and Oral Single-Dose Administration in Jennies (Equus asinus*). Journal of Equine Veterinary Science,* **35**, 13–18).

Gomel, M., Modi, S., Vyas, K. G., and Rajesh, K. S., (2011). Delivery approaches to bypass P-glycoprotein efflux pump. *Pharmaceutical Information*, **9,** 1.

Gonçalves, V.L., Laranjeira, M.C.M., Fávere, V.T., (2005). Effect of Crosslinking Agents on Chitosan Microspheres in Controlled Release of Diclofenac Sodium. *Polímeros: Ciência e Tecnologia*. **15**, 6-12.

Gungor, S., Bektas, A., Alp, F.I., et al., (2008). Matrix-type transdermal patches of verapamil hydrochloride: in vitro permeation studies through excised rat skin and pharmacodynamic evaluation in rats. *Pharmaceutical Development and Technology,* **4**, 283-289.

Guo, P., Wang, Y., Zhou, X., Xie, Y., Wu, H., Gao, X., (2013). Expression of soybean lectin in transgenic tobacco results in enhanced resistance to pathogens and pests. *Plant Science*, **211**, 17–22.

Gupta, P., Vermani, K., Garg, S., (2002). Hydrogels: From controlled release to pH responsive drug delivery. *Research Focus*, **7(10)**, 569-579.

Haney, M. J., Klyachko, N. L., Zhao, Y., et al., (2015). Exosomes as drug delivery vehicles for Parkinson's disease therapy. *Journal of Controlled Release***207**, 18–30.

Harsulkar, A.A., Sreenivas, S.A., Mandade, R.J., Wakada, R.B., (2011). Polymers in mucoadhesive drug delivery system- A Review. *International Journal of Drug Formulation and Research,* **2(3),** 61-67.

Hawkins, B. T., and Davis, T. P., (2005). The blood-brain barrier/neurovascular unit in health and disease. *Pharmacological Reviews*, **57 (2)**, 173–185.

Haznar-Garbacz, D., Garbacz, G., Eisenächer, F., Klein, S., Weitschies, W., (2012). A novel liquefied gas based oral controlled release drug delivery system for liquid drug formulations. *European Journal of Pharmaceutics and Biopharmaceutics*, **81**, 334–338.

He, G., Xuan, G., Ruan, H., Chen, Q., Yu, Y., (2005). Optimization of angiotensin I-converting enzyme (ACE) inhibition by rice dregs hydrolysates using response surface methodology. *Journal of Zhejiang University Science*, **6B (6)**, 508-513.

He, P., Davis, S.S., Illum, L., (1998). In vitro evaluation of the mucoadhesive properties of chitosan microspheres. *International Journal of Pharmaceutics*, **166**, 75–68.

Higgins, C. F., and Gottesman, M. M., (1992). Is the multidrug transporter a flippase? *Trends in Biochemical Sciences*, **17 (1)**, 18–21.

Hildebrand, H., McDonald, F.M. and Windt-Hanke, F., (1991). Characterization of oral sustained release preparations of iloprost in a pig model by plasma level monitoring. *Prostaglandins*, **41**, 473-486.

Himadri, S.S, Samit, K.R., (2014). Synthesis, characterization, swelling and drug release behavior of semi-interpenetrating network hydrogels of sodium alginate and polyacrylamide. *Carbohydrate Polymers,* **99**, 666– 678.

Hintzen, F., Perera, G., Hauptstein, S., Müller, C., Laffleur, F., Bernkop-Schnürch, A., (2014). In vivo evaluation of an oral self-microemulsifying drug delivery system (SMEDDS) for leuprorelin. *International Journal of Pharmaceutics*, **472**, 20–26.

Hitchcock, S. A., (2012). Structural modifications that alter the Pglycoprotein efflux properties of compounds. *Journal of Medicinal Chemistry*, **55 (11)**, 4877–4895.

Huang, J., Shu, Q., Wang, L., Wu, H., Wang, A.Y., Mao, H., (2015). Layer-by-layer assembled milk protein coated magnetic nanoparticle enabled oral drug delivery with high stability in stomach and enzyme-responsive release in small intestine. *Biomaterials*, **39**, 105-113.

Huang, X., Brazel, C.S., (2001). On the importance and mechanisms of burst release in matrix-controlled drug delivery systems. *Journal of Controlled Release*, **73**, 121-136.

Hugger, E. D., Audus, K. L., and Borchardt, R. T., (2002). Effects of poly (ethylene glycol) on efflux transporter activity in Caco-2 cell monolayers. *Journal of Pharmaceutical Sciences*, **91 (9)**, 1980–1990.

Hunter, R. L., McNicholl, J., and Lal, A. A., (1994). Mechanisms of action of non-ionic block copolymer adjuvants. *AIDS Research and Human Retroviruses*, **10 (2)**, 95–98.

Huo, X., Liu, Q., Wang, C., et al., (2013). Enhancement effect of Pgp inhibitors on the intestinal absorption and antiproliferative activity of bestatin. *European Journal of Pharmaceutical Sciences*, **50 (3-4)**, 420–428.

Huwyler, J., Cerletti, A., Fricker, G., Eberle, A. N., and Drewe, J., (2002). By-passing of P-glycoprotein using immunoliposomes. *Journal of Drug Targeting*, **10 (1)**, 73–79.

Huynh C.L., (2000). Using Partial Residual Plots in Assessing and Improving the Construct Validity of Multiple Regression Models. *Multiple Linear Regression Viewpoints*, **26(2)**, 29-335.

Ibrahim, S and Johan, M.R., (2012). Thermolysis and Conductivity Studies of Poly (Ethylene Oxide) (PEO) Based Polymer Electrolytes Doped with Carbon Nanotube. *International Journal of Electrochemical Science*, **7**, 2596 – 2615.

Insel, T. R., (2010). Rethinking schizophrenia. *Nature*, **468 (7321)**, 187–193.

Iqbal, J., Hombach, J., Matuszczak, B., and Bernkop-Schn¨urch, A., (2010). Design and in vitro evaluation of a novel polymeric Pglycoprotein (P-gp) inhibitor. *Journal of Controlled Release*, **147 (1)**, 62–69.

Izák, P., Hovorka, Š., Bartovský, T., Crespo, J.G., (2007). Swelling of polymeric membranes in room temperature ionic liquids. *Journal of Membrane Science*, **296**, 131-138.

Izumi, Y., Saito, S., Soma, K., (1999). Differential Scanning Calorimetry and Structural studies of the sol-gel transition of gellan gum in water. *Progress in colloid and polymer science*, **114**, 48-55.

Johnson, B. M., Charman, W. N., and Porter, C. J. H., (2002). An in vitro examination of the impact of polyethylene glycol 400, pluronic p85, and vitamin E d-a-tocopheryl polyethylene glycol 1000 succinate on p-glycoprotein efflux and enterocyte-based metabolism in excised rat intestine. *The Journal of the American Association of Pharmaceutical Sciences*, **4 (4)**, 193–205.

Kaur, G., Singh, D., Brar, V., (2014). Bioadhesive okra polymer based buccal patches as platform for controlled drug delivery. *International Journal of Biological Macromolecules*, **70**, 408-419.

Kaur, I. P., Bhandari, R., Bhandari, S., and Kakkar, V., (2008). Potential of solid lipid nanoparticles in brain targeting. *Journal of Controlled Release*, **127 (2)**, 97–109.

Khalid, M.N., Agnely, F., Yagoubi, N., Grossiord, J.L., Couarraze, G., (2002). Water state characterization, swelling behavior, thermal and mechanical properties of chitosan based networks. *European Journal of Pharmaceutical Sciences*, **15**, 425-432.

Khin, N. A., Chen, Y.-F., Yang, Y., Yang, P., and Laughren, T. P., Exploratory analyses of efficacy data from schizophrenia trials in support of new drug applications submitted to the US Food and Drug Administration. *Journal of Clinical Psychiatry*, **73 (6)**, 856–864.

Khutoryanskiy, V.V., (2011).Advances in mucoadhesion and mucoadhesive polymers. *Macromolecular Bioscience*, **11(6)**, 748-764.

Kiil, S., Dam-Johansen, K., (2003). Controlled drug delivery from swellable hydroxypropylmethylcellulose matrices: model-based analysis of observed radial front movements. *Journal of Controlled Release*, **90**, 1–21.

Kim, I.Y., Yoo, M.K., Seo, J.H., Park, S.S., Na, H.S., Lee, H.C., Kim, S.K., Cho, C.S., (2007). Evaluation of semi-interpenetrating polymer networks composed of chitosan and poloxamer for wound dressing application. *International Journal of Pharmaceutics*, **341**, 35-43.

Kim, S.-H., and Chu, C.-C., (2000). Synthesis and characterization of dextran-methacrylate hydrogels and structural study by SEM. *Journal of Biomedical Materials Research*, **49 (4)**, 517–527.

Kingdon, D. G., Ashcroft, K., Bhandari, B., et al., (2010). Schizophrenia and borderline personality disorder: similarities and differences in the experience of auditory hallucinations, paranoia, and childhood trauma. *Journal of Nervous and Mental Disease*, **198 (6)**, 99–403.

Kirschbaum, K. M., Henken, S., Hiemke, C., and Schmitt, U., (2008). Pharmacodynamic consequences of P-glycoprotein-dependent pharmacokinetics of risperidone and haloperidol in mice. *Behavioral Brain Research*, **188 (2)**, 298–303.

Kittipongpatana, O.S., Kittipongpatana, N., (2013). Physicochemical, in vitro digestibility and functional properties of carboxymethyl rice starch cross-linked with epichlorohydrin*. Food Chemistry,* **141**, 1438–1444.

Korbely, A., Kelemen, A., Kasa, J.P., Pintye-Hodi, K., (2012). Effects of processing on the release profiles of matrix systems containing 5-Aminosalicylic acid. *American Association of Pharmaceutical Scientists PharmSciTech*, **13(4)**, 1341-1347.

Kostewicz, E., Sansom, L., Fishlock, R., Morella, A. and Kuchel, T., (1996). Examination of two sustained release nifedipine preparations in humans and in pigs. *European Journal of Pharmaceutical Sciences*, **4**, 351-357.

Kreye, F., Hamm, G., Karrout, Y., Legouffe, R., Bonnel, D., Siepmann, F., Siepmann, J., (2012). MALDI-TOF MS imaging of controlled release implants. *Journal of Controlled Release*, **161**, 98–108.

Kreye, Y., Li, H., Guo, Z., Wu, L., Chen, F., de Matas, M., Shao, Q., Xiao, T., York, P., He, Y., Zhang, J., (2013). Quantification of Swelling and Erosion in the Controlled Release of a Poorly Water-Soluble Drug Using Synchrotron X-ray Computed Microtomography. *The American Association of Pharmaceutical Sciences Journal*, **15**, 4.

Krishna, R., McIntosh, N., Riggs, K. W., and. Mayer, L. D., (1999). Doxorubicin encapsulated in sterically stabilized liposomes exhibits renal and biliary clearance properties that are independent of valspodar (PSC 833) under conditions that significantly inhibit nonencapsulated drug excretion. *Clinical Cancer Research*, **5 (10)**, 2939–2947.

Krishnaraj, K., Chanrasekar, M.J.N., Nanjan, M.J., Muralidharan, S., Manikandan, D., (2012). Development of Sustained release antipsychotic tablets using novel polysaccharide isolated from Delonix regia seeds and its pharmacokinetic studies. *International Journal of Pharmaceutics,* **20**, 239–48.

Kruk, M.E., Schwalbe, N., (2006). The relation between intermittent dosing and adherence: Preliminary Insights. *Clinical Therapeutics*, **28(12)**, 1989-1995.

Kulhara, P., Kulhara, P., Chakrabarti, S., and Chakrabarti, S., (2001). Culture and schizophrenia and other psychotic disorder. *Psychiatric Clinics of North America*, **24 (3)**, 449–464.

Kulkarni, R.V., Baraskar, V.V., Setty, C.M., SA, B., (2011). Interpenetrating Polymer Network Matrices of Sodium Alginate and Carrageenan for Controlled drug delivery application. *Journal of Fibers and Polymers*, **12**, 352-358.

Kulkarni, R.V., Mangond, B.S., Mutalik, S., Sa, B., (2011). Interpenetrating polymer network microcapsules of gellan gum and egg albumin entrapped with diltiazem–resin complex for controlled release application. *Journal of Carbohydrate Polymers*, **83**, 1001–1007.

Kumar, R., and Sinha, V. R., (2013). Thiomer: a potential carrier for therapeutic delivery. *Reactive & Functional Polymers*, **73 (8)**, 1156–1166.

Kuo, Y.-C., and Chen, H.-H., (2006). Effect of nanoparticulate polybutylcyanoacrylate and methylmethacrylate-sulfopropylmethacrylate on the permeability of zidovudine and lamivudine across the in vitro blood-brain barrier. *International Journal of Pharmaceutics***, 327 (1-2)**, 160–169.

La Foug`ere, C., B¨oning, G., Bartmann, H., et al., (2010). Uptake and binding of the serotonin 5-HT1*A* antagonist [18F]-MPPF in brain of rats: effects of the novel P-glycoprotein inhibitor tariquidar. *NeuroImage*, **49 (2)**, 1406–1415.

Lalatsa, A., Sch¨atzlein, A. G., and Uchegbu, I. F., (2011). Drug delivery across the blood-brain barrier. *Current Drug Delivery*, **5 (50)**, 657–666.

Lamprecht, A., and Benoit, J.-P., (2006). Etoposide nanocarriers suppress glioma cell growth by intracellular drug delivery and simultaneous P-glycoprotein inhibition. *Journal of Controlled Release*, **112 (2)**, 208–213.

Larsen, W.A., McCleary, S.J., (1972). The use of Partial Residual Plots in Regression Analysis. Journal of the American Society for Quality and the American Statistical Association *Technometrics*, **14**, 781-790.

Lavon, I., Grossman, N., Kost, J., 2005. The nature of ultrasound-SLS synergism during enhanced transdermal transport. *Journal of Controlled Release* 107,484-494.

Lee, G., Dallas, S., Hong, M., and Bendayan, R., (2001). Drug transporters in the central nervous system: Brain barriers and brain parenchyma considerations. *Pharmacological Reviews*, **53 (4)**, 569–596.

Lee, I.P and Peppas, N.A., (1987). Prediction of polymer dissolution in swellable controlled-release systems. *Journal of Controlled Release*, **6(1)**, 207-215.

Lee, K. D., Hong, K., and Papahadjopoulos, D., (1992). Recognition of liposomes by cells: In vitro binding and endocytosis mediated by specific lipid headgroups and surface charge density. *Biochimica ET Biophysica Acta—Biomembranes*, **1103 (2)**, 185–197.

Leung, V., Ko, F., (2011). Biomedical applications of nanofibers. *Polymers for advanced Technologies*, **22**, 350-365.

Levinson, D.F., Umapathy, C., Musthaq, M., (1999). Treatment of Schizoaffective Disorder and Schizophrenia with Mood Symptoms. *American Journal of Psychiatry*, **156**, 8.

Li, M., Si, L., Pan, H., et al., (2011). Excipients enhance intestinal absorption of ganciclovir by P-gp inhibition: assessed *in vitro* by everted gut sac and *in situ* by improved intestinal perfusion. *International Journal of Pharmaceutics*, **403 (1-2)**, 37– 45.

Lin, S.J., Pascall, M.A., (2014). Incorporation of vitamin E into chitosan and its effect on the film forming solution (viscosity and drying rate) and the solubility and thermal properties of the dried film. *Food Hydrocolloids*, **35**, 78-84.

Lin, Y.-C., Ellingrod, V. L., Bishop, J. R., and Miller, D. D., (2006). The relationship between P-glycoprotein (PGP) polymorphisms and response to olanzapine treatment in schizophrenia. *Therapeutic Drug Monitoring*, **28 (5)** 668–672.

Liu, Y.C., Park, M.B., (2009). Hydrogel based interpenetrating polymer networks based on poly (ethylene glycol) methyl ether acrylate and gelatin for vascular tissue engineering. *Biomaterials*, **30**, 196-207.

Löscher, W and Potschka, H., (2005). Drug resistance in brain diseases and the role of drug efflux transporters. *Nature Reviews Neuroscience*, **6 (8)**, 591–602.

Löscher, W., and Potschka, H. (2005). Role of drug efflux transporters in the brain for drug disposition and treatment of brain diseases. *Progress in Neurobiology*, **76 (1)**, 22–76.

Löscher, W., and Potschka, H., (2005). Blood-brain barrier active efflux transporters: ATP-binding cassette gene family. *The Journal of the American Society for Experimental NeuroTherapeuticss (NeuroRx)*, **2 (1)**, 86–98.

Maderuelo, C., Zarzuelo, A., Lanao, J.M., (2011). Critical factors in the release of drugs from sustained release hydrophilic matrices. *Journal of Controlled Release*, **154**, 2-19.

Mandal, A.S., Biswas, N., Karim, K.M., Guha, A., Chatterjee, S., Behera, M., Kuotsu, K., (2010). Drug delivery system based on chronobiology- A review. *Journal of Controlled Release,* **147**, 314-325.

Mandal, B., Bhattacharjee, H., Mittal, N., et al., (2013). Core-shell-type lipid-polymer hybrid nanoparticles as a drug delivery platform. *Nanomedicine: Nanotechnology, Biology, and Medicine*, **9 (4)**, 474–491.

Marinich, J.A., Ferrero, C., Jiménez-Castellanos M.R., (2012). Graft copolymers of ethyl methacrylate on waxy maize starch derivatives as novel excipients for matrix tablets: Drug release and fronts movement kinetics. *European Journal of Pharmaceutics and Biopharmaceutics*, **80**, 674-687.

Matricardi, P., di Meo, C., Coviello, T., Hennink, W.E., Alhaique, F., (2013). Interpenetrating Polymer Networks polysaccharide hydrogels for drug delivery and tissue engineering. *Advanced Drug Delivery Reviews,* **65**, 1172–1187.

Matsson, P., Pedersen, J. M., Norinder, U., Bergstr¨om, C. A. S., and Artursson, P., Identification of novel specific and general inhibitors of the three major human ATP-binding cassette transporters P-gp, BCRP and MRP2 among registered drugs. *Pharmaceutical Research*, **26 (8)**, 1816–1831.

Mettler Toledo, (2000). UserCom, 1/2000, Information for users of METTLER TORLEDO thermal analysis systems.

Mettler Toledo, (2001), Mettler Toledo Thermal Analysis systems, Information for users.

Mignani, S., El Kazzouli, S., Bousmina, M., Majoral, J-P., (2013). Expand classical drug administration ways by emerging routes using dendrimer drug delivery systems: A concise overview*. Advanced Drug Delivery Reviews*, **65**, 1316–1330.

Miller, D. S., Bauer, B., and Hartz, A. M. S., (2008). Modulation of P-glycoprotein at the blood-brain barrier: opportunities to improve CNS pharmacotherapy. *Pharmacological Reviews*, **60 (2)**, 196–209.

Misra, A., Ganesh, S., Shahiwala, A., and Shah, S. P., (2003). Drug delivery to the central nervous system: a review. *Journal of Pharmacy and Pharmaceutical Sciences*, **6 (2)**, 252–273.

Mo, R., Jin, X., Li, N., et al., (2011). The mechanism of enhancement on oral absorption of paclitaxel by N-octyl-O-sulfate chitosan micelles. *Biomaterials*, **32 (20)**, 4609–4620.

Moa, R., Jin, X., Li, N., Ju, C., Sun, M., Zhang, C., Ping, Q., (2011). The mechanism of enhancement on oral absorption of paclitaxel by N-octyl-O-sulfate chitosan micelles. *Biomaterials*, **32**, 4609-4620.

Modi, S.A., Gaikwad, P.D., Bankar, V.H., Pawar, S.P., (2011). Sustained release drug delivery system: A review. *International Journal of Pharma Research and Development*, **2(12)**, 147-160.

Montesinos, R. N., B´eduneau, A., Pellequer, Y., and Lamprecht, A., (2012). Delivery of P-glycoprotein substrates using chemosensitizers and nanotechnology for selective and efficient therapeutic outcomes. *Journal of Controlled Release*, **161 (1)**, 50–61.

Murthy, P.S.K., Mohan, Y.M., Sreeramulu, J., Raju, K.M., (2006). Semi IPNs of starch and poly (acrylamide-co-sodium methacrylate): Preparation, swelling and diffusion characteristics evaluation. *Journal of reactive and functional polymers*, **66**, 1482-1493.

Musther, H., Olivares-Morales, A., Hatley, O.J.D., Liu, B., Hodjegan, A.R., (2014). Animal versus human oral drug bioavailability: Do they correlate? *European Journal of Pharmaceutical Sciences*, **57**, 280–291.

Muthu, M. S., and Singh, S., (2009).Poly (D, L-lactide) nanosuspensions of risperidone for parenteral delivery: formulation and in-vitro evaluation. *Current Drug Delivery*, **6 (1)**, 62–68.

Mythri, G., Kavitha, K., Kumar, M.R., Sd. Singh, J., (2011). Novel Mucoadhesive Polymers- a Review.*Journal of Applied pharmaceutical science, **1(8)**, 37-42.*

Nagar, M., Singhai, S., Chopra, V.S., Gautam, N., Trivedi, P., (2010). Chronotropic systems; an emerging trend in drug delivery for pulsed release in Chronopharmacotherapy. *International Journal of Pharmaceutical and Clinical Research*, **2(1)**, 10-19.

Nakagami, T., Yasui-Furukori, N**.,** Saito, M., Tateishi, T., and Kaneo, S., (2005). Effect of verapamil on pharmacokinetics and pharmacodynamics of risperidone: in vivo evidence of involvement of P-glycoprotein in risperidone disposition. *Clinical Pharmacology and Therapeutics*, **78 (1)**, 43–51.

Nasongkla, N., Bey, E., Ren, J., et al., (2006). Multifunctional polymeric micelles as cancer-targeted, MRI-ultrasensitive drug delivery systems. *Nano Letters*, **6**, 2427–2430.

Nassar, T., Rom, A., Nyska, A., and Benita, S., (2009). Novel double coated nanocapsules for intestinal delivery and enhanced oral bioavailability of tacrolimus, a P-gp substrate drug. *Journal of Controlled Release*, **133 (1)**, 77–84.

National Toxicology Program. Report on Carcinogens. 12th Edition, Department of Health and Human Services. 2011.

Negi, L. M., Tariq, M., and Talegaonkar, S., (2013). Nano scale self-emulsifying oil based carrier system for improved oral bioavailability of camptothecin derivative by P-Glycoprotein modulation. *Colloids and Surfaces B: Biointerfaces*, **111**,346–353.

Nnadi, C. U., and Malhotra, A. K., (2007). Individualizing antipsychotic drug therapy in schizophrenia: the promise of pharmacogenetics. *Current Psychiatry Reports*, **9 (4)**, 313–318.

Nokhodchi, A., Tailor, A., (2004). In situ cross-linking of sodium alginate with calcium and aluminum ions to sustain the release of theophylline from polymeric matrices. *IL FARMACO*, **59**, 999-1004.

Olivares, J.M., Rodriguez-Morales, A., Diels, J., Diels, J., Povey, M., Jacobs, A., Zhao, Z., Lam, A., (2009). Long-term outcomes in patients with schizophrenia treated with risperidone long-acting injection or oral antipsychotics in Spain: Results from the electronic Schizophrenia Treatment Adherence Registry (e-STAR). *European Psychiatry*, **24**, 287-296.

Özeroglu, C., and Birdal, A., (2009). Swelling properties of acrylamide-N, N′-methylene bis (acrylamide) hydrogels synthesized by using meso-2, 3-dimercaptosuccinic acid-cerium (IV) redox couple. *Express Polymer Letters*, **3**, 168–176.

Panda, P.K., Mukhopadhyay, S., Behera, B., Bhol, C.S., Dey, S., Das, D.N., Sinha, N., Bissoyi, A., Pramanik, K., Maiti, T.K., Bhutia, S.K., (2014). Antitumor effect of soybean lectin mediated through reactive oxygen species-dependent pathway. *Life Sciences*, **111,** 27–35.

Pang, K. S., (2003). Modeling of intestinal drug absorption: Roles of transporters and metabolic enzymes (for the Gillette review series). *Drug Metabolism & Disposition*, **31 (12)**, 1507– 1519.

Parikh, T., Bommana, M.M., Squillante III, E., (2010). Efficacy of surface charge in targeting pegylated nanoparticles of sulpiride to the brain. *European Journal of Pharmaceutics and Biopharmaceutics*, **74**, 442–450.

Peppas, N.A., Huang, Y., (2004). Nanoscale technology of mucoadhesive interactions. *Advanced Drug Delivery Reviews*, **56**, 1675-1687.

Perez-Vilar, J., Hill, R., (1999). The structure and assembly of secreted mucins. *Journal of biological chemistry,* **274(45)**, 31751-31754.

Petersen, S.B., Nolan, G., Maher, S., Rahbek, U.L., Guldbrandt, M., Brayden, D.J., (2012). Evaluation of alkylmaltosides as intestinal permeation enhancers: Comparison between rat intestinal mucosal sheets and Caco-2 monolayers. *European Journal of Pharmaceutical Sciences*, **47**, 701–712.

Peuskens, J., Bech, P., Möller, H-J., Bale, R., Fleurot, O., Rein, W., (1999). Amisulpiride vs. risperidone in the treatment of acute exacerbations of schizophrenia. *Psychiatry Research,* **88**, 107-117.

Phapale, P.B., Lee, H.W., Lim, M.S., Seong, S.J., Kim, E.H., Park, J., Lee, M., Hwang, S.K., Yoon, Y.R., (2010). Liquid chromatography- tandem mass spectrometry quantification of levosulpiride in human plasma and its application to bioequivalence study, *Journal of Chromatography B*, **878**, 2280-2285.

Pharoah, F., Mari, J. J., Rathbone, J., and Wong, W., (2006). Family intervention for schizophrenia. *Cochrane Database of Systematic Reviews*, **4**, Article ID CD000088.

Pignatello, R., Ferro, M., De Guidi, G., Salemi, G., Vandelli, M.A., Guccione, S., Geppi, M., Forte, C., Puglisi, G., (2001). Preparation, characterization and photosensitivity studies of solid dispersions of diflunisal and Eudragit RS100® and RL100®*. International Journal of Pharmaceutics,* **218,** 27–42.

Pillay, V and Fassihi, R., (2000). A novel approach for constant rate delivery of highly soluble bioactives from a simple monolithic system. *Journal of Controlled Release*, **67**, 67–78.

Ping, H.E., et al., (1998). In vitro evaluation of the mucoadhesive properties of chitosan microspheres. *International Journal of Pharmaceutics,* **166**, 68–75.

Prabakaran, D., Singh, P., Jaganathan, K.S., Vyas, S.P., (2004). Osmotically regulated asymmetric capsular systems for simultaneous sustained delivery of anti-tubercular drugs. *Journal of Controlled Release*, **95**, 239– 248.

Proença, P., Franco, J.M., Mustra, C., Marcos, M., Pereira, A.R., Corte-Real, F., Vieira, D.N. (2011). An UPLCeMS/MS method for the determination of valproic acid in blood of a fatal intoxication case. *Journal of Forensic and Legal Medicine*, **18**, 320-324.

Pund, S., Joshi, A., Vasu, K., Nivsarkar, M., Shishoo, C., (2011). Gastroretentive delivery of rifampicin: In vitro mucoadhesion and in vivo gamma scintigraphy. *International Journal of Pharmaceutics*, **411**, 106–112.

Pundir, S., Badola, A., Sharma, D., (2013). Sustained release matrix technology and recent advance in matrix drug delivery systems: A review. *International Journal of Drug Research and Technology*, **3(1)**, 12-20.

Raissi, S., Farsani, E.R., (2009). Statistical Process Optimization through Multi-Response Surface Methodology. *World Academy of Science, Engineering and Technology*, **51**, 267-271.

Rasve, G., Borade, G., Deshmukh, S., Tagalpallewar, A., (2011). Pulsatile drug delivery system: current scenario. *International Journal of Pharma and Bio Sciences*, **2(3)**, 332-343.

Reddy, K.R., Mutalik, S., Reddy, S., (2003). Once-Daily Sustained-Release Matrix Tablets of Nicorandil: Formulation and In Vitro Evaluation. *The Journal of American Association of Pharmaceutical Science PharmSciTech*. **4**, 1-9.

Reddy, M.M., Reddy, J.D., Moin, A., Shivakumar, H.G., (2012). Formulation of Sustained – Release Matrix Tablets using Crosslinked Karaya Gum. *Tropical Journal of Pharmaceutical Research*, **11**, 28-35.

Rege, B. D., Kao, J. P. Y., and Polli, J. E., (2002). Effects of nonionic surfactants on membrane transporters in Caco-2 cell monolayers. *European Journal of Pharmaceutical Sciences*, **16 (4-5)**, 237–246.

Reis, M.D and Pruitt, L., (2005). Effects of cross-linking on the microstructure and mechanical properties of ultra- high molecular weight. *Clinical Orthopedic related research*, **440**, and 149-56.

Rey-Raap, N., Szczurek, A., Fierro, V., Menéndez, J.A., Arenillas, A., Celzard, A. (2015). Towards a feasible and scalable production of bio-xerogels. *Journal of Colloid and Interface Science*, **456**; 138–144.

Richardson, J.C., Bowtell, R.W., Mäder, K., Melia, C.D., (2005). Pharmaceutical applications of magnetic resonance imaging (MRI). *Advanced Drug Delivery Reviews*, **57**, 1191– 1209.

Rinaki, E., Dokoumetzidis, A., and Macheras, P., (2003). The mean dissolution time depends on the dose/solubility ratio. *Pharmaceutical Research*, **20**, 406-408.

Roberts D. J., and Goralski, K. B., (2008). A critical overview of the influence of, inflammation and infection on P-glycoprotein expression and activity in the brain. *Expert Opinion on Drug Metabolism and Toxicology*, **4 (10)**, 1245–1264.

Roberts, M.S., 1991. Structure-permeability considerations in percutaneous absorption. In: R.C. Scott, R.H. Guy, J. Hadgraft *et al*., eds. 1991. London: IBC Technical Services, pp. 210-228.

Roger, E., Lagarce, F., Garcion, E., and Benoit, J.-P., (2010). Reciprocal competition between lipid nanocapsules and P-gp for paclitaxel transport across Caco-2 cells. *European Journal of Pharmaceutical Sciences*, **40 (5)**, 422–429.

Roine, J., Murtomaa, M., Myllys, M., Salonen, J., (2012). Dual-capillary electroencapsulation of mesoporous silicon drug carrier particles for controlled oral drug delivery. *Journal of Electrostatics*, **70**, 428-437.

Rokhade, A.P., Agnihotri, S.A., Patil, S.A., Malikarjuna, N.N., Kulkarni, P.V., Aminabhavi, T.M., (2006). Semi- Interpenetrating polymer network microspheres of gelatin and sodium Carboxymethyl cellulose for controlled release of ketorolac tromethamine. *Journal of carbohydrate polymers*, **65**, 243-252.

Rosenberg, M. F., Kamis, A. B., Callaghan, R., Higgins, C. F., and Ford, R. C., (2003). Three-dimensional structures of the mammalian multidrug resistance P-glycoprotein demonstrate major conformational changes in the transmembrane domains upon nucleotide binding. *Journal of Biological Chemistry*, **278 (10)**, 8294–8299.

Rossiter, D., (2010). South African Medicine Formulary, 9TH Edition.

Rowe, R.C., et al. (2006). Handbook of Pharmaceutical Excipients. *Pharmaceutical Press and American Pharmacists Association,* 5th edition.

Roy, P., Shahiwala, A., (2009). Multiparticulate formulation approach to pulsatile drug delivery: Current Perspectives. *Journal of controlled release*, **134**; 74-80.

Roy, S., Pal, K., Anis, A., Pramanik, K., Prabhakar, B., (2009). Polymers in Mucoadhesive Drug Delivery System: A Brief Note. *Designed Monomers and Polymers*, **12**, 483-495.

Ruvalcaba, A.M., Snchez- Diaz, J.C., Becerra, F., Cruz- Barba, L.E., Gonzalez- Alvarez, A., (2009). Swelling characterization and drug delivery kinetics of polyacrylamide-co-itaconic acid/chitosan hydrogels. *Express Polymer letters*, **3**, 25-32.

Sahin, M., Kocak, N., Arslan, G., Ucan, H.I., (2011). Synthesis of Crosslinked Chitosan with Epichlorohydrin Possessing Two Novel Polymeric Ligands and Its Use in Metal Removal. *Journal of Inorganic and Organometallic Polymers and Materials*, **21**, 69-80.

Salamat-Miller, N., Chittchang M., Johnston, T.P., (2005). The use of mucoadhesive polymers in buccal drug delivery. *Advanced Drug Delivery Reviews*, **57**, 1666 – 1691.

Sanchez, J., Charmette, C., Gramain, P., (2002). Poly (ethylene oxide-co-epichlorohydrin) membranes for carbon dioxide separation. *Journal of Membrane Science*. **205**, 259-263.

Sauna, Z. E., Smith, M. M., M¨uller, M., Kerr, K. M., and Ambudkar, S. V., (2001). The mechanism of action of multidrug-resistance linked P-glycoprotein. *Journal of Bioenergetics and Biomembranes*, **33 (6)**, 481–491.

Saxena, V., and Hussain, M. D., (2012). Poloxamer 407/TPGS mixed micelles for delivery of gambogic acid to breast and multidrug resistant cancer. *International Journal of Nanomedicine*, **7**, 713–721.

Scaccia, S., (2005). Water determination in composite PEO-based polymer electrolytes by volumetric Karl Fischer titration method. *The International Journal of Pure and Applied Analytical Chemistry (Talanta)*, **67**, 678–681.

Scherrmann, J.-M., (2002). Drug delivery to brain via the blood-brain barrier. *Vascular Pharmacology*, **38 (6)**, 349–354.

Schinkel, A. H., (1999). P-Glycoprotein, a gatekeeper in the blood brain barrier. *Advanced Drug Delivery Reviews*, **36 (2-3)**, 179–194.

Schlessinger, A., Khuri, N., Giacomini, K.M., and Sali, A., (2013). Molecular modelling and ligand docking for solute carrier (SLC) transporters. *Current Topics in Medicinal Chemistry*, **13 (7)**, 843–856.

Schmitt, U., El-Ela, A. A., Guo, L. J., et al., (2006). Cyclosporine a (CsA) affects the pharmacodynamics and pharmacokinetics of the atypical antipsychotic amisulpride probably via inhibition of P-glycoprotein (P-gp). *Journal of Neural Transmission*, **113 (7)**, 787–801.

Schnaare, R., Block, L., Rohan, L., (2005). Rheology in: Hendrickson, R., (ed) Remingtons the Science and Practice of Pharmacy, 21st edn. Lippincott, Williams and Wilkins, Philadelphia.

Sellimi, S., Younes, I., Ayeda, H.B., Maalej, H., Montero, V., Rinaudoc, M., Dahia, M., Mechichi, T., Hajji, M., Nasri, M., (2015). Structural, physicochemical and antioxidant properties of sodium alginate isolated from a Tunisian brown seaweed. *International Journal of Biological Macromolecules,* **72**, 1358–1367.

Shah, R.B., Tawakkul, M.A., Khan, M.A., (2008). Comparative Evaluation of Flow for Pharmaceutical Powders and Granules.*The Journal of American Association of Pharmaceutical Sciences (AAPS PharmSciTech)*, **9**, 250-258.

Sharma, S.K., Mohan, S., Jaimini, M., (2014). Formulation and in vitro evaluation of modified release tablets of gliclazide (antidiabetic drug). *International Journal of Pharmacy and Pharmaceutical Sciences,* **6 (2),** 259-261.

Sharom, F. J., (2014). Complex interplay between the P-glycoprotein multidrug efflux pump and the membrane: Its role in modulating protein function. *Frontiers in Oncology*, **4**, Article ID Article 41.

Shen, Q., Lin, Y., Handa, T., et al., (2006). Modulation of intestinal Pglycoprotein function by polyethylene glycols and their derivatives by in vitro transport and in situ absorption studies. *International Journal of Pharmaceutics*, **313 (1-2)**, 49–56.

Shen, Z., Mitragotri, S., (2002). Intestinal Patches for Oral Drug Delivery. *Pharmaceutical Research,* **19(4),** 391-395.

Shoaib, M.H., Tazeen, J., Merchant, H.A., Yousuf, R.I., (2006). Evaluation of Drug Release Kinetics from Ibuprofen Matrix Tablets Using Hpmc. *Pakistan Journal of Pharmaceutical Science,* **19**, 119-124.

Siepmann, J and Peppas, N.A., (2012). Modeling of drug release from delivery systems based on hydroxypropyl methylcellulose (HPMC). *Journal of Advanced drug delivery reviews*, **64**, 163-174.

Siepmann, J., Lecomte, F., Bodmeie, R., (1999). Diffusion- controlled drug delivery systems: calculation of the required composition to achieve desired release profiles. *Journal of controlled release*, **60**, 379-389.

Siepmann, J., Siepmann, F., (2013). Stability of aqueous polymeric controlled release film coatings. *International Journal of Pharmaceutics*, **457**, 437-445.

Sigma Aldrich, MDS (±) Sulpiride, Germany.

Singh, A., Sharma, P.K., Malviya, R., (2011). Release Behavior of Drugs from various Natural Gums and Polymers. *Journal of Polymer Medicine,* **4 (41)**.

Singh, B., Dahiya, M., Saharan, V., Ahuja, N., (2005). Optimizing Drug Delivery Systems Using Systematic “Design of Experiments.” Part II: Retrospect and Prospects. *Critical Reviews™ in Therapeutic Drug Carrier Systems*, **22(3)**, 215–293.

Singh, B., Kumar, R., Ahuja, N., (2004). Optimizing Drug Delivery Systems Using Systematic "Design of Experiments." Part I: Fundamental Aspects. *Critical Reviews™ in Therapeutic Drug Carrier Systems*, **22 (1)**, 27–105.

Soares, B.G.O., Fenton, M., Chue, P., (2011). Sulpiride for Schizophrenia. *The Cochrane Collaboration.*

Sperling, L.H., Klempner, D., Utracki, L.A., (1994). Interpenetrating Polymer Networks: An Overview.*American Chemical Society, Advances in Chemistry Series*, **239**, 3-38.

Sriamornsak, P., Thirawong, N., Weerapol, Y., Nunthanid, J., Sungthongjeen, S., (2007). Swelling and erosion of pectin matrix tablets and their impact on their behavior. *European Journal of Pharmaceutics and Biopharmaceutics,* **67**, 211-219.

Stolp H. B., and Dziegielewska, K. M., (2009). Review: role of developmental inflammation and blood-brain barrier dysfunction in neurodevelopmental and neurodegenerative diseases. *Neuropathology and Applied Neurobiology*, **35 (2)**, 132–146.

Streubel, A., Siepmann, J., Bodmeier, R., (2006). Drug delivery to the upper small intestine window using gastroretentive technologies. *Current Opinion in Pharmacology*, **6**, 501–508.

Strübing, S., Metz, H., Mäder, K., (2008). Characterization of poly (vinyl acetate) based floating matrix tablets. *Journal of Controlled Release*, **126**, 149–155.

Suri, S., Christine, E., (2009). Photo patterned collagen-hyaluronic acid interpenetrating polymer network hydrogels. *Acta Biomaterials*, **5**, 2385-2397.

Suzuki, T., Uchida, H., Takeuchi, H., Nakajima, S., Nomura, K., Tanabe, A., Yagi, G., Watanabe, K., Kashima, H., (2009). Augmentation of atypical antipsychotic with valproic acid an open-label study for most difficult patients with schizophrenia. *Human Psychopharmacology Clinical Experimental,* **24**, 628-638.

Svenson, S., (2009). Dendrimers as versatile platform in drug delivery applications. *European Journal of Pharmaceutics and Biopharmaceutics*, **71 (3)**, 445–462.

Syed, K.H.G., Al-Assaf, S., Phillips, G.O., (2011). Hydrogels: Methods of Preparation, characterization and Applications. *Progress in Molecular and Environmental Bioengineering from Analysis and Modeling to Technology Applications*. ISBN: 978-953,307-568-5.

Szakonyi, G and Zelkó, R., (2012). The effect of water on the solid state characteristics of pharmaceutical excipients: Molecular mechanisms, measurement techniques, and quality aspects of final dosage form. *International Journal of Pharmaceutical* Investigation, **2**, 18-25.

Takano, M., Yumoto, R., and Murakami, T., (2006). Expression and function of efflux drug transporters in the intestine. *Pharmacology and Therapeutics*, **109 (1-2)**, 137–161.

Tandon, R., Nasrallah, H. A., and Keshavan, M. S., (2009). Schizophrenia, 'just the facts' 4. Clinical features and conceptualization. *Schizophrenia Research*, **110 (1–3)**, 1–23.

Tangri, P. and Madav, N.V.S., (2011). Oral Mucoadhesive Drug Delivery Systems: A Review. *International Journal of Biopharmaceutics,* **2(1),** 36-46).

Tao, S.L., Desai, T, A., (2005). Gastrointestinal patch systems for oral drug delivery, *Drug Discovery Today*, **10(13)**, 909-915.

Taylor**,** E. M., (2002). The impact of efflux transporters in the brain on the development of drugs for CNS disorders. *Clinical Pharmacokinetics*, **41 (2)**, 81–92.

Thakkar, R., Saravaia, H., Ambasana, M., Patel, M., Shah, A., (2012). An IsocraticMethod for Quantification of Valproic Acid and Its Related Impurities Using Ion Pair Reagent by Ultraperformance Liquid Chromatography. *International Scholary Research Notices Chromatography*, 1-5.

Toti, U.S and Aminabhavi, T.M., (2004). Modified guar gum matrix tablet for controlled release of diltiazem hydrochloride. *Journal of Controlled Release*, **95**, 567– 577.

Tsume, Y., Incecayir, T., Song, X., Hilfinger, J.M., Amidon, G.L., (2014). The development of orally administrable gemcitabine prodrugs with D-enantiomer amino acids: Enhanced membrane permeability and enzymatic stability. *European Journal of Pharmaceutics and Biopharmaceutics*, **86**, 514–523.

Van derMeel, R., Fens, M. H. A. M., Vader, P., van Solinge, W.W., Eniola-Adefeso, O., and Schiffelers, R. M., (2014). Extracellular vesicles as drug delivery systems: lessons from the liposome field. *Journal of Controlled Release*, **195**, 72–85.

Van Dommelen, S. M., Vader, P., Lakhal, S.M, et al., (2012). Microvesicles and exosomes: opportunities for cell-derived membrane vesicles in drug delivery. *Journal of Controlled Release*, **161 (2)**, 635–644.

van Os, J., Kenis, G., and Rutten, B. P. F., (2010). The environment and schizophrenia. *Nature*, **468 (7321)**, 203–212.

Varma, M. V. S., Ashokraj, Y., Dey, C. S., and Panchagnula, R., (2003). P-glycoprotein inhibitors and their screening: a perspective from bioavailability enhancement. *Pharmacological Research*, **48 (4)**, 347–359.

Varma, M.V.S., Kausal, A.M., Garg, A., Garg, S., (2004). Factors affecting mechanism and kinetics of drug release from matrix –based oral controlled drug delivery systems. *American Journal of Drug Delivery*, **2(1)**, 43-57.

Wagner, D., Spahn-Langguth, H., Hanafy, A., Koggel, A., and Langguth, P., (2001). Intestinal drug efflux: formulation and food effects. *Advanced Drug Delivery Reviews*, **50 (1)**, S13–S31.

Wang Y., Nedelman J., 2002. Bias in the Wagner-Nelson estimate of the fraction of drug absorbed. *Pharmaceutical Research* **19(4)**, 470-476.

Wang, F., Zhang, D., Zhang, Q., et al., (2011). Synergistic effect of folate mediated targeting and verapamil-mediated P-gp inhibition with paclitaxel-polymer micelles to overcome multi-drug resistance. *Biomaterials*, **32 (35)**, 9444–9456.

Wang, J.-S., Ruan, Y., Taylor, R.M., Donovan, J. L., Markowitz, J. S., and DeVane, C. L., The brain entry of risperidone and 9- hydroxyrisperidone is greatly limited by P-glycoprotein. *International Journal of Neuropsychopharmacology*, **7 (4)**, 415–419.

Wang, J.-S., Zhu, H.-J., Donovan, J. L., et al., (2009). Aripiprazole brain concentration is altered in P-glycoprotein deficient mice. *Schizophrenia Research*, **110 (1-3)**, 90–94.

Wang, N., Wang, T., Zhang, M., Chen, R., Niu, R., Deng, Y., (2014). Mannose derivative and lipid A dually decorated cationic liposomes as an effective cold chain free oral mucosal vaccine adjuvant-delivery system. *European Journal of Pharmaceutics and Biopharmaceutics*, **88**, 194–206.

Wang, S., Ren, J., Li, W., Sun, R., Liu, S., (2014). Properties of polyvinyl alcohol/xylan composite films with citric acid. *Carbohydrate Polymers*, **103**, 94-99.

Werle, M., (2008). Natural and synthetic polymers as inhibitors of drug efflux pumps. *Pharmaceutical Research*, **25 (3)**, 500– 511.

Werle, M., and Bemkop-Schn¨urch, A., (2008). Thiolated chitosans: useful excipients for oral drug delivery. *Journal of Pharmacy and Pharmacology*, **60 (3)**, 273–281.

Werle, M., and Hoffer, M., (2006). Glutathione and thiolated chitosan inhibit multidrug resistance P-glycoprotein activity in excised small intestine. *Journal of Controlled Release*, **111 (1-2)**, 41–46.

Whitehead, K., Shen, Z., Mitragotri, S., (2004). Oral delivery of macromolecules using intestinal patches: applications for insulin delivery*, Journal of Controlled Release* **98**, 37:45.

Wong, H. L., Bendayan, R., Rauth, A. M., and Wu, X. Y., (2006). Simultaneous delivery of doxorubicin and GG918 (Elacridar) by new polymer-lipid hybrid nanoparticles (PLN) for enhanced treatment of multidrug-resistant breast cancer. *Journal of Controlled Release*, **116 (3)**, 275–284.

Wong, H. L., Wu, X. Y., and Bendayan, R., (2012). Nanotechnological advances for the delivery of CNS therapeutics. *Advanced Drug Delivery Reviews*, **64 (7)**, 686–700.

Woo, J. S., Lee, C. H., Shim, C. K., and Hwang, S.J., (2003). Enhanced oral bioavailability of paclitaxel by coadministration of the Pglycoprotein inhibitor KR30031. *Pharmaceutical Research*, **20 (1)**, 24–30.

Xua, L., Donga, M., Gonga, H., Suna, M., Lia, Y., (2015). Effects of inorganic cations on the rheology of aqueous welan, xanthan, gellan solutions and their mixtures. *Carbohydrate Polymers*, **121**, 147–154.

Yadav, V.K., Gupta, A.B., Kumar, R., Yadav, J.S., Kumar, B., (2010). Mucoadhesive Polymers: Means of Improving the Mucoadhesive Properties of Drug Delivery System. *Journal of Chemical and Pharmaceutical Research*, **2(5)**, 418-432.

Yallapu, M. M., Jaggi, M., and Chauhan, S. C., (2011). Design and engineering of nanogels for cancer treatment. *Drug Discovery Today*, **16 (9-10)**, 457–463.

Yang, N., Ashton, J., Kasapis, S., (2015). The influence of chitosan on the structural properties of whey protein and wheat starch composite systems. *Food Chemistry*, **179**, 60–67.

Yin, X., Li, H., Guo, Z., Wu, L., Chen, F., de Matas, M., Shao, Q., Xiao, T., York, P., He, Y., Zhang, J., (2013). Quantification of Swelling and Erosion in the Controlled Release of a Poorly Water-Soluble Drug Using Synchrotron X-ray Computed Microtomography. *The American Association of Pharmaceutical Science Journal*, **15**, 4.

Yu, T., Andrews, G.P., Jones, D.S., (2014). Mucoadhesion and Characterization of Mucoadhesive Properties. *Mucosal Delivery of Biopharmaceuticals*, DOI 10.1007/978-1-4614-9524-6_2, 35-44.

Yue, Y.M., Xu, K., Liu, X-G., Chen, Q., Shen, X., Wang, P-X., (2008). Preparation and characterization of interpenetration polymer network films based on Poly (vinyl alcohol) and Poly (acrylic acid) for drug delivery. *Journal of Applied Polymer Science,* **108**, 3836-3842.

Zhang, H., Zhao, Y., (2015). Preparation, characterization and evaluation of tea polyphenoleZn complex loaded b-chitosan nanoparticles. *Food Hydrocolloids*, **48**, 260-273.

Zhang, X.Z., Wu, D.Q., Chu, C.C., (2004). Synthesis, characterization and controlled drug release of thermosensitive IPN-PNIPAAm hydrogels. *Biomaterials*, **25**, 3793-3805.

Zhang, Y., Huo, M., Zhou, J., Xie, S., (2010). PKSolver: An add-in program for pharmacokinetic and pharmacodynamic data analysis in Microsoft Excel. *Computer methods and programs in biomedicine*, **99**, 306-314.

Zhuang, X., Tian, X., Zheng, Y., et al., (2011). Formulation and physicochemical characterization of a novel self-microemulsifying delivery system as hydrotropic and solubilizing agent for Penfluridol. *Procedia Engineering*, **18**, 59–65. Proceedings of the 2nd SREE Conference on Chemical Engineering (CCE ’11).

Zo-li, J.T.U., (2005). Morphology, Crystallization and Melting Behavior of Propylene-Ethylene Statistical Copolymers. Doctor of Philosophy. Virginia: Polytechnic Institute and State University.

11. Appendices

11.1. Doctoral Publication

11.1.1. Review Paper

Hindawi Publishing Corporation
BioMed Research International
Article ID 484963

Review Article

Bypassing P-Glycoprotein Drug Efflux Mechanisms: Possible Applications in Pharmacoresistant Schizophrenia Therapy

Famida G. Hoosain, Yahya E. Choonara, Lomas K. Tomar, Pradeep Kumar, Charu Tyagi, Lisa C. du Toit, and Viness Pillay

Wits Advanced Drug Delivery Platform Research Unit, Department of Pharmacy and Pharmacology, School of Therapeutic Sciences, Faculty of Health Sciences, University of the Witwatersrand, 7 York Road, Parktown, Johannesburg 2193, South Africa

Correspondence should be addressed to Viness Pillay; viness.pillay@wits.ac.za

Received 2 December 2014; Revised 8 May 2015; Accepted 10 May 2015

Academic Editor: Eberval G. Figueiredo

Copyright © 2015 Famida G. Hoosain et al. This is an open access article distributed under the Creative Commons Attribution License, which permits unrestricted use, distribution, and reproduction in any medium, provided the original work is properly cited.

The efficient noninvasive treatment of neurodegenerative disorders is often constrained by reduced permeation of therapeutic agents into the central nervous system (CNS). A vast majority of bioactive agents do not readily permeate into the brain tissue due to the existence of the blood-brain barrier (BBB) and the associated P-glycoprotein efflux transporter. The overexpression of the MDR1 P-glycoprotein has been related to the occurrence of multidrug resistance in CNS diseases. Various research outputs have focused on overcoming the P-glycoprotein drug efflux transporter, which mainly involve its inhibition or bypassing mechanisms. Studies into neurodegenerative disorders have shown that the P-glycoprotein efflux transporter plays a vital role in the progression of schizophrenia, with a noted increase in P-glycoprotein function among schizophrenic patients, thereby reducing therapeutic outcomes. In this review, we address the hypothesis that methods employed in overcoming P-glycoprotein in cancer and other disease states at the level of the BBB and intestine may be applied to schizophrenia drug delivery system design to improve clinical efficiency of drug therapies. In addition, the current review explores polymers and drug delivery systems capable of P-gp inhibition and modulation.

1. Introduction

The effectiveness of drug treatments for numerous disease states such as cancer, infectious diseases, and central nervous system (CNS) disorders (epilepsy, depression, and schizophrenia) is limited by poor therapeutic outcomes or drug resistance. The outcomes of drug treatment can be viewed as an interchange of several gene products that have an effect on pharmacokinetics and pharmacodynamics. These gene products mainly include metabolizing enzymes and drug transporters and alterations within any of these gene products may lead to a reduction in clinical outcomes [1]. In particular, the clinical treatment and management of CNS disorders necessitate that a sufficient amount of drug must enter the brain. The use of oral drug delivery systems is beneficial in the treatment of neurodegenerative disorders as compliance to therapy becomes challenging [2]. However, an imperative factor determining the entry of drug molecules into the brain via oral administration is its absorption through the intestinal epithelium and the permeability of the blood-brain barrier (BBB). Passive diffusion across the intestinal epithelium is dependent on many physiochemical characteristics of drugs such as lipophilicity, molecular weight, and hydrophobic bonding [3]. The same principle applies to passive diffusion across the BBB, although passive diffusion across the BBB is limited to small lipophilic molecules. Active efflux of the drug into the intestine and from BBB endothelium back into the blood are the most important mechanisms underlying reduced brain uptake of active drug molecules post oral dosing [4].

The development of drug delivery systems involved in the treatment of neurodegenerative disorders requires a vital consideration of achievable brain concentrations. Factors that impact the brain uptake and concentrations of drugs include (i) the extent of intestinal absorption after oral administration, (ii) the rate and extent of transport across the BBB

AAPS PharmSciTech, Vol. 15, No. 5, October 2014 (© 2014)
DOI: 10.1208/s12249-014-0153-4

Research Article

An Epichlorohydrin-Crosslinked Semi-Interpenetrating GG-PEO Network as a Xerogel Matrix for Sustained Release of Sulpiride

Famida G. Hoosain,[1] Yahya E. Choonara,[1] Pradeep Kumar,[1] Lomas K. Tomar,[1] Charu Tyagi,[1] Lisa C. du Toit,[1] and Viness Pillay[1,2]

Received 14 February 2014; accepted 14 May 2014; published online 12 June 2014

Abstract. The current study involved the development of a novel sustained release crosslinked semi-IPN xerogel matrix tablet prepared by chemical crosslinking of poly(ethylene) oxide (PEO) and gellan gum (GG) employing epichlorohydrin (EPI) as crosslinker. A Box–Behnken design was employed for the statistical optimization of the matrix system to ascertain the ideal combination of native polymeric and crosslinking agents. Characterization studies were performed by employing standard polymer characterization techniques such as Fourier transform infrared spectroscopy, differential scanning calorimetry, and scanning electron microscopy. Formulated matrix tablets displayed zero-order release kinetics, extending over 24 h. The mechanism of drug release was primarily by swelling and surface erosion. Crosslinked semi-IPN xerogel matrix tablets were compared to non-crosslinked polymer blends; results from the study conducted showed that the physicochemical properties of the PEO and GG were sufficiently modified to allow for sustained release of sulpiride with a 100% drug release at 24 h in a controlled manner as compared to non-crosslinked formulations which displayed further release beyond the test period. Crosslinked formulations displayed water uptake between 450 and 500% indicating a controlled rate of swelling and erosion allowing for sustained release. Surface morphology of the crosslinked system depicted a porous structure formed by interpenetrating networks of polymers, allowing for a greater degree of controlled penetration into the system affording it the ability to sustain drug release. Therefore, conclusively, based on the study performed, crosslinked PEO-GG allows for the sustained release of sulpiride from a hydrophilic semi-IPN xerogel matrix system.

KEY WORDS: epichlorohydrin; matrix tablet; semi-interpenetrating polymer network; sustained release; sulpiride.

INTRODUCTION

The use of hydrophilic matrix systems in order to achieve sustained drug delivery kinetics has been a widespread field of research studies in the pharmaceutical industry. The development of sustained release dosage forms is beneficial for the optimal therapeutic outcomes required for many disease states, which allows for improved patient compliance, and as an extension the safety and efficacy of drug therapy. There are various ways in which controlled release is achieved with regards to oral dosage forms. Amid the many approaches available, the most common is that of hydrophilic matrix systems due to their low-cost production, ability to modify, and closely control drug release kinetics [1], as well as define drug delivery according to desired release profile and improved patient compliance because of a fewer administrations by maintaining constant levels of drug within the circulatory system [2]. Sustained release systems allow for the modulation of drug delivery into circulation at predetermined time points depending on the release profile preferred, thereby sustained release formulations allow for optimum therapeutic outcomes, prolonged efficacy of drug molecule, and a reduction in toxicity profiles [3]. Natural polymers have been used with great recurrence lately for these very reasons. Natural polymers are readily available within the environment and thus they are cheap, they also undergo easy metabolism by naturally occurring enzymes thereby allowing for biodegradability and biocompatibility [4]. Among the many advantages of the use of natural polymer in the development of novel drug delivery systems is that they have no cytotoxic effects associated with the polymer or its products of degradation and are commonly considered safe as they are food grade materials. These naturally occurring polymers can undergo modification reactions so to allow for the enhancement of mechanical and release kinetic properties as per formulation requirements [5].

However, natural polymers are also subject to certain limitations, such as uncontrolled hydration rates and loss of viscosity on storage; it has been found that modifications such as crosslinking, blending and formation of interpenetrating polymer networks (semi-IPN) improve these limitations. In the current study, a semi-IPN has been used to modify the

[1] Wits Advanced Drug Delivery Platform Research Unit, Department of Pharmacy and Pharmacology, School of Therapeutic Sciences, Faculty of Health Sciences, University of the Witwatersrand, Johannesburg, 7 York Road, Parktown, 2193, South Africa.
[2] To whom correspondence should be addressed. (e-mail: viness.pillay@wits.ac.za)

11.1.3 Research Paper 2

Fabrication and characterization of Poly (ethylene) oxide- Gellan Gum semi – Interpenetrating Polymer Network Matrix (XePoMas) oral dosage form for the delivery of a low bioavailable active

Famida G.Hoosain[1], Lomas K.Tomar[1], Pradeep Kumar[1], Charu Tyagi[1], Lisa C. du Toit[1], Yahya E. Choonara[1], and Viness Pillay[1]*

[1]University of the Witwatersrand, Faculty of Health Sciences, Department of Pharmacy and Pharmacology, 7 York Road, Parktown, Johannesburg 2193, South Africa

***Corresponding Author**:

Professor Viness Pillay
Tel: +27-11-717-2274
Fax: +27-11-642-4355
Fax2Email: +27-86-553-4733
Email: viness.pillay@wits.ac.za

ABSTRACT

In this study, an optimized epichlorohydrin crosslinked semi-interpenetrating polymer network xerogel matrix system (XePoMas) for the controlled delivery of sulpiride was prepared. Its ability to sustain drug release was determined by *in vitro* and *in vivo* drug release experiments. Swelling of the xerogel over the 24 hour experimental period ranged from 346-648 %, swelling was observed to increase exponentially over the initial 8 hours. *In vitro* drug release depicted a linear zero-order drug release profile with an R^2 value of 0.9956.The ability of the fabricated XePoMas to sustain drug release and enhance bioavailability of sulpiride *in vivo* was investigated by evaluating the plasma drug concentration over 24 hours in the large pig model. The XePoMas was shown to increase intestinal absorption of sulpiride to a greater extent than the marketed Eglonyl® *in vivo*, with a C_{max} of 830.58ng/mL after 15 hours.

Keywords: Sulpiride, Epichlorohydrin, xerogel, matrix, bioavailability.

11.1.4. Research Paper 3

A Novel Dual-layered Oral Device for Delivery of Two Bioactives in the Treatment of Schizoaffective Disorder

Famida G.Hoosain[1], Lomas K.Tomar[1], Pradeep Kumar[1], Charu Tyagi[1], Lisa C. du Toit[1], Yahya E. Choonara[1], and Viness Pillay[1]*

[1]University of the Witwatersrand, Faculty of Health Sciences, Department of Pharmacy and Pharmacology, 7 York Road, Parktown, Johannesburg 2193, South Africa

***Corresponding Author:**

Professor Viness Pillay
Tel: +27-11-717-2274
Fax: +27-11-642-4355
Fax2Email: +27-86-553-4733
Email: viness.pillay@wits.ac.za

Schizoaffective disorder is a neurodegenerative disorder that affects the primary functional areas of the central nervous system, resulting in memory dissociations and dysfunctional social skills. Medical therapy involves complex therapeutic regimens of antipsychotic and mood stabilizing agents. The current delivery system allows for individualistic release of 2 bioactives from a single oral dosage. The fabricated system is aimed to enhance clinical management of schizoaffective disorder and overcome the related therapeutic limitations. Box-Behnken and Central Composite experimental designs were generated for statistical optimization of the respective components of the dual-layered system. The semi-Interpenetrating polymer network xerogel (s-IPN) was fabricated by the crosslinking of Gellan Gum and Polyethylene oxide (PEO) to formulate the sustained release matrix layer. The bioadhesive multilayered intestinal patch component was prepared via a combination of crosslinking, polymer blending and conjugation reactions to pulsatile release. The s-IPN xerogel matrix component showed zero-order sustained release kinetics, extending over 24 hours. Surface structure indicated porosity formed by interpenetrating networks of polymers, proving the formation of an IPN. FTIR spectra displayed peaks at 3276 cm^{-1} which is characteristic of the additional NaOH group due to crosslinking with epichlorohydrin. The intestinal patch component displayed pulsatile release, with the observed 3 pulses in 6 hour intervals over a 24 hour period. Degree of swelling for the drug-loaded and mucoadhesive layers ranged between 150-400%. Mucoadhesion was found to range between 61.2-88.1%.

35th Academy of Pharmaceutical Sciences Conference 2014

A novel semi-interpenetrating polymer network (IPN) matrix system for the delivery of sulpiride in schizophrenia

Famida Ghulam Hoosain, Viness Pillay, Yahya Choonara, Lisa du Toit and Pradeep Kumar

University of Witwatersrand, Department of Pharmacy and Pharmacology, 7 York Road, Johannesburg, 2193

Purpose: Schizophrenia is a neurodegenerative disease that affects the primary functional areas of the central nervous system, leading to memory dysfunction and reduction in social functionality. For the purpose of the current study sulpiride has been elected as the model drug to be delivered via a novel semi-IPN xerogel matrix drug delivery system.

Methods: A 3-factor, 3 level Box-Behnken experimental design was generated for statistical optimization which produced 15 formulations. A semi-IPN was formulated via crosslinking Gellan Gum (GG) in the presence of Poly (ethylene) oxide (PEO) the resulting polymeric was precipitated, dried and crushed to form matrix tablets. Characterization studies such as Fourier Transform Infrared spectrometry (FTIR), Differential Scanning Calorimetry (DSC), *in vitro* drug release studies, Textural Analysis and Scanning Electron Microscopy (SEM) were conducted. The properties of the synthesized xerogel as compared to crude polymers were evaluated.

Results: The fabrication of the semi-IPN xerogel was successful as evident from data derived from characterization studies such as SEM. Formulated matrix tablets displayed zero- order sustained release kinetics, extending over a period of 24 hours. The mechanism of drug release was observed to be initiated by swelling followed by surface erosion. A 100% drug release was achieved at 24 hours, thus proving its oral applicability. Crosslinked formulations displayed water uptake majorly between 450-500% which indicated a controlled rate of swelling and erosion further allowing for sustained release. Surface morphology of the crosslinked system depicted a porous structure formed by interpenetrating networks of polymers, thereby allowing for a greater degree of controlled penetration into the system affording it the ability to sustain drug release. Brinells hardness number ranged from 200-238, these results illustrate that despite its porous structure the matrix tablet maintains its structural integrity under compression. A peak at 215˚C due to crosslinking was observed in the DSC profile. FTIR showed an additional NaOH group at 3276 cm^{-1} due to crosslinking with EPI. An erosion of 80-86 % was observed in all formulations at the 24 hour mark.

Conclusion: The study validated that the crosslinking of PEO and GG enhanced the physiochemical and physicomechanical properties of the individual polymers, as well as the formation of a semi-IPN xerogel matrix that allows for sustained drug release. The porous structure of the matrix system further enhanced the ability to achieve sustained drug release.

A Novel Dual Layered Oral Semi-Interpenetrating Polymer Network Xerogel Matrix- Bioadhesive Intestinal Patch System for the Individualistic Delivery of Antipsychotics and Mood Stabilizing Agents in Schizoaffective Disorder

Famida Ghulam Hoosain, Viness Pillay*, Yahya Choonara, Lisa du Toit and Pradeep Kumar
University of Witwatersrand, Department of Pharmacy and Pharmacology, 7 York Road, Johannesburg, 2193

Purpose: Schizoaffective disorder is a neurodegenerative disease that affects the primary functional areas of the central nervous system, leading to memory dysfunction and reduction in social functionality.

Methods: *Preparation of Semi-IPN xerogel:* Gelation by crosslinking of Poly (ethylene) oxide (PEO) and Gellan Gum (GG) was employed in the formulation process of the xerogel, followed by precipitation, drying, crushing and compression. Intestinal patches were prepared via a combination of crosslinking and polymer blending techniques; the drug loaded layer of the intestinal patch was synthesized via crosslinking of Eudragit®RS100: sodium alginate with calcium chloride. The mucoadhesive layer of intestinal patch was prepared via the amalgamation of lectin with a hypromellose: chitosan (citric acid) polymer blend.
Characterization Process: Characterization studies such as Fourier Transform Infrared spectrometry, Differential Scanning Calorimetry, *In vitro* drug release studies, Textural Analysis and Scanning Electron Microscopy were conducted on the synthesized semi-IPN xerogel and intestinal patch mucoadhesive and drug loaded layers. To evaluate the properties of the synthesized system components as compared to crude polymers employed.

Results: The xerogel matrix component displayed zero-order sustained release kinetics, extending over a period of 24 hours. A 100% drug release was achieved at 24 hours. Water uptake between 450-500% indicated a controlled rate of swelling and erosion further allowing for sustained release. Surface morphology depicted a porous structure formed by interpenetrating networks of polymers, allowing a greater degree of controlled penetration into the system thus sustaining drug release. Brinells hardness ranged from 200-238 which illustrates structural integrity under compression. Endothermic melting peaks for all design formulations remained within a stable, constant range between 106-107˚C, in addition prominent peaks at a temperature of 215˚C relating to crosslinking was observed in all formulations. FTIR data plots displays peaks at 3276 cm^{-1} which is characteristic of the additional NaOH group due to crosslinking with epichlorohydrin. An erosion of 80-86 % was observed in all formulations at the 24 hour mark. The intestinal patch component displayed pulsatile release, with desired 3 pulses in 6 hour intervals over a 24 hour period. Percentage swelling for the drug loaded and mucoadhesive layers were respectively were satisfactory for the required purpose ranging between 150-400%. Mucoadhesion was between 61.2 -88.1% displaying appropriate mucoadhesion. The tensile strength of the drug loaded and mucoadhesive layers in respect of Young's Modulus were 0.15 and 0.09, indicating excellent flexibility.

Conclusion: The currently proposed system was successful in delivering the model drugs according to the desired drug release kinetics. All characterization studies proved that the system possesses good chemical and mechanical stability required for oral drug delivery.

A Novel Dual-layered Oral Device for Delivery of Two Bioactives in the Treatment of Schizoaffective Disorder

Famida Ghulam Hoosain, Viness Pillay*, Yahya Choonara, Lisa du Toit and Pradeep Kumar
University of Witwatersrand, Department of Pharmacy and Pharmacology, 7 York Road, Johannesburg, 2193

Purpose: Schizoaffective disorder is a neurodegenerative disorder that affects the primary functional areas of the central nervous system, resulting in dysfunction of memory and social functioning. Clinical treatment involves therapeutic regimens of antipsychotic and mood stabilizing agents. The present delivery system provides individualistic release of 2 bioactives within a single oral dosage. The developed system is aimed to enhance management of schizoaffective disorder and overcome related therapeutic limitations.

Methods: Box-Behnken experimental designs were generated for statistical optimization of the respective components of the dual-layered system. The semi-Interpenetrating polymer network xerogel (s-IPN) was fabricated by the crosslinking of Gellan Gum and Polyethylene oxide (PEO) to formulate the sustained release matrix layer. The bioadhesive multilayered intestinal patch component was prepared via a combination of crosslinking, polymer blending and conjugation reactions to pulsatile release. Characterization studies such as Fourier Transform Infrared spectrometry (FTIR), Differential Scanning Calorimetry (DSC), *in vitro* drug release studies, Textural Analysis, Scanning Electron Microscopy (SEM) and *in vivo* studies were conducted.

Results: The s-IPN xerogel matrix component showed zero-order sustained release kinetics, extending over 24 hours. Swelling in the range of 450-500% indicated controlled rate of swelling further allowing for sustained release. Surface structure indicated porosity formed by interpenetrating networks of polymers, proving the formation of an IPN. Brinell hardness number ranged from 200-238 which displays structural integrity under compression. DSC melting peaks for all design formulations remained within a stable, constant range of 106-107˚C, distinctive peaks at a temperature of 215˚C relating to crosslinking was observed in all formulations. FTIR spectra displayed peaks at 3276 cm^{-1} which is characteristic of the additional NaOH group due to crosslinking with epichlorohydrin. The intestinal patch component displayed pulsatile release, with the observed 3 pulses in 6 hour intervals over a 24 hour period. Degree of swelling for the drug-loaded and mucoadhesive layers were satisfactory for the required purpose ranging between 150-400%.
Mucoadhesion was found to range between 61.2-88.1%. Tensile testing of the drug-loaded and mucoadhesive layers in respect of Young's Modulus was 0.15 and 0.09, respectively, indicating excellent flexibility of the polymeric patch layers.

Conclusion: Clinical management of schizoaffective disorder involves the use of combination therapy to combat precipitating symptoms of the schizophrenia and the coexisting mood disorder. The advantage of a single dosage form able to deliver 2 bioactives lays in reduced pill burdens. The enhanced bioavailability of both agents will enhance compliance and therapeutic outcomes. The proposed system was successful in delivering the model drugs in accordance with desired release kinetics.

A Novel Dual Layered Oral Matrix System for the Individualistic Delivery of Antipsychotics and Mood Stabilizing Agents in Schizoaffective Disorder

Famida Ghulam Hoosain, Viness Pillay, Yahya Choonara, Lisa du Toit and Pradeep Kumar

Department of Pharmacy and Pharmacology, School of Therapeutic Sciences, University of Witwatersrand

Schizoaffective disorder is a neurodegenerative disease that affects functional areas of the CNS. Treatment regimens are complex, thus an oral dual-layered system for the concurrent-individualistic delivery of two bioactives was prepared via crosslinking, blending and solvent casting techniques. Box-Behnken and Central Composite design programs were employed for generation of a series of formulations with varying compositions for establishment of optimized s-IPN xerogel-bioadhesive intestinal patch components. Sulpiride and Valproic acid were employed as prototype drugs for experimental design. Subsequently, optimized formulations were characterized for physiomechanical, physiochemical, drug release and mucoadhesive properties. *In vitro* evaluation indicated that formulations met desired pharmaceutical requirements, such as tensile strength, swelling, mucoadhesion and drug release kinetics individualistic to each component. For the s-IPN xerogel component; *in vitro* and *in vivo* studies displayed zero-order sustained release extending over the 24 hour test period, with 100% drug released at 24 hours. A porous surface morphology of the xerogel was observed due to polymer interpenetration, and allows for drug entrapment and controlled release. The intestinal patch component displayed pulsatile release three pulses at 6 hour intervals. Mucoadhesion ranged between 61.2-88.1% appropriate for prolonged residence time required. The tensile strength of the patch layers was 0.09-0.15 indicating excellent flexibility.

Keywords: Xerogel, s-IPN, Bioadhesive Intestinal Patch, Sustained release, Pulsatile release.

11.3. Animal Ethics Clearance Certificate for ex vivo and in vivo studies (clearance was granted for 5 animals, hence the same 5 animals were used after a wash out period of 3 days between dosing, each test group thus consisted of the same 5 animals, and there were 3 groups, n=15)

STRICTLY CONFIDENTIAL

ANIMAL ETHICS SCREENING COMMITTEE (AESC)

CLEARANCE CERTIFICATE NO. 2013/23/04

APPLICANT: Ms FG Hoosain

SCHOOL: Therapeutic Sciences
DEPARTMENT: Pharmacy
LOCATION:

PROJECT TITLE: Synchronised release of sulpiride and lecithin from an inter-penetrating network (IPN) xerogel polymer matrix

Number and Species

5 adult white pigs

Approval was given for to the use of animals for the project described above at an AESC meeting held on 20130430. This approval remains valid until 20150429.

The use of these animals is subject to AESC guidelines for the use and care of animals, is limited to the procedures described in the application form and is subject to any additional conditions listed below:

Signed: _____ (Chairperson, AESC) Date: 6/5/13

I am satisfied that the persons listed in this application are competent to perform the procedures therein, in terms of Section 23 (1) (c) of the Veterinary and Para-Veterinary Professions Act (19 of 1982)

Signed: _____ (Registered Veterinarian) Date: 6/5/13

cc: Supervisor: Professor V Pillay
Director: CAS

Works 2000/Iain0015/AESCCert.wps